

**Wear and rim damage of UHMWPE acetabular cups in total  
hip replacement**

Susan Partridge

Submitted in accordance with the requirements for the degree of Doctor of  
Philosophy

The University of Leeds  
School of Mechanical Engineering

December 2016

The candidate confirms that the work submitted is his/her own, except where work which has formed part of jointly-authored publications has been included. The contribution of the candidate and the other authors to this work has been explicitly indicated below. The candidate confirms that appropriate credit has been given within the thesis where reference has been made to the work of others.

Results from Chapter 3 were published as part of a jointly authored publication: Influence of hip joint simulator design and mechanics on the wear and creep of metal-on-UHMWPE bearings; Murat Ali, Mazen Al-Hajjar, Susan Partridge, Sophie Williams, John Fisher and Louise M Jennings; Proc IMechE Part H: J Engineering in Medicine 2016, Vol. 230(5) 389–397.

Dr Murat Ali designed and conducted the study and carried out the electromechanical hip simulator testing (EM13). The pneumatic hip simulator (Prosim) testing of crosslinked UHMWPE acetabular liners under standard loading conditions outlined in the above publication was carried out by the candidate. All other authors had supervisory roles.

The results of Chapter 3 were subsequently included in a publication (*currently under review*) outlining the protocol development aspect of the tests: Evaluation of a New Methodology to Simulate Damage and Wear of Polyethylene Hip Replacements Subjected to Edge Loading in Hip Simulator Testing; Susan Partridge, Joanne Tipper, Mazen Al-Hajjar, Graham Isaac and Sophie Williams.

Susan partridge was first author and carried out all aspects of the protocol development experimental testing and analysis of results, Mazen Al-Hajjar was responsible for the design of the modifications to the simulator that were used in the testing, Graham Isaac was an employee of DePuy Synthes that provided the components. All other authors had supervisory roles.

This copy has been supplied on the understanding that it is copyright material and that no quotation from the thesis may be published without proper acknowledgement.

## Acknowledgements

I would like to acknowledge the National Institute for Health Research (NIHR) Leeds Musculoskeletal Biomedical Research Unit for funding my position at the Institute of Medical and Biological Engineering while I completed this PhD. I would also like to thank DePuy Synthes UK for supplying the test samples.

I would also like to thank my supervisors Dr Sophie Williams, Professor Joanne Tipper and Professor John Fisher for their support and guidance throughout this project. In particular, I would like to thank Dr Williams for recognising the importance of pursuing other goals in life and supporting my athletics career.

I am very grateful to Mazen Al-Hajjar, who was a constant source of knowledge on hip simulators, as well as Dawn Groves and Mahsa Shahi Avadi for their assistance in the day to day running of the simulator.

I acknowledge and thank Greg de Boer for writing the Matlab code that was used to analyse the rims of the acetabular liners, Nagitha Wijayathunga for assisting with the MicroCT scans and undergraduate and summer intern students Jack Davies, Charlie Howard and Leila Brown for assisting with some of the measurements.

Thanks also to Oscar O'Dwyer, Amritha Leo and Gregory Pryce for assisting with the repeatability and reproducibility evaluation of the method for measuring volume change in explants.

Thanks also for the support of the collaborating surgeons and support staff at Musgrave Park Hospital and Charlotte Maxeke Johannesburg Academic Hospital for assisting in the retrieval of the explants studied in this project.

Special thanks to the technical and administrative staff at the Institute of Medical and Biological Engineering as well as my fellow colleagues and PhD students for supporting my work and my well-being.

Finally, I would like to dedicate this to the ever present Piper.

## **Abstract**

Wear and fatigue of polyethylene acetabular cups have been reported to play a role in the failure of total hip replacements. Edge loading of hip replacements can occur where there is sub-optimal component positioning and/or joint laxity. Wear resistance can be improved by crosslinking but the manufacturing process of these materials involves post-irradiation thermal treatments to recombine free radicals and to stabilise the materials. Stabilisation can also be achieved by adding antioxidants. Material degradation due to oxidation and manufacturing process can result in rim cracking and/or fracture due to a reduction in mechanical properties and this has been observed *in vivo*. A requirement for pre-clinical hip simulator testing under edge loading conditions for all of these materials has therefore been identified.

This thesis describes the development and evaluation of a hip simulator edge loading protocol using accelerated aged conventional UHMWPE acetabular liners as positive controls and commercially available crosslinked UHMWPE acetabular liners as negative controls. The edge loading protocol was then used to evaluate antioxidant stabilised liners in hip simulator tests. Explanted UHMWPE acetabular liners were evaluated for wear and damage mechanisms and compared with the damage observed on the hip simulator tested liners and new methodologies were developed to measure and analyse these explanted liners.

The edge loading protocol produced cracking and subsurface damage in the aged UHMWPE liners but not in the non-aged crosslinked liners. Rim deformation was observed on all liners and the volume change produced was reduced under edge loading conditions for both types of UHMWPE liner. The antioxidant liners performed as well as the commercially available crosslinked liner in hip simulator tests and the rim deformation that was observed on explanted liners was replicated under edge loading conditions in the hip simulator tests.

The edge loading protocol can be used in the future to test a range of UHMWPE materials, including aged materials, and explant analysis using the methodologies developed in this study can be used to inform the design of future simulator tests.

## Contents

|   |             |
|---|-------------|
| <b>Contents</b> .....   | <b>v</b>    |
| <b>Figures</b> .....  | <b>x</b>    |
| <b>Tables</b> .....   | <b>xxii</b> |
| <b>Abbreviations</b> .....                                    | <b>xxiv</b> |
| <b>Chapter 1: Introduction</b> .....                          | <b>1</b>    |
| 1.1 Introduction .....  | 1           |
| 1.2 The Natural Hip .....                                     | 1           |
| 1.3 Osteoarthritis .....                                      | 2           |
| 1.4 Overview of Total Hip Replacement .....                   | 3           |
| 1.4.1 The National Joint Registry of England in Wales .....   | 4           |
| 1.4.2 Total Hip Replacement Bearings.....                     | 4           |
| 1.4.3 Acetabular Cup Design.....                              | 6           |
| 1.5 Overview of Ultra-High-Molecular-Weight Polyethylene..... | 7           |
| 1.5.1 Structure .....   | 7           |
| 1.5.2 Wear of UHMWPE.....                                     | 9           |
| 1.5.3 Lubrication Regime .....                                | 15          |
| 1.5.4 Sterilisation .....                                     | 16          |
| 1.5.5 Oxidation.....  | 17          |
| 1.5.6 Wear Debris and Osteolysis .....                        | 19          |
| 1.5.7 Crosslinked UHMWPE .....                                | 20          |
| 1.5.8 Additive Stabilised UHMWPE.....                         | 28          |
| 1.6 Clinical Aspects of Total Hip Replacement.....            | 30          |
| 1.6.1 Edge Loading .....                                      | 30          |
| 1.6.2 Cup Positioning .....                                   | 31          |
| 1.6.3 Pre-clinical Hip Simulator Testing .....                | 32          |
| 1.6.4 Modular Design Considerations.....                      | 36          |
| 1.6.5 Current Concepts in Explant Analysis .....              | 37          |
| 1.7 Aims and Objectives.....                                  | 44          |
| 1.7.1 Aims  | 44          |
| 1.7.2 Objectives.....   | 44          |
| 1.7.3 Thesis Outline.....                                     | 46          |

|  |           |
|--|-----------|
| <b>Chapter 2: Materials and Methods .....</b>                                | <b>47</b> |
| 2.1 Introduction .....   | 47        |
| 2.2 Materials .....  | 47        |
| 2.2.1 Simulator Components .....   | 48        |
| 2.2.2 Explants .....   | 49        |
| 2.3 General Methods .....  | 50        |
| 2.3.1 Component Cleaning.....  | 50        |
| 2.3.2 Microscopic and Macroscopic Observations .....                         | 50        |
| 2.3.3 Gravimetric Measurements .....   | 50        |
| 2.3.4 Geometric Measurement of Simulator Components .....                    | 51        |
| 2.3.5 General Statistical Methods.....                                       | 56        |
| 2.4 Development of a Geometric Measurement Methodology for Explants .....    | 56        |
| 2.4.1 Introduction .....   | 56        |
| 2.4.2 Materials .....  | 57        |
| 2.4.3 Methods .....  | 58        |
| 2.4.4 Results .....  | 64        |
| 2.4.5 Discussion and Conclusion .....  | 68        |
| 2.5 Development of Rim Deformation Measurement Methodology .....             | 70        |
| 2.5.1 Materials .....  | 70        |
| 2.5.2 Measurement Methods .....  | 71        |
| 2.5.3 Analysis Method.....   | 74        |
| 2.5.4 Validation .....   | 79        |
| 2.5.5 Discussion and Conclusion .....  | 83        |
| 2.6 Development of Subsurface Analysis using MicroCT.....                    | 84        |
| 2.6.1 Introduction .....   | 84        |
| 2.6.2 Materials .....  | 85        |
| 2.6.3 Methods .....  | 85        |
| 2.6.4 Results .....  | 87        |
| 2.6.5 Discussion and Conclusion .....  | 89        |
| 2.7 General Equipment Calibration .....                                      | 90        |
| 2.8 Conclusion .....   | 91        |
| <b>Chapter 3: Hip Simulator Edge Loading Protocol Development Study.....</b> | <b>92</b> |
| 3.1 Introduction .....   | 92        |

|       |  |            |
|-------|--|------------|
| 3.2   | Materials and Methods.....                                       | 94         |
| 3.2.1 | Materials .....  | 94         |
| 3.3   | Methods .....  | 96         |
| 3.3.1 | Simulator Set-up .....   | 96         |
| 3.3.2 | Standard and Edge Loading Conditions .....                       | 99         |
| 3.3.3 | Lubricant .....  | 102        |
| 3.3.4 | Calibration .....  | 102        |
| 3.3.5 | Measurement Points.....  | 104        |
| 3.3.6 | Soak and Load Controls.....                                      | 104        |
| 3.3.7 | Test for Liner Conformity of Aged PE Liners .....                | 104        |
| 3.3.8 | Subsurface Analysis.....   | 105        |
| 3.4   | Results .....  | 105        |
| 3.4.1 | Rim Deformation.....   | 105        |
| 3.4.2 | Subsurface Damage .....  | 107        |
| 3.4.3 | Damage to Acetabular Liners and Cups.....                        | 112        |
| 3.4.4 | Volume Change .....  | 116        |
| 3.4.5 | Creep .....  | 119        |
| 3.4.6 | Deformation of aged PE liners .....                              | 125        |
| 3.5   | Discussion.....  | 126        |
| 3.5.1 | Rim Deformation.....   | 127        |
| 3.5.2 | Subsurface Damage .....  | 127        |
| 3.5.3 | Damage to Acetabular Liners.....                                 | 129        |
| 3.5.4 | Volume Change .....  | 130        |
| 3.6   | Conclusion .....   | 132        |
|       | <b>Chapter 4: Hip Simulator - Antioxidant UHMWPE Study .....</b> | <b>133</b> |
| 4.1   | Introduction .....   | 133        |
| 4.2   | Materials .....  | 135        |
| 4.3   | Methods .....  | 137        |
| 4.4   | Results .....  | 138        |
| 4.4.1 | Rim Deformation.....   | 138        |
| 4.4.2 | Subsurface Damage .....  | 140        |
| 4.4.3 | Damage to the acetabular liners and cups .....                   | 141        |
| 4.4.4 | Volume Changes .....   | 142        |

|   |            |
|---|------------|
| 4.4.5 Comparison of AOPE Study with Protocol Development Hip Simulator Study..... | 147        |
| 4.5 Discussion.....   | 149        |
| 4.5.1 Volume Change .....   | 149        |
| 4.5.2 Damage to Acetabular Liners and Cups.....                                   | 151        |
| 4.6 Conclusion.....   | 152        |
| <b>Chapter 5: Wear and Damage Analysis of Explanted Acetabular Liners .....</b>   | <b>153</b> |
| 5.1 Introduction .....  | 153        |
| 5.2 Methods and Materials.....  | 153        |
| 5.2.1 Ethical Approval and Explant Collection .....                               | 154        |
| 5.2.2 Explant Selection.....  | 156        |
| 5.2.3 Analysis Methods for Explants.....  | 159        |
| 5.2.4 Semi-Quantative Damage Categorisation of Explants.....                      | 160        |
| 5.2.5 Calculation of Volume Change per Million Cycles for Explants ...            | 163        |
| 5.3 Results .....   | 164        |
| 5.3.1 Rim Deformation.....  | 164        |
| 5.3.1 Subsurface damage.....  | 168        |
| 5.3.2 Damage Categorisation.....  | 175        |
| 5.3.3 Volume change .....   | 182        |
| 5.3.4 Statistical Analyses and Correlations.....                                  | 187        |
| 5.4 Discussion.....   | 189        |
| 5.4.1 Rim Deformation of Explanted Acetabular Liners .....                        | 190        |
| 5.4.2 Subsurface Damage to Explanted Acetabular Liners.....                       | 195        |
| 5.4.3 Damage and Volume Change to Explanted Acetabular Liners ....                | 197        |
| 5.4.4 Damage and Wear of Crosslinked and Non-crosslinked Acetabular Liners .....  | 199        |
| 5.4.5 Statistical Analyses.....   | 200        |
| 5.4.6 Limitations to Explant Analysis Methodologies.....                          | 200        |
| 5.4.7 Summary and Conclusion .....  | 201        |
| <b>Chapter 6: Discussion and Future Work .....</b>                                | <b>203</b> |
| 6.1 Introduction .....  | 203        |
| 6.2 Comparative Analysis of Simulator Components and Explants.....                | 204        |
| 6.2.1 Rim Deformation of Simulator Components and Explants.....                   | 204        |
| 6.2.2 Subsurface Damage of Simulator Liners and Explants .....                    | 206        |

|   |            |
|---|------------|
| 6.2.3 Surface Damage to Simulator Liners and Explants .....   | 208        |
| 6.2.4 Volume Change of Simulator Components and Explants .....  | 210        |
| 6.3 Study Limitations.....  | 212        |
| 6.4 Conclusion .....  | 214        |
| 6.5 Future Work .....   | 215        |
| 6.5.1 Simulator Studies .....   | 215        |
| 6.5.2 Explant Studies.....  | 215        |
| 6.6 Final Summary.....  | 218        |
| <b>References.....</b>  | <b>219</b> |
| <b>Appendix 1: Simulator Components with Station Numbers and Labelling .....</b>                              | <b>245</b> |
| <b>Appendix 2: Inter and Intra-user variability of volume change<br/>    measurements on explant 6N .....</b> | <b>254</b> |
| <b>Appendix 3: Analysing Volume Change in Explants with Redlux .....</b>                                      | <b>255</b> |
| <b>Appendix 4: Analysing Rim Deformation in UHMWPE Liners.....</b>  | <b>258</b> |
| <b>Appendix 5: Images of Explanted Acetabular Liners.....</b>   | <b>264</b> |
| <b>Appendix 6: Informed Consent and Explant Collection Documents .....</b>                                    | <b>266</b> |

## Figures

|  |           |
|--|-----------|
| <b>Figure 1-1 The Natural Hip (BBC, 2014) .....</b>  | <b>1</b>  |
| <b>Figure 1-2 Total Hip Arthroplasty (Malik, 2007) .....</b>   | <b>3</b>  |
| <b>Figure 1-3 Comparison of cumulative probability of revision (Kaplan-Meier estimates) for uncemented primary hip replacements with different bearing surfaces (National Joint Registry, 2014) .....</b>                                | <b>5</b>  |
| <b>Figure 1-4 A schematic of (A) Ethylene and (B) UHMWPE Chemical Structures (Kurtz, 2009) .....</b>   | <b>8</b>  |
| <b>Figure 1-5 A Schematic of the Morphology of UHMWPE. Kurtz (2009).....</b>   | <b>8</b>  |
| <b>Figure 1-6 A schematic of Wear Produced by Microscopic Counterface Asperities. Adapted from Fisher (1994) .....</b>   | <b>9</b>  |
| <b>Figure 1-7 A Schematic of Macroscopic Polymer Asperity Wear. Adapted from Fisher (1994) .....</b>   | <b>10</b> |
| <b>Figure 1-8 A Schematic of Stress Fields Associated with Structural Failure. Adapted from Fisher (1994) .....</b>  | <b>11</b> |
| <b>Figure 1-9 Graph of Boundary, Mixed and and Hydrodynamic Lubrication Regimes. Adapted from Biresaw (2008).....</b>  | <b>15</b> |
| <b>Figure 1-10 Schematic of pathophysiology of wear debris-mediated osteolysis (Talmo et al., 2006) .....</b>  | <b>20</b> |
| <b>Figure 1-11 Molecular structure of conventional UHMWPE and cross-linked UHMWPE (Adapted from DePuy Orthopaedics Inc., 2009).....</b>  | <b>21</b> |
| <b>Figure 1-12 Schematic to outline the trade-offs in wear resistance, fatigue crack propagation resistance and oxidation resistance developed by Atwood et al., (2011).....</b>   | <b>27</b> |
| <b>Figure 1-13 Schematic of Edge Loading (A) Head and Cup Separation (B) Rim Contact (C) Relocation (Nevelos et al., 2000) .....</b>   | <b>30</b> |
| <b>Figure 1-14 Load (right) and motion (left) parameters described in ISO 1424-1 (2014) where AB = Abduction, AD = Adduction, E = Extension, F = Flexion, IR = Inward rotation and OR = Outward rotation (BS ISO 14242-1:2014) .....</b> | <b>33</b> |
| <b>Figure 1-15 schematic of the wear volumes for a Charnley acetabular cup showing the cylindrical and spherical regions and the wear volume (parallelogram EDCGFO; (Hall and Unsworth, 1995)).....</b>                                  | <b>41</b> |

|   |    |
|---|----|
| Figure 2-1 An assembled Pinnacle® acetabular shell showing the ARD tabs on the UHMWPE liner and the ARD scallops on the titanium shell.....   | 48 |
| Figure 2-2 A compression moulded acetabular cup (foreground; AOPE CM cup) and a Pinnacle® compatible liner with titanium shell (background; AOPE liner).....  | 49 |
| Figure 2-3 Schematic of a CMM scan of a UHMWPE liner showing measurement coordinates across the bearing surface .....   | 52 |
| Figure 2-4 Alignment of an acetabular cup on the CMM: origin ( $0_x, 0_y$ ) is set at ( $d_x, 0_y$ ) from the centre of one of the alignment holes and the x axis is aligned through the origin and the centre of one of the alignment holes. The horizontal liner rim is aligned with the z plane. ....  | 53 |
| Figure 2-5 SR3D image of a cross section of an AOPE acetabular liner (AOPE 2) after 5Mc of standard loading and 5Mc of edge loading. The maximum radial deviation at the area of articulation is marked with a red line (208.9 $\mu\text{m}$ ) and the radial deviation at the rim is marked with a green line (157.9 $\mu\text{m}$ ). Profile deviations are at x40 magnification.....   | 54 |
| Figure 2-6 Geometric reconstruction of volume change for an AOPE acetabular liner after 5Mc of standard loading and 5Mc of edge loading (AOPE 2). Volume change on the bearing surface and close to the inner rim is shown.....   | 55 |
| Figure 2-7 A flow chart showing the process for obtaining volume change in explanted acetabular liners using Redlux from measurement to volume calculation. ....  | 60 |
| Figure 2-8 Flow chart showing the process for evaluating the repeatability, reproducibility and accuracy of each volume change protocol. The volume change for the explants was determined by four different protocols, which were repeated three times by four different users. The accuracy was determined by comparing to gravimetric measurements of two different control liners.....  | 63 |
| Figure 2-9 Inter-user variability of the volume change analyses for the four protocols for each user for explant 3N ( $\pm 95\%$ Confidence intervals) .....  | 65 |
| Figure 2-10 Schematic of an acetabular liner showing the Talysurf traces taken from the bearing surface to the horizontal rim including: (A) three traces taken across the edge loaded region, (B) a fourth trace taken across an unworn region of the liner (the colours represent those used to plot the traces in Matlab in section 2.5.3) and (C) a photo of the liner showing the same traces in the schematic and (D) cross section of the rim showing where the stylus took the traces ..... | 72 |

|   |           |
|---|-----------|
| <b>Figure 2-11 Schematic of an explanted liner with the Talysurf traces taken at 30° intervals around the circumference of the liner. The colours are the same as those used to plot the traces in Matlab.....</b>  | <b>73</b> |
| <b>Figure 2-12 Example of an explanted acetabular liner with extensive damage to the rim. No talysurf traces were taken over the rim in this area to avoid damage to the stylus. ....</b>   | <b>73</b> |
| <b>Figure 2-13 Four Talysurf traces with the identified datum highlighted on each trace (Note: unworn trace = blue, worn traces = cyan, green and black; XLPE simulator liner, AM9). ....</b>   | <b>74</b> |
| <b>Figure 2-14 Two cases where (A) the constraint was not satisfied and the datum was not identified at <math>x_p</math> and (B) the constraint was satisfied and the datum was identified at <math>x_p</math>. Note that the datum is identified before the traces are levelled. ....</b>  | <b>75</b> |
| <b>Figure 2-15 Talysurf traces with an example of an explant with (A) a wrongly identified datum for one of the traces (red), (B) a close up of the scratch that caused the datum to be located in the wrong place and (C) correct identification of the datum after lowering the tolerance value (note that the traces have not been levelled yet). ....</b>   | <b>76</b> |
| <b>Figure 2-16 Four Talysurf traces that have been (A) datum matched and rotated to align with the unworn trace along the horizontal rim and (B) rotated about the datum to the horizontal plane (levelled) and scaled to plot both axes in mm (Note: unworn trace = blue, worn traces = cyan, green and black; XLPE simulator liner, AM9) ....</b>   | <b>77</b> |
| <b>Figure 2-17 The tolerance used to calculate the datum for the cyan trace was changed from (A) 0.5 to (B) 0.55 resulting in better alignment with the other traces (XLPE simulator liner, AM1). ....</b>  | <b>77</b> |
| <b>Figure 2-18 Four Talysurf traces with (A) the location of the point from which the penetration was calculated and (B) a close up with a red arrow to mark the penetration distance between the unworn (dark blue) and worn traces (black, cyan, green; mean=0.07mm) normal to the unworn trace (XLPE simulator liner, AM9).....</b>  | <b>78</b> |
| <b>Figure 2-19 Six Talysurf traces of untested liner NA14 with material removed at the inner rim. The blue, cyan and green traces were taken across an intact region of the rim and the black, magenta and red traces were taken across the region of the liner where the material was removed. (A) denotes the user defined data point where the distance between traces was calculated normal to the first unworn trace (0.54mm), (B) denotes the point where the distance between traces was calculated on the chamfer above the worn region (0.0076mm).....</b> | <b>79</b> |

|   |           |
|---|-----------|
| <b>Figure 2-20 Eight Talysurf traces taken at 45° intervals around the circumference of untested liner AM11 .....</b>   | <b>80</b> |
| <b>Figure 2-21 (A) A close up of the eight Talysurf traces taken at 45° intervals around the circumference of control liner AM11 showing how a difference in gradient along the length of the chamfer resulted in a misaligned trace at the inner rim and (B) a close up of the inner rim showing a mean difference of 0.04mm between traces.....</b>   | <b>81</b> |
| <b>Figure 2-22 Six traces taken across the rim of a ceramic liner. Three across a worn region of the liner (pink) and three across an unworn region (blue) .....</b>  | <b>82</b> |
| <b>Figure 2-23 Two Talysurf traces across the same region of a ceramic liner (without moving the liner between traces) showing (A) a full plot of the two traces and (B) a close up of the traces showing a distance between the two of 0.00083mm.....</b>  | <b>83</b> |
| <b>Figure 2-24 (A) A fixture for acetabular liners designed to fit the 73mm MicroCT sample holder with 3 tiers allowing multiple liners to be loaded at one time (sponge used to hold samples in place) and (B) a MicroCT image of an explanted acetabular liner with damage in the superior rim region. The view is of a 10µm 2D reconstruction and looks down onto a cross section of the rim. ....</b> | <b>86</b> |
| <b>Figure 2-25 (A) Initial scans for each type of material were made of the whole liner and (B) subsequent scans were of a reduced scan region measuring approximately 20-25mm from the horizontal rim towards the apex of the liner. ....</b>  | <b>87</b> |
| <b>Figure 2-26 MicroCT images of (A) an XLPE control liner, (B) an aged PE liner and (C) an AOPE liner, each with a close up of the material (right hand image).....</b>  | <b>88</b> |
| <b>Figure 2-27 MicroCT images of the AOPE control liner with (A) a void in the material and (B) a wrinkle effect around the inner rim.....</b>  | <b>89</b> |
| <b>Figure 3-1 Photo of an acetabular liner showing the barb around the circumference of the liner.....</b>  | <b>96</b> |
| <b>Figure 3-2 Group 1 of the Prosim ten station hip joint simulator showing five stations with serum in gaiters surrounding the joint interface. ....</b>   | <b>96</b> |
| <b>Figure 3-3 Single station on the Prosim simulator. The testing set-up is shown with the femoral head mounted on the metal spigot and the acetabular cup cemented into the simulator mount (note the image depicts a cemented cup rather than a shell and liner. The shells were cemented into the holder in the present study). ....</b>   | <b>97</b> |

|   |            |
|---|------------|
| <b>Figure 3-4 The backside of a titanium shell showing the hole through which the liner was pushed out by a screw at measurement points. ....</b>   | <b>97</b>  |
| <b>Figure 3-5 Schematic of an acetabular cup and femoral head showing (A) the joint reaction force during stance phase in the clinical conditions with the cup at 45° and (B) the joint reaction force in the simulator conditions with the cup angle at 35° (Adapted from Williams et al. 2008).....</b>   | <b>98</b>  |
| <b>Figure 3-6 Schematic of a side view of a single station of the Prosim hip simulator with the set-up for edge loading conditions. A back spring pushed the femoral head laterally during the swing phase of gait causing the femoral head to contact with the acetabular rim on heel strike (lateral sliding distance 0.5mm-1mm) .....</b>  | <b>99</b>  |
| <b>Figure 3-7 Load and motion output profiles for one cycle of gait with the femoral head position highlighted for heel strike, stance phase and toe off. ....</b>  | <b>100</b> |
| <b>Figure 3-8 Schematic of the dial gauge micrometer set-up to measure lateral sliding distance under microseparation (diagram not to scale) ....</b>   | <b>102</b> |
| <b>Figure 3-9 Automatic Load Calibration function on the Prosim pneumatic hip simulator.....</b>  | <b>103</b> |
| <b>Figure 3-10 Worn and unworn rim profiles for XLPE liners (A) AM1, (B) AM5, (C) AM7 and (D) AM9 showing the points at which the penetration values were measured for a section zoomed to the inner rim. The red circle highlights the sharp change in radius between the bearing surface and chamfer for the worn profiles. The unworn profile is the dark blue line. ....</b>  | <b>106</b> |
| <b>Figure 3-11 Worn and unworn rim profiles for aged PE liners A2, A4, A6 and A10 showing the points at which the penetration values were measured for a section zoomed to the inner rim. The red circle highlights the sharp change in radius between the bearing surface and chamfer for the worn profiles. ....</b>  | <b>107</b> |
| <b>Figure 3-12 MicroCT 2D reconstructed slices with no visible cracking: (A&amp;B) XLPE liner AM1 at 2.3mm and 7.7mm below the horizontal surface of the rim and (C&amp;D) XLPE liner AM5 at 2.1mm and 6mm below the horizontal surface of the rim. View is a cross section of the liner looking down onto the rim. ....</b>  | <b>108</b> |
| <b>Figure 3-13 MicroCT 2D reconstructed slices showing subsurface cracking on aged PE liner A10 showing (A) circumferential cracking at outer rim and at an anti-rotation tab 2.5mm below the horizontal surface of the rim (B) cracking around an anti-rotation tab 3mm below the horizontal surface (C) extensive multi-directional cracking near the outer rim and anti-tab 3.3mm below the horizontal surface and (D)</b> |            |

circumferential cracking near the inner rim 3.8mm below the horizontal surface. View is a cross section of the liner looking down onto the rim. .... 109

**Figure 3-14 MicroCT 2D reconstructed slices with the corresponding photos of an aged PE liner (A10) showing (A) cracks propagating circumferentially close to the inner rim and the corresponding whitening at the inner rim, (B) Cracks propagating circumferentially along the outer rim from at an anti-rotation tab and the corresponding photo and (C) a radial crack and the corresponding backside crack. The location of these damage mechanisms is shown in the first image. .... 110**

**Figure 3-15 Subsurface cracking on aged PE liner A2 showing (A) circumferential cracking at outer rim and around an anti-rotation tab 2.9mm below the horizontal surface of the rim (B) cracking around an anti-rotation tab 3.2mm below the horizontal surface (C) circumferential cracking near the inner rim 4mm below the horizontal surface and (D) Radial crack initiating at the outer rim and extending towards the inner bearing surface 9mm below the horizontal surface of the rim (see Figure 3-16 for detail). View is a cross section of the liner looking down onto the rim. .... 111**

**Figure 3-16 A MicroCT reconstruction with the corresponding photo of an aged PE liner (A2) showing a radial crack and the corresponding backside crack ..... 112**

**Figure 3-17 An XLPE liner with the polished wear area highlighted after standard loading and a microscopy image of the fine scratching on the bearing surface (AM1; x30 magnification) ..... 113**

**Figure 3-18 Images of cracking on aged PE liners after 5Mc of edge loading showing cracking along an anti-rotation tab (A, Aged PE liner A2; C, aged PE liner A10) and subsurface cracking and whitening at inner rim (B, aged PE liner A2 and C, aged PE liner A10) ..... 113**

**Figure 3-19 Radial cracking on the backside of aged PE liner (A) A2, (B) A4 & (C) A10 after 5MC of edge loading ..... 114**

**Figure 3-20 (Top image) Location of damage to aged PE liners (A10 shown) with respect to orientation during edge loading (Bottom image A) Subsurface cracking and whitening of the material at the inner rim (Bottom image B) cracking along anti-rotation scallop (Bottom image C) radial crack on backside..... 115**

**Figure 3-21 Microscopic image of scratching on a metal femoral head articulating with an XLPE acetabular cup (AM1). .... 116**

|   |            |
|---|------------|
| <b>Figure 3-22 Cumulative volume changes measured gravimetrically for the XLPE liners after 5Mc of standard loading (0-5Mc) and 5Mc of edge loading (5-10Mc) in a hip simulator.....</b>  | <b>117</b> |
| <b>Figure 3-23 Cumulative volume changes measured gravimetrically for the aged PE liners after 5Mc of standard loading (0-5Mc) and 5Mc of edge loading (5-10Mc) in a hip simulator.....</b>   | <b>118</b> |
| <b>Figure 3-24 Mean steady state wear rates calculated using gravimetric measurements for the XLPE and aged PE liners under standard and edge loading conditions in a hip simulator (<math>\pm 95\%</math> Confidence intervals; n=4) .....</b>           | <b>119</b> |
| <b>Figure 3-25 Cumulative volume change measured geometrically for the XLPE liners after 5Mc of standard loading in a hip simulator .....</b>   | <b>120</b> |
| <b>Figure 3-26 Mean volume change for the XLPE liners over 5Mc of standard loading: comparison of gravimetric, geometric, geometric corrected with load control (<math>\pm 95\%</math> Confidence Intervals; n=4), and load control measurement.....</b>  | <b>121</b> |
| <b>Figure 3-27 Cumulative volume change measured geometrically for the aged PE liners after 5Mc of standard loading in a hip simulator .....</b>  | <b>122</b> |
| <b>Figure 3-28 Mean volume changes for the aged PE liners over 5Mc of standard loading: comparison of gravimetric, geometric, geometric load control corrected (<math>\pm 95\%</math> Confidence Intervals; n=4), and load control measurements .....</b> | <b>123</b> |
| <b>Figure 3-29 Mean steady state wear rates calculated from the geometric and gravimetric measurements of the XLPE and the aged PE liners under standard loading conditions (<math>\pm 95\%</math> Confidence intervals; n=4) .....</b>                   | <b>124</b> |
| <b>Figure 3-30 SR3D geometric reconstructions of volume change after 5Mc standard loading and 5Mc edge loading conditions for XLPE liners (A &amp; B; AM9) and aged PE liners (C &amp; D; A10 ).....</b>  | <b>125</b> |
| <b>Figure 3-31 Pinnacle shells after the backside of the liners were covered in engineering blue then inserted and removed from the shell. (A &amp; B) areas of contact for an XLPE liner (C &amp;D) areas of contact for an aged PE liner.....</b>       | <b>126</b> |
| <b>Figure 4-1 A compression moulder acetabular cup (foreground; AOPE cup) and a Pinnacle® compatible liner with titanium shell (background; AOPE liner).....</b>  | <b>136</b> |
| <b>Figure 4-2 Schematic of a cross-section of the compression moulded acetabular cup.....</b>   | <b>137</b> |

|   |            |
|---|------------|
| <b>Figure 4-3 4-4 A close up of the inner rim showing worn and unworn rim profiles for the AOPE liners. The point at which the penetration values were measured is shown and a sharp change in radius at the inner rim can be observed. The dark blue liner is the unworn profile and the green, cyan and black lines are the worn profiles. ....</b> | <b>139</b> |
| <b>Figure 4-5 A close up of the inner rim showing worn and unworn rim profiles for the AOPE cups. The point at which the penetration values were measured is shown and a sharp change in radius at the inner rim can be observed. The dark blue liner is the unworn profile and the green, cyan and black lines are the worn profiles. ....</b>       | <b>140</b> |
| <b>Figure 4-6 MicroCT 2D reconstructed slices with no visible cracking: AOPE liner AOPE 5 at (A) 1.39mm. (B) 2.64mm, (C) 2.91mm and (D) 7.1mm below the horizontal surface of the rim. The holes are reference holes used in the CMM measurements. View is a cross section of the liner looking down onto the rim. ....</b>                           | <b>141</b> |
| <b>Figure 4-7 An AOPE liner (AOPE 5) with (A) the wear area highlighted after standard loading and (B) a microscopy image of the polished bearing surface (x30 magnification).....</b>  | <b>142</b> |
| <b>Figure 4-8 Cumulative volume changes measured gravimetrically for the AOPE liners after 4.8Mc of standard loading (0-5Mc) and 5Mc of edge loading (5-10Mc) in a hip simulator.....</b>   | <b>143</b> |
| <b>Figure 4-9 Cumulative volume changes measured geometrically for the AOPE liners after 4.8Mc of standard loading (0-5Mc) and 5Mc of edge loading (5-10Mc) in a hip simulator.....</b>   | <b>144</b> |
| <b>Figure 4-10 Cumulative volume changes measured geometrically for the AOPE cups after 4.8Mc of standard loading (0-5Mc) and 5Mc of edge loading (5-10Mc) in a hip simulator.....</b>  | <b>145</b> |
| <b>Figure 4-11 Mean steady state wear rates for the AOPE liners and AOPE cups after 4.8Mc of standard and 5Mc of edge loading conditions calculated using geometric measurements and gravimetric measurements (AOPE liners only); (<math>\pm 95\%</math> Confidence Intervals; n=4) .....</b>   | <b>146</b> |
| <b>Figure 4-12 SR3D geometric reconstructions of volume change after 5Mc standard loading and 5Mc edge loading conditions for the AOPE liners (A &amp; B; AOPE 6) and AOPE cups (C &amp; D; AOPE CM 2). Superior region of the liner/cup is at the top of the image.....</b>  | <b>147</b> |
| <b>Figure 4-13 Mean penetration values at the inner rim for the XLPE liners, Aged PE liners, AOPE liners and AOPE cups (95% Confidence Intervals; n=4) .....</b>  | <b>148</b> |
| <b>Figure 4-14 Mean steady state wear rates measured gravimetrically and geometrically for the AOPE liners, AOPE cups, XLPE liners and aged PE</b>  |            |

|  |     |
|--|-----|
| liners for standard loading and edge loading conditions ( $\pm 95\%$ Confidence internals; n=4 for each liner/cup; all XLPE and aged PE data previously presented in results sections 3.4.1) .....   | 149 |
| Figure 5-1 Schematic of a (a) neutral liner, (B) lipped liner and (C) an image of a dissociated neutral liner (liner 10D) .....  | 157 |
| Figure 5-2 Pre-operative x-ray showing the horizontal reference along the transischial line and the inclination angle of the acetabular cup .....  | 160 |
| Figure 5-3 Schematic of an acetabular liner divided into four quadrants with the wear area to the superior aspect where (a) denotes the rim subdivision and (b) the bearing surface subdivision .....  | 161 |
| Figure 5-4 Microscopy image taken at x30 magnification showing (A) pitting, (B) surface deformation (indentations), (C) unworn surface with machining marks still visible, (D) abrasion, scratching and embedded debris, (E) large scratch and (F) fine scratching and burnishing .....  | 162 |
| Figure 5-5 Close up of the inner rims of five of the neutral liners with no visible deformation and/or wear. Blue traces are taken over the unworn region and pink traces over the worn region. Cyan traces are taken from the anterior and posterior unworn regions of the liner. ....  | 165 |
| Figure 5-6 A close up of the inner rim showing a sharpening of the rim for (A) explant 5N with a mean penetration distance of 0.36mm and (B) explant 6N with a mean penetration of 0.5mm. Blue traces are taken over the unworn region and pink traces over the worn region. Cyan traces are taken from across the anterior and posterior regions of the liner. .... | 166 |
| Figure 5-7 Full traces and close up of the inner rims of the five dissociated neutral liners with large deformations in the form of a flattened curve on the superolateral rim (identified for one of the superolateral traces with an arrow) .....  | 167 |
| Figure 5-8 Talysurf traces of (A) a flattened inner rim on the superior region of dissociated neutral liner, explant 12D, (B) an undeformed region of the same liner (or less deformed) and (C) a photographic image of the deformed inner rim (explant 12D) .....   | 168 |
| Figure 5-9 A Photographic image and MicroCT images of the subsurface damage observed on a non-dissociated neutral liner (explant 3N) showing (A) a photo of the component and orientation <i>in vivo</i> , (B, C & D) visibly undamaged sections of the liner between 2.1mm and 4.5mm below the horizontal rim.....  | 169 |
| Figure 5-10 A Photographic image and MicroCT images of the subsurface damage observed on a non-dissociated neutral liner (explant 2N) showing (A) a photo of the component and orientation <i>in vivo</i> , (B)  |     |

visibly undamaged section of the liner 5mm below the horizontal rim (C) a visibly damaged section showing cracking 1.3mm beneath the surface damage and (D) a close up of the damage in (C) showing cracks extending circumferentially and perpendicular to the outer rim (arrow; scale bar 1mm)..... 170

**Figure 5-11** Photographic images and MicroCT images of the subsurface damage observed on a non-dissociated neutral liner (explant 5N) showing (A) a photo of the component and orientation *in vivo*, (B) a close up photographic section of the damaged rim showing surface damage in the posterior region, (C) a complete MicroCT slice at the top (horizontal section) of the liner rim, (D) a crack propagating circumferentially 0.4mm beneath the surface damage, (E) extensive multi-directional cracking 1mm underneath the surface damage and (F) a crack propagating circumferentially 1.6mm below the surface damage. .... 171

**Figure 5-12** Photographic images and MicroCT images of the subsurface damage observed on a dissociated neutral liner (explant 11D) showing (A.1) a photo of the fractured superior rim with absent anti-rotation tabs, (B) the fractured superior rim and cracking adjacent to the location of an absent anti-rotation tab 3.9mm below the horizontal liner rim, (C) a visibly undamaged section, except for the fracture in the superior region, 5.1mm below the horizontal rim, (D) a visibly undamaged section 6.8mm below the horizontal liner rim ..... 172

**Figure 5-13** Photographic images and MicroCT images of the subsurface damage observed on a dissociated neutral liner (explant 9D) showing (A.1) a photo of the superior rim with cracking, absent antirotation tabs and embedded debris, (B.1) a photo of the inferior rim with delamination and embedded debris, (A.2, A.3 & A.4) MicroCT images of circumferential cracking propagating parallel to the outer rim and multi-directional cracking with embedded debris at 1.8mm, 2.1mm and 3mm (B.2, B.3) multi-directional cracking 3.3mm and 3.9mm below the horizontal rim and (B.4) circumferential cracking near the inferior inner rim ..... 173

**Figure 5-14** Photographic images and MicroCT images of the subsurface damage observed on a dissociated neutral liner (explant 12D) showing (A.1) a photo of the deformed superior rim (B.1) a photo of the inferior rim with delamination and embedded debris, (A.2 & A.3) the visibly undamaged superior rim at 0.7mm and 3.1mm below the horizontal liner rim (B.2 & B.3) extensive multi-directional cracking on the inferior rim and cracking adjacent to an anti-rotation tab (arrow)..... 174

**Figure 5-15** Examples of damage modes observed on the non-dissociated neutral liners (A) Scratching with some embedded particles (explant 1N), (B) Abrasion (explant 2N), (C) embedded debris (explant 4N), (D)

|  |            |
|--|------------|
| elongation of the bearing surface (explant 5N and (E) rim damage in the form of two gouge like cracks (explant 5N) .....   | 176        |
| <b>Figure 5-16 Examples of damage mechanisms on the dissociated neutral liners: (A) Deformation at inner rim and embedded particles at the outer superior rim (explant 9D), (B) fractured superior rim (explant 11D) (C) gouge like rim fracture on the superior rim (explant 8D) and (D) Delamination, fracture and embedded particles on the inferior rim (explant 12D) .....</b>                              | <b>177</b> |
| <b>Figure 5-17 (A) Deformation, scratching and a ridge across the backside of the liner. (B) The other side of the liner was less damaged .....</b>  | <b>178</b> |
| <b>Figure 5-18 (A) Femoral head with typical metal transfer and scratching and (B) metal shell showing with deformation caused by articulation of the femoral head.....</b>  | <b>178</b> |
| <b>Figure 5-19 Images of lipped explants showing (A), (B), (C) areas of rim deformation (highlighted with blue pen) possibly due to impingement and (D) gross deformation to the superolateral rim .....</b>   | <b>179</b> |
| <b>Figure 5-20 A femoral head that articulated with a lipped liner (explant 15L) with heavy scratching to one side .....</b>   | <b>180</b> |
| <b>Figure 5-21 Redlux geometric reconstructions of the explanted non-dissociated neutral acetabular liners. Annotations apply to all liners: (A) a principal area of volume change due to wear and creep, (B) a secondary area of volume change and (C) creep on the bearing surface (red, white). Grey areas are screw holes excluded from the calculations. View looks down onto the bearing surface .....</b> | <b>184</b> |
| <b>Figure 5-22 Redlux geometric reconstructions of the explanted dissociated neutral acetabular liners showing areas of wear/deformation near the rim and extending on to the bearing surface (explants 8D, 10D &amp; 11D), atypical volume change on the bearing surface (explant 9D) and “typical” volume change on the bearing surface (explant 12D). View looks down onto the bearing surface .....</b>      | <b>186</b> |
| <b>Figure 5-23 Redlux images of the explanted lipped acetabular liners showing areas of volume change. The elevated rim is positioned at the top of the image and view looks down onto the bearing surface. ....</b>   | <b>187</b> |
| <b>Figure 5-24 Talysurf trace over the deformed region of (A) a non-dissociated neutral liner and (B) a dissociated neutral liner revealing distinct geometries between the two types of liner at the inner rim.....</b>   | <b>191</b> |
| <b>Figure 5-25 (A) Reassembled dissociated neutral explant (explant 10D) showing (A) the position of the head with respect to the liner following the dissociation, (B) the deformed region of the inner rim and (C) a close up of the relatively undamaged rim region and (D) a</b>   |            |

|   |            |
|---|------------|
| microscope image of the rim area with machining marks still visible (x30 magnification).....  | 192        |
| <b>Figure 5-26 (A) MicroCT image of a crack propagating circumferentially, appearing to initiate at an area of extensive damage (B) Cracks propagating circumferentially and parallel to the outer edge of the rim ..</b>   | <b>196</b> |
| <b>Figure 6-1 Talysurf rim traces of (A) a simulator sample (aged PE liner A10) and (B) an explanted liner (explant 5N) showing similar rim wear and/or deformation in the form of a sharpening of the inner rim and reduced radius of curvature.....</b>   | <b>206</b> |
| <b>Figure 6-2 MicroCT images of (A) cracks propagating circumferentially around the liner rim and at an anti-rotation tab on the superior rim of an aged PE liner (simulator sample A10), (B) a crack propagating circumferentially close to the outer edge of the superior rim of a dissociated explant (9D), (C) a crack along an anti-rotation tab on the inferior rim of a dissociated explant (11D), (D) a crack filled with third body debris along an anti-rotation tab on the inferior rim of an explant (12D) and (E) a crack propagating circumferentially around a non-dissociated explant (5N). .....</b> | <b>207</b> |
| <b>Figure 6-3 Microscope images of the surface of (A) an XLPE simulator liner with fine scratching on the surface (XLPE AM1) and (B) an explant with fine scratching as well as larger, deeper scratches (arrow; explant 4N; x30 magnification).....</b>  | <b>208</b> |
| <b>Figure 6-4 Rim damage on (A) a non-dissociated neutral explanted liner and a (B) dissociated neutral liner that may have been cause by femoral neck impingement.....</b>   | <b>209</b> |
| <b>Figure 6-5 Volume change per million cycles measured geometrically under standard loading conditions for all simulator components (n=4) and for the non-crosslinked non-dissociated neutral explanted liners (n=5; <math>\pm</math>95% Confidence Intervals) .....</b>   | <b>211</b> |

## Tables

|  |            |
|--|------------|
| <b>Table 1 Description of Wear Modes as Described by Mckellop &amp; Campbell (1995).....</b>   | <b>11</b>  |
| <b>Table 2 Damage Categories for UHMWPE Components. Adapted from Mckellop &amp; Campbell (1995).....</b>   | <b>12</b>  |
| <b>Table 3 Mechanical properties of non-aged, accelerated aged, 5 years shelf aged and 10 years shelf aged test specimens tested using the small punch technique; taken from Edidin et al., 2000.....</b>  | <b>18</b>  |
| <b>Table 4 Mechanical properties of UHMWPE as a function of radiation dose (Pruitt., 2005) .....</b>   | <b>22</b>  |
| <b>Table 5 Mean volume change <math>\pm</math> %RSD for three repeats of four different protocols by four different users using Redlux analysis software. Green = RSD&lt;5%, Yellow = RSD = 5%-10%, Red = RSD&gt;10%.....</b>  | <b>64</b>  |
| <b>Table 6 Associated p numbers for a Tukey HSD post hoc test of inter-user variation for four users and four protocols.....</b>   | <b>66</b>  |
| <b>Table 7 Mean volume change <math>\pm</math> %RSD for all users and all protocols. ....</b>  | <b>66</b>  |
| <b>Table 8 The volume change <math>\pm</math>RSD assessed gravimetrically and geometrically (Redlux) using four different protocols for two different control liners. Protocol 3 and 4 were not performed for liner NA14 because the absence of creep and deformation meant that there were no other obvious features on the cup to exclude.....</b> | <b>67</b>  |
| <b>Table 9 Details of the acetabular liners, femoral heads, sample sizes and labelling convention of the edge loading protocol development tests .....</b>   | <b>95</b>  |
| <b>Table 10 Details of acetabular components and femoral heads in the anti-oxidant hip simulator study .....</b>   | <b>135</b> |
| <b>Table 11 List of patient/implant data recorded and description of the data .....</b>  | <b>155</b> |
| <b>Table 12 Summary details of all explants included in the study.....</b>   | <b>158</b> |
| <b>Table 13 Scoring system for assessing damage mechanisms on explant bearing surfaces and rims .....</b>  | <b>163</b> |
| <b>Table 14 Summary of damage scores for each quadrant and subdivision for all explanted liners (mean is rounded to nearest whole number) .....</b>  | <b>181</b> |
| <b>Table 15 Mean damage scores for each different mechanisms and liner subset, divided into bearing surface and rim region .....</b>   | <b>182</b> |

**Table 16 Volume changes for the non-dissociated neutral acetabular liners  
with the mean of the non-crosslinked liner  $\pm$  95% CI ..... 183**

**Table 17 Mean values of patient and explant data for each subset (the p  
number is given where there is a statistically significant difference;  
 $p < 0.05$ )..... 188**

## Abbreviations

|        |  |
|--------|--|
| AO     | Antioxidant  |
| ARD    | Anti-rotation device                                 |
| BMI    | Body Mass Index                                      |
| CI     | Confidence Interval                                  |
| CMM    | Coordinate Measuring Machine                         |
| CoCr   | Cobalt Chromium                                      |
| CoCrMo | Cobalt Chromium Molybdenum                           |
| COP    | Ceramic on UHMWPE                                    |
| ECM    | Extracellular Matrix                                 |
| EtO    | Ethylene Oxide                                       |
| F      | load applied to press the friction surfaces together |
| FTIR   | Fourier transform infrared spectroscopy              |
| g/l    | Grammes/litre  |
| GVF    | Gamma Vacuum Sterilised                              |
| h      | Film thickness                                       |
| HA     | Hydroxyapatite                                       |
| HPAO   | Hindered phenol anti-oxidant                         |
| IL-1   | Interleukin-1  |
| IL-6   | Interleukin-6  |
| kGy    | Kilogray   |
| LMBRU  | Leeds Musculoskeletal Biomedical Research Unit       |
| Mc     | Million Cycles                                       |
| MOP    | Metal on UHMWPE                                      |
| MRad   | Megarads   |

|                  |  |
|------------------|--|
| n                | Number of samples  |
| NJR              | National Joint Registry  |
| P                | Applied Load   |
| PE               | Polyethylene   |
| PGE <sub>2</sub> | Prostaglandin E2   |
| PMMA             | Polymethylmethacrylate   |
| PTFE             | Polytetrafluoroethylene  |
| R&D              | Research and development   |
| R <sub>a</sub>   | Average Surface Roughness  |
| RSD              | Relative Standard Deviation or Coefficient of Variation                |
| SEM              | Scanning Electron Microscope   |
| THA              | Total Hip Arthroplasty   |
| THR              | Total Hip Replacement  |
| TNF- $\alpha$    | Tumor necrosis factor-alpha  |
| u                | Speed  |
| UHMWPE           | Ultra-High Molecular Weight Polyethylene                               |
| v/v              | Volume per volume  |
| w/v              | Weight per volume  |
| z                | lubrication process parameter  |
| $\lambda$        | Lambda ratio: ratio of lubricating film thickness to surface roughness |
| $\mu$            | Coefficient of friction  |

## Chapter 1: Introduction

### 1.1 Introduction

People in the UK are living longer and the percentage of the population aged over 65 is increasing. Not only has the basic life expectancy at birth continued to rise, the expectation of a healthy and disability free life for longer is also increasing (Office for National Statistics, 2014). As a result of this ageing population, medical science is faced with an increasing demand to keep more people active for longer and hip replacements play a vital role in achieving this. Historically, hip replacements have generally been implanted in elderly, less active patients with limited life expectancy. However, advancements in available technology leading to hip replacements in younger patients and a more active elderly population have given rise to patients with greater expectations in terms of continued activity levels and implant lifetime. As a result, researchers and manufacturers are faced with the challenge of developing implants that are able to meet the demands of our longer living, more active population.

### 1.2 The Natural Hip

The hip is a ball and socket joint made up of the head of the femur articulating against the acetabulum of the pelvis (Figure 1-1).

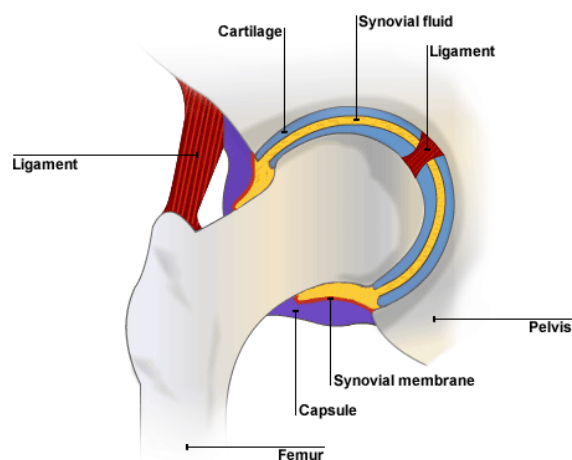


Figure 1-1 The Natural Hip (BBC, 2014)

Both the head and acetabulum are covered by a layer of cartilage that promotes the smooth articulation of the joint. A synovial membrane lines the joint to form the joint capsule and secretes synovial fluid, which acts as lubrication to the joint. Ligaments, tendons and muscles surround the joint to stabilise and control movement. The hip joint has three degrees of freedom: flexion/extension; abduction/adduction; and external/internal rotation. It must withstand forces of around four times body weight for normal everyday activities and peak loads of up to eight times body weight have been recorded in stumbling patients (Paul, 1976; Bergmann et al., 2004).

### **1.3 Osteoarthritis**

Osteoarthritis is a degenerative joint disease affecting not only the cartilage but the entire synovial joint. The initial stages of osteoarthritis are characterised by a thickening of the articular cartilage as the chondrocytes attempt to repair the tissue. However, as the disease progresses a softening and thinning of the cartilage takes place as the concentration of proteoglycans is reduced. The surface of the cartilage begins to break down and fibrillation occurs. In the later stages of osteoarthritis the cartilage can become completely worn exposing underlying eburnated bone. Cartilage does not have a blood supply, which means that once damaged it is difficult to repair. Fibrocartilage may form as part of a repair process but the mechanical properties are inferior to those of the original hyaline cartilage and it may degrade over time. Although cartilage damage is normally considered the main identifying feature of osteoarthritis, changes also occur in the bone and surrounding tissue. Sclerosis of subchondral bone, osteophyte formation, subchondral cysts and localised osteonecrosis may occur while inflammation of the synovial membrane and the joint capsule, bursitis, degradation of tendons, ligaments and muscle atrophy have all been linked to osteoarthritis (Fauci, 2006). In England, 2.46 million people are living with osteoarthritis of the hip (Arthritis Research UK, 2014) and this was the diagnosis in 91% of total hip replacements in

2014 (National Joint Registry, 2014). Other diagnoses include, rheumatoid arthritis and genetic disorders.

#### **1.4 Overview of Total Hip Replacement**

In total hip replacement the femoral head is removed and replaced by an artificial head, which articulates against an artificial cup implanted into the acetabulum. The head is attached to a stem that is fixed to the inside of the femoral shaft (Figure 1-2). Fixation of the femoral component is achieved using cement (cemented) or by adding a porous coating and press fitting into the shaft of the femur (uncemented), promoting bone growth directly on to the component. Likewise, the acetabular cup can be cemented directly into the acetabulum or it can be fixed to the acetabulum with screws, spikes or bone ingrowth.



**Figure 1-2 Total Hip Arthroplasty (Malik, 2007)**

The bearing is a ball and socket joint. Femoral heads are typically metal or ceramic and the acetabular component can be metal, ceramic or ultra-high-molecular weight polyethylene (UHMWPE).

#### **1.4.1 The National Joint Registry of England in Wales**

Total hip replacement is generally considered a successful procedure. In the 12<sup>th</sup> Annual Report (2014), The National Joint Registry for England and Wales (NJR) reported that 85.6% of patients said they were much better following a primary hip replacement. In the same report, the overall risk of revision at 11 years was reported as 5%. However, the revision rate depended on a variety of factors including the age and gender of the patient. For example, the overall risk of revision at 10 years was 8.87% for men aged under 55 year's old compared to only 3.34% in men over 75 year's old. The corresponding figures for women were 12.15% and 2.55%, respectively. This emphasises the importance of long-lasting joint replacements for the younger more active patient.

The failure and revision rate of total hip replacement is multifactorial and the complexity of the data in the National Joint Registry reflects this. The NJR annual reports present data on implant usage by bearing type, fixation (cemented, cementless, hybrid) and design as well as collecting and presenting surgeon and patient data. The clinical outcome is presented for a range of factors including, age, gender, surgeon, bearing type, fixation method and component design. Any one of these factors may influence the clinical outcome of a hip replacement and one of the primary purposes of the NJR is early identification of failure trends. In combination with laboratory research and pre-clinical testing it can be used to inform the design of implants and to help establish recommendations for patient suitability.

#### **1.4.2 Total Hip Replacement Bearings**

Total hip replacement bearings can be metal on UHMWPE (MoP), ceramic on UHMWPE (CoP), ceramic on ceramic (CoC), metal on metal (MoM) or ceramic on metal (CoM).

The National Joint Registry for England and Wales report survival rates by bearing type and fixation method for total hip replacement (National Joint Registry, 2014). For uncemented hip replacements, metal on metal hip replacements have the highest predicted failure rate at 10 years and ceramic on ceramic and ceramic

on UHMWPE have the lowest (Figure 1-3). Cemented components show similar trends.

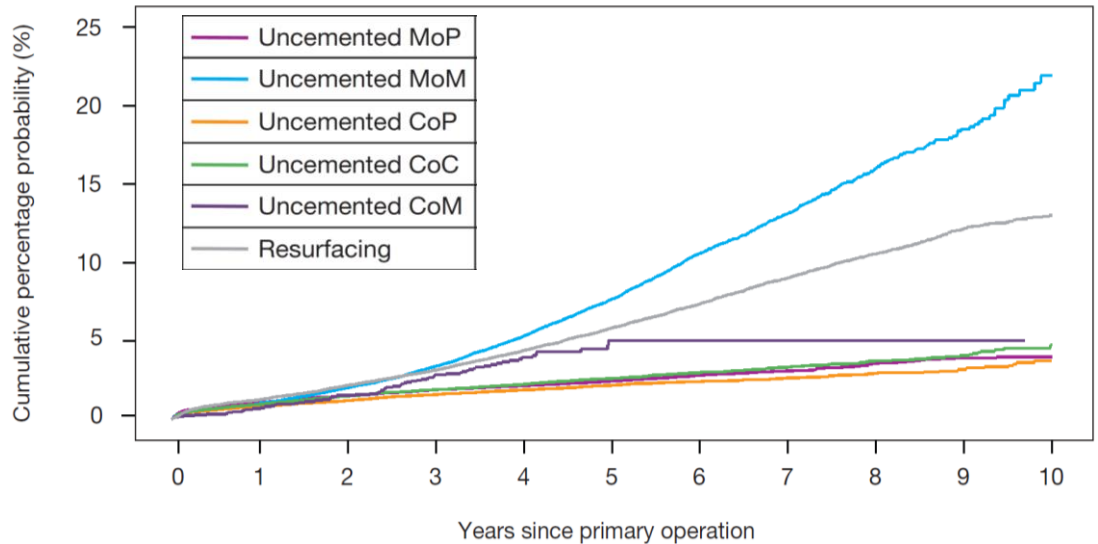


**Figure 1-3 Comparison of cumulative probability of revision (Kaplan-Meier estimates) for uncemented primary hip replacements with different bearing surfaces (National Joint Registry, 2014)**

Metal on UHMWPE is the most commonly implanted bearing combination followed by ceramic on UHMWPE (CoP). However, UHMWPE is susceptible to high wear rates. Wear debris has been implicated in the failure of these components due to osteolysis and subsequent aseptic loosening (Ingham and Fisher, 2000). Osteolysis refers to an inflammatory response that results in bone resorption and can be diagnosed by radiolucencies surrounding the total joint replacement. Studies carried out since the late 1970s have presented evidence that UHMWPE wear debris is the primary catalyst in the development of osteolysis around total joint replacements (Willert et al., 1977; Amstutz et al., 1992). Highly crosslinked UHMWPE was introduced in the 2000s to improve the wear resistance. This was achieved by exposing the material to gamma radiation, which breaks the chemical bonds and creates free radicals that recombine to form crosslinks. Post-irradiation

thermal treatments were then used to stabilise the material. Ceramic on UHMWPE bearings have been shown to wear less than metal on UHMWPE bearings, which is thought to be due to a higher resistance to scratching and damage (Derbyshire et al., 1994; Galvin et al., 2010).

Ultra high molecular weight polyethylene wear debris may be generated at non-articulating surfaces, for example between the shell and liner, known as back-side wear, or by contact of the femoral stem against the rim of the acetabular cup. However, the predominant particle found in the periprosthetic tissue of a metal on UHMWPE arthroplasty is UHMWPE, most of which is generated at the articulating surfaces (Kurtz et al., 1999). Much progress has been made since the first hip replacements to improve the wear resistance of UHMWPE bearings and to provide a relatively inexpensive and clinically reliable total hip replacement.

Ceramic on ceramic bearings have good wear resistance but can be susceptible to fracture (Barrack et al., 2004). Furthermore, mal-positioning of these components can lead to edge loading of the acetabular rim and an increase in wear (Nevelos et al., 2000). Metal on metal total hip replacements and resurfacings constitute only 0.1% of all primary hip replacements (National Joint Registry, 2014). They offer superior wear resistance but relatively high failure rates have been recorded (20% at 10 years for uncemented components) and concerns over toxicity due to the release of metal ions have been raised.

### **1.4.3 Acetabular Cup Design**

Acetabular cups can be cemented, cementless, modular or monoblock cups.

Cemented, monoblock all UHMWPE cups date back to the first prostheses in the 1960s and are still available clinically today. The UHMWPE cups are cemented directly into the acetabulum using PMMA cement. The all-UHMWPE cup can be unforgiving intra-operatively, due to the design, as it cannot be repositioned once implanted and surgical inconsistency can yield varying clinical results. Manufacturers are continually seeking design improvements to achieve better fixation, to reduce dislocation potential and to reduce wear and as a result a vast

array of design features are available clinically, not all of which have a proven track record.

Cementless cups are composed of a metal shell into which an UHMWPE, ceramic or metal liner is fixed by means of a mechanical locking mechanism. The metal shells are fixed to the acetabulum with screws, pegs or spikes or are press fit into the acetabulum. A porous and/or hydroxyapatite exterior coating achieves biological fixation of the component. Modularity of these components allows the surgeon to choose from a range of head diameters, liner materials, geometrical design features and liner offset. An additional benefit is that the liner can potentially be changed without revising other components if excessive wear occurs.

Some monoblock designs have an UHMWPE liner and porous coated metal shell that have been assembled during manufacture, usually by compression moulding of the UHMWPE. As well as limiting micromotion between shell and liner, this removes the requirement for a locking mechanism thus reducing potential areas of thin UHMWPE and high stress fields around notches. A study by Young et al. (2002) compared head penetration and incidence of osteolysis for modular and non-modular acetabular cups using radiographs. They reported lower wear rates (not significant) for the non-modular cups and a significantly lower rate of osteolysis for the non-modular cups. They attributed this to reduced micromotion between shell and liner, increased polyethylene thickness and greater shell-liner conformity.

## **1.5 Overview of Ultra-High-Molecular-Weight Polyethylene**

### **1.5.1 Structure**

Ultra-high molecular weight polyethylene remains the most commonly implanted bearing material and can reasonably be expected to perform well clinically for 10-15 years (National Joint Registry, 2014). However, beyond 10 years the survival of UHMWPE total hip replacements becomes limited by wear of the UHMWPE primarily at the articulating surface. Ultra-high molecular weight

polyethylene for orthopaedic components is made up of ethylene monomer units joined together by covalent bonds to form a linear homopolymer, an un-branched chain of identical repeated units (Figure 1-4; Kurtz 2009).

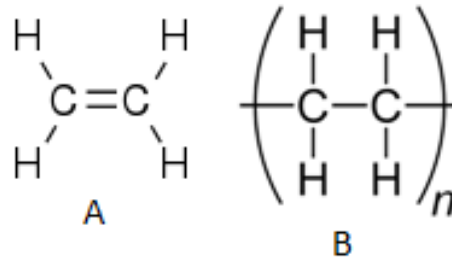


**Figure 1-4 A schematic of (A) Ethylene and (B) UHMWPE Chemical Structures (Kurtz, 2009)**

A UHMWPE chain can have between 71,000 and 214,000 repeated units equating to a molecular weight of between 2 and 6 million g mol<sup>-1</sup> (Kurtz 2009). These polymer chains rotate around the C-C bond to form chain folds and ordered crystalline lamellae. However, the extremely long length of the polymer chains hinders the formation of these crystalline regions and therefore limits the overall crystallinity of the material. The resulting structure consists of crystalline lamellae interconnected via tie molecules embedded within an amorphous matrix consisting of randomly oriented, entangled polymer chains (Figure 1-5).

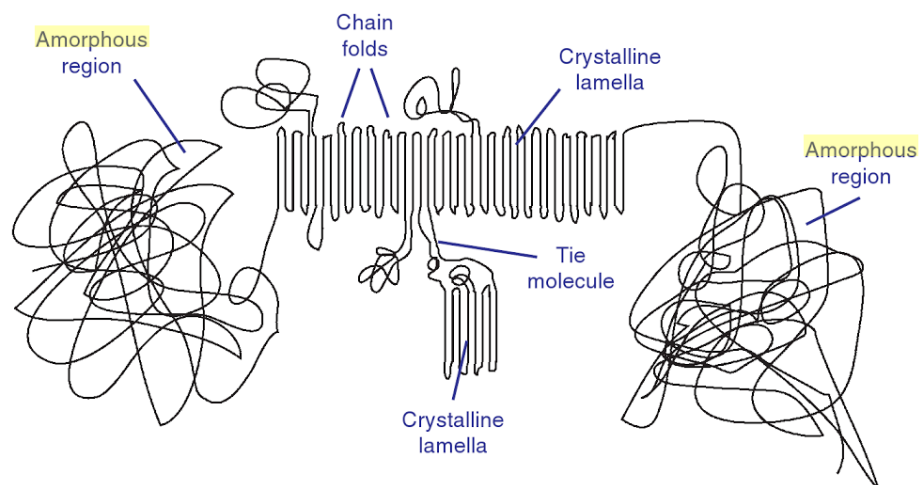


**Figure 1-5 A Schematic of the Morphology of UHMWPE. Kurtz (2009)**

In comparison to other forms of polyethylene, UHMWPE has high impact strength, tensile strength and wear resistance (Kurtz 2009). Currently there are two medical grades of UHMWPE available for implants, GUR 1050 and GUR 1020, where the main difference is the average molecular weight ( $5.5-6$  and  $3-3.5 \times 10^6$  gmol<sup>-1</sup>, respectively).

### 1.5.2 Wear of UHMWPE

Fisher (1994) identified the three main wear processes for UHMWPE: wear produced by microscopic counterface asperities; macroscopic polymer asperity wear and structural failure and wear.

Wear produced by microscopic asperities on the smooth femoral head involves the smallest scale of cyclic stress (Figure 1-6). Repeated sliding of the femoral head over the UHMWPE surface causes the polymer to deform elastically and plastically and finally results in detachment of a particle through fatigue failure. A rougher femoral head results in increased wear as fewer sliding cycles are required to detach the particle as it is subjected to greater cyclic stress.

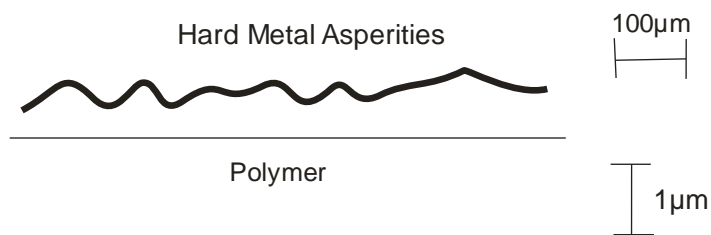


**Figure 1-6 A schematic of Wear Produced by Microscopic Counterface Asperities. Adapted from Fisher (1994)**

Unlike wear produced by microscopic counterface asperities, macroscopic polymer asperity wear assumes a polymer surface roughness that is much greater than that of the femoral counterface (Figure 1-7). On loading of the polymer the macroscopic asperities initially deform elastically. However, after some cycles the deformation becomes plastic producing local stress concentrations in the polymer

asperity. Under cyclic loading the deformation of the macroscopic polymer asperity can produce crack propagation and surface fatigue to within  $10\mu\text{m}$  of the surface under the asperity. This process is also known as micro-delamination and produces much larger UHMWPE particles due to the larger scale cyclic stresses involved. Both wear produced by microscopic counterface asperities and macroscopic polymer asperity wear occur within  $10\mu\text{m}$  of the surface.

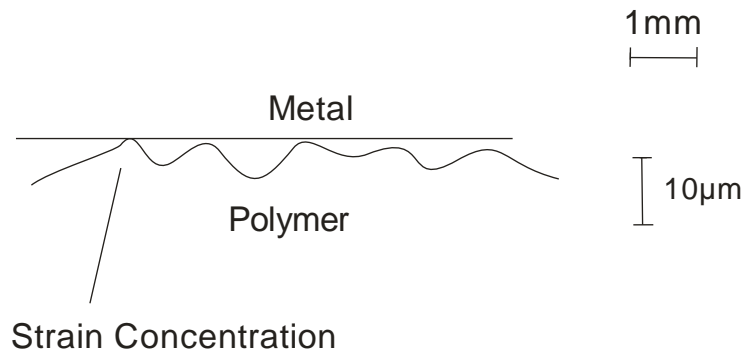


**Figure 1-7 A Schematic of Macroscopic Polymer Asperity Wear. Adapted from Fisher (1994)**

Structural failure and wear involves larger stress fields and is associated with the overall structural stress field, which is of the order 1-10mm and varies with time as the load is applied and spatially as the contact area moves over the polymer. In this wear process it is assumed the two surfaces are smooth (Figure 1-8). The stress field is determined by the geometry of the contact, the load and the elastic modulus of the materials. Under cyclic loading conditions, if the stress field exceeds the yield stress and fatigue limit of the material it can cause structural fatigue after relatively few cycles. This wear process otherwise known as delamination can produce large amounts of wear debris but is much more common in total knee replacements than total hip replacements (Mayor et al., 2003; Patten et al., 2010).

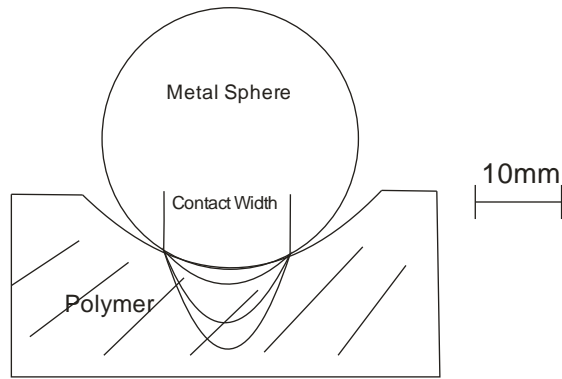


**Figure 1-8 A Schematic of Stress Fields Associated with Structural Failure.**

**Adapted from Fisher (1994)**

Mckellop & Campbell (1995) defined wear modes as the general conditions under which a joint functions in vivo (Table 1). All modes produce wear particles but modes 2,3 and 4 can produce significantly more wear because in these modes the prosthesis is not functioning in the manner intended by the designers.

**Table 1 Description of Wear Modes as Described by Mckellop & Campbell (1995)**

| <b>Mode</b>   | <b>Description</b>   | <b>Example</b>  |
|---------------|--|---|
| <b>Mode 1</b> | Two bearing surfaces moving together as intended by the designer |   |
| <b>Mode 2</b> | A bearing surface wearing against a non-bearing surface          | Wear through of femoral head to metal shell <i>and/or</i> Ball contacting with shell rim during dislocation |
| <b>Mode 3</b> | Third body particles interposed between bearing surfaces         | Bone, PMMA, metal or ceramic particles  |
| <b>Mode 4</b> | Two non-bearing surfaces moving against each other               | Neck impingement <i>and/or</i> Backside wear  |

A joint prosthesis functioning in any of these modes will be subject to one of the three fundamental wear mechanisms: adhesion, abrasion, and fatigue. Wear mechanisms are the processes that cause wear and damage to the UHMWPE. Adhesion involves bonding of two contacting surfaces under load with material being pulled away from at least one of the surfaces when enough relative motion is experienced (macroscopic polymer asperity wear). Abrasion involves asperities on a rough hard surface cutting through a smooth softer surface, resulting in material removal (microscopic counterface asperity wear). Fatigue failure occurs when local stresses exceed the fatigue strength of a material causing it to fail after a certain number of loading cycles (structural failure and wear; McKellop 2007). McKellop (2007) differentiated between wear and damage because a material can undergo substantial damage despite very little or no particle generation or wear occurring. The most commonly observed forms of wear damage have been divided into two categories, macrodamage and microdamage, and several subdivisions (Table 2).

**Table 2 Damage Categories for UHMWPE Components. Adapted from**  
Mckellop & Campbell (1995)

| <b>Macrodamage</b>   | <b>Microdamage – observed in the glossy, smooth surface</b>   |
|--|---|
| <ul style="list-style-type: none"> <li>• Smoothing or Polishing – a glossy smooth surface relative to the original machined surface</li> <li>• Scratching – a rough surface relative to the original machined surface</li> <li>• Cracks, Pits and/or Delamination</li> </ul> | <ul style="list-style-type: none"> <li>• Nodules several microns in diameter</li> <li>• Ripples – aligned rows of nodules</li> <li>• Smearred nodules – from slight surface deformation to complete obliteration of nodular structures</li> <li>• Fibrils of elongated polymer</li> <li>• Microcracks – usually located between nodules or ripples</li> <li>• Scratches – up to 10s of microns wide</li> <li>• Shreds of elongated polymer – larger than fibrils</li> <li>• Pits</li> </ul> |

Volumetric wear ( $V$ ;  $\text{mm}^3$ ) is widely thought to be proportional to applied load ( $W$ ;  $N$ ) and sliding distance ( $x$ ;  $m$ ) and is described by the Lancaster equation

(1.1), where  $K$  is the wear factor ( $\text{mm}^3/\text{Nm}$ ) and dependant on material factors relating to the sliding surfaces such as hardness, lubrication and real contact area (Lancaster, 1973).

$$V = K.W.x \quad (1.1)$$

The Lancaster equation is a simplified version of the Archard equation (Archard, 1953). Archard theorised that the wear rate for metal on UHMWPE was proportional to the load and independent of the apparent area of contact.

Several studies have challenged the idea that the wear rate is more dependent on the normal load rather than the contact area or the contact stress. In pin on plate tests, Rose et al. (1983) found that wear increased exponentially with increasing load and Rostoker and Galante (1979) reported substantial increases in wear with contact stress at contact pressures above 7MPa. However, Barbour et al. (1995) reported a decrease in wear factor with increasing contact stress in pin on plate tests. Similarly, Vassiliou and Unsworth (2004) reported a decrease in wear factor with increasing nominal stress while Mazzucco et al. (2003) reported that wear rate increased with increasing contact area but was independent of normal load in pin on disk tests for a range of contact stresses.

The wear behaviour of UHMWPE is very sensitive to the direction and mode of sliding motion. Unidirectional reciprocating motion results in the molecules becoming stretched and orientated along the direction of sliding causing strain hardening to occur and resulting in relatively low wear rates. Pooley & Tabor (1972) reported that when UHMWPE is subject to unidirectional sliding the molecules align along the direction of sliding. This results in a reduced coefficient of friction and a potential reduction in wear. Bragdon et al. (1996) found that multidirectional motion, which was representative of the natural human hip joint, resulted in the polymer surface being “redrawn and reoriented at acute angles” causing shearing of the UHMWPE into particles and producing wear. Similarly Wang et al. (1997) developed a model to describe multidirectional wear. The model separates flexion/extension and abduction/adduction into principal and secondary stress components, respectively. These authors described a strain hardening effect in the principal direction and a strain softening and weakening of the material in

the secondary direction. This strain softening led to shear rupture during multidirectional movement and hence the generation of wear particles. This phenomenon resulted in higher wear rates being observed when multidirectional wear paths were present. The above studies emphasise the importance of multidirectional motion on the wear behaviour of UHMWPE and the requirement to replicate this *in vitro* if clinically relevant wear rates are to be obtained. At this stage it is important to mention the effect of cross-linking on this wear behaviour. Cross-linking reduces the mobility of molecules and therefore reduces the strain hardening and corresponding strain softening, resulting in lower wear rates under multidirectional motion. A theoretical model developed by Wang (2001) related wear factor to coefficient of friction ( $\mu$ ), the cross-link density ( $X_c$ ) and the maximum cross shear angle  $\alpha$  for multi-directional motion in a hip joint simulator. These authors reported increasing wear rate with increasing coefficient of friction and increasing maximum cross shear angle but decreasing wear rate with increasing radiation crosslinking.

During the initial stages of functioning, a joint prosthesis will undergo a process termed 'bedding-in' whereby penetration of the femoral head into the acetabular cup is a result of both creep and wear of the UHMWPE. Creep or cold flow refers to the deformation of the material over time under the application of a stress such as body weight. The two articulating surfaces increasingly conform over the first 12-24 months, increasing the contact area and reducing contact stresses, after which a steady state of wear is reached and penetration is mainly a result of particulate debris removal or 'true wear'. Studies by Estok et al. (2005) and Glyn-Jones et al. (2008) measured the penetration of the femoral head into the acetabulum using radiographs and compared the creep and wear of conventional and cross-linked UHMWPE. Both studies reported similar creep deformation for both types of material and both studies concluded that the majority of the creep occurs during the early stages of implantation. Estok et al. (2005) reported a creep dominated phase during the first two years of implantation and Glyn-Jones et al. (2008) reported a shorter creep phase of six months, predicting that virtually all creep would have occurred after one year of implantation. A simulator study by Galvin et al. (2007) also reported a creep dominated phase of two years for cross-

linked UHMWPE for a ceramic on UHMWPE bearing and one year for a metal on UHMWPE bearing.

Measurement of wear in UHMWPE components must therefore take into account the difference between volume change due to creep and volume change due to wear during the early stages of testing or implantation and that this may change depending on material characteristics and bearing combinations.

### 1.5.3 Lubrication Regime

Metal on metal and ceramic on ceramic bearings have been shown to function in fluid film or hydrodynamic lubrication regimes, assuming bearing surfaces are smooth enough (Jin et al. 1996). In this regime the presence of a relatively thick lubricant film between surfaces prevents rubbing between bearing surfaces and therefore greatly reduces wear. However, metal and ceramic on UHMWPE bearings have been shown to function in mixed lubrication regimes (dominated by boundary lubrication; Auger et al. (1993)), whereby high polymer surface roughness and a thin lubricant film allow surface asperities to rub together producing wear.

The effect of altering lubricant viscosity, speed and applied load on the film thickness, coefficient of friction and lubrication regime are shown in Figure 1-9.

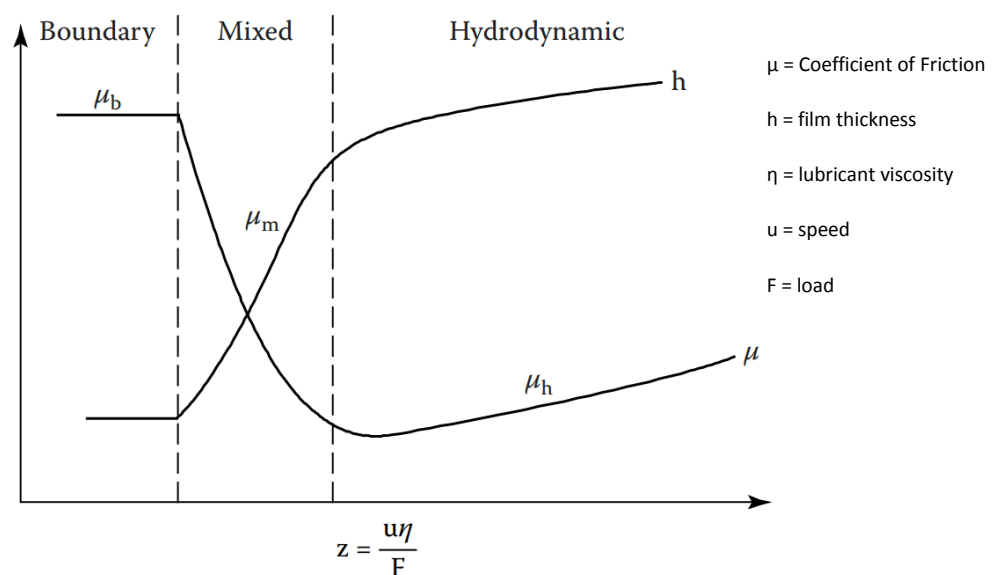


**Figure 1-9 Graph of Boundary, Mixed and and Hydrodynamic Lubrication Regimes. Adapted from Biresaw (2008)**

As it is not possible to alter the viscosity of synovial fluid or the load applied, it is therefore not possible to achieve fluid film lubrication by altering these variables for UHMWPE bearings. Jin et al. (1996) reported on the importance of surface roughness and fluid film thickness on the lubrication regime. The lambda ratio used to predict lubrication regime is given in equation (1.2):

$$\lambda = \frac{h_{\min}}{[(R_{a1})^2 + (R_{a2})^2]^{1/2}} \quad (1.2)$$

where  $R_{a1}$  and  $R_{a2}$  are the surface roughness of the femoral head and the acetabular cup, respectively, and  $h$  is the film thickness. If  $\lambda > 3$  then fluid film lubrication is expected. For  $\lambda < 1$ , boundary lubrication, whereby a significant amount of asperity contact and wear occurs, is expected. For  $1 < \lambda < 3$ , mixed lubrication occurs. Jalali-Vahid et al. (2001) found that increasing the femoral head diameter and the UHMWPE thickness and decreasing the radial clearance and the elastic modulus would increase the fluid film thickness. However, these authors reported that the film thickness achieved for all of these variables was much smaller than the surface roughness of the polymer and therefore a mixed lubrication regime would prevail. As it is unlikely that modern surface finishes could be improved significantly it is therefore necessary to reduce the wear produced by mixed lubrication by other means, such as modifying the mechanical properties of the polymer.

#### **1.5.4 Sterilisation**

Sterilisation of the UHMWPE components is an important step in obtaining long term performance and the sterilisation method chosen can influence the mechanical properties of the material. Previously, orthopaedic components were sterilised by gamma radiation in the presence of air and then packaged in air permeable packaging. Gamma irradiation results in crosslinking, which despite improving the wear resistance of the material is known to generate free radicals. Free radicals can react with oxygen in the air or *in vivo* to cause oxidative

degradation of the component. In the 1990s it was reported that these air sterilised components were undergoing oxidative degradation or shelf ageing, resulting in an increase in density and crystallinity and a decrease in ductility and toughness. Oxidative damage was observed as a white band below the surface of these implants and was responsible for fatigue damage and increased wear of the material (Premnath et al. 1996; Collier et al. 1996) Consequently, manufacturers have ceased to use this method of sterilisation and a range of other methods are used in its place.

Gamma irradiation in an inert environment in conjunction with barrier packaging removes the availability of oxygen to react with free radicals. Argon, nitrogen and vacuum conditions are used. However, in recent years concerns have been raised over the effectiveness of this packaging and oxidation again becomes a problem once the packaging has been opened. Additionally, the degree of effectiveness in terms of preventing oxidation during shelf ageing can be affected by the type of packaging used, as outlined in a survey by Costa et al. (2006) on contemporary packaging.

Ethylene oxide (EtO) sterilisation does not alter the physical structure of the UHMWPE and does not generate free radicals. Studies on oxidation levels after EtO sterilisation by Collier et al. (1996) revealed that damage modes such as rim cracking and delamination observed in components that had been gamma radiated were not observed in EtO sterilised components.

Gas plasma sterilisation is a relatively modern sterilisation technique and therefore it is too early to evaluate its performance clinically. However, it is becoming more widely accepted as a cheap and quick sterilisation method that does not generate free radicals or alter material properties but as with EtO sterilisation it does not promote cross-linking of the UHMWPE and therefore does not offer the improvement to wear resistance of gamma radiation.

### **1.5.5 Oxidation**

When UHMWPE is subjected to gamma radiation for either the purposes of sterilisation or crosslinking, the chemical bonds within the material are broken in a

process known as chain scission. This generates free radicals within the polymer. The more mobile free radicals will recombine to form crosslinks but residual free radicals that do not recombine will react with oxygen to form unstable hydroperoxides that decay causing embrittlement of the material through chain scission and recrystallization (Kurtz, 2009). This embrittlement of the material compromises wear resistance and fatigue resistance and can lead to failure of the material through fracture (Table 3).

Eddin et al. (2000) compared the surface and subsurface mechanical properties of shelf aged and naturally aged UHMWPE test specimens using the small punch technique and compared them with non-aged controls. They reported an increase in elastic modulus and a decrease in ductility, ultimate strength and toughness resulting from post-irradiation ageing that was “consistent with a progressive embrittlement process. The accelerated ageing process that they used in the study (4 weeks at 80C in an atmospheric oven) produced mechanical degradation at the surface but not the subsurface, highlighting the difficulty in replicating the natural ageing process in these materials.

**Table 3 Mechanical properties of non-aged, accelerated aged, 5 years shelf aged and 10 years shelf aged test specimens tested using the small punch technique; taken from Eddin et al., 2000**

| Shelf age when tested (yrs) | Specimen Location | Elastic Modulus (Mpa) | Initial Peak Load (N) | Ultimate Load (N) | Ultimate Displacement (mm) | Work to Failure (mJ) |
|-----------------------------|-------------------|-----------------------|-----------------------|-------------------|----------------------------|----------------------|
| 0                           | Surface           | 485 ± 85              | 64.6 ± 2.9            | 55.1 ± 2.1        | 4.11 ± 0.04                | 191 ± 8              |
| 0                           | Subsurface        | 589 ± 121             | 64.9 ± 3.1            | 60.9 ± 3.4        | 4.07 ± 0.08                | 196 ± 13             |
| A.A                         | Surface           | 1281 ± 363            | 62.5 ± 8.5            | 17.7 ± 12.1       | 2.20 ± 1.57                | 78 ± 71              |
| A.A                         | Subsurface        | 672 ± 188             | 70.3 ± 1.0            | 65.4 ± 1.8        | 4.06 ± 0.04                | 207 ± 5              |
| 5                           | Surface           | 1100 ± 129            | 72.6 ± 1.5            | 56.7 ± 6.2        | 4.13 ± 0.20                | 214 ± 17             |
| 5                           | Subsurface        | 1056 ± 134            | 69.7 ± 1.3            | 39.0 ± 3.7        | 4.11 ± 0.15                | 190 ± 5              |
| 10                          | Surface           | 1326 ± 313            | 58.1 ± 7.7            | 22.5 ± 16.9       | 2.64 ± 0.32                | 99 ± 29              |
| 10                          | Subsurface        | 1487 ± 150            | 34.7 ± 1.7            | 8.9 ± 0.0         | 1.91 ± 0.12                | 43 ± 4               |

\*A.A = accelerated aged specimens

Sutula et al. (1996) found that gamma induced oxidation from sterilisation in air had a significant correlation with component cracking and delamination and resulted in reductions in ultimate tensile strength and elongation. Oxidation of the components can occur when the implant is exposed to oxygen during shelf storage and/or during implantation.

Currier et al. (2007) reported that *in vivo* oxidation of components sterilised in barrier packaging with gamma radiation occurred via the same mechanisms as those sterilised in air and the long term results were expected to be a loss of mechanical properties leaving the components susceptible to fatigue failure with increasing time and loading cycles.

Puolakka et al. (2003) retrieved 20 gamma sterilised acetabular liners and measured the oxidation index and wear. All liners exhibited oxidation and crystallisation but the liners with a shelf life of more than 3 years exhibited significantly higher wear rates. These authors observed extensive abrasive wear on the component surface using scanning electron microscopy.

### **1.5.6 Wear Debris and Osteolysis**

During normal functioning of a UHMWPE hip replacement, UHMWPE wear debris is generated at the articulating surfaces. Macrophages are activated as the body attempts to rid itself of the foreign particles (Figure 1-10). The normal role of macrophages is to engulf and destroy micro-organisms and initiate the tissue repair process by releasing cytokines such as tumor necrosis factor-  $\alpha$  (TNF- $\alpha$ ), interleukin-1(IL-1) and interleukin-6(IL-6) and other mediators of inflammation such as prostaglandin E2 (PGE2), RANKL, collagenases and gelatinase. However, UHMWPE particles are bioinert and phagocytosis is therefore ineffective. This results in the controlled release of cytokines and the formation of giant cells. Several of the cytokines produced are known to promote the activation of osteoclasts, the key players in bone resorption, which leads to the ultimate loosening of the implant (Ingham and Fisher, 2000). Revell et al. (1997) reported a critical number of UHMWPE particles that would cause osteolysis of around  $1 \times 10^{10}$  particles/gram of

tissue. The mean number of particles per mg of wear debris for gamma sterilised acetabular cups was estimated by Tipper et al. (2000) to be  $1.3 \times 10^{10}$ .

The total volume of wear debris is not the only factor to influence the osteolytic reaction but also the concentration of particles within the critical size range ( $0.2\mu\text{m}$ - $0.8\mu\text{m}$ ) for macrophage activation. Ingram et al. (2004) reported an increase in the percentage of particles within this critical size range for crosslinked UHMWPE compared to a non-crosslinked material.

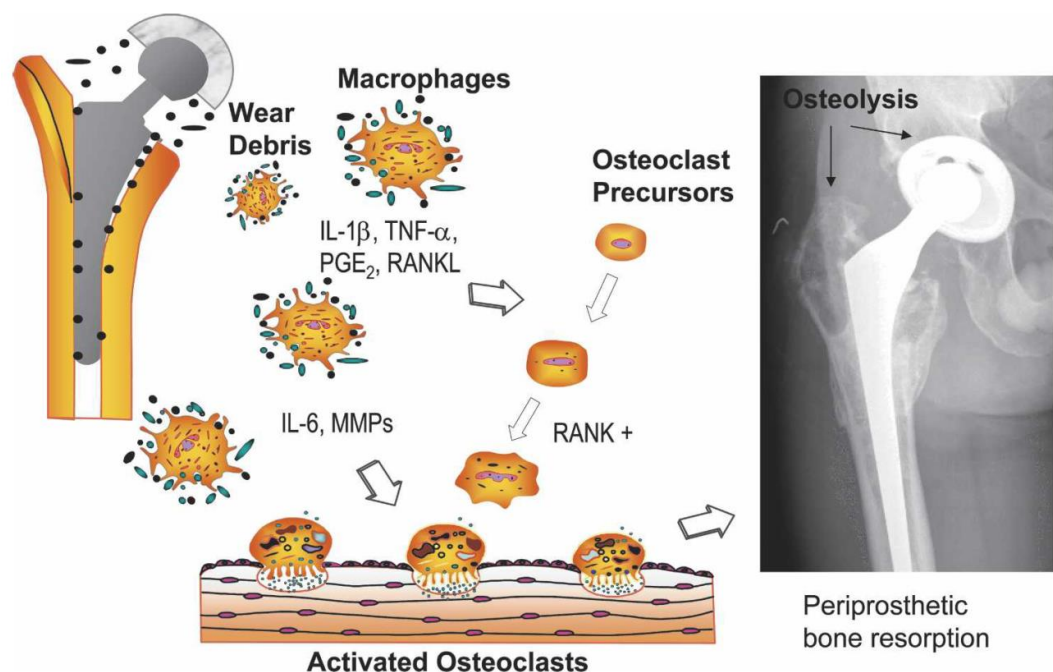


**Figure 1-10 Schematic of pathophysiology of wear debris-mediated osteolysis** (Talmo et al., 2006)

### 1.5.7 Crosslinked UHMWPE

Highly cross-linked UHMWPE (generally considered to be UHMWPE that has been exposed to radiation doses of 5Mrad and above and then stabilised with thermal treatments) was introduced clinically for total hip replacement in 1998 to improve the wear resistance of the polymer. Since then it has been widely used in the United States and is being used increasingly in the UK, with all major manufacturers offering a proprietary version of the material. The advantages of crosslinked UHMWPE over low wearing hard on hard bearings include a reduced

surgeon learning curve in terms of implantation technique and a forgiving nature with respect to surgeon variations at implantation.

When UHMWPE is exposed to ionising radiation the C-C and C-H bonds are cleaved in a process known as chain scission. Free radicals are generated in this process and two free radicals may then go on to combine forming cross-links (Figure 1-11). Crosslinking is detrimental to the mechanical properties such as strength, ductility, toughness, elastic modulus and fatigue crack propagation resistance (Pruitt, 2005).

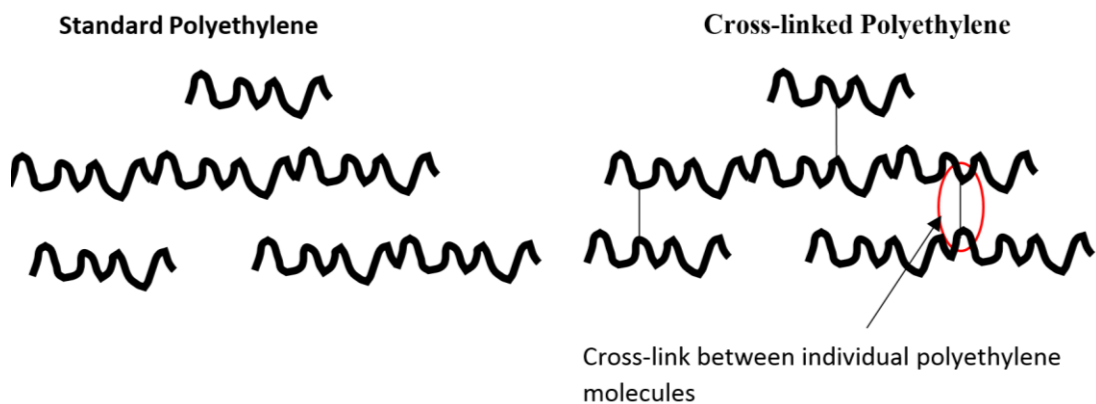


**Figure 1-11 Molecular structure of conventional UHMWPE and cross-linked UHMWPE (Adapted from DePuy Orthopaedics Inc., 2009)**

As discussed previously (section 1.5.5), the crosslinks between the polymer chains prevent slippage and make the UHMWPE more resistant to surface orientation, which in turn reduces the wear debris generation that occurs when conventional UHMWPE is subjected to cross shear during multidirectional movement (Bragdon et al., 1996).

Most of the free radicals that are produced during the crosslinking process are not mobile enough to recombine and these residual free radicals pose an oxidation risk to the material as they can go on to react with oxygen in the environment. To avoid oxidation of the polymer, the radiation dose and post-irradiation thermal treatment must be carefully selected. Increasing the radiation dose will increase the cross-link density up to a dose of around 10Mrad, after which the cross-linking begins to saturate (Muratoglu et al., 1999). Increasing the radiation dose up to this threshold will increase the wear resistance but conversely

results in reducing mechanical properties and increasing free radicals. A post-irradiation thermal treatment is required to quench these free radicals and eliminate the oxidation risk of the material. This can be done by heating the polymer to above its melting temperature, known as re-melting, or heating the polymer to below the melting temperature, known as annealing. Post-irradiation re-melting reduces the crystallinity of the material allowing the free radicals to mobilise and recombine but has an adverse effect on the strength of the material. Annealing in contrast allows the microstructure to be maintained but is less efficient at eliminating free radicals. Achieving a cross-linked UHMWPE that will provide implant longevity requires a balance to be achieved between the wear resistance, mechanical properties, free radicals and crystallinity of the material.

Pruitt (2005) conducted a review of the mechanical properties of conventional and highly crosslinked UHMWPE. The properties as a function of radiation dose are provided in Table 4. They reported that the improved resistance to plastic deformation and corresponding improvement in wear was offset by reductions in ultimate tensile stress, ductility, modulus, toughness and crack propagation resistance.

**Table 4 Mechanical properties of UHMWPE as a function of radiation dose**  
(Pruitt., 2005)

| Property   | GUR 1050   | 25kGy     | 50kGy      | 100kGy           | 200kGy           |
|--|------------|-----------|------------|------------------|------------------|
| Crystallinity (%)  | 50.7±0.5   | 45.4±0.7  | 46.2±0.7   | 46.9±0.8         | 47.7±0.4         |
| Yield Stress (MPa)   | 20.2±1.0   | 19.0±0.4  | 19.9±0.8   | 19.8±0.7         | 21.2±1.0         |
| Modulus (Mpa)  | 495±56     | 433±14    | 412±50     | 386±23           | 266±30           |
| True Stress at Break (MPa)   | 315.5±31.6 | 284.8±18  | 237.6±12.3 | 185.7±7.5        | 126.0±14         |
| True strain at Break   | 1.82±0.01  | 1.74±0.03 | 1.59±0.01  | 1.50±0.02        | 1.37±0.06        |
| Fracture Toughness (J <sub>IC</sub> /kJ/m <sup>2</sup> )               | 2.1        | 23.8      | 76.2       | =J <sub>SS</sub> | =J <sub>SS</sub> |
| Steady State Fracture Toughness (J <sub>SS</sub> , kJ/m <sup>2</sup> ) | 116.9±0.1  | 101.2±0.1 | 98.5±0.2   | 87.6±0.01        | 79.3±1.9         |

Several in vitro studies have been performed on the wear resistance of cross-linked UHMWPE (McKellop et al., 1999; Ries et al., 2001; Endo et al., 2002; Galvin et al., 2010). The results have demonstrated a remarkable decrease in wear when compared to conventional UHMWPE and these findings are beginning to be corroborated by clinical experience (Martell et al. 2003; Dorr et al. 2005; Calvert et al. 2009; Engh et al. 2012; García-Rey et al. 2012; Glyn-Jones et al. 2015).

McKellop et al. (1999) studied the wear of cross-linked UHMWPE cups for a range of radiation doses. These authors found that the wear rate decreased markedly for increasing radiation dose and that wear rates for gamma radiation doses above 200kGy were extremely low with machining marks still observable in the main contact zone. However, in practice the trade off in mechanical properties for radiation doses of 200kGy would be undesirable and a compromise between wear and material properties is essential. The wear rates in the McKellop study at more clinically relevant radiation doses were  $9.3 \pm 0.9 \text{mm}^3/\text{yr}$  and  $2.2 \pm 0.2 \text{mm}^3/\text{yr}$  (for 4.5Mrad and 9.5Mrad, respectively). Galvin et al. (2007) reported significantly lower wear rates for UHMWPE materials crosslinked at 7.5Mrad and 10Mrad and then re-melted, compared to a control material subjected to a radiation dose of 2.5Mrad in air (conventional UHMWPE). The steady state wear rate for the highly crosslinked material (10Mrad) was  $4.6 \text{mm}^3/\text{million cycles}$  compared to over  $40 \text{mm}^3/\text{million cycles}$  for the conventional UHMWPE.

Ries et al. (2001) reported the gravimetric wear rates from hip simulator testing of ethylene oxide sterilised UHMWPE, gamma inert sterilised UHMWPE and two crosslinked UHMWPEs subjected to clinically relevant radiation doses (5Mrad and 10Mrad) and aged. Both crosslinked materials were lower wearing than the non-crosslinked materials. These authors reported negative wear rates for the 10Mrad crosslinked UHMWPE. However, they noted that fluid absorption of the UHMWPE material would make it difficult to correctly measure very low wear rates gravimetrically. Furthermore, these tests were run using 100% bovine serum rather than the 25% bovine recommended by ISO standards for hip simulator testing. Additionally, these tests were run with the bulk fluid at 37°C. Studies have shown that the temperature at the bearing is significant higher than 37°C and that increased protein precipitation may occur at these higher temperatures (Lu and

McKellop, 1997). Protein concentration and precipitation influence the wear of UHMWPE and may explain the negligible wear reported in the above study (Wang et al., 1998; Liao et al., 1999). Zero wear has not been observed clinically for these materials.

Medium term clinical results for highly crosslinked materials have now been reported. As part of a prospective, randomised study, Engh et al. (2012) carried out a 10 year follow up of highly crosslinked acetabular cups (5Mrad and heat treated) and non-crosslinked cups of the same design (DePuy Duraloc® cups). They reported an 83% reduction in the wear rate of the crosslinked cup compared to the non-crosslinked cup (0.04mm/yr and 0.22mm/yr, respectively) and this corresponded with a clinically significant reduction in incidences of osteolysis for the crosslinked group.

Similarly, Garcia-Rey et al. (2012) reported the results of the mean yearly linear penetration rates measured on radiographs of a highly crosslinked UHMWPE and a nitrogen sterilised UHMWPE at 10 to 12 year follow up and reported significantly lower rates for a highly crosslinked UHMWPE compared to a non-crosslinked UHMWPE (a 64% reduction; 0.08mm/yr and 0.16mm/yr respectively).

In a study by Babovic & Trousdale (2013) of 50 patients younger than 50 at the time of primary surgery, the authors reported 100% survivorship and a very low head penetration rate of 0.02mm/yr at 10 year follow up. They suggested that the younger patients in the study would be more active and therefore place higher demand in terms of wear on the materials and concluded that the crosslinked material had excellent long-term potential.

The above studies all included creep and wear in the calculation of linear penetration rate. Creep in UHMWPE is known to vary depending on the type of UHMWPE and the material properties such as percentage crystallinity, which depends on factors such as radiation dose, thermal processing and oxidative degradation. Wear debris is linked to osteolysis and it is therefore important to distinguish wear from creep, which cannot be assumed to be the same for all UHMWPE materials. The majority of creep has been shown to occur within the first 6 months to 2 years of implantation.

Glyn-Jones et al. (2015) reported the volumetric wear between 1 and 10 years, excluding the first year of implantation, in a study of a crosslinked UHMWPE and a non-crosslinked UHMWPE of the same design. These authors observed lower wear volumes for the crosslinked liners (98mm<sup>3</sup> and 14 mm<sup>3</sup>, respectively). All of the above studies are limited by the measurement of wear and penetration using radiographs, which can be subject to error due to patient positioning, poor quality images and observer variation, rather than direct wear measurement on an explanted liner. Furthermore, backside wear is not measurable using radiographs but may be a source of wear debris.

A variety of factors can affect the wear rates of UHMWPE acetabular cups, such as component design, radiation dose, thermal processing, material degradation, adverse loading, all of which should be taken into consideration when interpreting results. However, the medium term performance of crosslinked UHMWPE in terms of wear is promising. Furthermore, while many studies have reported lower wear rates for crosslinked UHMWPE than non-crosslinked UHMWPE, there is currently limited evidence that this will equate to improved clinical outcomes in the long term.

Despite the promising results in terms of the wear resistance of cross-linked UHMWPE, concerns remain about the effect of the alteration to mechanical properties on the clinical performance of the polymer. Baker et al. (2002) carried out a study on the degree of cross-linking and its effect on the fatigue crack initiation and propagation resistance. These authors found that although cross-linking can be beneficial in preventing the initiation of flaws within the material, the resistance to crack propagation is reduced as a result of the decrease in plasticity at the crack tip. Crack propagation resistance is important if we are to assume the worst case scenario that clinically available components will contain some flaws or defects capable of propagating when subjected to cyclic loading. These authors concluded that a lower degree of crosslinking is optimal when designing for both wear resistance and fatigue crack propagation resistance. In a separate study by Bradford et al. (2004) of 21 retrieved acetabular cups, all explants exhibited surface cracking, abrasions, pitting and scratching after only 10 months of implantation. This is in contrast to in vitro studies of cross-linked

UHMWPE cups that still display machining marks after simulation of long-term implantation. This may be because the less ductile material does not permit cold flow or creep of the polymer at the articulating surface.

The choice of post-irradiation thermal treatment may also play a role in the survivorship of cross-linked UHMWPE. It is widely believed that irradiated and annealed UHMWPE is at risk of *in vivo* oxidation as a result of residual free radicals.

Wannomae et al. (2006) reported increased crystallinity and unprecedented levels of *in vivo* oxidation of irradiated and annealed components after 3 years of implantation. These authors reported embrittlement and subsurface white bands comparable with those observed in traditional UHMWPE components sterilised in air. Furthermore these findings were compared to components that were irradiated and melted to remove all free radicals. No oxidation was observed and no change in crystallinity occurred *in vivo* for the re-melted components.

Similarly, Currier et al. (2007) reported that a series of retrieved Crossfire® (annealed) liners had oxidised to a measurable degree and were susceptible to fatigue damage after only 3 years.

Kurtz et al. (2006) analysed traditional gamma air sterilised liners, conventional gamma inert sterilised liners and annealed highly cross-linked liners for *in vivo* degradation. These authors found that all three groups of liners had undergone *in vivo* degradation. However, they also found that the most severe oxidation occurs at areas experiencing the lowest amount of wear such as the liner rim. This was most likely to be due to the bearing itself being protected against exposure to oxidising bodily fluids. Consequently, the authors were able to conclude that in the absence of impingement and providing that the locking mechanism was not exposed to large volumes of oxidising fluid, *in vivo* degradation of annealed highly cross-linked UHMWPE was not clinically relevant during the first 5 years of implantation and can be considered a long-term failure mode.

Irradiated and re-melted UHMWPE is a solution to the problem of *in vivo* oxidation as free radicals are completely quenched during the re-melting process. However, as mentioned previously this presents another problem as it decreases the crystallinity of the material.

Atwood et al., (2011) reviewed the clinical trade-offs between fatigue, wear and oxidation of highly crosslinked and thermally processed materials. They devised a schematic that effectively showed the relationship between these properties for untreated controls, a moderately crosslinked and re-melted UHMWPE, a highly crosslinked and re-melted UHMWPE and a highly crosslinked and annealed UHMWPE (Figure 1-12). The untreated controls show good oxidation and fatigue crack propagation resistance but poor wear resistance. The moderately crosslinked and re-melted UHMWPE showed good oxidation resistance but moderate fatigue crack propagation and wear resistance. The highly crosslinked re-melted UHMWPE showed good oxidation resistance and wear resistance but poor fatigue crack propagation resistance. Finally, the highly cross linked and annealed UHMWPE showed good wear resistance and fatigue crack propagation resistance but poor oxidation resistance.

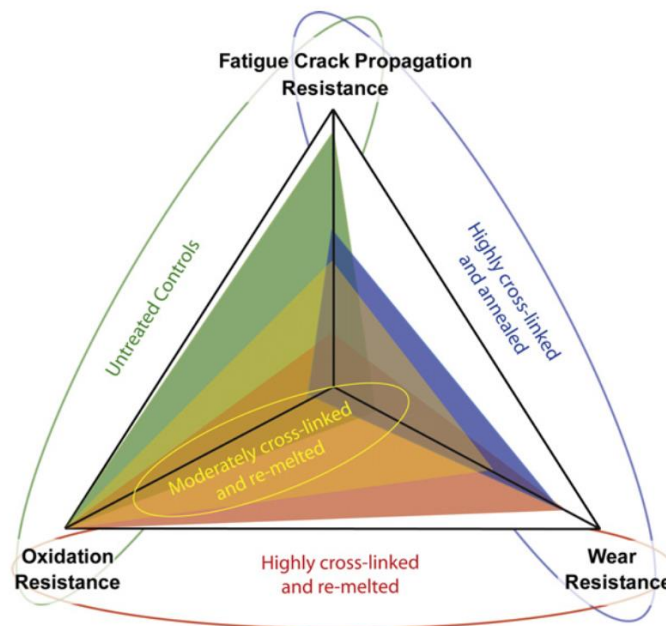


**Figure 1-12 Schematic to outline the trade-offs in wear resistance, fatigue crack propagation resistance and oxidation resistance developed by Atwood et al., (2011)**

The inconclusive nature of the evidence surrounding the best post-irradiation thermal treatment led to a search for alternative methods to stabilise UHMWPE.

### **1.5.8 Additive Stabilised UHMWPE**

More recently, antioxidants such as vitamin E ( $\alpha$ -tocopherol) have been added to crosslinked UHMWPE in order to stabilise residual free radicals and improve the materials resistance to oxidation. This eliminated the requirement for post-irradiation thermal treatments of varying effectiveness or that are detrimental to the mechanical properties of the material.

Vitamin E is a biocompatible free radical scavenger and can therefore replace post-irradiation re-melting without the associated loss of crystallinity and reduced fatigue strength. Initial studies on vitamin E have been promising but long term clinical performance is yet to be determined. Oral et al. (2006) reported comparable wear performance for vitamin E stabilised UHMWPE acetabular liners when compared to highly crosslinked and re-melted UHMWPE in hip simulator tests. These authors also reported higher strength and fatigue crack propagation resistance of the material, which they attributed to the higher crystallinity of the base material.

Grupp et al. (2014) evaluated the wear performance of Vitamin-E stabilised UHMWPE acetabular liners after prolonged ageing in hip simulator tests and compared it with standard and highly crosslinked re-melted UHMWPE. The standard UHMWPE began to oxidise after two weeks of accelerated ageing, the crosslinked UHMWPE after 5 weeks and the Vitamin-E stabilised UHMWPE was oxidation resistant after 6 weeks of accelerated ageing. Wear correlated with oxidation in this study.

Other antioxidants have been investigated for use as free radical scavengers in UHMWPE such as nitroxide tempo, anthocyanin extracts and hindered phenol antioxidants.

Ultra-high-molecular weight polyethylene stabilised with hindered phenol antioxidants (HPAOs) has been less widely studied than Vitamin E stabilised UHMWPE. However, some evidence of its efficacy exists. Narayan et al. (2009) carried out pin on disk tests of hindered phenol doped UHMWPE. They observed inferior wear rates for three different formulations of hindered phenols when compared to a moderately crosslinked and re-melted control sample for a given

radiation dose but observed a decrease in wear rates with decreasing antioxidant loading and increased radiation dose. It was suggested that the higher loading of HPAO interfered with the crosslinking process resulting in higher wear. The authors suggested that the wear behaviour of HPAO doped UHMWPE was a complex interdependent relationship between formulation, antioxidant loading and radiation dose and that appropriate optimization would achieve a material that matched the performance of current UHMWPE with added oxidative stability. However, this study does not demonstrate superior wear performance of the material over other highly crosslinked UHMWPEs.

King et al. (2009) compared the mechanical properties and oxidation resistance of HPAO doped UHMWPE (75kGy radiation dose), a conventional UHMWPE (radiation dose 40kGy) and a highly crosslinked and re-melted UHMWPE (50kGy). The HPAO stabilised UHMWPE showed better oxidation resistance compared to the conventional UHMWPE and was similar to that of the re-melted UHMWPE (Oxidation Index; 0.000, 0.045, 0.506 for the HPAO, re-melted and conventional UHMWPE, respectively). However, the mechanical properties were superior to those of the re-melted material. The strength (UTS; 40.1Mpa and 46.1Mpa for the re-melted and HPAO materials, respectively) and crack propagation resistance ( $\Delta K_{incept}$ ; 1.57Mpa $\sqrt{m}$  and 1.88Mpa $\sqrt{m}$  for the re-melted and HPAO materials, respectively) were improved in the HPAO material. The wear rates in pin on disk tests for the re-melted and HPAO materials were comparable and decreased in comparison to the conventional UHMWPE, suggesting that the material provides good wear resistance, improved tensile strength and fatigue crack propagation resistance and oxidation resistance. Narayan et al. (2010) carried out a follow up study and reported that HPAO stabilised UHMWPE continued to exhibit good oxidation resistance after 40 days of accelerated ageing.

Despite these promising results, HPAO1 (hindered phenol 3,5-di-tert-butyl-4-hydroxyhydrocinnamate) was reported to be cytotoxic to certain cells in a study by Bladen et al. (2013) and these authors cautioned the use of hindered phenols as stabilisers for UHMWPE.

## 1.6 Clinical Aspects of Total Hip Replacement

### 1.6.1 Edge Loading

Edge loading occurs when there is microseparation of the femoral head and the acetabular cup during the swing phase of gait. The head then contacts with the rim of the cup on heel strike before relocating to the articulating surface on the stance phase (Figure 1-13).

Edge loading can result from rotational and/or translational mal-positioning of the cup. Rotational malposition refers to excessive inclination of the acetabular cup resulting in the contact area approaching the acetabular rim and translational malposition refers to a mismatch in the centres of rotation of the femoral head and acetabular cup. Translational malposition can be caused by medialisation of the cup, lever out of the head due to femoral neck impingement, head offset deficiency, stem subsidence or joint laxity (Jennings et al. 2012).

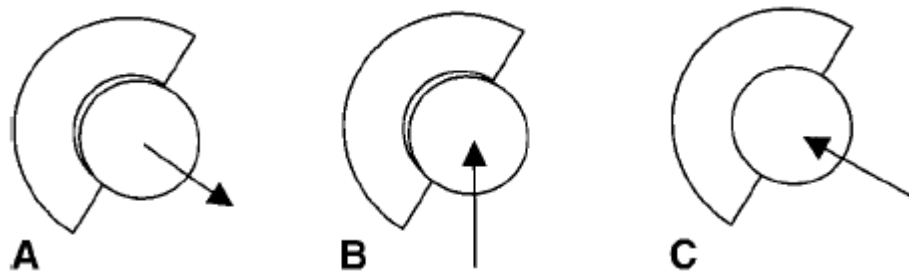


**Figure 1-13 Schematic of Edge Loading (A) Head and Cup Separation (B) Rim Contact (C) Relocation** (Nevelos et al., 2000)

Fluoroscopy studies have been carried out to determine the prevalence of edge loading in total hip replacements. Lombardi et al. (2000) used fluoroscopy to study the extent of microseparation during adduction/abduction manoeuvres and normal walking gait for 10 metal on UHMWPE total hip replacements. These authors found that microseparation was present in all 10 THR studied with an average of 1.2mm & 2.4mm separation for adduction/abduction leg lifts and walking gait respectively. In a separate study by Dennis et al. (2001), an average femoral head separation of 3.3mm was observed in all of 10 total hip

replacements. Similarly, Komistek et al. (2002) observed a medial sliding of the femoral head during the swing phase of gait. The average sliding distance was 2mm.

### **1.6.2 Cup Positioning**

Incorrect cup placement is associated with restricted range of motion, rim damage through edge loading, impingement, dislocation and high contact stresses potentially leading to increased UHMWPE wear. At the time of implantation the surgeon can control cup inclination and anteversion as well as its depth in the acetabulum. Factors such as femoral anteversion and femoral offset play a role in restricting range of motion because of impingement and correct cup placement is critical.

Several authors have carried out studies to determine recommendations for optimal cup positioning. Lewinnek et al. (1978) recommended a safe range of  $40^{\circ} \pm 10^{\circ}$  abduction and  $15^{\circ} \pm 10^{\circ}$  anteversion. This was considered a realistic range to allow a reasonable surgical envelope while permitting an adequate range of motion without impinging. Outside this range these authors found a significant increase in dislocation rate. D'Lima et al. (2000) used three dimensional computer aided design to investigate the effect of acetabular and femoral orientation on range of motion before cup/liner impingement for varying head/neck ratios. These authors found that for a given head/neck ratio a complex interaction of acetabular abduction and anteversion and femoral anteversion is required for optimal range of motion, concluding that overall, with the correct acetabular and femoral anteversion, abduction angles of between  $45^{\circ}$  and  $55^{\circ}$  permitted the maximum range of motion and stability without impingement.

This 'safe range' has been widely adopted clinically. This has been largely driven by the prevalence of dislocation as a reason for revision (third most likely cause of revision in 2014; NJR 2014). While steeper inclination angles, such as those suggested by D'Lima, are desirable in terms of impingement free range of motion,

high cup inclination angles have been associated with higher risk of edge loading and greater wear.

Hua et al. (2014) developed a finite element model to predict the contact mechanics of metal on UHMWPE acetabular cups for varying cup inclination angles and microseparation distances. These authors showed that, as the cup inclination angle increased, the microseparation distance required to create edge loading decreased. Microseparation distances of 2mm resulted in high stresses that were centralised on the rim of the cup and plastic strain was shown to increase with increasing microseparation.

Patil et al. (2003) carried out a study using finite element analysis, simulator tests and explant analysis to determine the effect of cup abduction angle on UHMWPE wear. These authors reported a significant association between UHMWPE wear and cup abduction in all three elements of their study. In the clinical element of the study these authors observed a 40% increase in linear wear for cups with abduction angles of  $\geq 45^\circ$ .

Similarly, excessive lateralisation of the cup has been associated with impingement (Malik 2007) but excessive medialisation may result in edge loading of the rim.

### **1.6.3 Pre-clinical Hip Simulator Testing**

Currently, international ISO standards outline loading and displacement recommendations for a standard walking cycle (BS ISO 14242:2002). The standard recommends the following load and motion parameters for physiological hip simulators with three axes of rotation: a twin peak time dependant loading cycle with a maximum load of 3kN and a minimum load of 300N, an abduction/adduction angle of  $+7^\circ$  to  $-4^\circ$ , a flexion/extension angle of  $+25^\circ$  to  $-18^\circ$  and an internal/external rotation angle of  $\pm 10^\circ$  (Figure 1-14). The complexities of a simulator with three axes of rotation, particularly 15 to 20 years ago when simulators were less advanced, was addressed by Barbour et al. (1999). These authors developed simplified load and motion input cycles using one load vector and two motion vectors (flexion/extension and internal/external rotation;

excluding abduction/adduction) by applying the motions 90° out of phase to generate an open elliptical wear track replicating physiological wear paths and rates. They compared the three axis physiological wear paths with that of the simplified two axis paths and similarities were reported. Ali et al. (2016) recently compared the wear rates of metal on UHMWPE bearings on a three axis of rotation hip simulator and a two axis of rotation hip simulator (using the simplified input profiles) and reported no significant difference in the wear rates between the two simulators.

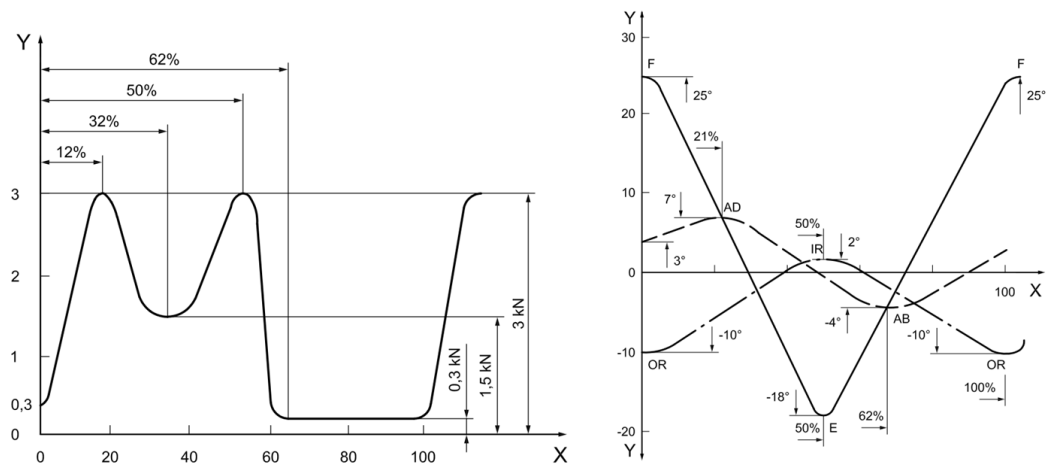


**Figure 1-14 Load (right) and motion (left) parameters described in ISO 1424-1 (2014) where AB = Abduction, AD = Adduction, E = Extension, F = Flexion, IR = Inward rotation and OR = Outward rotation (BS ISO 14242-1:2014)**

ISO standards do not currently recommend input parameters for hip simulator testing of edge loading conditions. Microseparation and edge loading caused by a mismatch in the centres of rotation of the femoral head and acetabular cup due to rotational and/or translational malposition has been observed in vivo and therefore the requirement for more robust and clinically relevant pre-clinical testing conditions has been identified.

Nevelos et al. (2000) first replicated clinically relevant stripe wear patterns observed on retrieved ceramic on ceramic bearings by applying a mediolateral displacement of the femoral during the swing phase of gait. Stewart et al. (2001) tested ceramic on ceramic bearings under mild and severe microseparation and edge loading conditions in hip simulator tests and found that wear rates were

increased during microseparation compared to standard walking cycles and these replicated clinically relevant wear rates and patterns. Manaka et al. (2004) replicated the work of Stewart et al., obtaining wear rates that were consistent with those obtained in the mild and severe separation modes of Stewart's group, demonstrating "good interlaboratory validation and credibility". These authors compared the stripe wear observed on the simulator samples with retrieved femoral heads. The reported narrower wear scars on the retrievals, attributing this to the more varied load and motions experienced *in vivo* when carrying out common activities such as stair climbing and rising from a chair. Leslie et al. (2009) tested metal on metal hip surface replacements in simulator tests and reported that wear rates increased 9-fold under a high cup inclination angle and 17-fold when a high cup inclination angle and microseparation were combined. More recently, Al-Hajjar et al. (2010) reported increased wear rates under microseparation conditions for ceramic on ceramic bearings but no significant difference in wear rates was observed between inclination angles of 55° and 65° for either standard or microseparation conditions. The same authors also showed that wear rates were greater for 36mm diameter ceramic on ceramic bearings than 28mm diameter bearings for dynamic microseparation and edge loading conditions but not standard conditions (Al-Hajjar et al. 2013), highlighting the importance of testing under more adverse conditions. It was also reported in a later study by these authors that increased translational mismatch between the centres of rotation of the head and the cup (translational malposition) and increased cup inclination angle (rotational malposition) would result in an increase in the magnitude of dynamic microseparation and wear in ceramic on ceramic bearings (Al-Hajjar et al. 2015). In contrast, a study by Williams et al. 2003 reported reduced wear rates in ceramic on UHMWPE bearings under edge loading conditions. However, the degree of microseparation studied by these authors was small in comparison to microseparation observed clinically (Komistek et al., 2002) and a deformation was observed on the rims of these cups that raised concerns over the fatigue performance of these cups under edge loading, particularly where material degradation exists. Similarly, Clarke et al. (2005) tested UHMWPE acetabular cups of a range of crosslinking levels in a hip simulator under standard conditions and

two different microseparation protocols. They reported higher wear rates under standard conditions compared to both microseparation protocols (up to 60% lower) regardless of crosslinking. The authors suggested the reduction in contact time was responsible for the reduction in wear.

These studies highlight the advances made in this field in recent years. It is now better understood that a mismatch in the centres of rotation of the head and cup due to translational malposition (a medial translation of the acetabular cup) and rotational malposition (excessive inclination and/or version of the acetabular component) may lead to dynamic microseparation and edge loading. Furthermore, these advances in understanding have been the driver to introducing adverse loading conditions into ISO standards. Jennings et al. (2012) have presented a Stratified Approach For Enhanced Reliability (SAFER) for pre-clinical simulator testing that describes a wider range of clinical conditions including surgical delivery, variations in kinematics, variations in the patient population and degradation of the biomaterial properties.

Current ISO standards do not describe testing conditions for components that have undergone material degradation during implantation. To replicate oxidative degradation during service, ASTM standard F2003-02 describes a process for the accelerated ageing of UHMWPE. This allows the mechanical and chemical stability of components to be evaluated without waiting long periods of time for the material to degrade naturally. Currier et al. (1998), reported cracking and delamination of knee components sterilised in air and then accelerated aged in simulations of fatigue loading. This damage was not observed in non-sterilised controls, highlighting the role of subsurface oxidation in these failure modes. Similarly, Oral et al. (2016) found that *in vitro* ageing of UHMWPE had detrimental effects on the mechanical properties of the material where even a small amount of oxidation existed. These studies emphasise the need to include an ageing element into hip simulator studies to determine the wear and fatigue performance of components. While accelerated ageing methods have been widely used to test the effect of oxidative degradation, comparisons between accelerated ageing and natural ageing are less widely reported and those that do exist highlight important differences between the two types of ageing. Edidin et al. (2000) compared the

mechanical behaviour of naturally and accelerated aged tibial inserts using the small punch test. The accelerated ageing process produced embrittlement of the surface area consistent with natural ageing for 10 years but embrittlement of the subsurface region was not replicated. In addition, a study by Saikko (2014) observed fracture and delamination of gamma-air-sterilised, shelf aged components on knee simulators after only a few hours of testing but equivalent components that were subjected to accelerated ageing showed only moderate adhesive wear after 8 weeks. These authors suggested that “established accelerated ageing methods may result in an underestimation of the oxidative damage”.

Despite limitations in the methods, testing of UHMWPE total joint components after accelerated aging has been shown to be an important aspect of pre-clinical testing of these components.

#### **1.6.4 Modular Design Considerations**

Cementless modular acetabular cups were originally introduced to prevent cement disease and to allow greater component flexibility for the surgeon. However, certain factors relating to modular designs have proven to be of concern.

Motion between shell and liner can lead to backside wear of the UHMWPE liner creating a further source of UHMWPE debris in addition to that produced at the articulating surfaces. The UHMWPE particles generated can migrate to the acetabulum leading to periacetabular osteolysis. Fehrig et al. (1999) studied the prevalence of shell/liner motion in modular cups from eight different manufacturers. These authors found evidence of motion in all designs and concluded that the extent of motion was greater where sharp anti-rotation devices that dig into the UHMWPE were used, rather than multiple protruding anti-rotation tabs or serrations in the internal rim. In a similar study by Lieberman et al. (1996) evidence of micromotion between shell and liner was found in cups from five different manufacturers. These studies did not quantify the degree of backside wear, nor did they attempt to relate the degree of micromotion to duration of implantation. However, a reasonable hypothesis would be that an increase in micromotion would increase backside wear and a locking mechanism undergoing

repetitive loading would deteriorate over time allowing micromotion to increase. These authors also found evidence to suggest that polishing the inner surface of the shell would reduce backside wear but noted that this was dependant on other design factors such as an effective locking mechanism. Kurtz et al. (1998) reported that shell/liner conformity facilitates the load transfer between liner and shell. A non-conforming liner will be supported at the rim until the liner is sufficiently deformed during loading to reduce micromotion and to distribute the load between the shell and liner. However, until a load transfer path is established, the liner is vulnerable to fatigue damage. For modular components shell/liner non-conformity can result from radial clearances, which are required to ensure ease of insertion of the liner, or manufacturing tolerances (Young et al., 2002) . Screw holes in the shell create large areas of unsupported UHMWPE and deformation of the UHMWPE has been linked to this lack of support (Simon et al., 1998). Optimising shell/liner conformity will ultimately increase the contact area of supported UHMWPE and decrease contact stresses and UHMWPE damage. Suboptimal locking mechanisms can also contribute to a lack of conformity between shell and liner. A design feature of modular cups includes a locking mechanism to fix the liner into the shell and this often results in areas of thinner UHMWPE close to the rim. A number of studies have reported rim fracture of cross-linked liners. Tower et al. (2007) observed rim cracking in four liners that had been retrieved after 7 to 27 months. These authors concluded that thin UHMWPE in the equatorial region, relatively vertical cup alignment and the material properties of the re-melted UHMWPE were responsible for the failures and that the reduced toughness of the cross-linked UHMWPE would make it more susceptible to fatigue failure than conventional UHMWPE.

#### **1.6.5 Current Concepts in Explant Analysis**

Implants retrieved at revision surgery have been widely used to assess wear and fatigue performance of total hip replacements and to determine failure mechanisms. The information gathered from these analyses can be used to inform implant design and to validate hip simulator tests. Explant analysis has varied from

basic macroscopic categorisation of damage (Hood et al., 1983; Wasielewski et al., 1994; Lombardi et al., 2008; Brandt et al., 2012) to more complex analyses such as Fourier Transform Infrared Spectroscopy (FTIR; Kurtz et al. 1999) to determine oxidation levels following implantation and geometrical measurements using coordinate measurement machines and MicroCT to determine wear volumes (Raimondi et al. 2000; Bowden et al. 2005; Jedenmalm et al. 2009; Matthew G Teeter et al. 2010; Uddin 2014).

UHMWPE explants present unique difficulties relating to analysis and measurement that are not encountered or encountered to a lesser extent when measuring simulator samples and/or hard bearing materials. Iatrogenic damage caused by the removal process is often observed on UHMWPE explants and can be difficult to distinguish from damage sustained prior to revision surgery. Furthermore, explants may have sustained damage *in vivo* to such an extent that measurements and basic observations beyond the most obvious relating to damage mechanisms are difficult to make.

The most significant challenge encountered when analysing explants results from the lack of original data relating to the component before it was implanted. Simulator samples can be measured prior to testing and then worn components can be compared to the original data. Gravimetric measurements can be performed to assess volume change as the original weight of the component is known (although errors relating to fluid absorption are acknowledged). Geometrical volume change measurements for hard on hard bearings can be complex but the lack of creep and plastic deformation means that it is easier to create nominal or reference spheres for comparison. Furthermore, for hard on hard bearings deformation of the component is primarily attributable to wear, unlike UHMWPE bearings that undergo extensive plastic deformation both during manufacture and implantation (Nevelos et al., 1999; Nevelos et al., 2000; Nevelos et al., 2001; Leslie et al., 2009; Williams et al., 2008). Wear and deformation *in vivo* is often calculated by measuring the penetration of the femoral head into the acetabular cups from radiographs. Penetration in mm/yr provides information relating to the wear of the acetabular cup if it assumed that most creep occurs in the first one to two years and thereafter the measurement relates to wear only.

The two most common techniques are radiostereometric analysis (RSA) and the Martell Method. RSA uses tantalum beads implanted in the implant and bone to provide reference markers to track migration (Bottner et al., 2005) and the Martell method uses a computer assisted vector wear technique that uses best fit circles of the head and acetabular cup (Martell & Berdia 1997; Martell et al. 2003; Manning et al. 2005). The RSA technique is more accurate but the Martell technique can be used for more patients as the tantalum beads are not required. These methods and others have been used to measure femoral head penetration *in vivo*, before the implant has been revised but do not measure wear or deformation on the rim of the cup.

Explanted acetabular cups allow direct measurement of volume change to be performed. Methods to measure wear and volume change in explanted UHMWPE acetabular cups include fluid displacement methods, shadowgraph methods as well as methods using coordinate measuring machines (CMM) and MicroCT. Experimental methods vary between studies but are generally based on similar principles. For the fluid displacement method, a femoral head is placed in the unworn region of the cup and fluid is introduced to the bearing using a micropipette, the resulting fluid volume is then compared to an unworn cup and femoral head to determine the volume attributable to the radial clearance of the femoral head and acetabular cup (Masaoka et al., 2003). The shadowgraph, radiograph and CMM techniques have been used to measure penetration depth  $d$  and then mathematical conversions are carried out based on these linear measurements to obtain volume change. For the shadowgraph method, casts are made of the worn sockets and the penetration of the worn and unworn profiles is measured in the superior and medial directions. The penetration angle  $\beta$  is then calculated using trigonometry. Hall & Unsworth (1995) compared a radiograph technique, a shadowgraph technique and a CMM technique to calculate wear volumes for 28 explanted Charnley cups. These authors modified an equation by Kabo et al. (1993), which utilised the penetration angle and penetration depth to calculate the volume of a hemispherical cup only, to calculate the volume change of a hemispherical Charnley cup with a cylindrical portion near the rim as seen in Figure 1-15.

$$V_{kabo} = \pi r^2 - r^2 \left[ d \cos^{-1} \left( \frac{d \tan \beta}{r} \right) - \sqrt{\left( \frac{r^2}{\tan^2 \beta} - d^2 \right)} + \frac{r}{\tan \beta} \right] - \frac{r^3}{3 \tan \beta} \left[ \left( 1 - \frac{d^2 \tan^2 \beta}{r} \right)^{3/2} - 1 \right] \quad (1.3)$$

$$V_{modified\ kabo} = V_{Kabo} + \frac{2rfd}{\cos \beta} \quad (1.4)$$

In equations (1.3) and (1.4)  $d$  is the penetration depth determined using the shadowgraph, radiograph or CMM technique,  $f$  is the depth of the cylindrical portion of a Charnley cup and  $\beta$  is the penetration angle determined using the shadowgraph, radiograph or CMM technique. They concluded that there was no significant difference in terms of penetration for the shadowgraph and the CMM techniques. A difference between the radiograph and the CMM techniques was observed and this was thought to be a result of measuring the wear in the coronal plane for the radiograph technique.

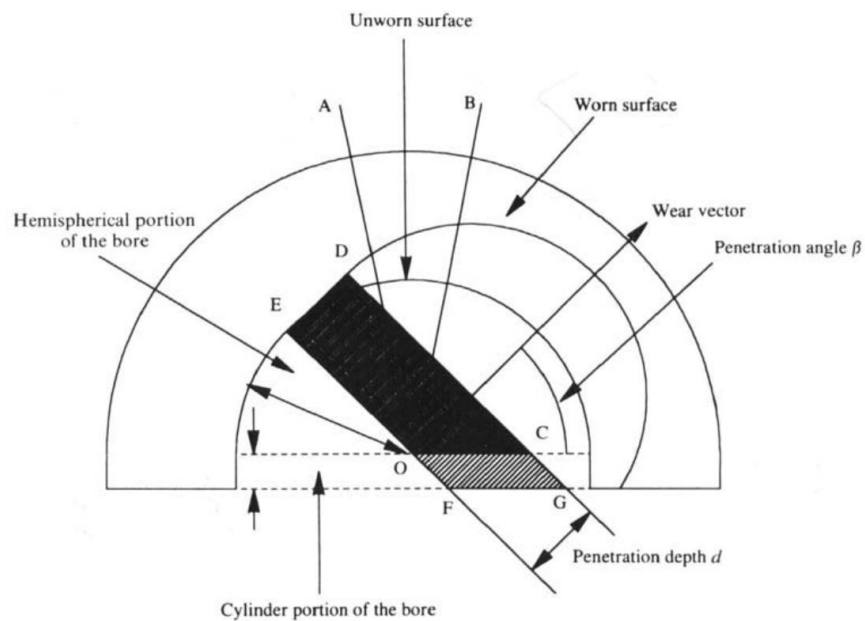


**Figure 1-15 schematic of the wear volumes for a Charnley acetabular cup showing the cylindrical and spherical regions and the wear volume (parallelogram EDCGFO; (Hall and Unsworth, 1995))**

Chuter et al. (2007) compared the radiographic method of measuring wear volumes to three *ex-vivo* methods: a shadowgraph method, a fluid-displacement method and a CMM method. For all of the methods except the fluid-displacement method, the volumetric wear or volume change was calculated from the penetration using the equations (1.3) and (1.4). Chuter concluded that the fluid displacement method was the most accurate method and that all *ex-vivo* methods were better than the radiograph method. However, they note that the radiograph method is the only method suitable for *in vivo* measurements.

For explants, the shadowgraph method and the fluid displacement method are time consuming and the fluid displacement method does not identify the location of the volume change. Furthermore, while they have been used successfully to measure cups with high wear volumes, their effectiveness for highly crosslinked UHMWPE cups exhibiting very low wear volumes is less well understood. Recently, CMM methods and MicroCT methods have been favoured

for the measurement of wear in explanted acetabular cups. Raimondi et al. (2000) presented a method for measuring wear volumes in UHMWPE acetabular cups using a coordinate measuring machine. The method involved sampling several points on the unworn area of the bearing surface and several points on the worn surface (identified by a ridge) and calculating the best-fit sphere from these points. The difference in volume of the two spheres was then calculated mathematically. The authors reported reasonable accuracy for cups with wear volumes of  $100\text{mm}^3$  but stressed that lower wear volumes would require a different method. Uddin (2014) used a similar method, to calculate wear volumes for highly crosslinked UHMWPE acetabular cups. These authors validated their method using gravimetric measurements. They reported that the method measured volumetric wear as low as  $0.49\text{mm}^3$  and with a maximum volumetric certainty of  $\pm 3.12\text{mm}^3$ .

MicroCT has also been used to assess volume change of UHMWPE acetabular explants. Bowden et al. (2005) described a validated method using manual rigid 3D image registration for measuring volume change in acetabular cups that had a scanner maximum uncertainty of 0.6% and that was shown to be repeatable through intra-observer analysis. Jedenmalm et al. (2009) used MicroCT to measure volume change and found the accuracy for linear wear to be 0.6mm and the angle to be  $27^\circ$ , which they concluded was a clinically relevant level of accuracy. Teeter et al. (2010) described a MicroCT method that created 3D deviation maps for the bearing surface and backside of UHMWPE liners. They measured UHMWPE acetabular cups and the penetration rate of  $0.15\text{mm/yr}$  corresponded with previous clinical results for the same type of cups. However, the method required comparison with an unworn cup. They used an unworn cup of the same design, which introduces errors due to the manufacturing tolerances. Another limiting factor of MicroCT analysis of volume change is the extremely large data sets and the length of time required to complete the image reconstruction. Both CMM and MicroCT methods for measuring volume change are susceptible to error due to creep of the UHMWPE as neither method isolates wear from creep.

Damage assessment and categorisation of explants has been extensively used to understand wear and failure mechanisms of UHMWPE acetabular cups and liners. One of the first authors to describe a method to categorise damage in total

knee replacements was Hood et al. (1983). These authors defined seven surface degradation mechanisms: surface deformation, pitting, embedded poly(methyl methacrylate) (PMMA) debris, scratching, burnishing, abrasion, and delamination. Tibial components were divided into four quadrants and each quadrant was given a score from 0-3 depending on the percentage coverage of each damage mechanism for each quadrant. The method did not factor the severity of each mechanism into the damage score, which was a limitation of the method. Wasielewski et al. (1994) recognised this limitation and graded prevalence and severity separately, combining the two to give an overall score for each tibial quadrant. Similarly, Brandt et al. (2012) graded both severity and prevalence separately and defined six damage features: burnishing, grooving, indentations, pitting, deformation and stippling. Lombardi et al. (2008) assessed backside wear on tibial inserts. These authors divided the baseplate into six zones and scored the damage for prevalence, severity and depth of the major defect. They defined nine damage mechanisms: pitting, scratching, abrasion, delamination, embedded debris, burnishing, deformation, discoloration and fraying of locking mechanism. More recently, Childs et al. (2016) assessed glenoid liners using each of the methods developed by Hood, Wasielewski, Lombardi and Brandt and carried out an assessment of observer consistency and the preferred method of scoring damage. They concluded that the method by Brandt was the best method in terms of accuracy and highlighted the importance of using several observers. Damage scoring methods adapted from the Hood method have also previously been applied to acetabular cups. Bradford et al. (2004) used the Hood method to assess for pitting, scratching, burnishing, abrasion, embedded particles, and permanent plastic deformation on highly crosslinked UHMWPE liners. Pang et al. (2015) used the same method to compare the damage in highly crosslinked and conventional acetabular liners but scored the rim separately, creating eight damage zones to be assessed.

MicroCT has previously been used to assess subsurface damage of UHMWPE total joint components. Kurtz et al. (2005) and Kurtz et al. (2007) were able to observe the trajectory of subsurface cracks and identify possible pit formation in explanted total disc arthroplasties using MicroCT scans. Teeter et al. (2010) described a method to visualise and quantify subsurface cracks due to fatigue wear

and delamination in explanted tibial inserts. As mentioned previously, MicroCT techniques for analysing UHMWPE total joint components are time consuming and require storage of large amounts of data. However, they offer a non-destructive method to analyse subsurface cracking in UHMWPE components. Non-destructive testing of explants allows further testing out of components to be carried as well avoiding legal and/or ethical implications relating to destruction of the components. Furthermore, MicroCT could be used in simulator testing to follow subsurface crack propagation over time by scanning at multiple measurement points, which would not be possible with destructive methods, but the sensitivity of the method in detecting very small cracks is yet to be fully determined.

## **1.7 Aims and Objectives**

### **1.7.1 Aims**

The overall aim of the study was to develop and evaluate clinically relevant simulation methods for edge loading and to investigate the wear and fatigue performance of a range of different types of UHMWPE acetabular liners under these conditions. The study also aimed to develop and evaluate methodologies for measuring and analysing wear and damage of explanted acetabular cups and to compare the results of these analyses with the wear and damage observed on simulator components.

### **1.7.2 Objectives**

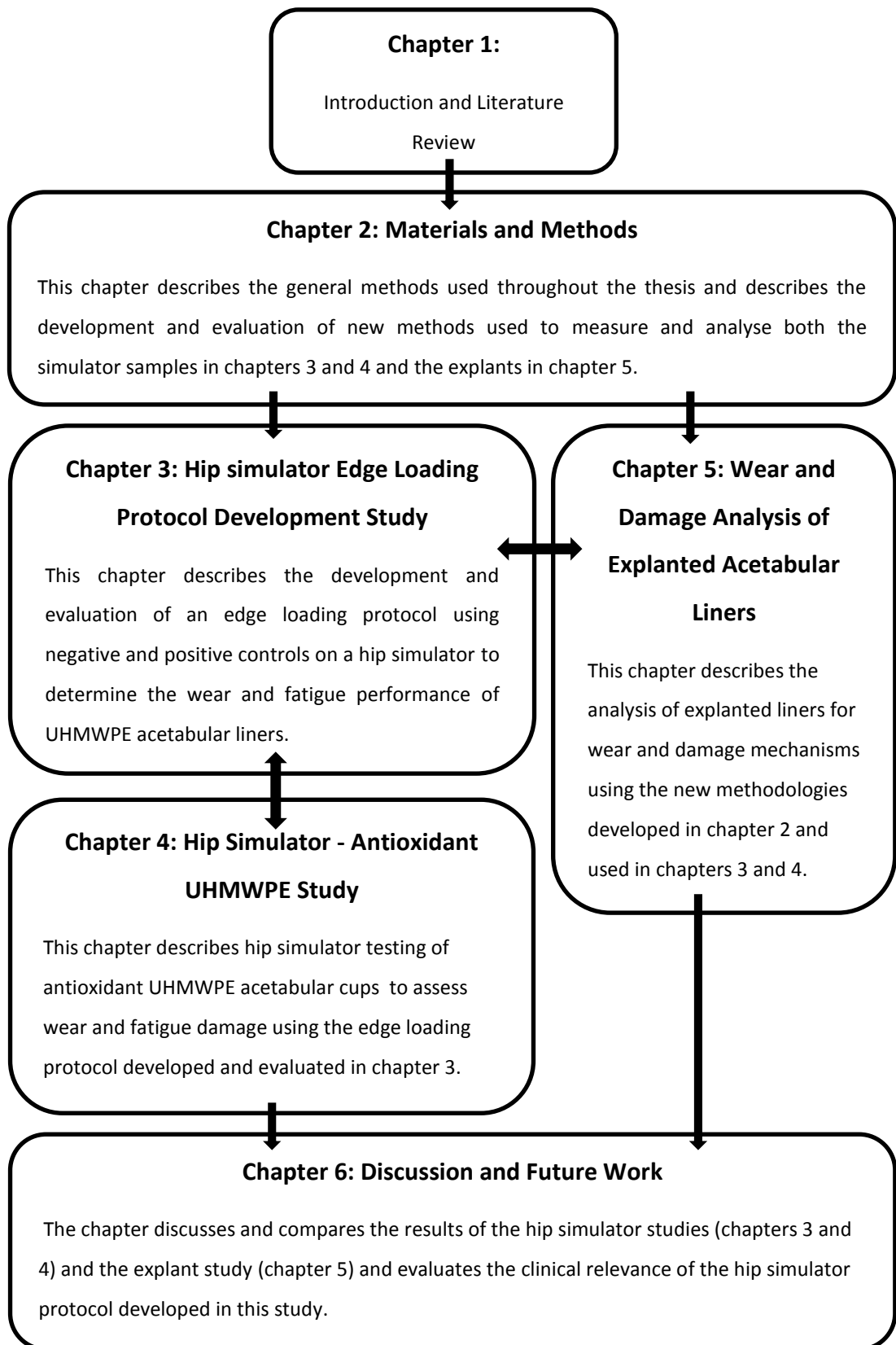
The aims of the study were achieved by completing the following objectives:

- Assess the wear and fatigue damage on the bearing surface and rim region of non-aged moderately crosslinked UHMWPE acetabular liners as negative controls and compare to aged UHMWPE liners as positive controls under standard and edge conditions in a hip simulator;
- Assess the wear and fatigue damage of two different designs of novel antioxidant UHMWPE acetabular cups under standard and edge

loading conditions in a hip simulator and compare with positive and negative controls from the edge loading protocol development tests and compare the two different cup designs for wear and fatigue behaviour;

- Evaluate new methodologies for the measurement and analysis of explanted acetabular liners with specific emphasis on damage and wear due to edge loading and carry out analyses of explanted acetabular liners;
- Compare wear and damage observed on simulator samples and explants and evaluate hip simulator protocols for replication of clinically relevant wear and damage mechanisms;
- Identify key areas for future studies to investigate the wear and fatigue performance of acetabular components under a range of clinically relevant conditions.

### 1.7.3 Thesis Outline



## Chapter 2: **Materials and Methods**

### **2.1 Introduction**

Hip simulator testing under standard and adverse edge loading conditions and analysis of explanted acetabular liners was carried out to develop and evaluate the edge loading method, to determine the wear and fatigue performance of different acetabular cups and to determine the clinical relevance of these simulator testing protocols. This chapter outlines the general methods and materials that were common to all areas of the research. Methods specific to the work carried out in a particular chapter and specific details of the materials used, such as sample size, can be found at the beginning of each relevant chapter.

Analysing the explants raised challenges that were not encountered when measuring and analysing the simulator samples. It was difficult to distinguish between damage sustained during implantation and iatrogenic damage caused at revision surgery. Furthermore, the lack of pre-implantation data relating to the cup meant that comparative measurements to determine wear volumes and/or rim deformation were not possible. Although some work has previously been undertaken to analyse explants at the Institute of Medical and Biological Engineering (Nevelos et al. 1999), there are not currently any Institute standard operating protocols relating to the analysis of explanted orthopaedic components or acetabular cups in particular, and therefore a significant proportion of the research presented in this thesis involved developing methodologies for analysing explants. This chapter also describes and discusses this methodology development.

### **2.2 Materials**

This section provides a general overview of the components tested as part of the hip simulator studies as well as the components selected to form part of the explant study. Information relating to these components is provided here because the components are used to develop and evaluate the measurement methodologies discussed in this chapter. More detailed descriptions of the

components including sample size can be found in each relevant chapter. A list of component images, lot numbers and the labelling conventions used in each study can be found in Appendix 1 (simulator study) and Appendix 5 (explant study).

### **2.2.1 Simulator Components**

In the Hip Simulator Protocol Development Study (Chapter 3) two types of UHMWPE acetabular liners were studied: Marathon® moderately crosslinked UHMWPE Pinnacle® liners (XLPE) and aged Gamma Vacuum Foil® UHMWPE liners (aged PE; DePuy Synthes, UK) compatible with the Pinnacle® total hip replacement system.

In the Antioxidant UHMWPE Hip Simulator Study (Chapter 4) two different acetabular cup designs were tested. A modular acetabular liner compatible with the Pinnacle® total hip replacement system (AOPE Liner; DePuy Synthes, UK) and a monoblock prototype compression moulded acetabular cup design (AOPE cup; DePuy Synthes, UK).

The Pinnacle® total hip replacement liners (XLPE, Aged PE and AOPE liners) in these studies comprised a 56mm outer diameter titanium alloy shell and a press fit 36mm inner diameter UHMWPE liner with taper lock and anti-rotation device (ARD) tabs that mate with anti-rotation device scallops (Figure 2-1).



**Figure 2-1 An assembled Pinnacle® acetabular shell showing the ARD tabs on the UHMWPE liner and the ARD scallops on the titanium shell**

The liner thickness for all materials was 7.8mm at the apex and 5.1mm at the rim. The compression moulded acetabular cup design comprised of a 36mm inner diameter non-removable compression moulded UHMWPE interior with Gription® porous coating on both the inner and outer surfaces of a 48mm outer diameter titanium shell (Figure 2-2). The UHMWPE in the compression moulded cup was 2.7mm thick.



**Figure 2-2 A compression moulded acetabular cup (foreground; AOPE CM cup) and a Pinnacle® compatible liner with titanium shell (background; AOPE liner)**

### **2.2.2 Explants**

Failed explants were collected at total hip replacement revision surgery and transported to the University of Leeds. Explants were selected for study with a view to making the best comparison with the simulator components. For this reason, UHMWPE Pinnacle® acetabular liners were selected for analysis from the collection at the University of Leeds. Crosslinked and non-crosslinked components and a range of thicknesses and Pinnacle® sub-designs (i.e., lipped, face changing, etc.) were selected but all were part of the Pinnacle® total hip replacement system. Further details including inclusion and exclusion criteria are provided in section 5.2.2.

## **2.3 General Methods**

This section outlines the general methods that are common to all areas of the research.

### **2.3.1 Component Cleaning**

The simulator components were cleaned prior to testing and at each measurement point to remove all debris and proteins that may have adhered to the surface. The components were cleaned in soapy water with soft tissue, soaked in Distil (Tristel Solutions Ltd, Cambridge, UK) for 10 minutes, rinsed in water and then placed in an ultrasonic bath for 10 minutes in 70% (v/v) isopropanol before being dried with soft tissue or left to air dry.

The explants were cleaned and decontaminated prior to storage and analysis. To decontaminate, explants were immersed in 10% neutral buffered formalin (NBF) for a minimum of 7 days at room temperature. Following decontamination, the explants were cleaned to remove any tissue and/or blood spots using Distil and a soft brush, rinsed using distilled water and dried using soft tissue paper or air dried.

### **2.3.2 Microscopic and Macroscopic Observations**

Following testing of the simulator components and during damage categorisation of the explants, the surfaces of the components were cleaned according to the cleaning protocol described in section 2.3.1, photographed and visually inspected for damage.

Further microscopic inspection was carried out using a Nikon SMZ800 Stereomicroscope (Nikon UK Ltd, Surrey, UK) at x30 magnification.

### **2.3.3 Gravimetric Measurements**

The gravimetric measurements assessed weight change due to material loss and fluid absorption of the simulator components. Weight change was not determined for the explants as no pre-implantation weight was available for comparison.

Prior to simulator testing and at each measurement point the liners were cleaned according to the cleaning protocol described in section 2.3.1 and left to stabilise for 72 hours in a controlled environment. The acetabular liners were weighed using a Mettler XP205 balance (Mettler Toledo, Leicester, UK; resolution 0.01mg) until five measurements within a range of 0.1mg were obtained for each liner. The balance was re-zeroed after every measurement and the mean of the five measurements was taken. The mass was converted to volume (mm<sup>3</sup>) by dividing by the density of the UHMWPE (Equation 2.1). The volume change for each acetabular cup design was plotted as a function of the number of simulator cycles. The wear rate in mm<sup>3</sup>/Million cycles (Mc) of simulator testing was calculated by dividing the overall volume change by the number of cycles of testing (Equation 2.2).

$$Volume = \frac{Mass}{Density} \quad (2.1)$$

$$Wear\ rate = \frac{Total\ volume\ change\ in\ mm^3}{Number\ of\ cycles \times 10^6} \quad (2.2)$$

Soak controls were used to compensate for fluid absorption when weighing the components. The soak control samples were stored in serum next to the simulator during testing. The serum was replaced with the same frequency as the serum in the simulator stations. The weight change of the soak control was deducted from the mean weight change of the test components. All of the liners were pre-soaked in water before testing for a minimum of one month (3 months for the aged PE and the XLPE liners and 1 month for the AOPE liners) to minimise fluid uptake during testing.

#### **2.3.4 Geometric Measurement of Simulator Components**

The three dimensional geometry of the bearing surface was determined using a Legex 322 coordinate measuring machine (CMM; Mitutoyo, Halifax, UK) with an accuracy of 0.8µm. The CMM scanning function was used to take 36 tracks of 68

points each at 10° intervals, starting in the centre of the cup and finishing on the cup rim (Figure 2-3).

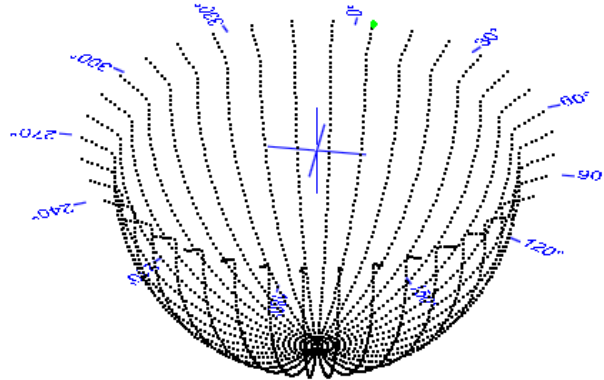


**Figure 2-3 Schematic of a CMM scan of a UHMWPE liner showing measurement coordinates across the bearing surface**

Alignment of the UHMWPE liner to the machine coordinates was achieved by aligning the horizontal rim of the cup with the z plane and using two small holes (diameter and depth 1.7mm) drilled in the cup rim to align the x and y axes (Figure 2-4). This was done by finding the intersection point along the x axis between the centres of the two holes and setting this as the origin. The x axis was aligned through the origin and the centre of one of the holes. Aligning the component coordinates with the machine coordinates allowed a comparison to be made between measurements when the components were removed and replaced on the CMM between measurement points. The cups and liners were measured before testing to obtain the original profile and then at each measurement point to determine a new worn profile.

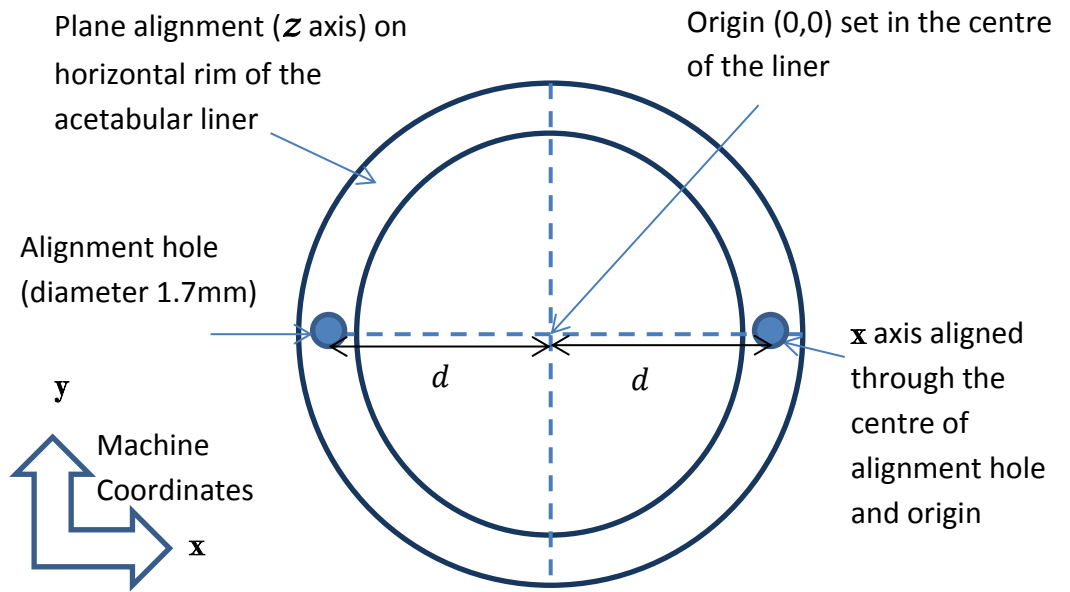


**Figure 2-4 Alignment of an acetabular cup on the CMM: origin  $(0_x, 0_y)$  is set at  $(d_x, 0_y)$  from the centre of one of the alignment holes and the x axis is aligned through the origin and the centre of one of the alignment holes. The horizontal liner rim is aligned with the z plane.**

To reduce measurement error, manufacturers recommend the largest possible probe diameter. In the case of the simulator cups the probe needed to be sufficiently small so as to fit into the alignment holes in the cup and therefore a 1mm diameter ruby probe was selected for the measurements.

SR3D software (Tribosol Ltd, UK) was used to analyse the CMM measurement data, which was exported from the CMM as a text file containing the coordinates and vector directions of the points along each track. SR3D compared the pre-wear profile of the component with the worn component and calculated the maximum radial deviation of a given track from the original profile to give the maximum penetration into the cup. An example of the output from the SR3D software is shown in Figure 2-5.

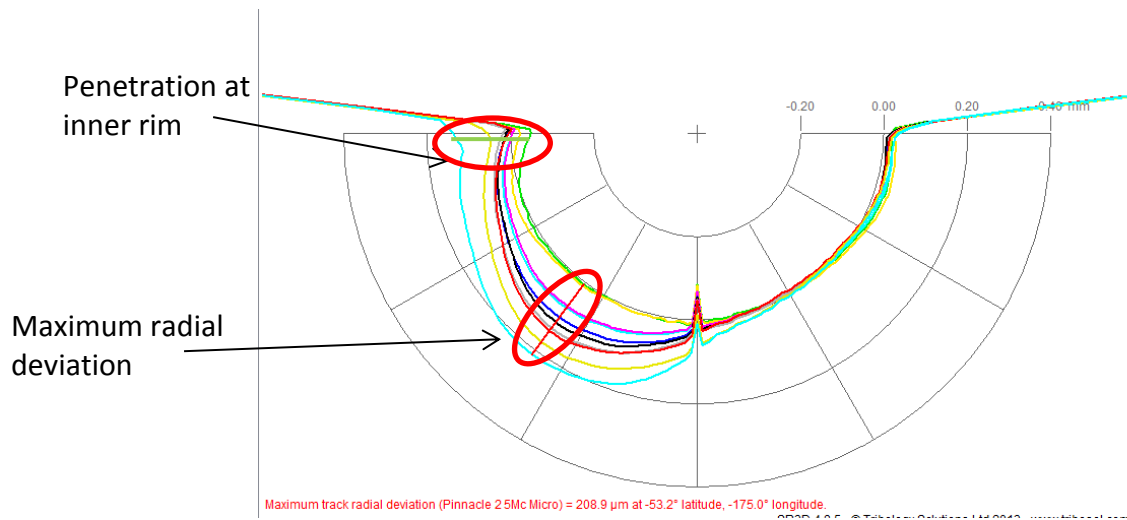


**Figure 2-5 SR3D image of a cross section of an AOPE acetabular liner (AOPE 2) after 5Mc of standard loading and 5Mc of edge loading. The maximum radial deviation at the area of articulation is marked with a red line (208.9  $\mu\text{m}$ ) and the radial deviation at the rim is marked with a green line (157.9 $\mu\text{m}$ ). Profile deviations are at x40 magnification**

The enclosed volume of the bearing surface was calculated by the SR3D software for both the original profile and the worn profile and a positive change indicated wear and/or deformation. A difference in the height of the average z value for the worn profile and the original profile was noted in the data and a z-compensation was applied. This was done by subtracting the average z coordinate of the original rim ( $Z_0$ ) from the average z coordinate of the measurement ( $Z_1$ ) and subtracting this value from the z coordinate of all the points of the measurement. The CMM measurements included both volume changes caused by wear of the UHMWPE as well as volume changes due to creep (Section 1.5.2). The SR3D software also produced geometric reconstructions of volume change (Figure 2-6).

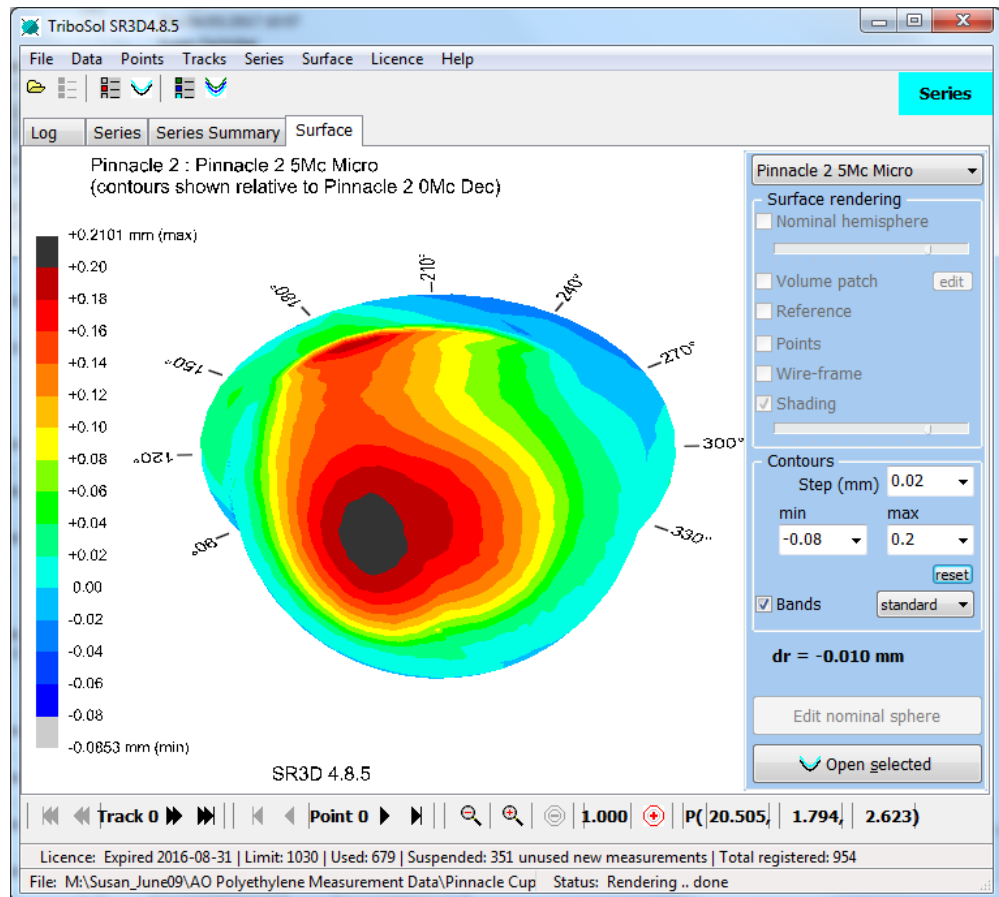


**Figure 2-6 Geometric reconstruction of volume change for an AOVE acetabular liner after 5Mc of standard loading and 5Mc of edge loading (AOPE 2). Volume change on the bearing surface and close to the inner rim is shown.**

The volume change for each acetabular cup design was plotted as a function of the number of cycles. As previously described in section 2.3.3, the rate of volume change was calculated by dividing the total volume change by the number of cycles, giving the volume change per million cycles in  $\text{mm}^3/\text{Mc}$ . The steady state wear rate was determined by calculating the volume change per million cycles between 1Mc and 5Mc (or 1Mc to the end of the test) to exclude the effect of creep in the first million cycles. This is a standard method for calculating steady state wear rates and has previously been used in similar studies (Galvin et al., 2010).

To evaluate measurement accuracy using this method, measurements of an unworn UHMWPE acetabular liner were repeated 4 times and a standard deviation

of 3.27mm<sup>3</sup> was obtained, which was assumed sufficiently small to measure volume change in these liners with relative accuracy.

### **2.3.5 General Statistical Methods**

For all data sets in the simulator and explant studies, the mean and 95% confidence intervals were calculated and statistical analyses were performed using a one-way ANOVA ( $p < 0.05$  for significance). A Tukey post-hoc analysis was performed for multiple datasets, where applicable.

Relationships between volume change, volume change per year or damage score and time *in vivo*, patient age, patient activity levels, patient BMI, liner thickness or cup inclination angle were assessed using a Spearman's correlations.

The relative standard deviation (%RSD) was used to compare the variation of datasets with different means.

## **2.4 Development of a Geometric Measurement Methodology for Explants**

### **2.4.1 Introduction**

Accurately measuring volume change in explants presents difficulties that are not encountered when measuring simulator samples. Iatrogenic damage caused by the removal process at hip replacement revision surgery is often observed on UHMWPE explants and can be difficult to distinguish from damage sustained during implantation. Furthermore, explants may have sustained damage *in vivo* to such an extent that measurements and basic observations relating to damage mechanisms are difficult to make. This damage contributes to one of the most significant challenges encountered when analysing explants, which is the lack of original data relating to the component before it was implanted. Simulator samples can be measured prior to testing and worn components can be compared to this original data. Gravimetric measurements can be performed to assess volume change as the original weight of the component is known (although errors relating to fluid absorption are acknowledged) and geometrical measurements can be compared to

original pre-wear profiles. Geometrical volume change measurements in explants require a nominal or reference sphere to be created from unworn, undamaged areas of the explants, which is then used for comparison with the worn profiles. However, damage and extensive plastic deformation can inhibit the identification of a reference sphere to represent the unworn geometry.

Various methods that attempt to overcome the challenges associated with explants have been developed and used to measure wear volume in explants. These include fluid displacement methods, microCT methods, radiostereometric methods and CMM methods (discussed in section 1.6.5). However, all of these methods have limitations.

This section describes and discusses the development and evaluation of a new geometric methodology for measuring and analysing explants using CMM measurements and Redlux software (Redlux, UK). The SR3D software (used for analysis in the simulator studies; section 2.3.4) was not used to determine the volume change or create geometric reconstructions of the explants as the software was no longer available when the explants were being analysed. A CMM based method was selected in this study to maintain consistency with the geometrical measurement methods used in the simulator studies in this project. Standard operating protocols for obtaining the volume change of UHMWPE acetabular explants do not currently exist at the Institute of Medical and Biological engineering and validation of the Redlux software reported in the literature primarily relates to hard on hard bearings (Tuke et al., 2010). A requirement to develop and evaluate a method to measure volume change in explanted UHMWPE acetabular liners was therefore identified.

#### **2.4.2 Materials**

Two explants from the explants study (Chapter 5), a simulator liner from the hip simulator study (Chapter 3) and an additional untested control liner were selected to develop and evaluate the method.

Both explants were non-crosslinked UHMWPE Pinnacle® liners (explant 6N and explant 3N; see section 2.2.1 for a description of the Pinnacle® liners). These explants were decontaminated and cleaned according to section 2.3.1.

The simulator liner was an XLPE Pinnacle® liner that had been pre-soaked and tested in a hip simulator for five million walking cycles (control liner AM1; DePuy Synthes, UK). Control liner AM1 was cleaned and weighed before and after testing and the volume change was calculated.

The additional control liner was an untested 36mm diameter Gamma Vacuum Foil® UHMWPE Pinnacle® compatible liner (Liner NA14; DePuy Synthes, UK). Liner NA14 was untested and had not been put in soak in order to reduce the effect of creep and fluid absorption on the results of the analyses. This liner was cleaned and weighed according to sections 2.3.1 and 2.3.3. A small amount of material was removed from the bearing surface of liner NA14 using a ball drill. The liner was weighed again and the volume change was calculated according to section 2.3.3.

### **2.4.3 Methods**

#### Measurements

Three dimensional geometric measurements assessed the total volume change at the surface of the cup comprising volume change due to creep and material loss due to wear. The cups were cleaned according to the cleaning protocol described in section 2.3 and left to stabilise in a controlled environment.

The CMM measurements of the explants were performed in the same way as the measurements of the simulator liners (section 2.3.4) except a 2mm ruby probe was selected and Redlux software was used to create geometric reconstructions of the bearing surface of the explants as well as to calculate volume change. Also, the number of measurement points was increased to 72 tracks of 140 points each at 5° intervals. The larger probe was used for the CMM scans of the explants because alignment holes on the horizontal rim were not used. This was because no unworn measurements were available for the explants and therefore exact re-alignment of the components between measurements was not required and it was not necessary to align the component to the machine coordinates.

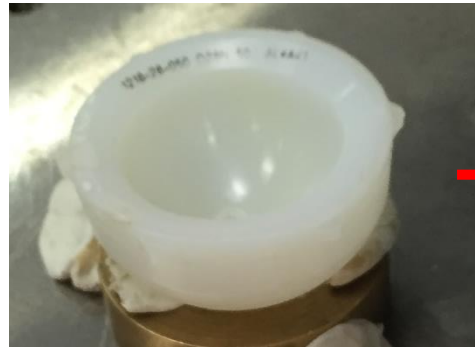
### Analyses

This section describes the basic Redlux analysis method as described in Redlux software manuals and the variations (protocols) of this basic method that were assessed in this study for analysing volume change in explants.

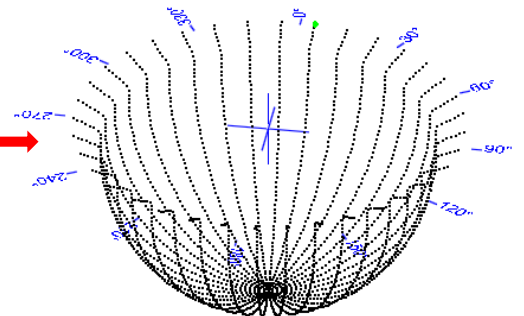
In the absence of an unworn cup for comparison, the volume change analysis using Redlux involved defining a best-fit nominal sphere using unworn, undeformed regions of the liner to represent the unworn liner and then determining the volume change of the worn liner caused by creep and wear compared to the defined nominal sphere (Figure 2-7). The nominal sphere was defined by excluding any features that were perceived by the user to be volume change due to creep, wear or damage and then calculating the nominal sphere using the remaining surface areas. This was done using the “Sphere (advanced)” feature of the software, which fitted a sphere to the data using a linear least squares fit (Tukey et al., 2010). The user manually drew around each area to be excluded and therefore the features that were excluded as well as the size of each excluded area were user dependent.

After the nominal sphere was defined, it was saved to the software and the profile for the worn liner was compared to this nominal sphere. A specific area of the worn cup was selected to perform the volume change calculation (i.e. the wear scar). This was done by excluding all other regions of the liner from calculations and selecting the desired area to be included in the calculation. The “Volume” tool feature of the software was then used to determine the volume of the black areas, which represented area below the nominal sphere (i.e. wear). Again the size of the area included in the volume change calculation was dependent on user judgement.

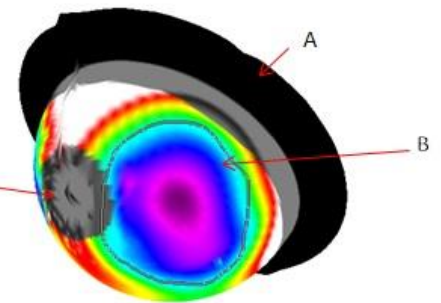
The method was not suitable for measuring volume change at the rim, as the method relied on being able to fit the data points to a sphere. It is therefore suggested that the actual volume change for each cup or liner was marginally larger than the values obtained in this study. However, it was assumed that any volume change and/or wear at the rim would be small in comparison to the wear on the bearing surface because the contact area was significantly larger at the bearing surface (Mazzucco and Spector, 2003).



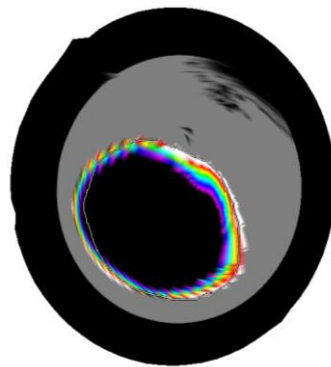
The explant is measured on the CMM



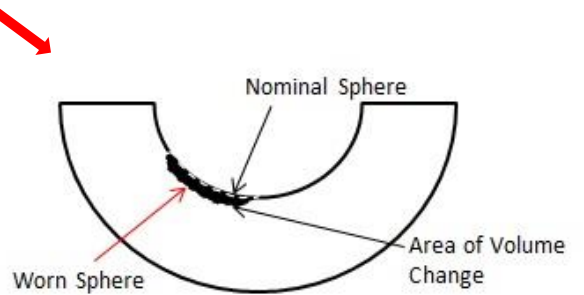
The CMM measurement coordinates are imported into the Redlux software



The nominal sphere is defined by the user. To do this, (A) the rim (B) areas of wear and deformation, and (C) damage are selected and excluded and a sphere is fit to the remaining data points.



The volume change is calculated as the difference between the best fit nominal sphere and the worn sphere. The wear area is selected (black) and the remaining areas (grey & black rim area) are excluded from calculations



The "Volume" tool is used to calculate the volume ( $\text{mm}^3$ ) and area ( $\text{mm}^2$ ) of the selected area compared to the nominal sphere.

**Figure 2-7 A flow chart showing the process for obtaining volume change in explanted acetabular liners using Redlux from measurement to volume calculation.**

In this study, variations in the basic method (protocols) were assessed to determine if this influenced the final volume change result. This was because the Redlux software manual provided a basic method but this method was subject to adaptation or refinement for specific applications.

The four protocols that were assessed were:

**Protocol 1:** The nominal sphere was defined by excluding the rim, damage (screw hole) and the basic wear area only;

**Protocol 2:** The nominal sphere was defined by excluding the rim, damage (screw hole) and the wear area only. In this protocol the wear area was excluded by increasing the size of the selection until the radius of the nominal sphere stopped increasing and/or the excluded area was deemed too large to continue by the user (e.g. the selected area is covering more than half the cup);

**Protocol 3:** As protocol 1 but also excluding other features not in the wear area caused by creep and/or damage;

**Protocol 4:** As protocol 2 but also excluding other features not in the wear area caused by creep and/or damage.

The protocols were selected to determine the effect of the size of the wear area that was excluded (protocol 1 & 2) and the effect of excluding other features caused by creep and/or damage (protocols 3 & 4) on the repeatability, reproducibility and accuracy of the protocol.

### Statistical Evaluation

The Redlux software and method were sensitive to user variation when measuring volume change in explants. The size of the areas excluded when defining the reference sphere depended on the user's judgement, as did the final area selected in the volume calculation. For this reason, evaluation of this method to

determine repeatability, reproducibility and accuracy when analysing explants for volume change was carried out prior to using it to measure volume change in explants. Four users, two with experience using the software (users 1 & 3) and two that were newly trained (2 & 4), assisted with the evaluation.

The four protocols were assessed by four different users and repeated three times by each user. A flowchart outlining the evaluation process is given in Figure 2-8.

For each protocol the relative standard deviation (RSD) was calculated for each user to determine the intra-user variation (repeatability) of the volume change calculation. The repeatability of a single user on different days was determined by a single user (user 1). To do this, the volume change analysis using protocol 2 was repeated three times on three different days and the RSD was calculated for all values. A one-way ANOVA was performed to test for a significant difference between the results for each day ( $p < 0.05$ ).

The mean volume change for each protocol and user was plotted with 95% confidence intervals and the inter-user variation (reproducibility) of each protocol was assessed by calculating the relative standard deviation for all users for each protocol. A one-way ANOVA and a Tukey HSD posthoc test were performed to determine if there was a significant difference ( $p < 0.05$ ) between the results of each user.

The accuracy of the protocol was assessed by one user only. The volume changes for liner AM1 and liner NA14 were determined geometrically using each protocol and compared to gravimetric volume change calculations of the same liners. Protocol 3 and protocol 4 could not be performed for liner NA14 because the absence of creep and deformation meant that there were no other obvious features on the cup to exclude.

The repeatability and reproducibility measurements for each user and protocol were performed for explant 3N and explant 6N. The statistical results are presented in the following section for explant 3N and in Appendix 2 for explant 6N.

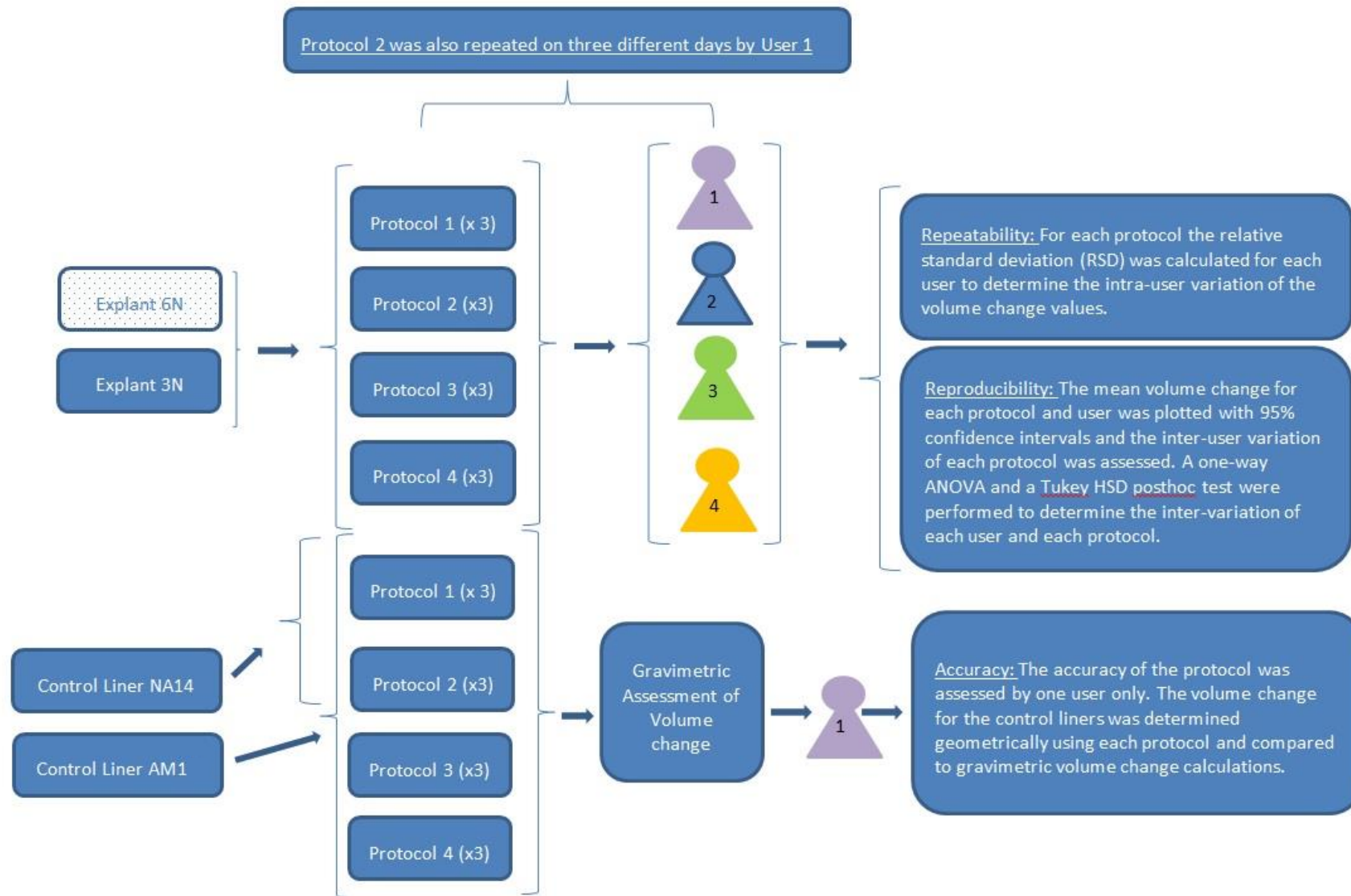


**Figure 2-8** Flow chart showing the process for evaluating the repeatability, reproducibility and accuracy of each volume change protocol. The volume change for the explants was determined by four different protocols, which were repeated three times by four different users. The accuracy was determined by comparing to gravimetric measurements of two different control liners

## 2.4.4 Results

### Repeatability

The mean volume change  $\pm$  %RSD for each user and protocol is given in Table 5.

**Table 5 Mean volume change  $\pm$  %RSD for three repeats of four different protocols by four different users using Redlux analysis software. Green = RSD<5%, Yellow = RSD = 5%-10%, Red = RSD>10%**

| Explant<br>3N | Protocol 1<br>(mm <sup>3</sup> ) | Protocol 2<br>(mm <sup>3</sup> ) | Protocol 3<br>(mm <sup>3</sup> ) | Protocol 4<br>(mm <sup>3</sup> ) |
|---------------|----------------------------------|----------------------------------|----------------------------------|----------------------------------|
| User 1        | 11 $\pm$ 12.2%                   | 23 $\pm$ 13%                     | 8 $\pm$ 4.3%                     | 18 $\pm$ 14.6%                   |
| User 2        | 10 $\pm$ 7.5%                    | 21 $\pm$ 16%                     | 8 $\pm$ 1.3%                     | 20 $\pm$ 2%                      |
| User 3        | 14 $\pm$ 7.1%                    | 36 $\pm$ 7%                      | 14 $\pm$ 25.5%                   | 27 $\pm$ 3.5%                    |
| User 4        | 12.9 $\pm$ 6.8%                  | 30 $\pm$ 5.2%                    | 11.7 $\pm$ 6.6%                  | 28.6 $\pm$ 4.4%                  |

For user 1, protocol 3 was the most repeatable (4.3 %RSD). For user 2, protocol 3 was the most repeatable (1.3 %RSD). For user 3, protocol 4 was the most repeatable (3.5 %RSD). For user 4, protocol 4 was the most repeatable (4.4%RSD).

The mean volume change  $\pm$ %RSD for a single user using protocol 2 on three different days was 24  $\pm$  11%RSD and there was no statistically significant difference between the data sets for each different day (p=0.144).

The results for the expert users (1&3) were no more repeatable than those of the newly trained users (2&4).

### Reproducibility

The mean volume change for each user and each protocol and then all users and each protocol were compared using a one-way ANOVA and a Tukey posthoc analysis to test for significant differences between the users and protocols. There was no significant difference between the mean volume changes for user 1 and user 2 for any of the protocols (Figure 2-9). The mean volume changes for user 3 were significantly different to the volume changes for both user 1 and user 2 for all protocols. There was a significant difference between the mean volume changes for user 1 and user 4 for protocol 4 only. There was a significant difference in the mean volume change for user 2 and user 4 for protocols 1, 2 and 3. There was no significant difference between the mean volume changes for user 3 and user 4 for any of the protocols.

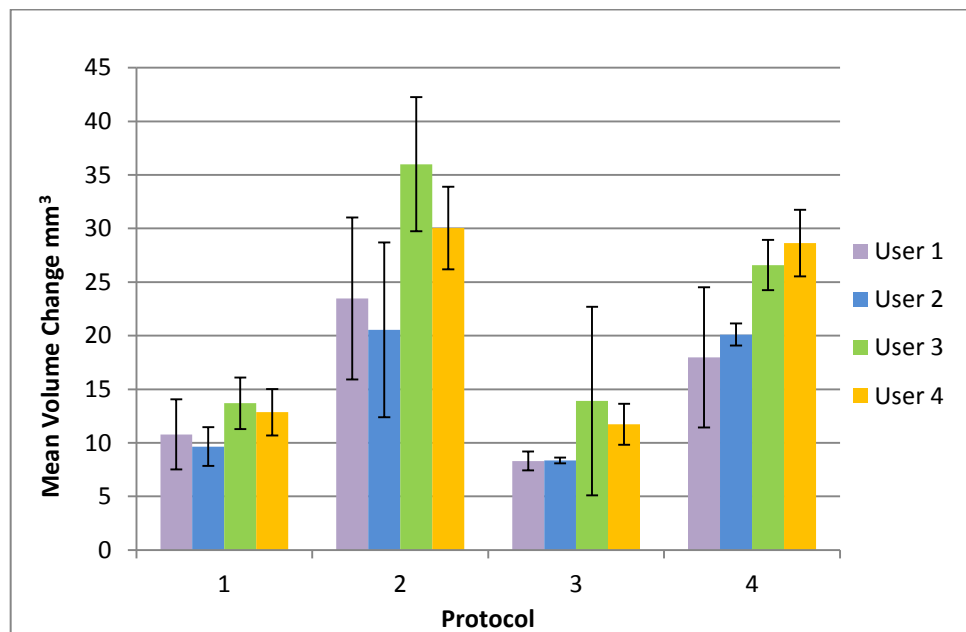


**Figure 2-9 Inter-user variability of the volume change analyses for the four protocols for each user for explant 3N ( $\pm 95\%$  Confidence intervals)**

The p numbers associated with the Tukey post hoc analysis are shown in Table 6.

**Table 6 Associated p numbers for a Tukey HSD post hoc test of inter-user variation for four users and four protocols**

| Users         | Protocol 1 (p)  | Protocol 2 (p)  | Protocol 3 (p) | Protocol 4 (p)  |
|---------------|-----------------|-----------------|----------------|-----------------|
| User1/User2   | 0.531           | 0.572           | 1              | .388            |
| User 1/User 3 | <u>0.03</u>     | <u>&lt;0.01</u> | <u>0.023</u>   | <u>&lt;0.01</u> |
| User 1/User 4 | 0.125           | 0.066           | 0.179          | <u>&lt;0.01</u> |
| User 2/User 3 | <u>&lt;0.01</u> | <u>&lt;0.01</u> | <u>0.024</u>   | <u>&lt;0.01</u> |
| User 2/User 4 | 0.18            | <u>0.011</u>    | .187           | <u>&lt;0.01</u> |
| User 3/User 4 | 0.740           | 0.099           | .502           | 0.420           |

\*underlined p number are significant (p<0.05)

The mean volume changes and the relative standard deviations for all users for each protocol are shown in Table 7. The most reproducible protocols were protocols 1 and 4. There was no statistically significant difference between protocols 1 and 3 (p=0.916) or protocols 2 and 4 (p=0.113) for all users but there was a significant difference between the other protocols (p<0.01 for all).

**Table 7 Mean volume change ± %RSD for all users and all protocols.**

|                    | Protocol 1 | Protocol 2   | Protocol 3   | Protocol 4   |
|--------------------|------------|--------------|--------------|--------------|
| <b>Mean ± %RSD</b> | 11.8 ± 16% | 27.5 ± 24.2% | 10.6 ± 27.6% | 23.3 ± 20.5% |

The repeatability and reproducibility measurements were also performed for explant 6N and were found to show similar trends to explant 3N. However, the larger volume change associated with explant 6N appeared to adversely affect the repeatability and reproducibility for this explant, which is evidenced by the slightly higher relative standard deviations. The values are presented in Appendix 2.

Accuracy

The geometric volume change for liner AM1 and liner NA14 was determined using Redlux for each protocol and compared to the volume change calculated from the gravimetric measurements for the same liners (Table 8).

**Table 8 The volume change  $\pm$ RSD assessed gravimetrically and geometrically (Redlux) using four different protocols for two different control liners. Protocol 3 and 4 were not performed for liner NA14 because the absence of creep and deformation meant that there were no other obvious features on the cup to exclude.**

| Liner NA14  | Gravimetric (mm <sup>3</sup> ) | Protocol 1 (mm <sup>3</sup> $\pm$ RSD) | Protocol 2 (mm <sup>3</sup> $\pm$ RSD) | Protocol 3 (mm <sup>3</sup> $\pm$ RSD) | Protocol 4 (mm <sup>3</sup> $\pm$ RSD) |
|-------------|--------------------------------|--|--|--|--|
| Repeat 1    | <b>1034.96</b>                 | 756.47                                 | 941.14                                 |  |  |
| Repeat 2    |                                | 776.56                                 | 910.72                                 |  |  |
| Repeat 3    |                                | 771.12                                 | 939.19                                 |  |  |
| <b>Mean</b> |                                | <b>768.05 <math>\pm</math> 1.35</b>    | <b>930.35 <math>\pm</math> 1.83</b>    |  |  |
| Liner AM1   | Gravimetric (mm <sup>3</sup> ) | Protocol 1 (mm <sup>3</sup> $\pm$ RSD) | Protocol 2 (mm <sup>3</sup> $\pm$ RSD) | Protocol 3 (mm <sup>3</sup> $\pm$ RSD) | Protocol 4 (mm <sup>3</sup> $\pm$ RSD) |
| Repeat 1    | <b>56.35</b>                   | 22.89                                  | 52.39                                  | 15.99                                  | 30.17                                  |
| Repeat 2    |                                | 24.28                                  | 52.80                                  | 18.67                                  | 32.22                                  |
| Repeat 3    |                                | 23.68                                  | 39.25                                  | 16.19                                  | 47.98                                  |
| Repeat 4    |                                | 24.46                                  | 51.71                                  | 18.42                                  | 40.45                                  |
| Repeat 5    |                                | 26.71                                  | 54.86                                  | 22.67                                  | 42.25                                  |
| <b>Mean</b> |                                | <b>24.40 <math>\pm</math> 5.85</b>     | <b>50.20 <math>\pm</math> 12.42</b>    | <b>18.39 <math>\pm</math> 14.65</b>    | <b>38.61 <math>\pm</math> 19.05</b>    |

The volume change measured gravimetrically was 1035mm<sup>3</sup> and 56.4mm<sup>3</sup> for control liner NA14 and control liner AM1, respectively. For both control liners, protocol 2 was closest to the gravimetric value and therefore the most accurate of all of the protocols. During drilling a small amount of material was unintentionally removed from the rim of control liner NA14. This was small in comparison to the area being measured on the bearing surface and would not greatly influence the total volume change. However, it can be assumed that the actual volume change calculated from the Redlux analysis would be even closer to the gravimetric data for this liner if the volume change at the rim was factored into the calculation.

#### **2.4.5 Discussion and Conclusion**

Protocol 2 was the most accurate of all the protocols. A relative standard deviation of  $\pm 12.42\%$  was obtained with this protocol when measuring the volume change for control liner AM1 and it was thought that this was representative of the accuracy of the method for measuring volume change in explants. The repeatability and reproducibility was comparable to that of the other three protocols and protocol 2 was therefore selected to analyse the volume change of the explants. A standard operating protocol was written and is provided in Appendix 3.

Protocols 2 and 4 produced higher volume changes than protocols 1 and 3. As there was no significant difference between the results of protocols 1 and 3 or protocols 2 and 4, it was assumed that excluding "other features" (protocols 3 and 4) when defining the reference sphere had less influence on the final volume change than the size of the wear area that was excluded. In terms of repeatability and reproducibility, the most repeatable and reproducible protocols varied depending on the user and no protocol was notably more repeatable or reproducible than the others. For this reason, the final protocol for use in the explant study was decided based on the analysis of accuracy. This protocol was repeatable and reproducible relative to previous studies reporting user variability for measurement of volume change (Bowden et al. 2005; Chuter et al. 2007; Teeter et al. 2011).

A method has been developed to measure volume change in explanted acetabular liners for which no pre-wear data was available. There were some limitations to the method. The accuracy of the method was determined by comparing with gravimetric measurements of two control liners (AM1 and NA14). However, it is known that gravimetric measurements of UHMWPE liners that have been soaked in water or serum are affected by fluid absorption (Affatato et al., 2000) and this would have affected the gravimetric measurements and therefore the calculated volume change of control liner AM1. The unsoaked and untested liner (NA14) eliminated the effect of fluid absorption but also minimised the effect of creep. The method may be more accurate for liners, such as control liner NA14, where minimal creep has occurred. This was because the material removal resulted in a more defined edge between the volume change and the rest of the bearing surface and it was therefore less subjective when selecting areas to exclude. However, explanted liners will have undergone more extensive deformation during implantation and the method may therefore be less accurate for explanted liners. Furthermore, the volume change for control liner NA14 was large in comparison to clinically relevant volume changes, the accuracy of the method may be reduced for smaller volume changes.

The method measures volume changes on the bearing surface only and does not include volume changes at the rim. It is thought that because of the reduced contact area volume changes at the rim would be small in comparison to that sustained at the bearing surface, but it should be acknowledged that the method may obtain volume changes that are smaller than the actual values.

Also, the method does not separate volume change due to creep and volume change due to wear and the resulting volume change is a combination of both. The volume change of an explant can only be measured at one time point and therefore it is not possible to exclude the first million cycles volume change to minimise the effect of creep, as would be possible with simulator samples.

While the limitations are acknowledged, the method has been assessed for accuracy using two different control liners and has been shown to be repeatable

and reproducible relative to previous studies and can therefore be used to measure the volume change in explanted acetabular liners.

## **2.5 Development of Rim Deformation Measurement Methodology**

Studies have reported microseparation of the femoral head and cup *in vivo* leading to edge loading of the acetabular rim (Lombardi et al., 2000; Dennis et al., 2001; Komistek et al., 2002). Fatigue damage such as fracture and cracking as well as deformation of the rim have been observed in explanted liners (Tower et al., 2007; Furmanski et al., 2009; Furmanski et al., 2011). Qualitative and quantitative analyses of rim damage in explanted cups and liners provide information relating to the prevalence and severity of edge loading during implantation. Current CMM measurement techniques for the rim of explants are often of limited accuracy because they depend on best fit methods of the spherical bearing surface to estimate the original geometry of the component before implantation (section 2.4). The inner rim does not lie on the spherical bearing surface and the method therefore lacks accuracy in this region. Furthermore, defining an original rim geometry for UHMWPE components is challenging because of the creep and deformation experienced by the material during loading.

Alternatively, two dimensional contacting profilometry can be used to measure rim wear and deformation. The issues that arise with this method relate to aligning traces taken across the rim at unworn and worn regions so that a comparison between the two can be made.

This section describes the development and evaluation of a new method for measuring wear and deformation at the inner rim of simulator components and explanted liners using two dimensional contacting profilometry.

### **2.5.1 Materials**

The method was developed and evaluated in order to measure the liners from the hip simulator studies (Chapters 3 and 4) and the explant study (Chapter 5). Descriptions of these components can be found in sections 2.2.1, 3.2.1 and 4.2

(simulator components) and sections 2.2.2 and 5.2.2 (explants) and images and labelling conventions can be found in Appendix 1 and Appendix 5.

Three untested liners were used to validate the rim deformation measurement and analysis methodology (section 2.5.4). These were an untested non-aged 36mm diameter Gamma Vacuum Foil® Pinnacle® compatible liner (liner NA14; see section 2.2.1 for a description of the Pinnacle® liner), an untested 36mm diameter Marathon® Pinnacle® acetabular liner (liner AM11) and a BioloX® delta ceramic explanted Pinnacle® liner. The ceramic liner was a taper fit liner that mated with the same titanium shell as the UHMWPE liner. Liner AM11 was a soak control for a hip simulator test and therefore had been soaked in water for several months. Liner NA14 was unsoaked and untested. All liners were supplied by DePuy Synthes, UK.

### **2.5.2 Measurement Methods**

A two dimensional contacting profilometer (Talysurf, Taylor and Hobson, Leicester, UK) was used to obtain profile traces of the liner rims for both simulator samples and explants. For all traces, a 2µm diamond tipped recess stylus was used. The liners were positioned at an angle of approximately 45° to prevent collision of the stylus with the liner. Measurement points were 0.25µm apart.

For the liners from the simulator studies (Chapters 3 and 4), three traces were taken across the area of the rim that was edge loaded (Figure 2-10A). The liner was rotated by approximately 5°-10° between these traces. A fourth trace was taken across an unworn area of the rim (Figure 2-10B). The traces were 9mm to 12mm long and the exact length varied depending on the geometry of the cup but covered a section of the bearing surface, the chamfer and a section of the horizontal rim (Figure 2-10D). The colours in Figure 2-10 represent those used to plot the traces in Matlab in the following section (section 2.5).

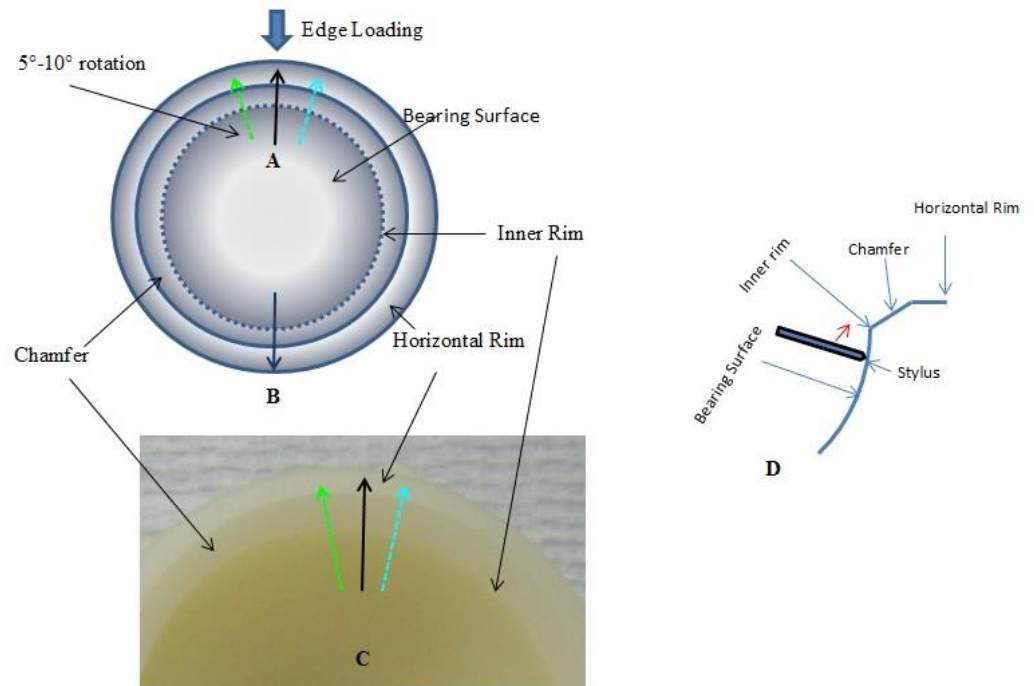


**Figure 2-10 Schematic of an acetabular liner showing the Talysurf traces taken from the bearing surface to the horizontal rim including: (A) three traces taken across the edge loaded region, (B) a fourth trace taken across an unworn region of the liner (the colours represent those used to plot the traces in Matlab in section 2.5.3) and (C) a photo of the liner showing the same traces in the schematic and (D) cross section of the rim showing where the stylus took the traces**

For the liners from the explant study (Chapter 5), rim traces were taken at 30° intervals around the circumference of the liners (Figure 2-11). The colours represent those used to plot the traces in Matlab (Section 2.5.3). The blue traces were the traces taken on the unworn side of the liner and the pink traces were taken across the worn side of the liner. This was identified from Redlux geometric reconstructions. The two cyan traces were taken across the anterior and posterior sections of the liner rim.

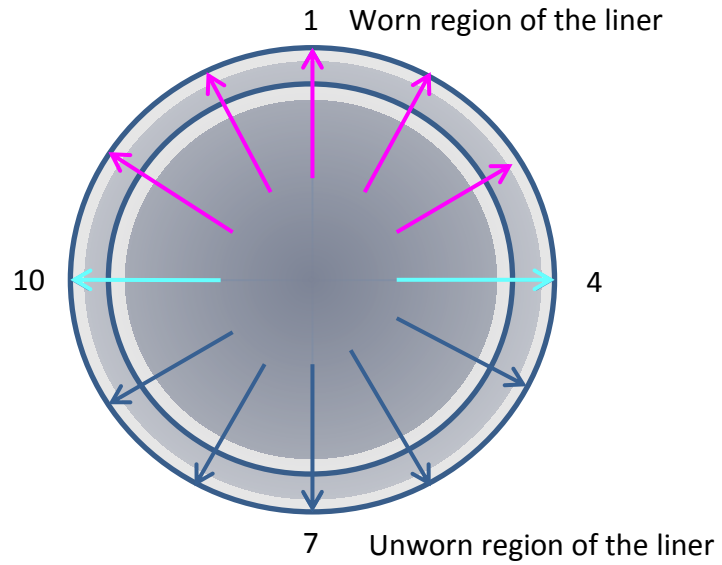


**Figure 2-11 Schematic of an explanted liner with the Talysurf traces taken at 30° intervals around the circumference of the liner. The colours are the same as those used to plot the traces in Matlab.**

Occasionally, a trace was omitted due to extensive damage to the liner in that region, which may have resulted in damage to the stylus (Figure 2-12).



**Figure 2-12 Example of an explanted acetabular liner with extensive damage to the rim. No talysurf traces were taken over the rim in this area to avoid damage to the stylus.**

### 2.5.3 Analysis Method

A Matlab (version R2014b, The MathWorks Inc, Natick, MA, USA) code was developed to plot and align profile traces taken across a worn region of a liner rim (worn trace) and an unworn region of a liner rim (unworn trace) and to calculate the rim deformation (penetration) at the region of edge loading. This was developed in collaboration with Dr Greg de Boer, who wrote the code. This section describes the Matlab code used to analyse the Talysurf traces of the liner rims. A protocol for using the code is provided in Appendix 4.

Measurement files with the x and z coordinates (y coordinate is fixed at 0) for the worn and unworn traces were exported from the Talysurf and converted to text files using Talymap Gold (Taylor Hobson, Leicester, UK). The text files with the data were then exported to Excel to be processed in Matlab.

For the simulator samples and most of the explants, the point at which the chamfer met the horizontal rim (Figure 2-10D) was unworn and not deformed by loading and could therefore be used as a reference point (datum) to align all of the traces along the same coordinates. The unscaled and unlevelled data for a simulator sample, as exported from excel, are shown in Figure 2-13 with the datum indicated.

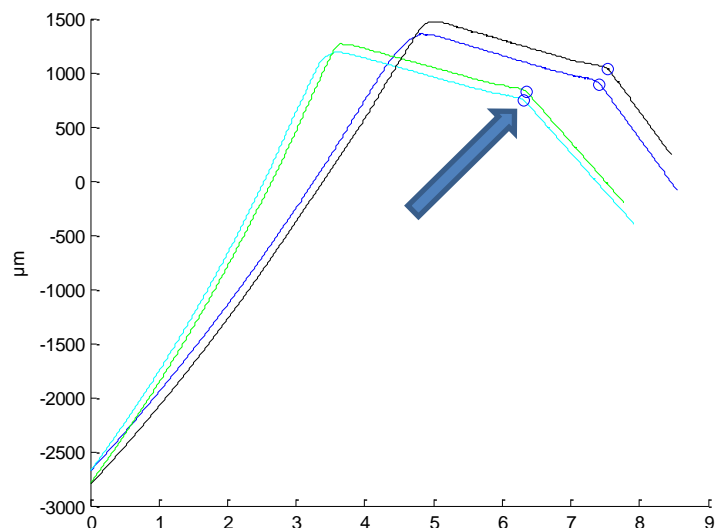


**Figure 2-13 Four Talysurf traces with the identified datum highlighted on each trace (Note: unworn trace = blue, worn traces = cyan, green and black; XLPE simulator liner, AM9).**

To identify the datum, the points on each trace were down-sampled to one in every hundred to reduce noise in the data. The Matlab code iterated along each x value starting on the horizontal rim and working towards the centre of the cup. The datum was identified as the point where the differences in the y values upstream were less than the differences in the y values downstream by a given tolerance (tol), where  $x_p, y_p$  is the current x, y location, r is 10 data points from p (defining the upstream and downstream regions) and  $y_{p+r}, y_{p-r}$  are the y values of the upstream and downstream regions respectively. Two cases where the constraint ( $y_{p+r} - y_p \leq \text{tol} (y_{p-r} - y_p)$ ) is and is not satisfied are shown in Figure 2-14.

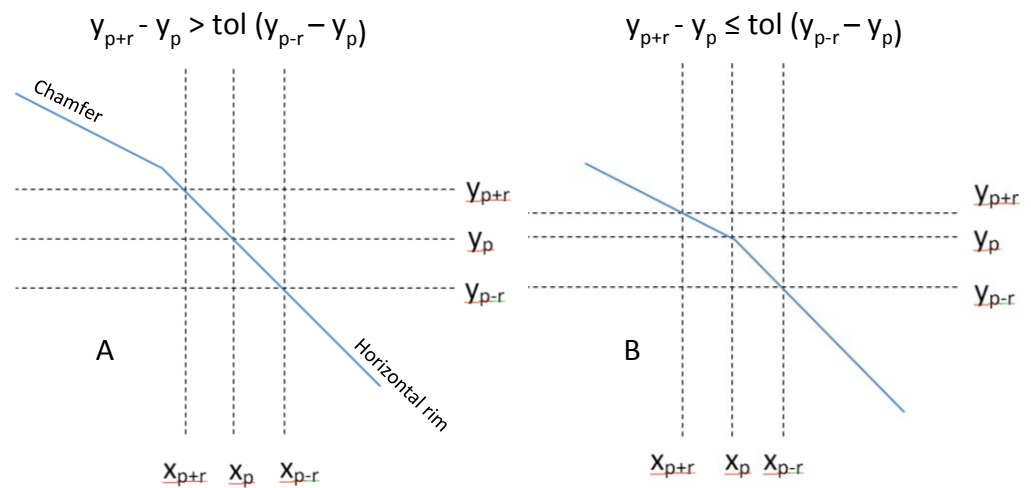


**Figure 2-14 Two cases where (A) the constraint was not satisfied and the datum was not identified at  $x_p$  and (B) the constraint was satisfied and the datum was identified at  $x_p$ . Note that the datum is identified before the traces are levelled.**

The default tolerance was 0.5 but it could be modified for each individual trace. Setting the wrong tolerance may result in the datum being identified at the inner rim or a small localised deformation such as a scratch (Figure 2-15).

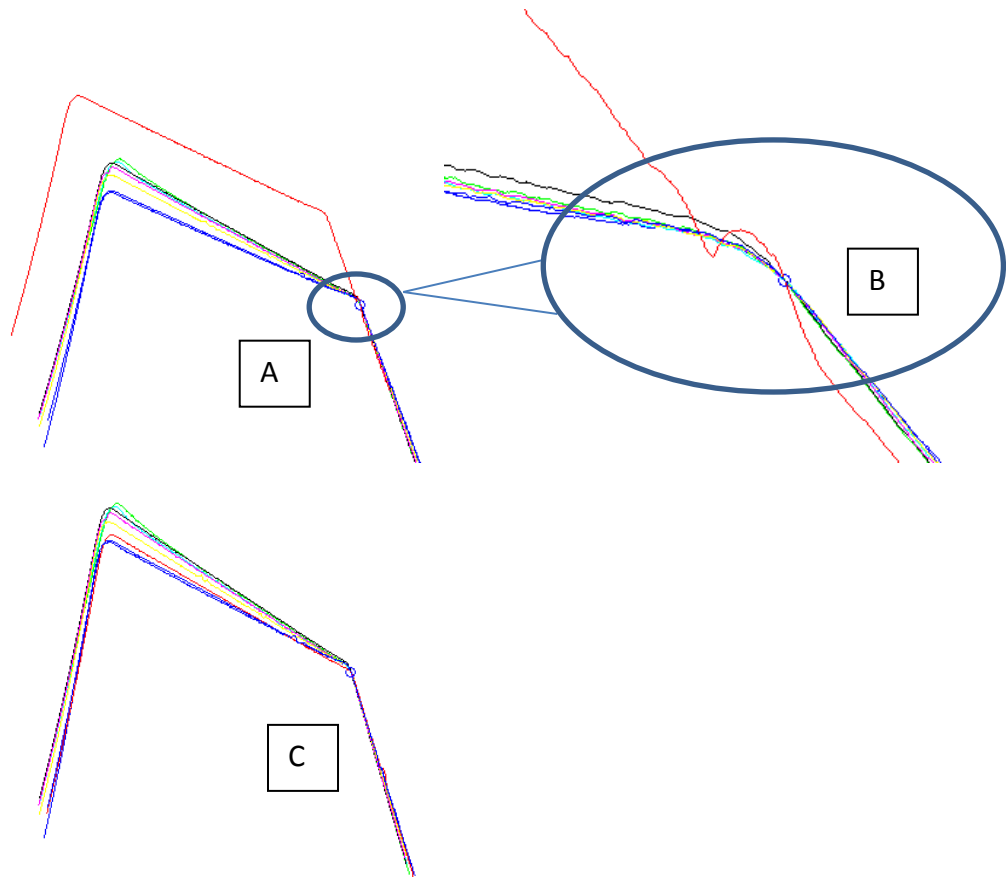


**Figure 2-15 Talysurf traces with an example of an explant with (A) a wrongly identified datum for one of the traces (red), (B) a close up of the scratch that caused the datum to be located in the wrong place and (C) correct identification of the datum after lowering the tolerance value (note that the traces have not been levelled yet).**

Following identification of the datum, the datum for each trace was matched. All of the worn traces were rotated about the datum to align with the unworn trace along the horizontal liner rim and then all traces were rotated to the horizontal plane (levelled) and scaled to plot both axes in mm (Figure 2-16).

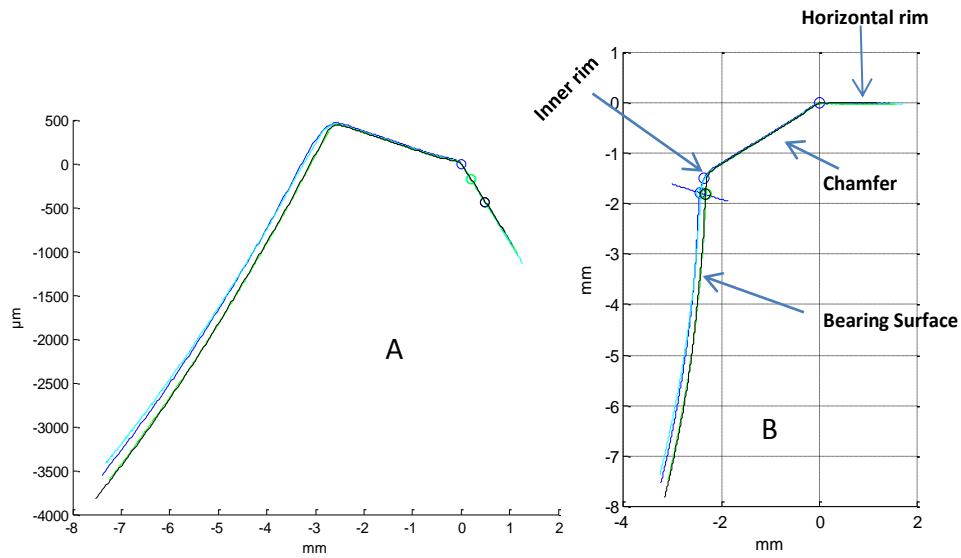


**Figure 2-16 Four Talysurf traces that have been (A) datum matched and rotated to align with the unworn trace along the horizontal rim and (B) rotated about the datum to the horizontal plane (levelled) and scaled to plot both axes in mm (Note: unworn trace = blue, worn traces = cyan, green and black; XLPE simulator liner, AM9)**

After alignment and levelling, finer adjustments were made to the tolerance if the datum was considered by the user to be inaccurately determined on any of the traces (Figure 2-17).

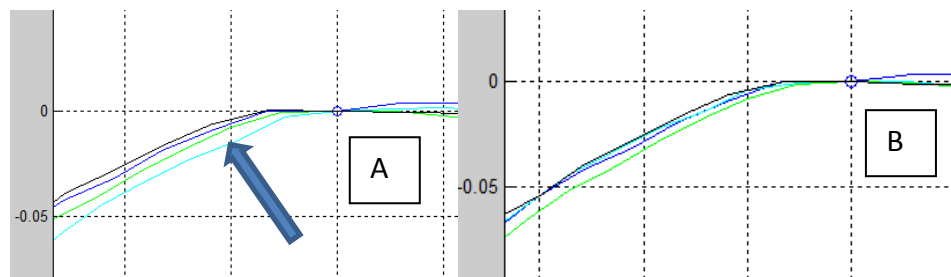


**Figure 2-17 The tolerance used to calculate the datum for the cyan trace was changed from (A) 0.5 to (B) 0.55 resulting in better alignment with the other traces (XLPE simulator liner, AM1).**

A point on the x axis of the unworn trace near the inner rim where edge loading occurred was selected by the user. The distance in mm between the unworn trace and the worn traces (penetration) was calculated normal to the unworn trace from this point (Figure 2-18). This point roughly corresponded with  $z = -1.8\text{mm}$  for the XLPE liners,  $z = -1.5\text{mm}$  for the aged PE liners and  $z = -1.8\text{mm}$  for the AOPE liners and cups. These values were selected because they were close to the inner rim but did not extend too far onto the articulating surface and were based on analysis of geometric mapping images to identify the most likely location of maximum penetration caused by edge loading. The penetration values were calculated by determining the tangential and normal directions of the unworn trace at the specified point, projecting a vector normal to the trace at this point and determining where it intercepted the worn traces and calculating the magnitude of the vector between the unworn and worn traces. The mean penetration between the unworn trace and each worn trace was calculated.

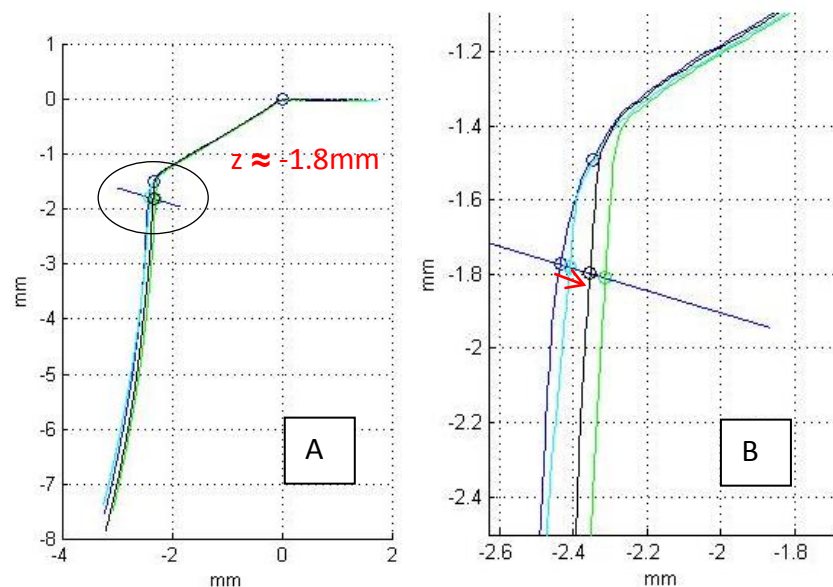


**Figure 2-18 Four Talysurf traces with (A) the location of the point from which the penetration was calculated and (B) a close up with a red arrow to mark the penetration distance between the unworn (dark blue) and worn traces (black, cyan, green; mean=0.07mm) normal to the unworn trace (XLPE simulator liner, AM9).**

### 2.5.4 Validation

For control liner NA14, a section of the inner rim was scraped away using a scalpel to replicate wear and/or deformation caused by edge loading. Three traces were taken across the region of the inner rim where the material was removed (worn traces) and three traces were taken across an intact region (unworn traces) of the rim as described in section 2.5.2. The liner was not rotated between traces on each side. The Matlab code correctly identified the datum and aligned the traces (Figure 2-19). Only very small variations between the points in traces of the same type (worn and unworn) were observed. The mean difference in worn and unworn traces just below the radius of curvature at the inner rim where the material was removed was 0.54mm. The mean difference on the chamfer above the area of material removal was 0.0076mm.

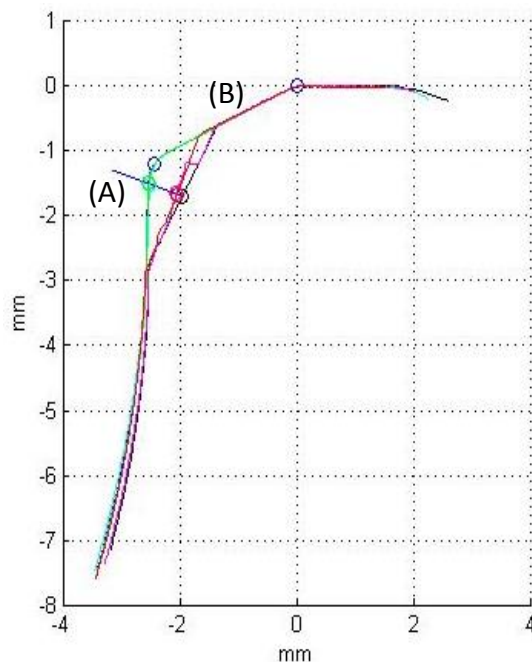


**Figure 2-19 Six Talysurf traces of untested liner NA14 with material removed at the inner rim. The blue, cyan and green traces were taken across an intact region of the rim and the black, magenta and red traces were taken across the region of the liner where the material was removed. (A) denotes the user defined data point where the distance between traces was calculated normal to the first unworn trace (0.54mm), (B) denotes the point where the distance between traces was calculated on the chamfer above the worn region (0.0076mm).**

For control liner AM11, traces were taken at 45° intervals around the entire circumference of the liner. The Matlab code correctly identified the datum and aligned the traces (Figure 2-20).

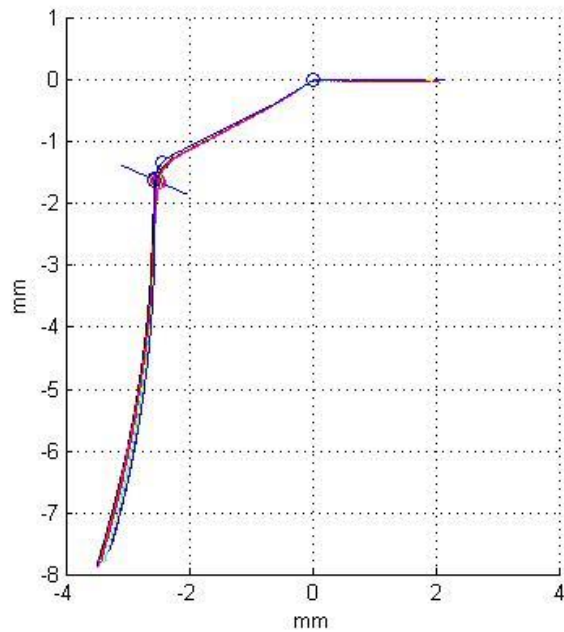


**Figure 2-20 Eight Talysurf traces taken at 45° intervals around the circumference of untested liner AM11**

A difference in the gradient of the chamfer was observed between separate traces for control liner AM11 (Figure 2-21). As the liner is unworn and the datum appeared to have been correctly identified, this may have been due to deformation during the manufacturing process or as a result of marginal differences when setting the liner up between each trace after rotating the liner (a small tilt in the liner on set-up may result in a slightly longer/shorter trace length in the chamfer region and therefore a difference in gradient and misalignment at the inner rim). The mean difference between the traces at  $z=-1.6\text{mm}$  was  $0.04\text{mm}$ .

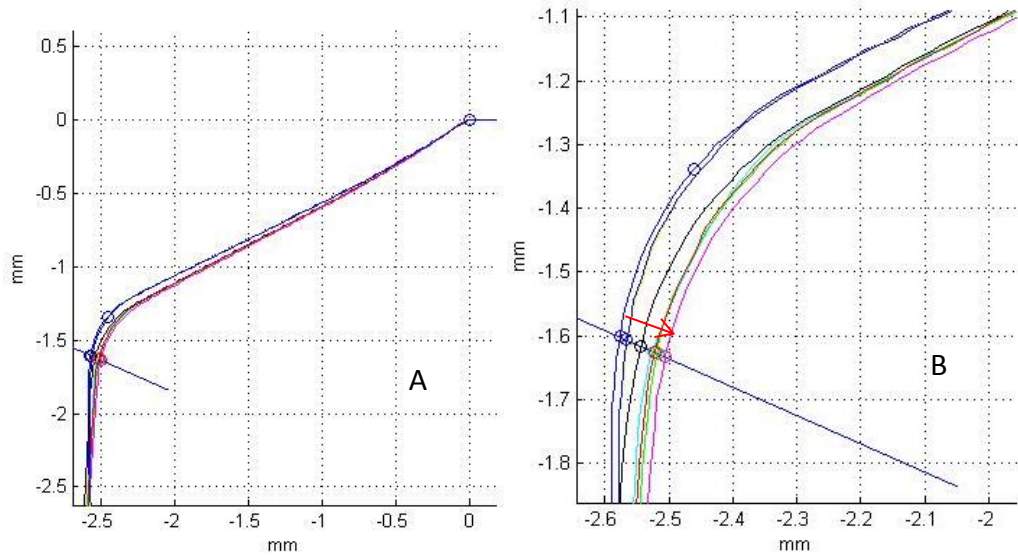


**Figure 2-21 (A) A close up of the eight Talysurf traces taken at 45° intervals around the circumference of control liner AM11 showing how a difference in gradient along the length of the chamfer resulted in a misaligned trace at the inner rim and (B) a close up of the inner rim showing a mean difference of 0.04mm between traces.**

To investigate this further and to minimise the effect of UHMWPE deformation and manufacturing tolerances, six traces were taken across the rim of a ceramic liner by Jack Davies, an MSc student: three across a known area of rim wear and three across an unworn region of the rim. The liner was rotated between traces (Figure 2-22).

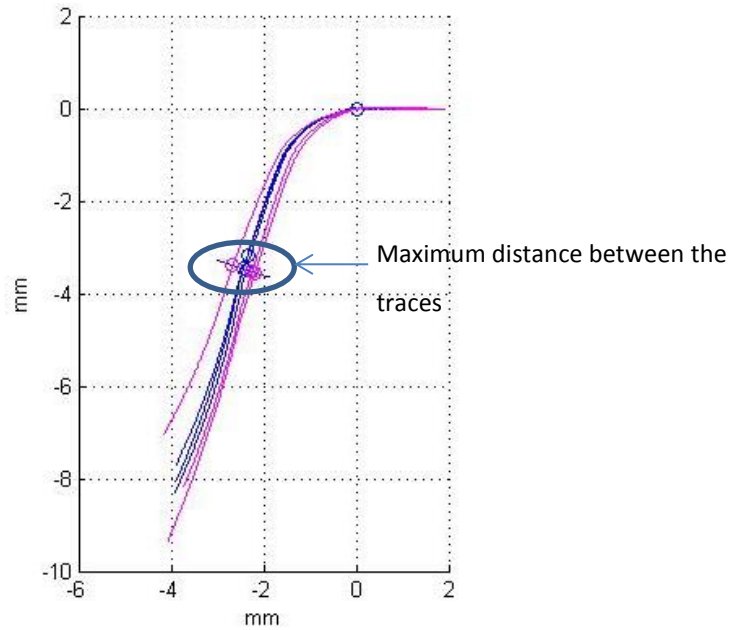


**Figure 2-22 Six traces taken across the rim of a ceramic liner. Three across a worn region of the liner (pink) and three across an unworn region (blue)**

The maximum distance between the six traces at a selected point for the ceramic liner was 0.27mm. Two further traces were repeated on the ceramic liner. These traces were taken across the same unworn region of the liner. The stylus was raised and replaced between traces but the liner was not moved. The difference between the traces was much smaller than when the liner was moved and rotated (0.00083mm; Figure 2-23).

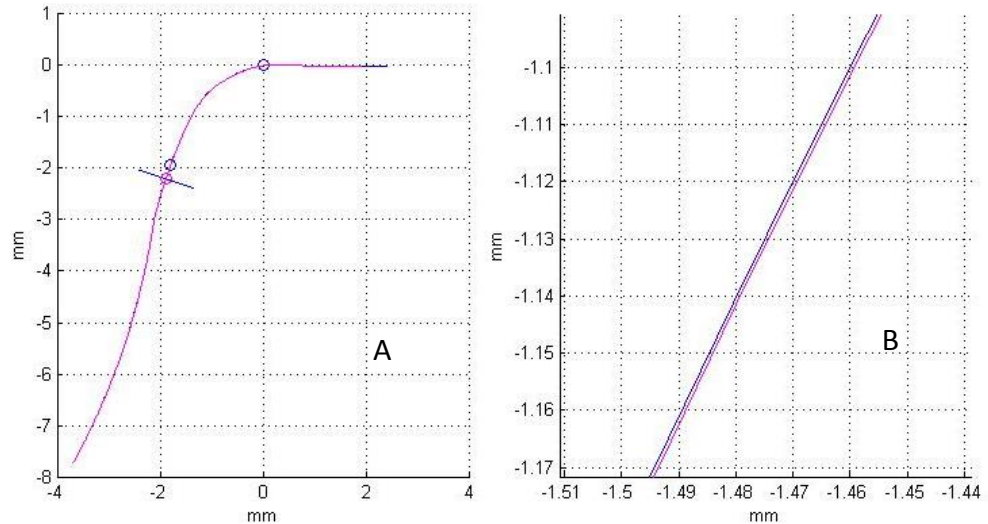


**Figure 2-23 Two Talysurf traces across the same region of a ceramic liner (without moving the liner between traces) showing (A) a full plot of the two traces and (B) a close up of the traces showing a distance between the two of 0.00083mm**

### 2.5.5 Discussion and Conclusion

A method has been developed to measure and analyse rim deformation on UHMWPE liners. Limitations to determining the penetration distance at the inner rim were identified. A difference in gradient and therefore a misalignment at the inner rim was observed for both the UHMWPE rims and the ceramic rims. When the ceramic rims were measured, a difference in gradient was observed when the liners were moved between traces but it was much smaller when the liners were not moved between traces. Unlike UHMWPE, ceramic liners do not deform and any rim wear in the liners would be significantly smaller than the distance observed between the traces in this study (Al-Hajjar et al. 2013). It was therefore concluded that the difference between the traces was mostly a result of variations in set-up positioning rather than deformation of the UHMWPE. Further work, to improve the measurement technique would be required for future development of the methodology. A fixture that allowed rotation of the liner without having to remove and replace it between traces may prevent misalignment of the liners when taking

measurements. However, this fixture would need to accommodate a range of acetabular liner shapes and sizes.

Despite the limitations of the method in accurately determining penetration, the Matlab code also allowed visual inspection of the shape of the inner rim following edge loading. For the purposes of this study, it was suggested that rim wear and deformation for UHMWPE acetabular components can be effectively analysed using a combination of quantitative (penetration values) and qualitative (shape of inner rim) methods.

## **2.6 Development of Subsurface Analysis using MicroCT**

### **2.6.1 Introduction**

Cracking and fatigue fracture has been observed in explanted acetabular liners (Bradford et al., 2004; Tower et al., 2007; Furmanski et al., 2009; Furmanski et al., 2011), particularly around the superior rim region. Understanding crack propagation and initiation in UHMWPE components is important to understanding liner failure and informing liner design.

Various methods such as CMM and stereomicroscopy have been used to measure and assess damage in explanted liners but have various limitations. Extensive surface cracking and damage can be measured by CMM techniques but it is not possible to measure subsurface cracking in this way. Stereomicroscopy with transillumination has been used to study subsurface cracking in UHMWPE liners but this method does not accurately detect and measure smaller cracks (Birman et al., 2005). Ong & Sa (1998) described an ultrasonic crack detection method but reported poor image resolution. Scanning electron microscopy (SEM) has successfully been used to measure subsurface damage in UHMWPE components with good resolution and image quality (Furmanski et al., 2009; Furmanski et al., 2011; Pruitt et al., 2013) However, this method is destructive.

Non-destructive methods are desirable when analysing explants so that further analyses can be performed in the future and to avoid any of the legal/ethical implications that may arise with destructively testing explanted liners.

Teeter et al. (2010) described a non-destructive microCT method with high image resolution (50  $\mu\text{m}$ ) to quantify subsurface cracking in explanted tibial inserts. Similar methods have been used by other researchers to analyse subsurface cracking in total joint components at up to 18 $\mu\text{m}$  resolution (Kurtz et al. 2007).

A non-destructive microCT method was developed in this study to create 2D reconstructions of subsurface cracking with a higher resolution (10 $\mu\text{m}$ ) than previously reported techniques. Previously reported methods using microCT at lower resolutions have described subsurface cracking in explanted acetabular liners. The method described in this study compared explanted acetabular liners with simulator samples, which to the author's knowledge has not been previously reported. Dr Nagitha Wijayathunga assisted with the scans.

### **2.6.2 Materials**

Three untested liners from each material group in the simulator tests were selected as control liners for the subsurface analysis methodology: an XLPE Pinnacle<sup>®</sup> liner, a GVF Pinnacle<sup>®</sup> compatible liner (chapter 3) and an AOPE Pinnacle<sup>®</sup> compatible liner (chapter 4). It was not possible to scan the AOPE compression moulded cups because the different density of the titanium shells would inhibit visualisation of the UHMWPE.

For the simulator tests and explant study, a selection of liners for each material was scanned. This was because of time constraints arising from the length of time required to perform the scan and subsequent reconstruction. However, based on initial visual observations, it is believed that the liners selected were representative of the whole set for each material. The details of the liners that were scanned are outlined in the materials section of the relevant chapters.

### **2.6.3 Methods**

Components were imaged using a micro-computed tomography scanner (MicroCT;  $\mu\text{CT}100$ , Scanco Medical AG, Brüttisellen, Switzerland). A bespoke fixture for the liners was constructed to fit into the 73mm machine sample containers (Figure 2-24A). This was marked on one side to ensure the orientation was the same for all liners. The scan was carried out at 55kV and 72 $\mu\text{A}$  with an integration

time of 400s. A 2D reconstruction of the stacked images was completed using built-in software and an image resolution of  $10\mu\text{m}$  was obtained (Figure 2-24B). The images were converted to .TIF files and viewed using ImageJ (Version 1.49, National Institute for Health, USA).

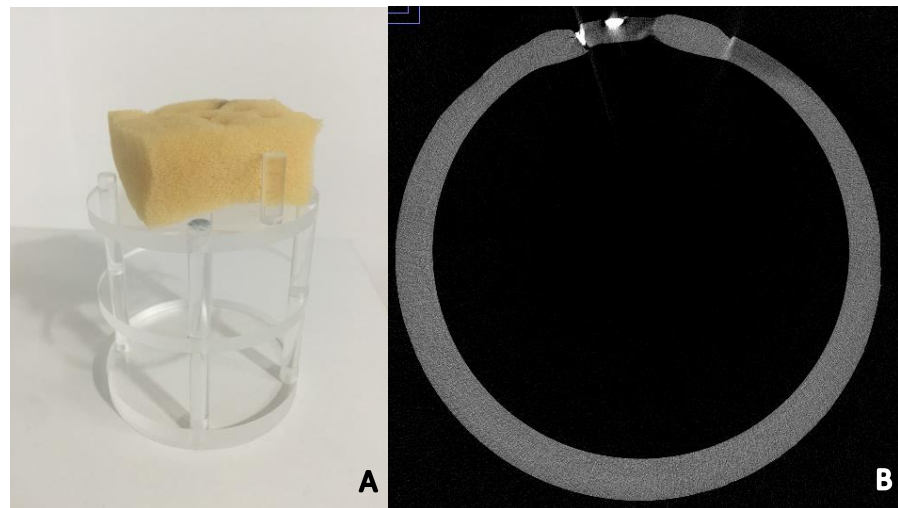


**Figure 2-24 (A) A fixture for acetabular liners designed to fit the 73mm MicroCT sample holder with 3 tiers allowing multiple liners to be loaded at one time (sponge used to hold samples in place) and (B) a MicroCT image of an explanted acetabular liner with damage in the superior rim region. The view is of a  $10\mu\text{m}$  2D reconstruction and looks down onto a cross section of the rim.**

Initial scans were made of the whole liner for the control liners and for one tested liner of each different material subset (XLPE liner, Aged PE liner, AOPE liner and explanted liner). Subsequent scans were made of the superior region only, encompassing the rim and extending approximately 20-25mm (depending on the size of the liner) towards the apex, to reduce reconstruction time (Figure 2-25). The scan region was identified as the area of interest from the initial full size scans. The results of the scans of the tested liners and explants are presented in each relevant chapter. The results of the scans of the control liners are presented here.

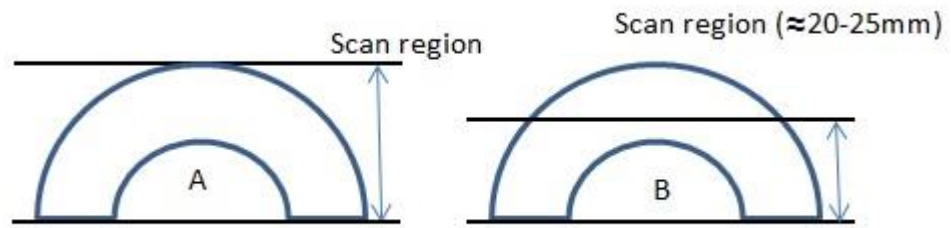


**Figure 2-25 (A) Initial scans for each type of material were made of the whole liner and (B) subsequent scans were of a reduced scan region measuring approximately 20-25mm from the horizontal rim towards the apex of the liner.**

Each 10  $\mu\text{m}$  slice was viewed sequentially from the surface of the rim moving down towards the apex of the liner. Initially, 1 in every 50 slices was viewed. Adjoining slices were then viewed to inspect any features of interested in more detail, particularly in the rim region. The approximate distance of each slice from the horizontal liner rim was calculated by counting the number of slices. The slices were inspected for micro-cracking and other subsurface damage. For the purposes of this study, micro-cracking was defined as cracks smaller than 1mm and subsurface damage was defined as cracks larger then 1mm.

#### **2.6.4 Results**

This section provides the results of the microCT scans of the control liners. The results of the scans for the other liners (simulator liners and explants) are given in each relevant chapter (sections 3.4.2, 4.4.2 and 5.3.1).

No identifiable subsurface micro-cracking or visible subsurface damage was observed in any of the control liners (Figure 2-26). Small, infrequent voids were observed in the material for all control liners (Figure 2-27A). These were observed throughout the material and were rarely observed over more than one slice (10 $\mu\text{m}$ ). A wrinkle effect was observed in all of the liners (Figure 2-27B). This was observed at various depths from the horizontal surface of the liner for all of the control liners.

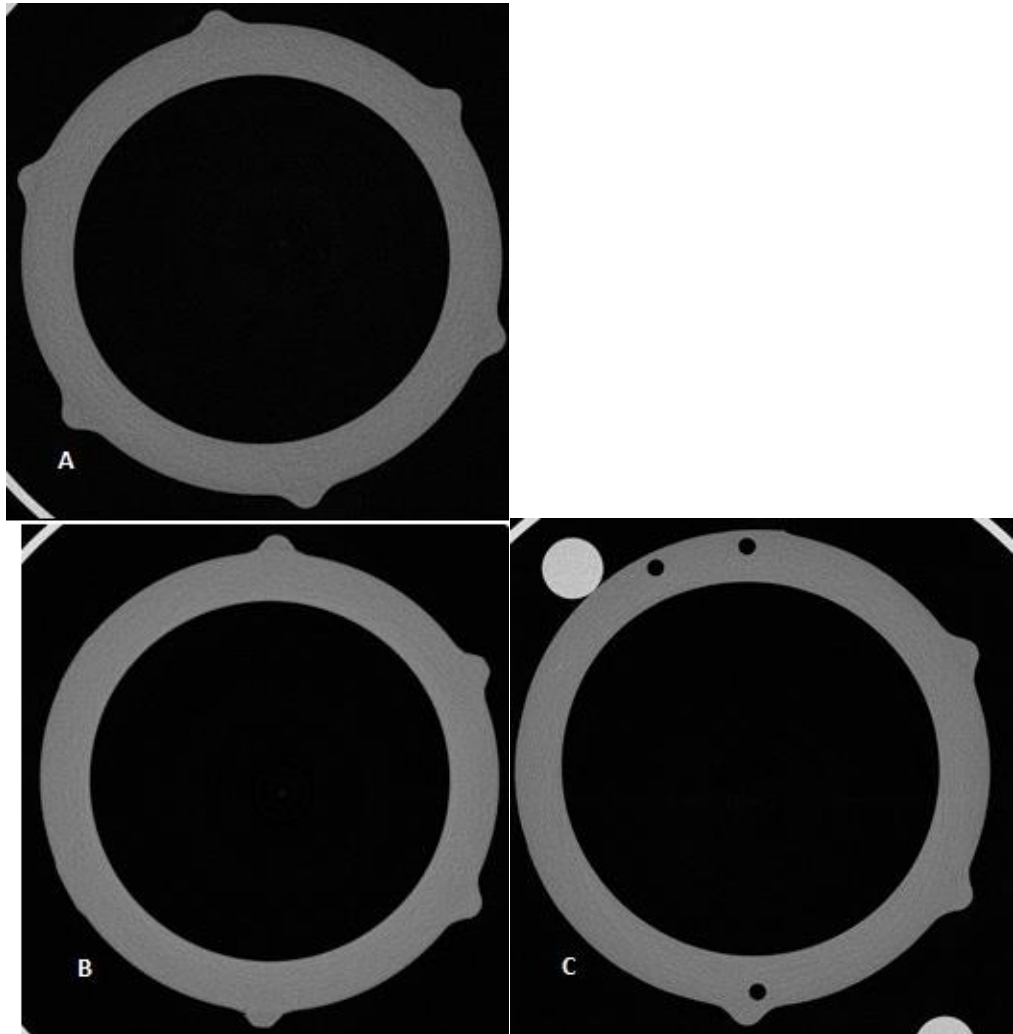
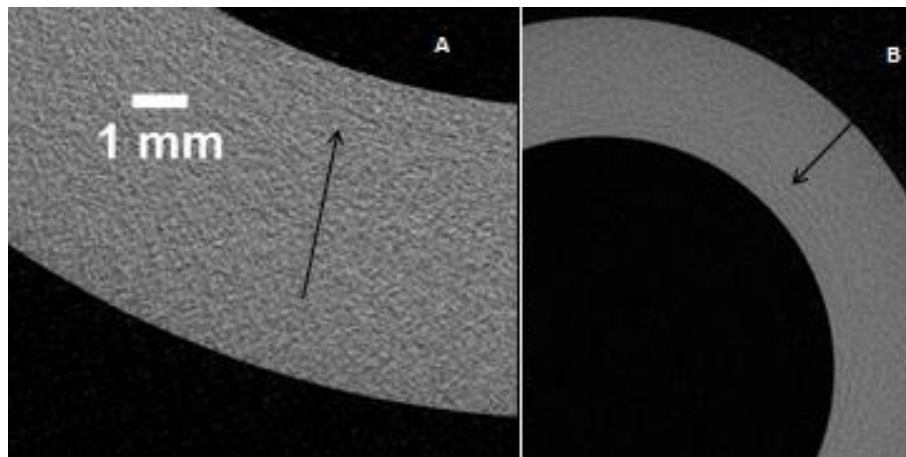


Figure 2-26 MicroCT images of (A) an XLPE control liner, (B) an aged PE liner and (C) an AOPE liner



**Figure 2-27 MicroCT images of the AOPE control liner with (A) a void in the material and (B) a wrinkle effect around the inner rim**

### **2.6.5 Discussion and Conclusion**

Identifying subsurface micro-cracking and damage in simulator samples and explants may allow potential fatigue failure mechanisms in UHMWPE acetabular liners to be identified and the effects of edge loading to be better understood.

The MicroCT method for analysing subsurface damage to liners used in this study achieved a resolution of 10 $\mu$ m, which is higher than existing methods described in the literature (Bowden et al. 2005; Kurtz et al. 2007; Teeter et al. 2010). It was therefore possible to observe features in the material that were too small to observe in previously described methods. Three control liners have been scanned that can be used as a comparison to help identify damage sustained by liners in simulators and during implantation.

The method had some limitations. Firstly, it relied on an observer individually checking up to 2000 microCT slices. Observer fatigue may result in misidentification of features such as micro-cracking or result in certain features being missed. This was minimised by reducing the size of the scan after the area of interest was identified from full scans.

Furthermore, very small cracks may not be easily distinguished from the surrounding material and therefore may not be identified by the observer. The control liners all exhibited small voids in the material. These are most likely created during the manufacture of the components, either during consolidation of the material or during machining of the liner. In practice it would be difficult to distinguish these voids from very small micro-cracks and therefore the method may require refining to enhance the appearance of micro-cracking and subsurface damage. Further to this, subsurface damage and cracks are only visible in microCT scans where a void is present between either sides of the crack. If the material was pushed together, it may not be visible on microCT images and therefore not all cracks would be visible. A key area of development would be to determine the sensitivity of this method for identifying micro-cracking.

A wrinkle effect was observed on all of the control liners. This may have been deformation of the material but as it was observed in untested and never-implanted control liners, it was thought that this was more likely a reconstruction artefact of the scanner. These artefacts and other reconstruction artefacts may inhibit observation of subsurface damage.

Despite the limitations, the method can be used to non-destructively analyse simulator liners and explants for larger macro-sized subsurface cracking and damage resulting from adverse loading conditions such as edge loading. Some development is required for micro-analysis of cracking.

## **2.7 General Equipment Calibration**

All laboratory equipment is calibrated and serviced yearly by service engineers. In addition to this, the following calibration and verification steps were performed on measurement and testing equipment.

For the CMM measurements, a 20mm ceramic masterball supplied by the manufacturer (Mitutuyo, Halifax, UK) was used to calibrate the machine before each use and after each probe change. The deviation in probe dimensions was checked and accepted for values less than 2 $\mu$ m.

For two dimensional contacting profilometry measurements, a 22mm stainless steel hemisphere supplied by the manufacturer (Taylor Hobson, Leicester, UK) was used to calibrate the stylus at each change. Calibration verification was performed before every use with a  $0.8\mu\text{m} \pm 0.05 \text{ Ra}$  standard (Taylor Hobson, Leicester, UK). This verified the equipment calibration and monitored the stylus condition.

For the gravimetric measurements, correct functioning of the balance was verified by measuring a metal component of a known weight.

## **2.8 Conclusion**

This chapter described standard and previously validated methods to measure volume change and damage in simulator components. In addition, new methods to measure and analyse volume change, damage and deformation in simulator samples and explanted acetabular liners were developed to be used in combination with existing standard methods in both simulator studies and explant studies. Both simulator samples and explants were used in the development of these new methods and the methods are in applied subsequent chapters in this project.

## Chapter 3: Hip Simulator Edge Loading Protocol Development Study

### 3.1 Introduction

Total hip replacements (THR) comprising of an ultra-high molecular weight polyethylene (UHMWPE) acetabular cup are widely implanted and generally regarded as successful (National Joint Registry, 2014). Historically, wear debris from these components was identified as one of the primary factors leading to aseptic loosening and the long term failure of these prostheses (Revell et al., 1997; Tipper et al., 2000; Ingham and Fisher, 2000). Conventional UHMWPE irradiated in air to sterilise the UHMWPE, was subject to oxidative degradation and ageing that not only increased surface wear but also made components susceptible to fatigue damage (Collier et al. 1996; Kurtz et al. 2006; Currier 2007; Mayor et al. 2008). Introduced in the year 2000, highly crosslinked UHMWPE cups with improved wear resistance were developed to reduce the volume of wear particles produced. Most importantly the manufacturing process of these materials also involved annealing or heat treatment above the melting temperature after irradiation to recombine free radicals and to stabilise the materials. Gamma irradiation doses of between 50kGy and 100kGy are used in the processing of crosslinked UHMWPE, this promotes crosslinking and increases wear resistance, and these are combined with various heat treatment protocols. Increased cross linking produces a corresponding decrease in ductility and fatigue crack propagation resistance of the UHMWPE (McKellop et al., 1999; Muratoglu et al., 1999). Over time further degradation may also occur. There have been reports of crosslinked acetabular liners being susceptible to rim fracture in vivo, particularly where liner designs or biomechanical conditions lead to stress concentrations from notched locking mechanisms and/or thin UHMWPE at the rim (Birman et al., 2005; Tower et al., 2007; Currier, 2007; Furmanski et al., 2009). Furthermore, an increasing radiation dose and a greater degree of crosslinking produce free radicals in the material and increase the oxidation potential. Acetabular components that have degraded through oxidation are more susceptible to wear and fatigue failure (Collier et al. 1996; Currier 2007; Kurtz et al. 2006; Currier et al. 2007). Recent studies have

reported in vivo oxidation of crosslinked components (Muratoglu et al., 1999; Baker et al., 1999; Currier et al., 2013; Kurtz et al., 2014). Initial reports on the clinical performance of these materials in terms of wear resistance have been favourable but the performance under more severe conditions such as edge loading or impingement has not been widely reported and has therefore yet to be fully determined.

Prior to clinical use, new hip replacement designs and materials are required to be tested in vitro on hip simulators to mimic aspects of the in vivo service of the hip replacement. Current ISO standards for hip simulator wear testing of THRs recommend loading and motion parameters that represent a standard walking cycle for correctly positioned prostheses with no degradation of the materials (Fisher et al. 2012; BS ISO 14242:2002). This does not consider many aspects of the highly variable kinematics and biomechanics of in vivo service of the THR that are apparent, for example, gait studies have revealed that THRs are subjected to elevated loads (eight times body weight in stumbling) and retrieval studies demonstrate that UHMWPE cups experience edge loading and impingement *in vivo* (Bergmann et al., 1995; Bergmann et al., 2004; Birman et al., 2005; Shon et al., 2005; Usrey et al., 2006; Duffy et al., 2009; Marchetti et al., 2011). Edge loading can result from non-optimal component positioning, the cup may be steeply inclined or the head and cup centres mismatched (Nevelos et al. 2000; Stewart et al. 2001; Leslie et al. 2009; Al-Hajjar et al. 2010; Al-Hajjar et al. 2013; Al-Hajjar et al. 2013). Fluoroscopy studies have revealed that such conditions can result in a separation of the head and cup in vivo leading to edge loading of the liner rim (Dennis et al., 2001; Komistek et al., 2002).

The aim of this study was to develop and evaluate a hip simulator edge loading protocol to determine the wear and fatigue behaviour of UHMWPE acetabular components in total hip replacement using aged PE liners as positive controls and XLPE liners as negative controls. Edge loading of UHMWPE liners where mechanical properties have been modified by the material processing and by oxidation and ageing may lead to early failure of the components. It is therefore appropriate to consider a positive control that involves ageing (and has shown

fatigue failure *in vivo*) in the evaluation of a new hip simulator method alongside a currently produced material as a negative control.

The study had the following objectives:

- Assess the wear and deformation of moderately crosslinked UHMWPE acetabular liners under standard and edge loading hip simulator conditions as a negative control and compare to aged UHMWPE liners as a positive control;
- Assess the rim deformation and subsurface damage to moderately crosslinked UHMWPE liners under edge loading conditions as a negative control and compare to aged UHMWPE liners as a positive control;

## **3.2 Materials and Methods**

The following sections describe the materials that were assessed and the testing and measurement methods that were specific to the edge loading protocol development study. General methods are described in Chapter 2.

### **3.2.1 Materials**

Two different types of 36mm diameter UHMWPE liner that were part of or compatible with the modular Pinnacle® total hip replacement system (DePuy Synthes, UK) were assessed. The Pinnacle® compatible design comprised a 56mm outer diameter titanium shell and a press fit 36mm inner diameter anti-oxidant UHMWPE liner with taper lock and anti-rotation device (ARD) tabs that mate with scallops on the titanium shell. The liner thickness was 7.8mm at the apex and 5.1mm at the rim.

The two types of UHMWPE studied were: Marathon®, a moderately crosslinked UHMWPE (XLPE; n=4) and an aged Gamma Vacuum Foil® UHMWPE (aged PE; n=4).

The XLPE liners were manufactured from GUR 1050 UHMWPE resin, gamma irradiated at 5Mrad and re-melted. These liners were commercially available as part of the Pinnacle® hip system.

The aged PE liners were manufactured from GUR 1020 UHMWPE resin, gamma irradiated at 2.5Mrad for sterilisation purposes and packaged in an inert environment. These liners subsequently underwent an accelerated ageing process (ASTM F2003-02(2015)) whereby they were exposed to 70° and 70psi in oxygen for two weeks to replicate ageing and oxidation of the material. The aged PE liners were compatible with the Pinnacle® acetabular shell.

All liners articulated against 36mm cobalt chromium femoral heads (DePuy Synthes, UK). The UHMWPE density was 0.934 g/cm<sup>3</sup>. The details of all the components are outlined in Table 9. Further details of the test components, reference and lot numbers and labelling are provided in Appendix 1.

**Table 9 Details of the acetabular liners, femoral heads, sample sizes and labelling convention of the edge loading protocol development tests**

| Cup   | Head  | n | Liner Labelling          |
|---|---|---|--------------------------|
| Marathon® UHMWPE<br>Pinnacle® liner (DePuy<br>Synthes Ltd)                                    | 36mm CoCr Articul/eze®<br>femoral head<br>(DePuy Synthes Ltd) | 4 | AM1<br>AM5<br>AM7<br>AM9 |
| GVF UHMWPE Pinnacle®<br>liner. Aged at 70psi and<br>70°C for two weeks<br>(DePuy Synthes Ltd) | 36mm CoCr Articul/eze®<br>femoral head<br>(DePuy Synthes Ltd) | 4 | A2<br>A4<br>A6<br>A10    |

A barb located around the circumference of the liners was removed prior to testing. Failure to remove this would have resulted in the barb detaching from the liner on removal from the shell at the first measurement point and influencing the gravimetric data.

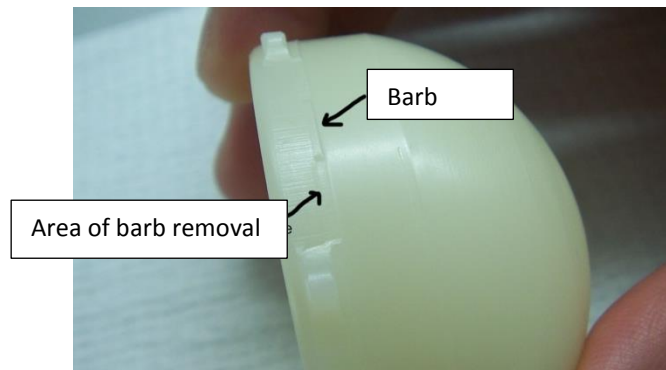


**Figure 3-1 Photo of an acetabular liner showing the barb around the circumference of the liner**

### **3.3 Methods**

#### **3.3.1 Simulator Set-up**

A ten station Prosim pneumatic hip joint simulator (Simulation Solutions Ltd, UK) was used in this study (Figure 3-2). A simulator station comprised a femoral head and acetabular cup positioned anatomically and surrounded by a silicone gaiter containing lubricating fluid.



**Figure 3-2 Group 1 of the Prosim ten station hip joint simulator showing five stations with serum in gaiters surrounding the joint interface.**

The titanium shells were mounted in the simulator cup holders using PMMA resin, so it was possible to remove the liners from the shells at each measurement point (Figure 3-3).

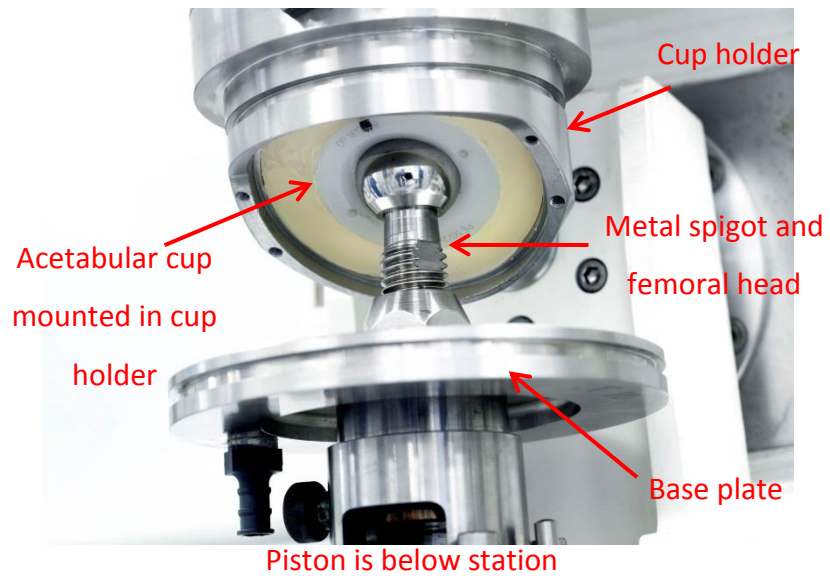


**Figure 3-3 Single station on the Prosim simulator. The testing set-up is shown with the femoral head mounted on the metal spigot and the acetabular cup cemented into the simulator mount (note the image depicts a cemented cup rather than a shell and liner. The shells were cemented into the holder in the present study).**

A hole and a screw in the back of both the simulator cup holder and the titanium shell allowed the UHMWPE liner to be pushed from behind to remove it from the shell at measurement points. A small UHMWPE tab was placed in the hole in the titanium shell to protect the liner from damage.



**Figure 3-4 The backside of a titanium shell showing the hole through which the liner was pushed out by a screw at measurement points.**

The cups were mounted in the cup holders at 35° to the horizontal, which is the equivalent of 45° *in vivo* as the loading was applied along the vertical axis (upwards from the piston below each station). Clinically the direction of the joint reaction force during stance phase is 10° medial, 55° to the face of the cup. For a force applied vertically on the simulator, altering the inclination angle to 35° preserved the 55° angle between the joint reaction force and cup face and replicated the clinical situation (Figure 3-5). The clinical inclination angle of 45° was selected as this is currently the most cited safe range for cup inclination angles *in vivo* and is commonly recommended by orthopaedic manufacturers (Lewinnek et al., 1978).

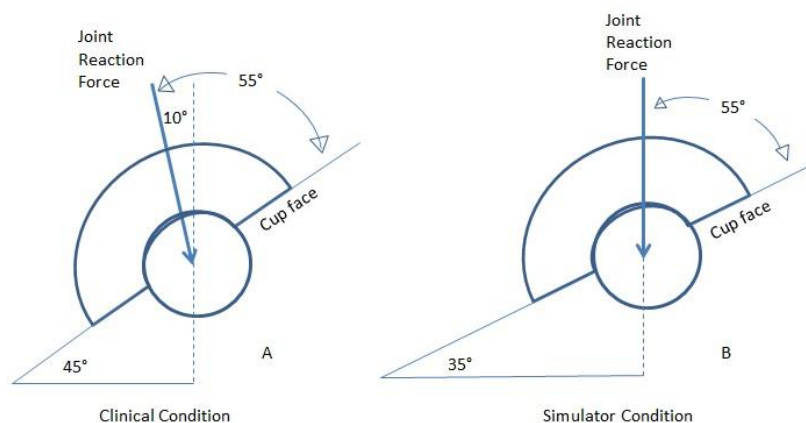


**Figure 3-5 Schematic of an acetabular cup and femoral head showing (A) the joint reaction force during stance phase in the clinical conditions with the cup at 45° and (B) the joint reaction force in the simulator conditions with the cup angle at 35° (Adapted from Williams et al. 2008)**

The femoral heads were mounted by means of a taper on a stainless steel spigot and alignment marks on the head and spigot allowed them to be removed and replaced in the same position at each measurement point if required. The centre of rotation of the femoral head was set to match the centre of rotation of the machine by a technician and the cup holder was adjusted so that the acetabular liner sat on top of the head.

A silicone gaiter was placed around the femoral head and acetabular cup and held in place with a metal clip and was filled with lubricant during the test.

A schematic of a single station of the Prosim hip simulator is shown in Figure 3-6 (acknowledgement: Philippa Clarkson).

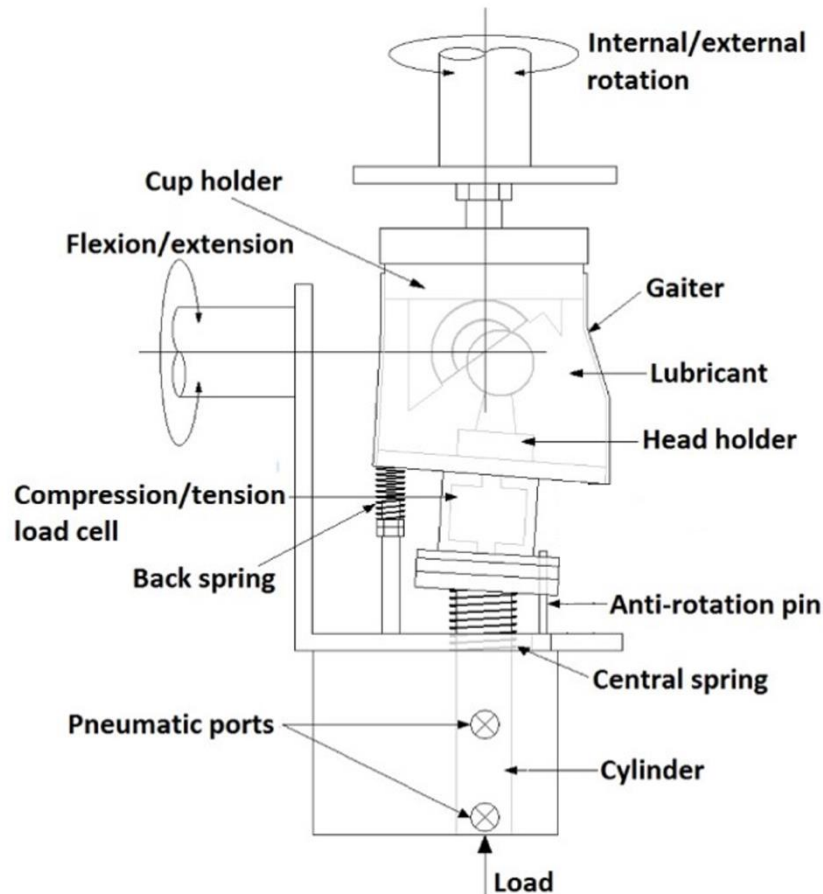


**Figure 3-6 Schematic of a side view of a single station of the Prosim hip simulator with the set-up for edge loading conditions. A back spring pushed the femoral head laterally during the swing phase of gait causing the femoral head to contact with the acetabular rim on heel strike (lateral sliding distance 0.5mm-1mm)**

### **3.3.2 Standard and Edge Loading Conditions**

For both standard and edge loading conditions, a twin peak time dependant loading curve was applied through the vertical axis with a maximum load of 3000N at heel strike and a minimum load of 300N in the swing phase (Figure 3-7). Two motions were applied to each station: the head underwent a flexion/extension

motion of  $+30^\circ$  to  $-15^\circ$  and the cup underwent an internal/external rotation motion of  $\pm 10^\circ$ . The motions were applied  $90^\circ$  out of phase to create an open elliptical wear track. This has previously been shown to give wear results comparable to a three axis physiological simulator under standard walking gait conditions (Barbour et al., 1999). The simulator was run at 1Hz. During edge loading conditions, a microseparation of the femoral head and the acetabular cup occurred during swing phase, causing the femoral head to strike the acetabular rim on heel strike and relocate during stance phase.

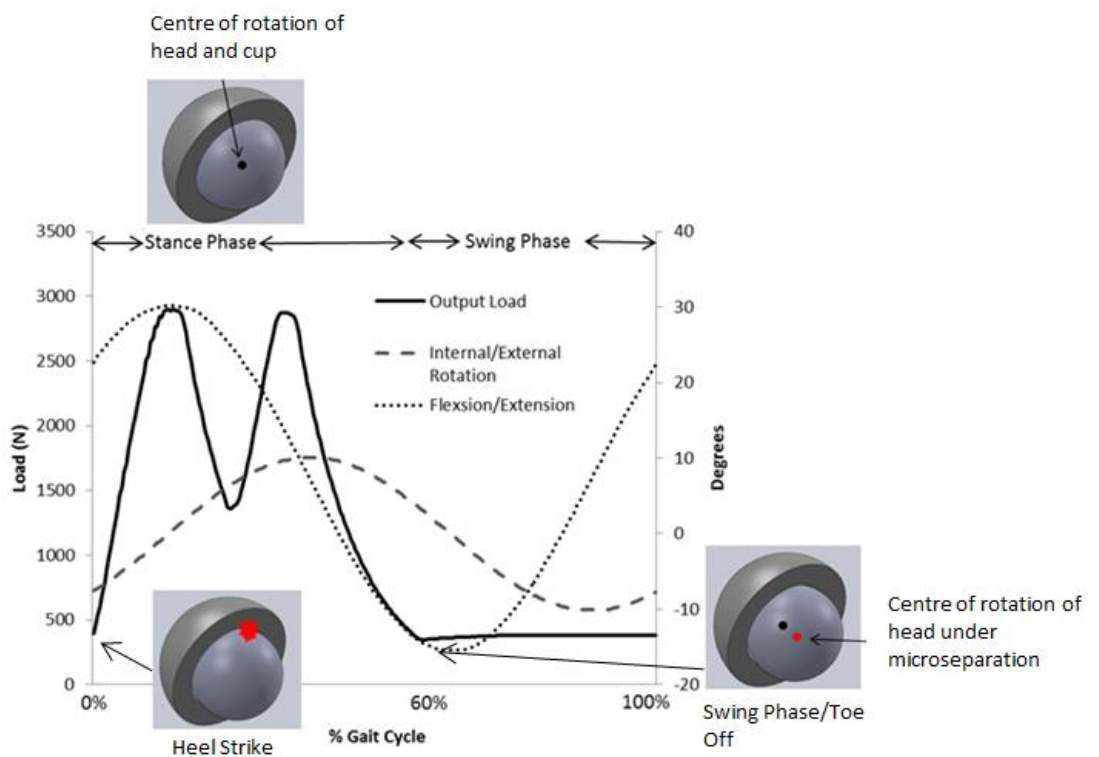


**Figure 3-7 Load and motion output profiles for one cycle of gait with the femoral head position highlighted for heel strike, stance phase and toe off.**

The loading was applied vertically through the femoral head by a piston underneath the station, which was controlled by a series of hoses through which a pneumatic pressure was applied. The set-up of the Prosim simulator allowed the load to be adjusted for group 1 and group 2 separately, but not for individual stations. This was because the loading for each group was applied by means of a single pneumatic value for the entire group. Group 1 is comprised of stations 1 to 5

and group 2 of stations 6 to 10. Real-time feedback was obtained from a dynamic load cell located on one of the articulating stations for each group. As the load was variable between each station, a nominal input load that would obtain a mean output load of 3kN across all stations in each group was applied. This input load was determined at the time of calibration. The XLPE and aged PE acetabular liners were mounted on alternate stations (1-10) to reduce any simulator bias.

During the edge loading test a separate constant downward pressure was applied to the piston through the vertical axis by means of one of the pneumatic inlet hoses attached to the station. This was sufficient to overcome the upward force during swing phase of gait and cause the piston and therefore the femoral head to drop, resulting in a dynamic microseparation of head and cup. A spring placed medially below the base plate provided a lateral sliding displacement of the femoral head causing it to contact with the superior edge of the cup on heel strike, representing translational malpositioning of the cup (Figure 3-8).

A lateral sliding displacement of the centre of the femoral head of between 0.5mm and 1mm was used and this was measured using a dial gauge micrometer (Figure 3-8). The magnitude of this displacement was assessed at serum changes and measurement points and could be adjusted by tightening or loosening the medial spring. It was not possible to measure the lateral displacement while the test was running due to the serum surrounding the bearing. Medial springs were regularly checked and adjusted during the test to prevent loosening.

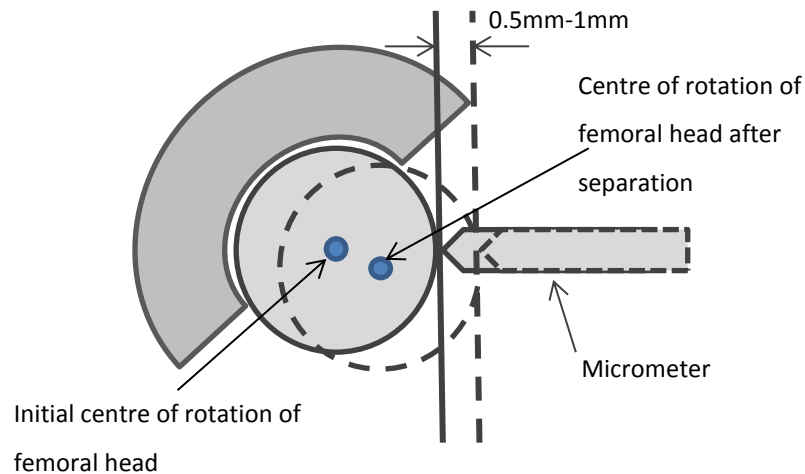


**Figure 3-8 Schematic of the dial gauge micrometer set-up to measure lateral sliding distance under microseparation (diagram not to scale)**

### **3.3.3 Lubricant**

The lubricant used in the simulator tests was 25% (v/v) newborn bovine serum with 0.03% sodium azide (v/v) to retard bacterial growth. Serum changes were carried out *in situ* without removing the components from the machine. Serum was contained in silicone gaiters that surrounded the bearings and that were held in place using metal jubilee clips. The test was stopped approximately every 0.33Mc to replace the serum. During each serum change the serum was drained from the silicone gaiter and either stored for future analysis or discarded. The stations and gaiters were flushed with soapy water, immersed in Distel for 10 minutes and then flushed again once using tap water then twice using deionised water. The serum solution was then replenished. Excess air was squeezed out of the gaiters.

### **3.3.4 Calibration**

The simulator was calibrated and the load verified before each test (including between standard and edge loading tests). To achieve this, the machine was switched to calibration mode and the 'Automatic Load Calibration' function was used. Group 1 (stations 1-5) and group 2 (stations 6-10) were calibrated separately. An external load cell and the machine load cell were placed on one station in each

group. The valve was opened to a pre-determined position to apply increasing loads and the actual load measured by the external load cell was input by the user (Figure 3-9). A calibration report was created providing the calibration constants and the deviation of the actual load from the desired load. This step was repeated until the deviation between the actual load and the simulator load was as small as possible. The calibration constants were checked to ensure they were similar to previously used values. To verify the loads on each station, the simulator was taken out of calibration mode and the motions were disabled. The simulator testing cycle was run with the external load cell placed on each station. The maximum and minimum loads for each station were recorded and the median of these values was used for the input loading profile for the testing cycles.

|                  | 1 | 2     | 3     | 4     | 5     |
|------------------|---|-------|-------|-------|-------|
| Valve:           | 0 | 16250 | 32500 | 48750 | 65000 |
| Loadcell ADC:    |   |       |       |       |       |
| Calibrated:      |   |       |       |       |       |
| Actual Loadcell: |   |       |       |       |       |

**Figure 3-9 Automatic Load Calibration function on the Prosim pneumatic hip simulator.**

The flexion/extension and the internal/external rotations were verified visually using markings on the simulator while the simulator was running with the motions enabled. The frequency was checked and confirmed as 1 cycle per second.

### **3.3.5 Measurement Points**

Measurement points were at 1, 2, 3 and 5Mc during the standard loading test and 1, 1.8, 2.9, 3.5 and 5Mc during the edge loading test for the aged PE and XLPE liners. At each measurement point, all cups were observed visually for evidence of cracking and/or subsurface damage. Total volume changes of the UHMWPE liners were measured gravimetrically using a balance (Mettler Toledo, Leicester, UK) and geometrically using a coordinate measuring machine (Legex 322, Mitutoyo, UK) as described in sections 2.3.3 and 2.3.4.

### **3.3.6 Soak and Load Controls**

Soak and load control samples were used during the simulator testing to compensate for fluid absorption and creep respectively.

The soak control samples were stored in 25% (v/v) serum (section 3.3.3) next to the simulator during testing. The serum was replaced and the liners were cleaned with the same frequency as the serum in the simulator stations. The soak controls were used to correct for fluid uptake rather than the load controls (section 2.3.3) because the load controls were not used during the edge loading tests and consistency between the two testing conditions was maintained.

The load control samples were mounted on stations three and eight of the hip simulator. These stations were run with the motions disabled under the same loading profile as the test stations. For standard hip simulator loading conditions, load controls were used to correct for creep in order to approximate a value for volume change relating to wear only. This was done by subtracting the volume change of the load control from the volume change of the worn samples at each measurement point. The load controls were only used during standard loading due to the difficulty in applying a load to the rim only with the motions disabled.

### **3.3.7 Test for Liner Conformity of Aged PE Liners**

A rocking motion was observed when the aged PE liners were inserted into the shells. It was thought that this was a shell/liner conformity issue and to test this theory, the backside of the liners was covered in engineering blue and pressed into

the shells by hand. When the liner was removed the areas of shell/liner contact were observed on the inside of the titanium shell and photographs were taken.

### **3.3.8 Subsurface Analysis**

Two liners from each material subset were selected to be assessed in the MicroCT subsurface analysis (section 2.6). The liners that were selected were aged PE liners A2 and A10 and XLPE liners AM1 and AM5. The aged PE liners were selected because cracking was observed on the surface of these liners and the XLPE liners were a random selection. A selection of liners were scanned and analysed rather than the entire set because of time constraints.

## **3.4 Results**

The following sections outline the results of the simulator test for the XLPE and aged PE liners for 5Mc of standard loading and 5Mc of edge loading conditions. The rim deformation, subsurface damage, surface damage and volume change of the acetabular liners are described.

### **3.4.1 Rim Deformation**

Two dimensional contacting profilometry (Talysurf) traces were taken across the liner rim to measure deformation due to edge loading. The method is described in section 2.5. Matlab plots of the traces over the inner rim and the mean penetration  $\pm$  confidence intervals are presented in this section.

The mean penetration value for the XLPE liners at the inner rim was  $0.08 \pm 0.04$ mm (Figure 3-10). A sharp change in gradient at the radius of curvature between the chamfer and the bearing surface was observed for the worn profiles. This was in contrast to the unworn profile, which exhibited a more gradual change in gradient and larger radius of curvature. The reader is referred back to section 2.5.4 for discussion on interpretation of the Matlab plots and limitations of the method.

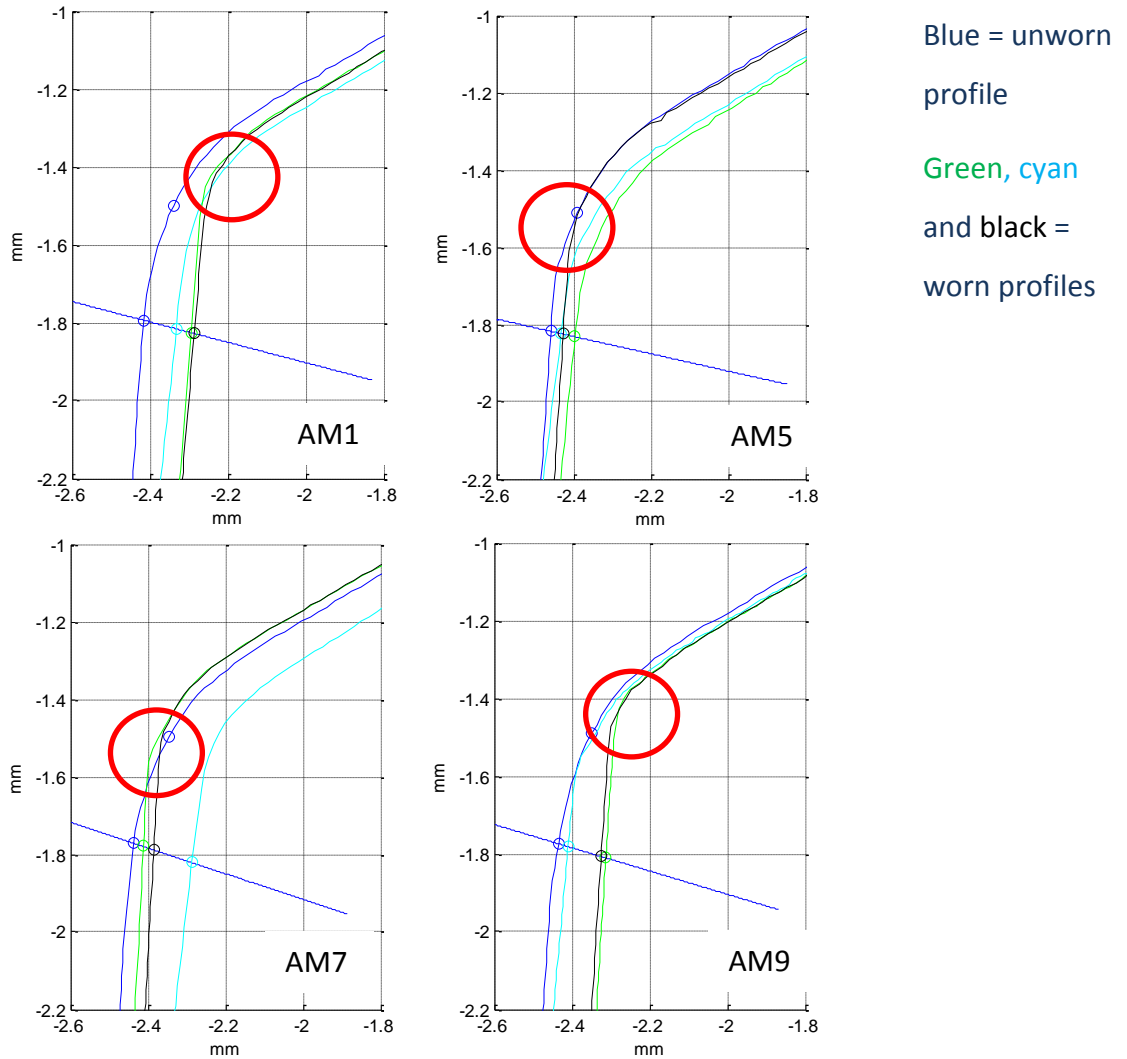


**Figure 3-10 Worn and unworn rim profiles for XLPE liners (A) AM1, (B) AM5, (C) AM7 and (D) AM9 showing the points at which the penetration values were measured for a section zoomed to the inner rim. The red circle highlights the sharp change in radius between the bearing surface and chamfer for the worn profiles. The unworn profile is the dark blue line.**

The mean penetration value for the aged PE liners at the inner rim was  $0.18 \pm 0.15$  mm (Figure 3-11). A sharp change in gradient at the radius of curvature between the chamfer and the bearing surface was observed for the worn profiles for all liners except liner A2, which only showed a moderately sharpened rim on one of the traces (cyan). This was in contrast to the unworn profile, which exhibited a more gradual change in gradient and larger radius of curvature. The sharpening in

the radius of curvature that was observed between the chamfer and the bearing surface was more pronounced for the aged PE liners than the XLPE liners.

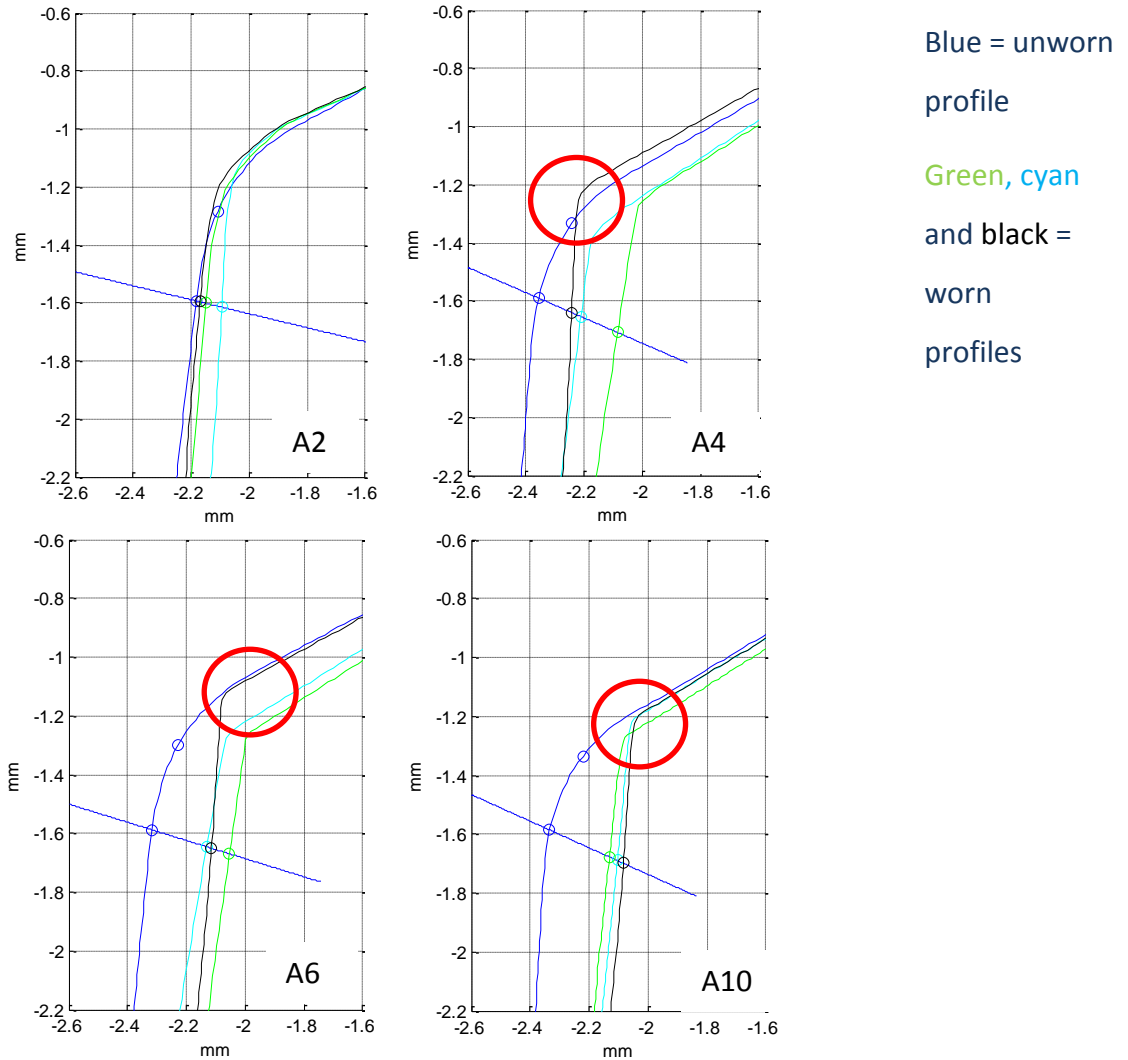


**Figure 3-11 Worn and unworn rim profiles for aged PE liners A2, A4, A6 and A10 showing the points at which the penetration values were measured for a section zoomed to the inner rim. The red circle highlights the sharp change in radius between the bearing surface and chamfer for the worn profiles.**

### 3.4.2 Subsurface Damage

Subsurface damage was evaluated using MicoCT scans as described in section 2.6. A selection of each type of material was scanned and analysed (A2, A10, AM1 and AM5)

No micro-cracking and/or obvious visible damage were observed on the XLPE liners when compared to the XLPE controls in section 2.6 (Figure 3-12).

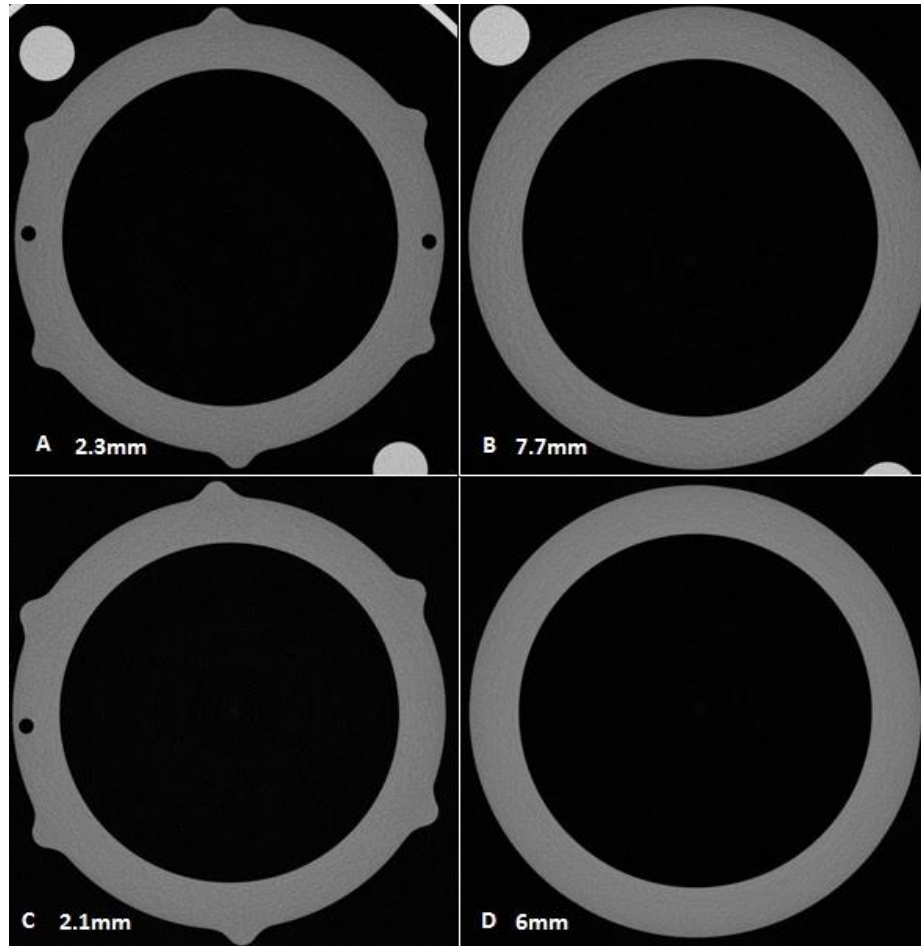


**Figure 3-12 MicroCT 2D reconstructed slices with no visible cracking: (A&B) XLPE liner AM1 at 2.3mm and 7.7mm below the horizontal surface of the rim and (C&D) XLPE liner AM5 at 2.1mm and 6mm below the horizontal surface of the rim. View is a cross section of the liner looking down onto the rim.**

Extensive subsurface cracking was observed on the aged PE liners (aged PE liners A2 & A10). The subsurface cracking on liner A10 appeared to initiate near the outer rim close to the horizontal surface of the rim at an anti-rotation tab, and propagated towards the inner rim further down the liner towards the apex (Figure 3-13).

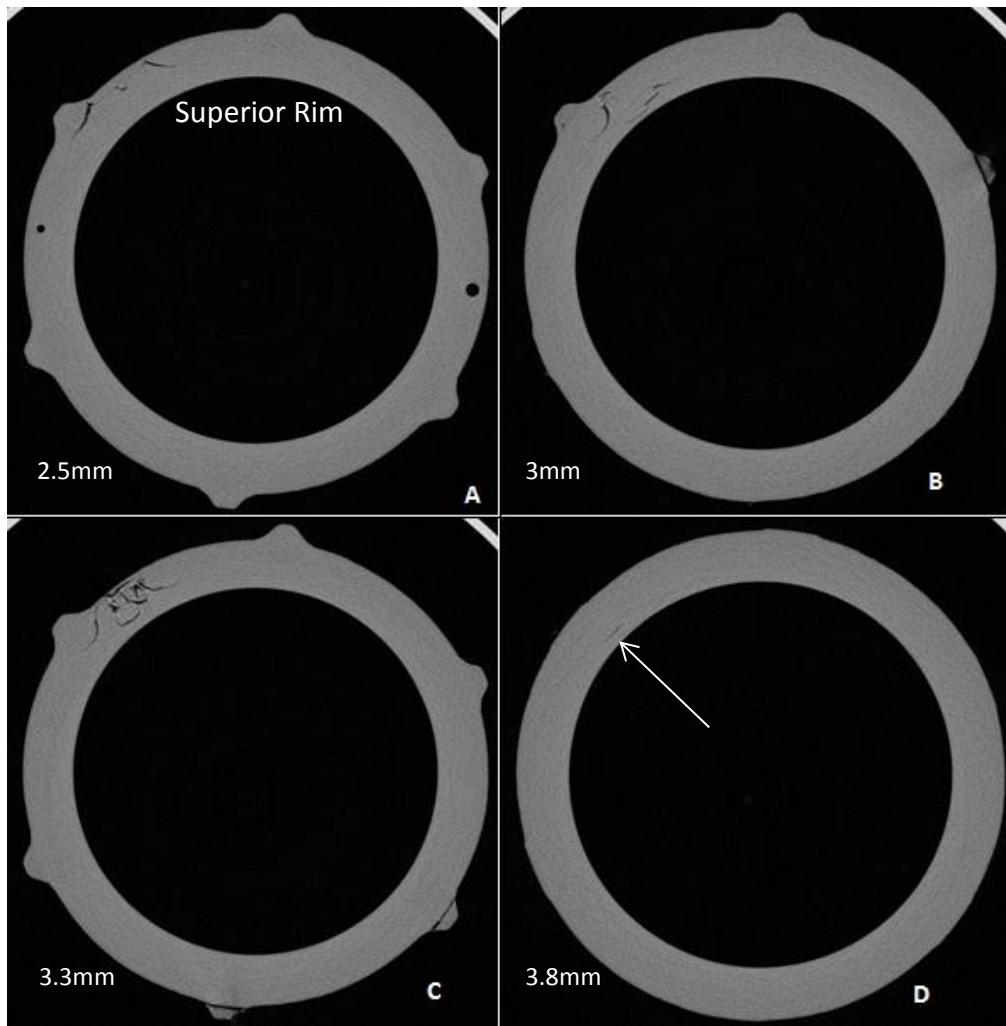


**Figure 3-13 MicroCT 2D reconstructed slices showing subsurface cracking on aged PE liner A10 showing (A) circumferential cracking at outer rim and at an anti-rotation tab 2.5mm below the horizontal surface of the rim (B) cracking around an anti-rotation tab 3mm below the horizontal surface (C) extensive multi-directional cracking near the outer rim and anti-tab 3.3mm below the horizontal surface and (D) circumferential cracking near the inner rim 3.8mm below the horizontal surface. View is a cross section of the liner looking down onto the rim.**

The subsurface damage was observed in the corresponding location to the damage that was visible from the surface (Figure 3-14). Circumferential subsurface cracks could be seen close to the inner rim where the whitening was observed at the surface and circumferential cracks propagating along the outer edge of the rim and at an anti-rotation tab were observed where the same type of damage was visible from the surface. Some subsurface damage was observed close to the

backside cracks but it was not extensive and appeared to propagate radially from the outer edge of the liner.

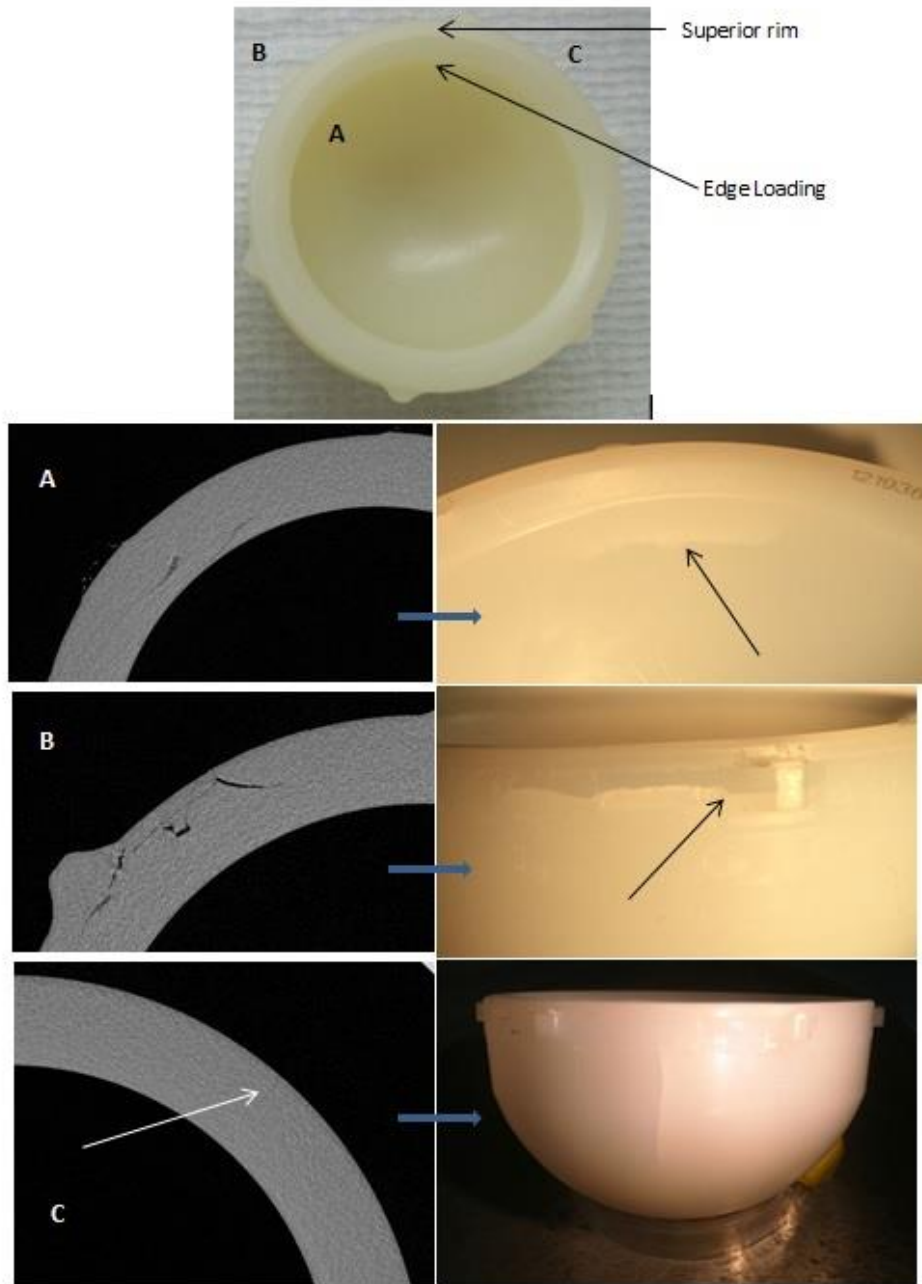


**Figure 3-14 MicroCT 2D reconstructed slices with the corresponding photos of an aged PE liner (A10) showing (A) cracks propagating circumferentially close to the inner rim and the corresponding whitening at the inner rim, (B) Cracks propagating circumferentially along the outer rim from at an anti-rotation tab and the corresponding photo and (C) a radial crack and the corresponding backside crack. The location of these damage mechanisms is shown in the first image.**

A similar damage pattern was observed for aged PE liner A2. Cracks appeared to initiate at the outer edge of the rim around an anti-rotation tab and then propagated down towards the inner rim and the apex of the liner and the subsurface damage was observed in the corresponding location to the damage that was visible from the surface (Figure 3-15).

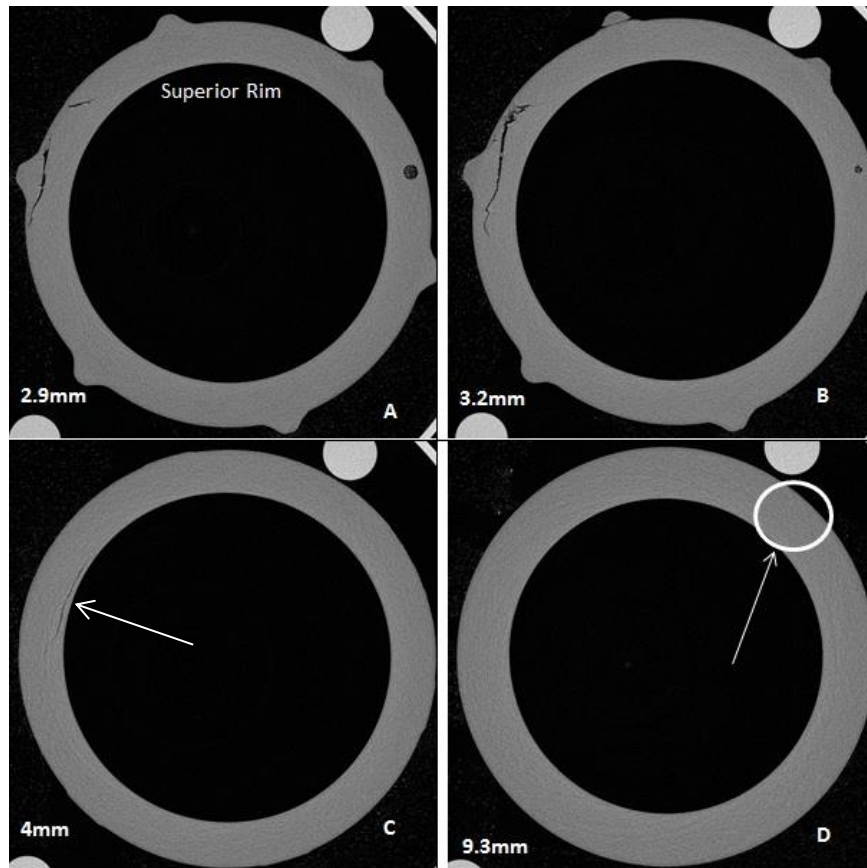
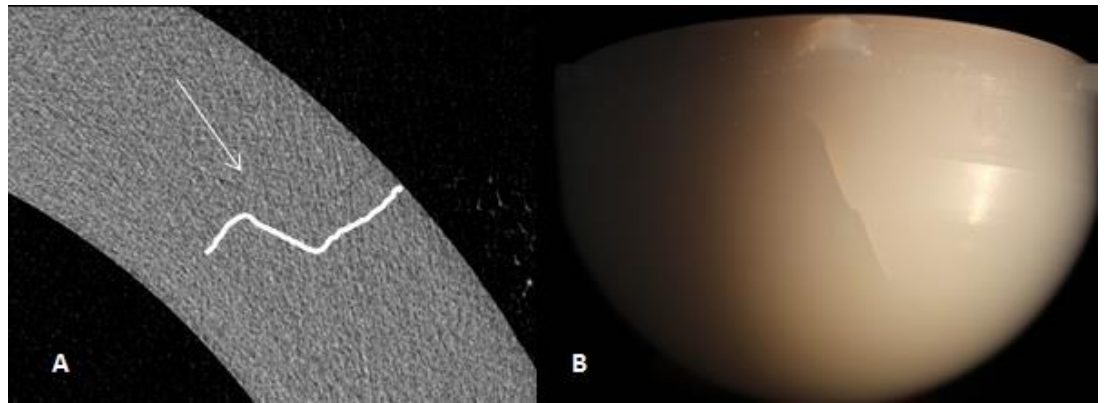


Figure 3-15 Subsurface cracking on aged PE liner A2 showing (A) circumferential cracking at outer rim and around an anti-rotation tab 2.9mm below the horizontal surface of the rim (B) cracking around an anti-rotation tab 3.2mm below the horizontal surface (C) circumferential cracking near the inner rim 4mm below the horizontal surface and (D) Radial crack initiating at the outer rim and extending towards the inner bearing surface 9mm below the horizontal surface of the rim (see Figure 3-16 for detail). View is a cross section of the liner looking down onto the rim.

Similar to aged PE liner A10, the subsurface cracking corresponding to the backside crack was less easily identified but some radial cracking was observed that was thought to be the backside crack Figure 3-16 .



**Figure 3-16 A MicroCT reconstruction with the corresponding photo of an aged PE liner (A2) showing a radial crack and the corresponding backside crack**

### **3.4.3 Damage to Acetabular Liners and Cups**

This section describes the wear and damage mechanisms observed on the liners throughout the test and the location of wear and damage with respect to liner orientation.

A polishing or burnishing of the articulating surface in the superior region of the cup, characterised by a shiny appearance, was observed on all liners, both XLPE and aged PE (Figure 3-17). Fine multidirectional scratching was observed on the bearing surfaces using a microscope. The XLPE liners did not exhibit any other visible signs of damage on the bearing surface or the rim after standard loading or edge loading.

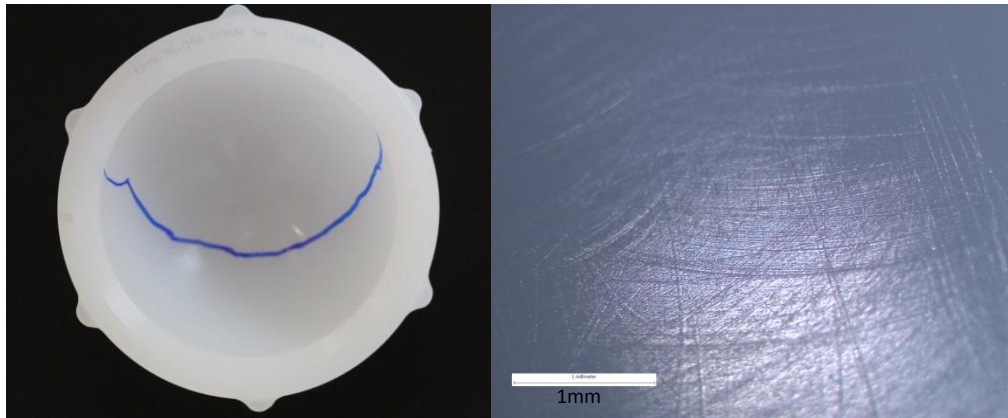


**Figure 3-17 An XLPE liner with the polished wear area highlighted after standard loading and a microscopy image of the fine scratching on the bearing surface (AM1; x30 magnification)**

Damage in the form of subsurface cracking and a whitening of the material at the inner rim and circumferential cracking along anti-rotation tabs was observed after 2Mc of standard loading on aged PE liners A2 and A10 (Figure 3-18). The same types of damage were observed on aged PE liner A4 after 1Mc of edge loading.

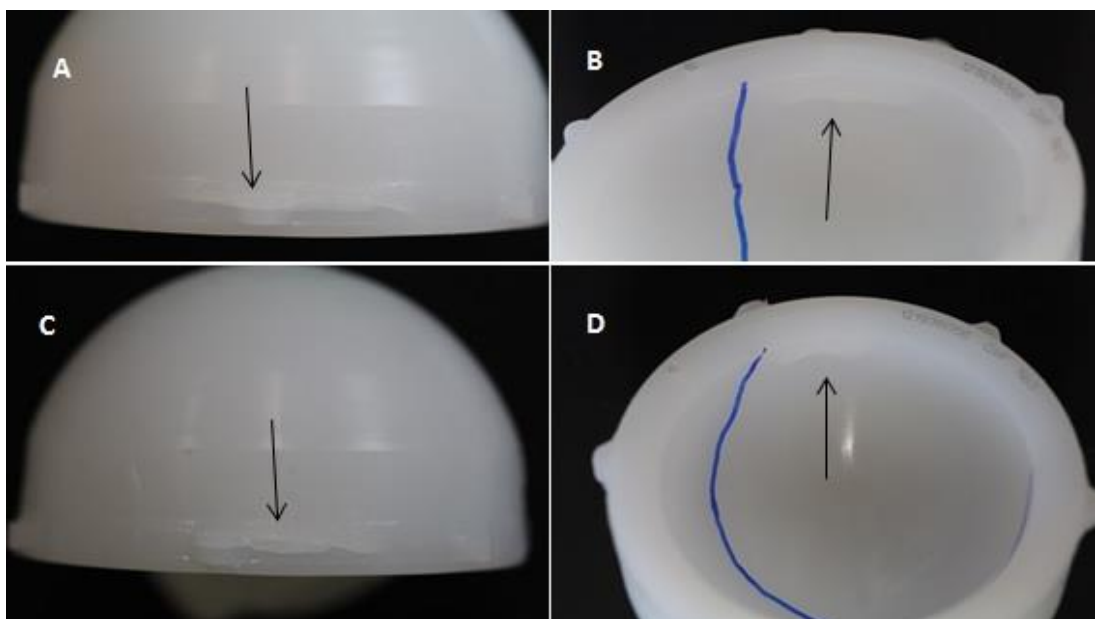


**Figure 3-18 Images of cracking on aged PE liners after 5Mc of edge loading showing cracking along an anti-rotation tab (A, Aged PE liner A2; C, aged PE liner**

**A10) and subsurface cracking and whitening at inner rim (B, aged PE liner A2 and C, aged PE liner A10)**

Radial cracks on the backside of the liners were observed on liner A4 after 1Mc of edge loading and after 3.5Mc for liners A2 and A10 (Figure 3-19).

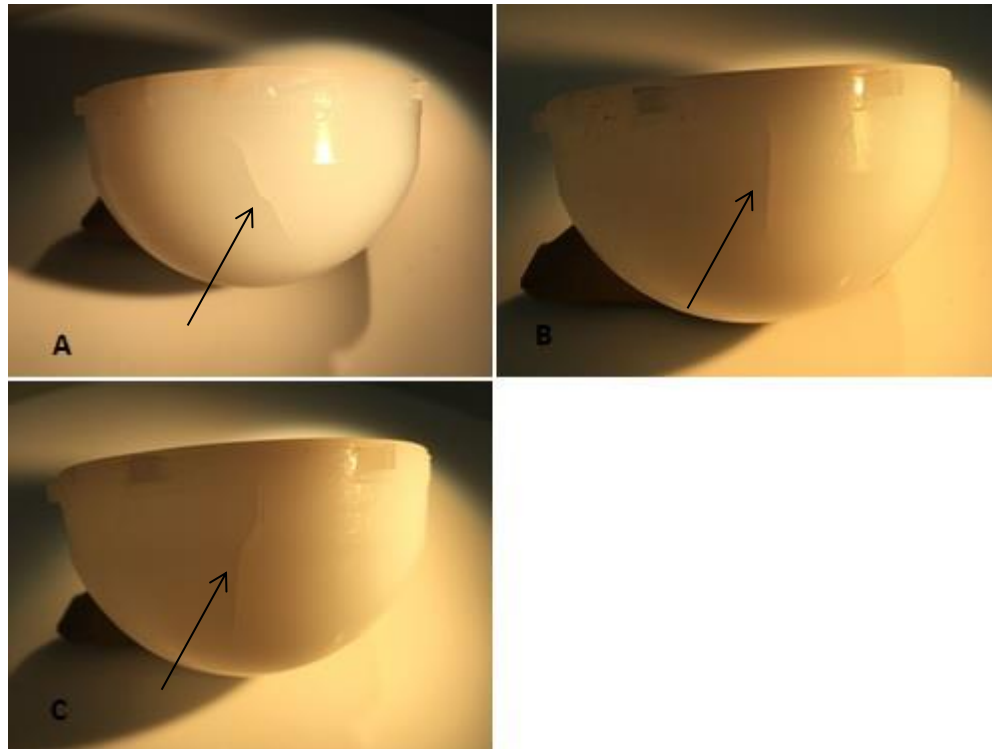


**Figure 3-19 Radial cracking on the backside of aged PE liner (A) A2, (B) A4 & (C) A10 after 5Mc of edge loading**

The damage was observed in the same location on the superior aspect of all of the liners. The location of this damage with respect to the orientation of the liners during edge loading as well as images of the damage after 5Mc of edge loading can be seen in Figure 3-20.

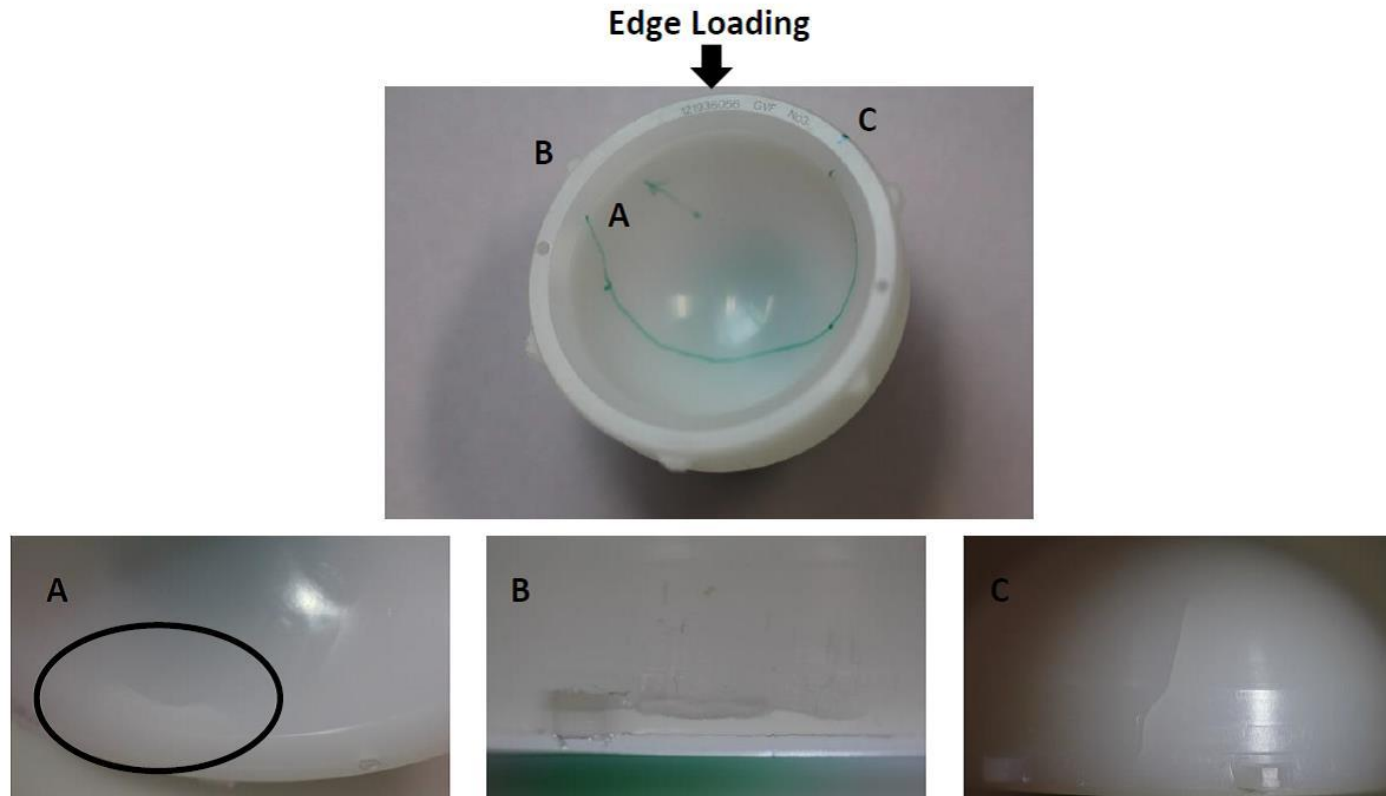
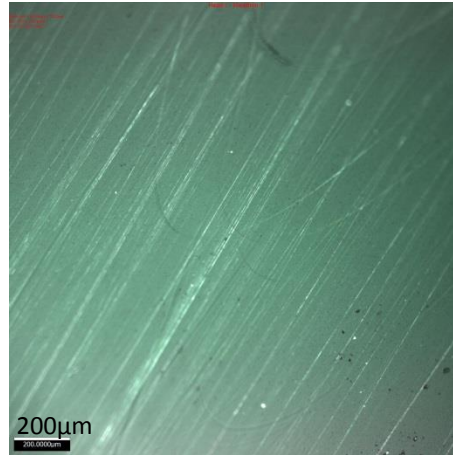


Figure 3-20 (Top image) Location of damage to aged PE liners (A10 shown) with respect to orientation during edge loading (Bottom image A) Subsurface cracking and whitening of the material at the inner rim (Bottom image B) cracking along anti-rotation scallop (Bottom image C) radial crack on backside.

No visible signs of damage were observed on aged PE liner A6.

Light scratching was observed on the femoral heads following testing (Figure 3-21).



**Figure 3-21 Microscopic image of scratching on a metal femoral head articulating with an XLPE acetabular cup (AM1).**

#### **3.4.4 Volume Change**

Volume change of the acetabular liners was calculated from the gravimetric measurements using the method described in section 2.3.3. They relate to material loss only and compensation for fluid absorption was applied. The mean volume change  $\pm$  the 95% confidence intervals are given and data sets are compared using a one-way ANOVA.

The mean total volume change for the XLPE liners after 5Mc of standard loading was  $44.3 \pm 13.3\text{mm}^3$  and the mean total volume change for the XLPE liners between 0Mc and 5Mc of edge loading (5-10Mc of testing) was  $13.5 \pm 12.6\text{mm}^3$  (Figure 3-22).

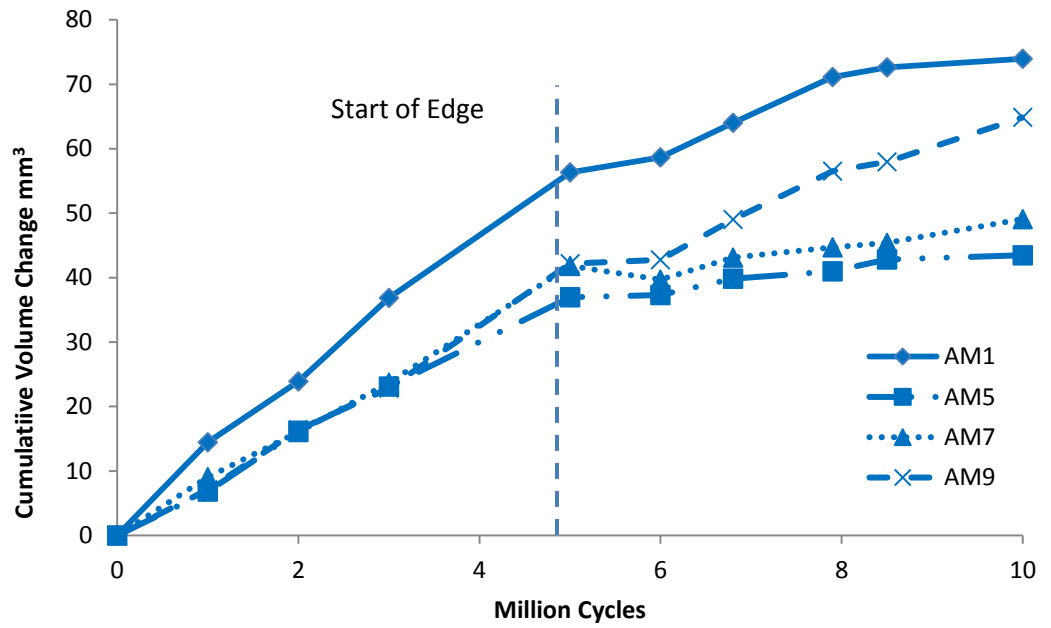


**Figure 3-22 Cumulative volume changes measured gravimetrically for the XLPE liners after 5Mc of standard loading (0-5Mc) and 5Mc of edge loading (5-10Mc) in a hip simulator**

The mean total volume change for the aged PE liners after 5Mc of standard loading was  $121 \pm 28.6\text{mm}^3$  and the mean total volume change for the aged PE liners between 0Mc and 5Mc of edge loading (5-10Mc of testing) was  $31.1 \pm 10.4\text{mm}^3$  (Figure 3-23).

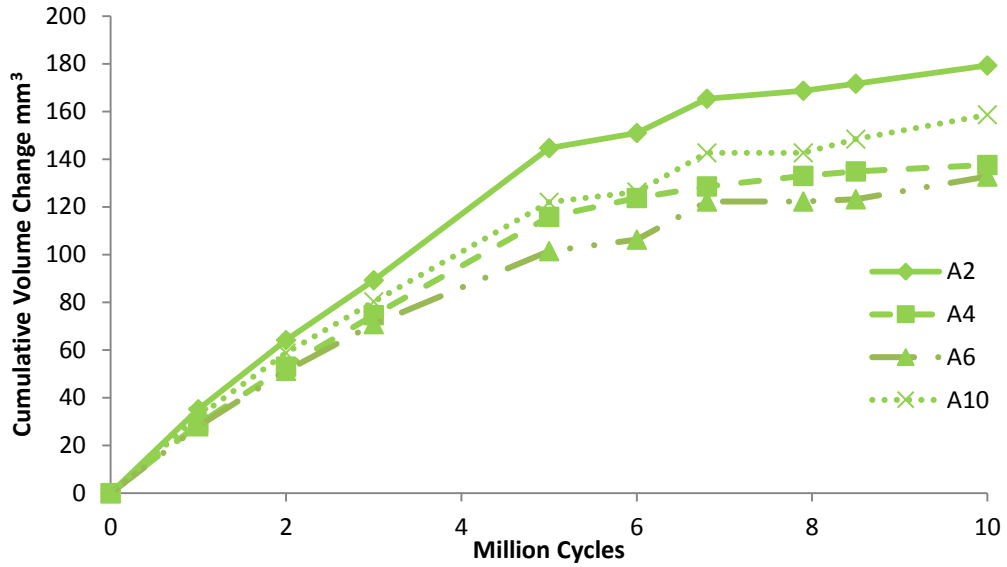


**Figure 3-23 Cumulative volume changes measured gravimetrically for the aged PE liners after 5Mc of standard loading (0-5Mc) and 5Mc of edge loading (5-10Mc) in a hip simulator**

The variation in the volume changes between XLPE liners increased during edge loading ( $44.3\text{mm}^2 \pm 19\% \text{RSD}$  for standard loading and  $13.5\text{mm}^2 \pm 59\% \text{RSD}$  for the edge loading conditions). This was less marked for the aged PE liners ( $43.2\text{mm}^2 \pm 14.7\% \text{RSD}$  and  $31.1 \pm 21\% \text{RSD}$  for standard and edge loading conditions, respectively).

The volume changes were converted to steady state wear rates as described in 2.3.3. These are shown in Figure 3-24.

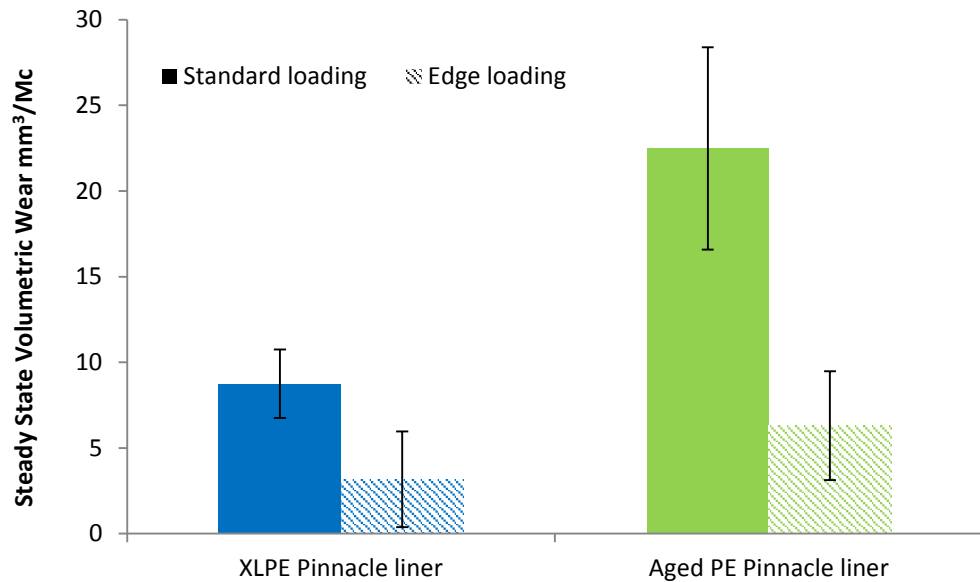


**Figure 3-24 Mean steady state wear rates calculated using gravimetric measurements for the XLPE and aged PE liners under standard and edge loading conditions in a hip simulator ( $\pm 95\%$  Confidence intervals;  $n=4$ )**

The aged PE liners were significantly higher wearing than the XLPE liners under standard loading conditions ( $p=0.0004$ ). The difference was not significant under edge loading conditions ( $p=0.06$ ). The steady state wear rates were significantly lower under edge loading conditions than under standard loading conditions for both types of liner ( $p=0.002$  and  $p=0.0002$ , for the XLPE and the aged PE liner respectively).

### 3.4.5 Creep

The volume change of each liner was measured geometrically using a coordinate measuring machine as described in section 2.3.4. The geometric

measurements measured volume change relating to both wear and creep of the material. Creep was assessed for standard loading conditions only.

The mean total volume change for the XLPE liners measured geometrically after 5Mc of standard loading was  $77.5 \pm 20\text{mm}^3$  (Figure 3-25).

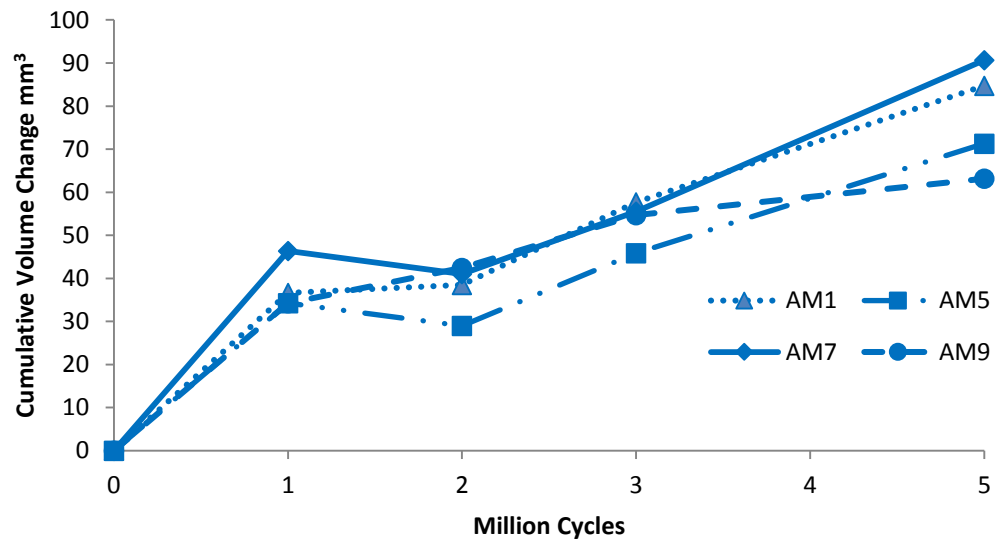


**Figure 3-25 Cumulative volume change measured geometrically for the XLPE liners after 5Mc of standard loading in a hip simulator**

The rate of volume change of the XLPE liners in the first million cycles was higher than the volume change for each of the subsequent 4 million cycles. An increase in volume between 1 and 2 million cycles, which may have been due to measurement error at the 1 million cycle measurement point or the 2 million cycle measurement point, was observed. The measurements were repeated at the 2Mc measurement point and were comparable to the first set of measurements taken at 2Mc. The method of volume change measurement was shown have an accuracy of  $\pm 3.27\text{mm}^3$  (SD; section 2.5.2), which may in part explain the volume change observed in these tests, given that a steady state wear rate of approximately  $10\text{mm}^3$  was expected. Other likely explanations included swelling of the liners due to temperature differences or excessive fluid absorption.

The mean volume changes for the geometric measurements were corrected for creep using the load control liner as described in section 3.3.6. These are shown for the XLPE liners in Figure 3-26 along with the gravimetric measurements, the geometric measurements before correction and load control measurements for comparison.

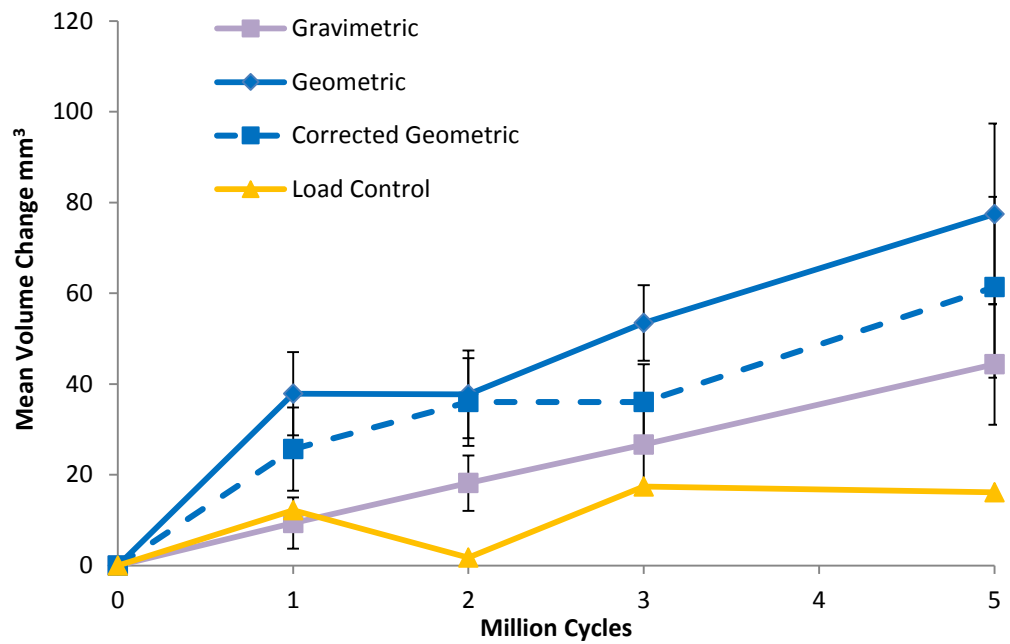


**Figure 3-26 Mean volume change for the XLPE liners over 5Mc of standard loading: comparison of gravimetric, geometric, geometric corrected with load control ( $\pm 95\%$  Confidence Intervals;  $n=4$ ), and load control measurement**

When the load control is used to compensate for creep, a volume increase at 2Mc is no longer observed.

The volume changes for the corrected geometric measurements of the XLPE liners were higher than the volume changes measured gravimetrically, particularly in the first 1 to 2 million cycles.

The mean total volume change for each aged PE liner measured geometrically after 5Mc of standard loading was  $124 \pm 22.5\text{mm}^3$  (Figure 3-27).

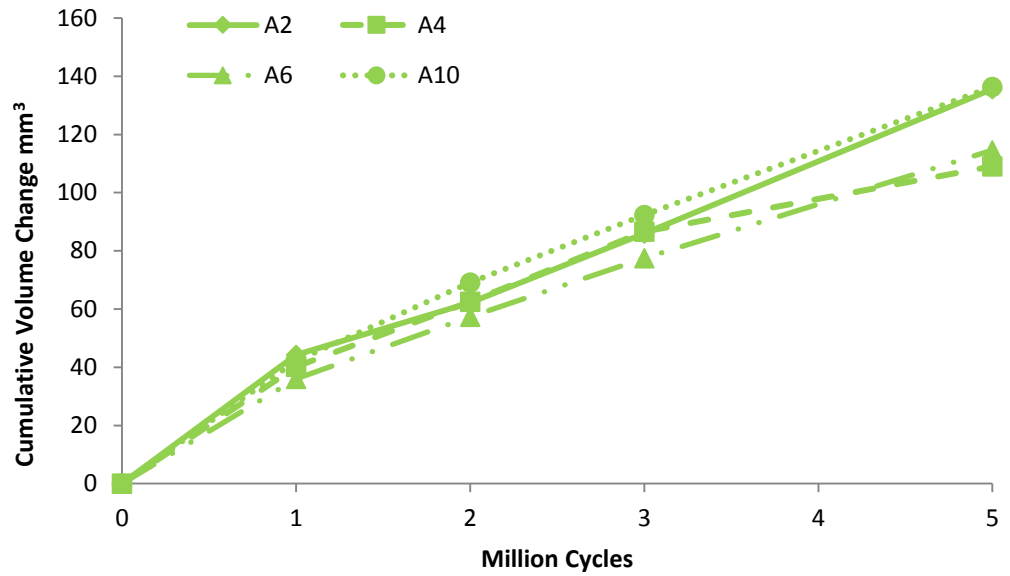


**Figure 3-27 Cumulative volume change measured geometrically for the aged PE liners after 5Mc of standard loading in a hip simulator**

The mean volume change for the geometric measurements is shown for the aged PE liners in Figure 3-28 along with the gravimetric, corrected geometric and load control measurements for comparison.

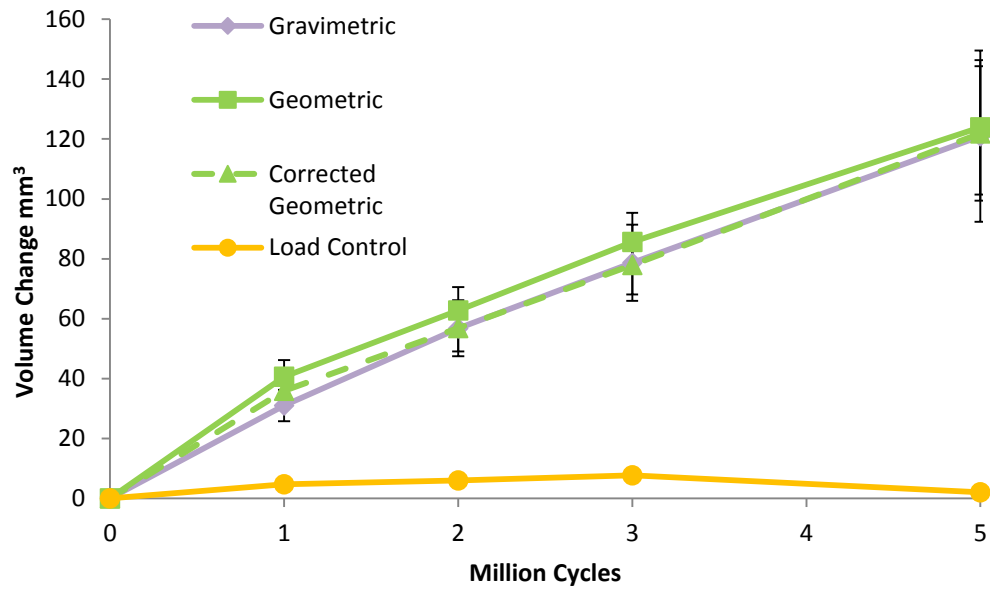


**Figure 3-28 Mean volume changes for the aged PE liners over 5Mc of standard loading: comparison of gravimetric, geometric, geometric load control corrected ( $\pm 95\%$  Confidence Intervals;  $n=4$ ), and load control measurements**

In contrast to the load corrected geometric measurements of the XLPE liners, the load corrected measurements of the aged PE liners show good agreement with the gravimetric measurements. The volume change observed for the aged PE load control liner was smaller than the volume change observed for the XLPE load control liner, indicating that the aged PE liners underwent less creep.

The steady state wear rates calculated using the geometric measurements and the gravimetric measurements can be seen in Figure 3-29.

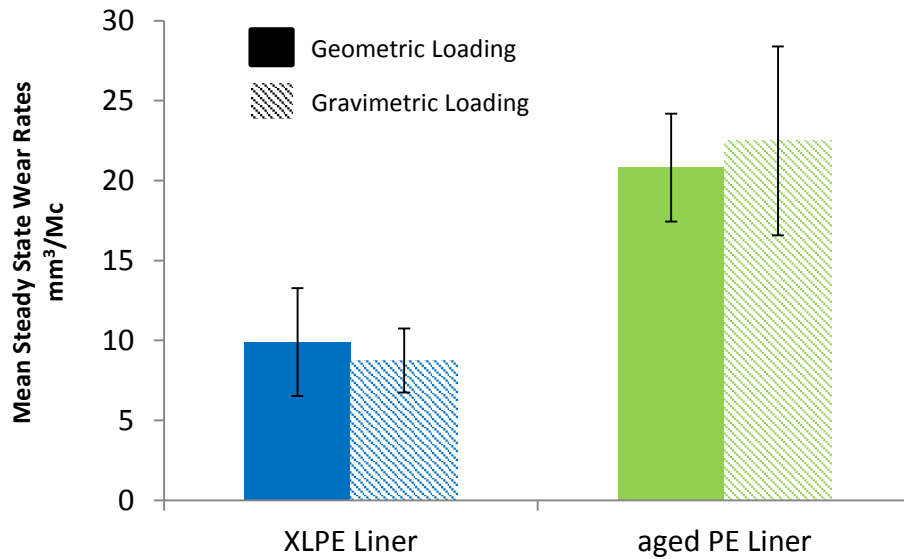


**Figure 3-29 Mean steady state wear rates calculated from the geometric and gravimetric measurements of the XLPE and the aged PE liners under standard loading conditions ( $\pm 95\%$  Confidence intervals;  $n=4$ )**

There was no significant difference between the steady state wear rates for the geometric measurements and the gravimetric measurements for either liner ( $p=0.51$  and  $p=0.38$  for the aged PE and XLPE liners respectively), suggesting that creep does not significantly affect the steady state wear rate for the liners where geometric measurements are taken.

Volume change was observed on the superior region of the bearing surface after standard loading and superiorly in the form of a thin narrow strip on the inner rim of all liners after edge loading. This can be seen on the SR3D geometric reconstructions (Figure 3-30). Greater deformation at the inner rim was observed on the aged PE liners and the areas of volume change had clearly defined edges on both the bearing surface and the inner rim. The volume change at the inner rim was separate to the volume change on the bearing surface. In comparison, the volume change for the XLPE liners was more variable in size and shape and did not have clearly defined edges. The narrow strip of deformation at the inner rim was not clearly separated from the main area of volume change on the bearing surface.

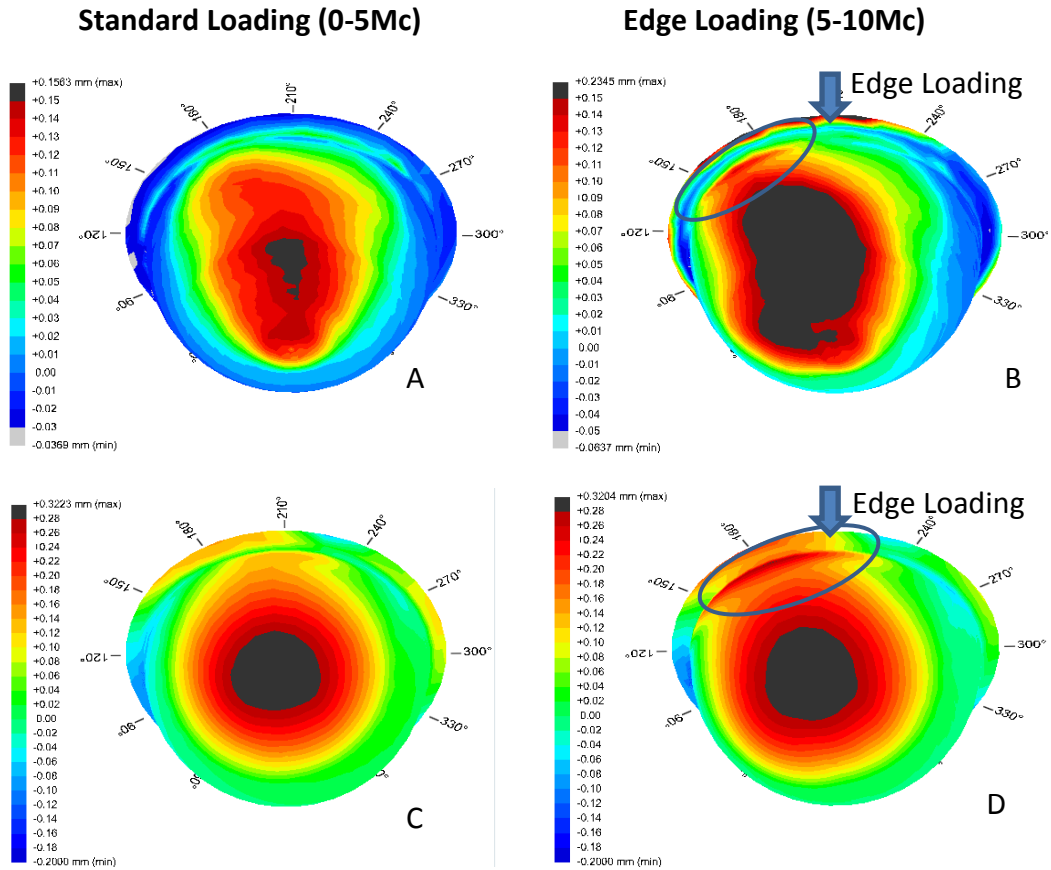


**Figure 3-30 SR3D geometric reconstructions of volume change after 5Mc standard loading and 5Mc edge loading conditions for XLPE liners (A & B; AM9) and aged PE liners (C & D; A10 )**

### 3.4.6 Deformation of aged PE liners

A rocking motion was observed when the aged PE liners were inserted into the shells. This was observed pre-test and throughout the duration of the test. This was investigated further using engineering blue to reveal areas of shell/liner contact. The areas of contact between shell and liner for the aged PE liners and the XLPE liners can be seen in Figure 3-31.



**Figure 3-31 Pinnacle shells after the backside of the liners were covered in engineering blue then inserted and removed from the shell. (A & B) areas of contact for an XLPE liner (C &D) areas of contact for an aged PE liner**

The XLPE liner made contact around the superior circumference but, with the exception of a few patches, the engineering blue was not transferred to the rest of the shell (Figure 3-31A&B). The aged PE liner made contact around the superior circumference of the shell but also made contact at the apex over a large area, as indicated by the blue dye that was transferred from the liner to the shell (Figure 3-31C&D). This shell liner contact/non-contact was consistent over all liners of each type. This shell liner contact was considered to be the source of the rocking motion observed for all aged PE liners.

### **3.5 Discussion**

The aim of the protocol development study was to evaluate a hip simulator edge loading protocol to determine the wear and fatigue behaviour of UHMWPE

acetabular components in total hip replacement using aged PE liners as positive controls and XLPE liners as negative controls. The edge loading protocol produced cracking and subsurface damage in the aged PE liners but not in the non-aged XLPE liners. Rim deformation was observed on all liners and volume change was reduced under edge loading conditions for both types of UHMWPE liner.

### **3.5.1 Rim Deformation**

Rim deformation was observed on the superior rim of all liners following edge loading. This deformation could be attributed to both plastic deformation and wear of the material. As expected, the aged PE liners exhibited a larger mean deformation at the rim than the XLPE liners. This was expected because the aged PE liners were higher wearing than the XLPE liners. An interesting finding in this part of the study was the shape of the 2D profilometry traces of the aged PE liners (Figure 3-11). A sharp change in gradient was observed between the bearing surface and the chamfered region of the rim for the aged PE liners (the inner rim). While this was also observed for the XLPE liners, the change in gradient was less pronounced with a larger radius of curvature being observed. It is postulated that this difference could be attributed to the more brittle nature of the oxidised aged PE material, resulting in more wear and less plastic deformation when edge loading occurs. This is supported by the findings in Section 3.4.5, indicating that less creep deformation occurs for the aged PE liners. The less defined area of volume change at the inner rim observed on the CMM SR3D geometric reconstructions for the XLPE liners (Figure 3-30) may also be attributed to increased creep of the XLPE material compared to the aged PE.

### **3.5.2 Subsurface Damage**

The MicroCT 2D reconstructions revealed extensive subsurface cracking in areas corresponding to surface cracking and damage on the positive controls, the aged PE liners. No visible damage was observed on the negative controls, the XLPE liners (compared to the XLPE controls in section 2.6). This may be a limitation of the analysis method as micro-cracking is not easily identified by the observer from the surrounding structure or it can be confused with reconstruction artefacts.

However, it may also suggest that no subsurface micro-cracking was sustained by the XLPE liners during the edge loading hip simulator tests.

For the aged PE liners, the MicroCT allowed a more thorough non-destructive analysis of crack initiation and propagation to be performed than a simple visual analysis. The MicroCT scans were performed at the end of the test after 5Mc of standard loading and 5Mc of edge loading and it is difficult to confidently identify crack initiation sites and to fully understand the propagation of these cracks without scanning at defined intervals throughout the testing cycle. However, from the MicroCT reconstructions of the post-test scans, the cracking appeared to initiate around one of the anti-rotation tabs on the superior edge loaded region of the rim and extended circumferentially along the outer edge of the rim away from the anti-rotation tab. It is therefore reasonable to suggest that the crack initiated at the anti-rotation tab because, as discussed already (section 3.5.1), previous studies have identified anti-rotation devices and locking mechanisms as areas of high stress concentrations and features where cracking commonly initiates (Furmanski et al., 2009; Furmanski et al., 2011; Tower et al., 2007).

For both cracked liners (A2 and A10), multidirectional cracking was observed approximately 3mm below the horizontal rim and this was more severe than could be determined from visual observations of the surface cracks. As the cracking extended down towards the apex of the liner it approached the inner rim and this was most likely the whitening that could be seen from the surface. This supports the previous hypothesis that the whitening was the initial stages of delamination, as these cracks seemed to propagate parallel to the liner surface.

Interestingly, the backside cracks were not easily identified on the MicroCT reconstructions. This was surprising as these cracks were fairly extensive and visible to the eye. This may be because the MicroCT reconstructions will only reveal cracks if there is a void between each side of the crack. If the two sides are pushed together then the crack may be less visible on the reconstruction. Alternatively, the direction of propagation was different to the other cracks and this may have been more difficult to identify on the 2D reconstruction slices.

The MicroCT scans support the hypothesis made during the damage analysis that cracking initiates at the outer edge of the rim and around anti-rotations tabs and propagates circumferentially (section 3.5.2). Furthermore, the MicroCT scans help provide a better understanding of the severity of subsurface cracking, which could not be determined from a surface analysis.

### **3.5.3 Damage to Acetabular Liners**

The circumferential cracks along the anti-rotation tabs of the aged PE liners observed during this study were similar to damage that has previously been observed on retrievals. Retrieval studies have reported crack initiation at notched locking mechanisms on UHMWPE liners and it was hypothesised that these were a result of high stress concentrations at these features (Furmanski et al., 2009; Furmanski et al., 2011; Tower et al., 2007). The whitening on the inner rim between the bearing surface and the chamfered region of the rim in this study indicated the presence of subsurface cracking. Its location adjacent to the cracking observed at the anti-rotation tab suggests that these cracks may have originated at the anti-rotation tab on the backside of the liner and propagated through the thickness of the UHMWPE towards the bearing surface.

The damage was observed in the form of a white patch, which may be indicative of the initial stages of delamination. Delamination is often characterised by large sections of material removal but during initial stages subsurface cracks propagate parallel to the material surface (Shibata et al., 2003; Blunn et al., 1992; Blunn et al., 1997). Oxidative degradation is known to decrease the resistance of the material to this cyclic fatigue mechanism (Bell et al., 1998; Blunn et al., 1992; Hood et al., 1983). It could therefore be hypothesised that the whitening observed at the inner rim in this study was characteristic of the early stages of delamination resulting from oxidative degradation of the material. Delamination has previously been observed on this region of the rim in retrieval studies (Tower et al., 2007). The damage observed in this simulator test was characteristic of fatigue damage caused by cyclic loading and was observed either on the liner rim or originating at the rim. In addition, the UHMWPE liner is thinnest at the rim giving rise to high stress concentrations in this area and leaving it vulnerable to fatigue failure.

To the author's knowledge, the cracking on the backside of the liners has not been observed in other simulator studies or on retrievals. Studies have shown that a shell/liner non conformity and areas of unsupported UHMWPE can lead to cracking in UHMWPE liners (Furmanski et al., 2009; Birman et al., 2005). According to a study by Kurtz et al. (1998), shell/liner conformity facilitates the load transfer between liner and shell. A non-conforming liner will be supported at the rim until the liner is sufficiently deformed during loading to reduce micromotion and to distribute the load between the shell and liner. However, until a load transfer path is established, the liner is vulnerable to fatigue damage. It is hypothesised that the radial cracks observed on the backside of the liners in this study were caused by the nonconforming shell and liner and the areas of unsupported UHMWPE. The cause of this irregular non-conformity and micromotion in the aged PE liners is not known but it is suggested it may have been caused by the accelerated ageing process.

#### **3.5.4 Volume Change**

The aged PE liners exhibited increased volume change compared to the XLPE liners for standard loading conditions. This finding was expected as XLPE components are known to be more wear resistant than conventional UHMWPE and the steady state wear rates observed in this study were consistent with wear rates previously reported in the literature for hip simulator studies (Galvin et al., 2007; Galvin et al., 2010). Furthermore, studies have shown that components with oxidative degradation exhibit increased wear, as in the case of the aged PE liners in this study (Collier et al. 1996; Kurtz et al. 2006; Currier et al. 2007). The difference in wear rates between the XLPE liners and the aged PE liners was not significant under edge loading conditions and this was likely because of the more variable nature of the volume changes measured during the edge loading tests.

The volume change for one of the XLPE liners was higher than the other liners during the standard loading test. This may be a result of variation in the loading conditions of individual simulator stations rather than a variation in material properties, as the volume changes for the other XLPE liners were similar. As discussed previously (section 3.3.2), the loading profile can be adjusted for each

group on the simulator but not individual stations and feedback was only obtained from one station (the station with the load cell). It is therefore possible that one individual station experienced different loading conditions to the other three, resulting in elevated wear volumes.

The volume changes observed for each liner during the edge loading test were more variable than those observed during the standard loading test for both the aged PE liners and the XLPE liners. This may be attributed to the requirement for regular adjustment of the microseparation and lateral displacement during the edge loading test, as discussed in Section 3.3.2. Variations in microseparation and lateral displacement values between stations may explain the larger relative standard deviation observed for edge loading conditions.

Both the aged PE liners and the XLPE liners exhibited reduced volume change under edge loading conditions than under standard loading conditions. This was previously observed in a simulator test of a moderately cross-linked UHMWPE articulating against ceramic heads (Williams et al., 2003). In contrast, studies of hard on hard bearings subjected to edge loading conditions have reported an increase in wear compared to standard loading conditions (Nevelos et al. 2000; Stewart et al. 2001; Nevelos et al. 2001; Williams et al. 2006; Leslie et al. 2009). It has been suggested that wear is increased for hard on hard bearings because of a disruption to fluid film lubrication and an increase in contact stress when edge loading occurs (Williams et al., 2008). Ultra-high-molecular-weight-polyethylene components function under a mixed lubrication regime, which is dominated by boundary lubrication mechanisms, and it is therefore hypothesised that the decrease in wear was due to a reduction in contact area during edge loading. Fluoroscopic studies have reported larger microseparations between the centre of the head and cup *in vivo* (between 0.8mm and 3.1mm; Lombardi et al. 2000; Dennis et al. 2001; Komistek et al. 2002). More recent advances in simulator technology allow these larger separations to be more readily replicated in simulator studies on edge loading. Increased translational malpositioning and increased cup inclination angles have been shown to cause increased magnitudes of dynamic microseparation and wear in hip simulator studies of ceramic on ceramic bearings (Al-Hajjar et al. 2015). It is yet to be determined if wear rates will

increase under more physiologically relevant dynamic microseparations for UHMWPE bearings.

The XLPE liners appeared to creep more than the aged PE liners, as evidenced by the larger volume change for the XLPE load control liner. Significantly higher volume changes were observed for the geometric measurements compared to the gravimetric measurements for these liners, particularly in the first million cycles of testing. A small difference was observed for the aged PE liners but this was effectively compensated using the load control liner. Estok et al. (2005) observed significantly higher creep for crosslinked 28mm acetabular liners compared to non-crosslinked liners in a load only simulator test but reported no difference in creep for 32mm liners. A study by Glyn-Jones et al. (2008) reported no difference in the mean creep values for highly cross-linked polyethylene and standard polyethylene hip replacement retrievals. It is therefore suggested that the higher creep observed for the XLPE liners relative to the aged PE liners in this study is related to the increase in percentage crystallinity and embrittlement of the aged material, resulting in an increased resistance to creep deformation (Narayan. et al. 2010; Brach del Prever et al. 2009). The study by Glyn-Jones et al. (2008) also reported that almost all (95%) creep of UHMWPE occurred within the first six months, which would explain why there was no difference between the steady state wear rates for the gravimetric and geometric measurements in the present study, as steady state wear rates are calculated over 1-5Mc.

### **3.6 Conclusion**

This study developed an edge loading protocol that simulated subsurface damage and rim cracking in aged PE liners as positive controls but not non-aged XLPE liners as negative controls. It supports previous findings that edge loading of UHMWPE components may cause rim failure as observed *in vivo*, particularly where component positioning is sub-optimal or in the case of material degradation. The protocol can be used in the future to test the effect of ageing on a range of crosslinked UHMWPE materials as well as to test components under larger microseparations.

## Chapter 4: Hip Simulator - Antioxidant UHMWPE Study

### 4.1 Introduction

Simulator tests and medium term clinical data indicate that cross-linked UHMWPE has a superior wear performance to conventional UHMWPE and as a result is now widely implanted in the UK and overseas (McKellop et al., 1999; Ries et al., 2001; Endo et al., 2002; Galvin et al., 2007; Calvert et al., 2009; Galvin et al., 2010; García-Rey et al., 2012; Engh et al., 2012; Babovic and Trousdale, 2013; Glyn-Jones et al., 2015). Despite the promising wear results reported to date, concerns remain regarding the long-term performance of these materials in relation to reduced mechanical properties and susceptibility to fatigue damage and fracture (Baker et al., 2003; Pruitt, 2005; Gencur et al., 2006; Atwood et al., 2011; Pruitt et al., 2013; Sobieraj et al., 2013). Furthermore, highly cross-linked materials are exposed to radiation doses of 5Mrad or higher. This produces free radicals, which can lead to oxidative degradation of the material *in vivo* (Collier et al. 1996; Collier et al. 1996; Currier et al. 2007). Thermal treatments are used to remove free radicals following irradiation: re-melting involves heating the UHMWPE to above the melting temperature and is effective at removing the free radicals but at the expense of the crystallinity and strength of the material (Oral et al. 2006) and annealing involves heating the material to below the melting temperature, which preserves the mechanical properties but does not effectively remove all of the free radicals (Gencur et al., 2006).

More recently, manufacturers have sought alternative means of protecting components from oxidation and eradicating free radicals after irradiation. This has been achieved by adding antioxidants such as hindered phenols to the UHMWPE to act as free radical scavengers (Oral et al. 2007; King et al. 2009). Mechanical properties are maintained in hindered phenol antioxidant doped UHMWPE relative to melted UHMWPE, which exhibits reduced properties due to a decrease in crystallinity (Narayan et al. 2009). The exact formulation and loading (% w/w) of the antioxidant influences the final mechanical properties of the UHMWPE and the wear rates increase with increasing antioxidant loading. However, studies have

shown that the addition of hindered phenols does not significantly inhibit the crosslinking process during irradiation of the UHMWPE and good oxidative stability is obtained when compared with non-stabilised crosslinked UHMWPE (Narayan et al. 2009).

Modular acetabular shells with UHMWPE liners offer a degree of choice in terms of component geometry and materials as well as giving the option to revise a liner independently of the metal shell. However, disadvantages include backside wear between shell and liner and the requirement for locking mechanisms, which may result in high stress concentrations and fatigue failure. Compression moulded acetabular cups are an alternative to modular cups to eliminate backside wear, improve shell liner conformity and eliminate locking mechanisms and other features that may be a source of stress concentrations (Young et al., 2002).

The aim of this study was to assess the wear and failure mechanisms of antioxidant UHMWPE for two different acetabular cup designs under standard and adverse edge loading conditions in a hip simulator. Validation of the method was completed in Chapter 3 by replicating failures seen in vivo for conventional GVF aged UHMWPE cups (positive control) and comparing this with marathon cross-linked UHMWPE cups (negative control). It was hypothesised that the antioxidant UHMWPE will have sufficient fatigue strength to withstand rim loading and therefore no rim failure or fracture of the acetabular cups will be observed when tested under edge loading conditions for 5Mc.

The oxidative degradation was not investigated in this study. Antioxidant UHMWPE provides an alternative method of stabilising the material, which in contrast with post-irradiation thermal treatments should eliminate free radicals whilst maintaining the mechanical properties of the material. This study investigates the wear and fatigue damage resistance of the material under edge loading conditions as compared to thermally treated liners. The resistance to oxidative degradation and any subsequent reduction in material properties would be the focus of another study.

The study had the following objectives:

- Evaluate and compare the volume change of the cups under standard and edge loading conditions and compare with positive and negative controls from protocol development tests (Chapter 3);
- Evaluate the rim damage to the acetabular cups after edge loading and compare with positive and negative controls from protocol development tests (Chapter 3);
- Compare the wear and damage mechanisms of the two different cup designs.

## 4.2 Materials

Two different designs of 36mm anti-oxidant UHMWPE (AOPE) acetabular cups were studied (Table 10). Further details of the test components, reference and lot numbers and labelling are provided in Appendix 1.

**Table 10 Details of acetabular components and femoral heads in the anti-oxidant hip simulator study**

| Cup   | Head  | n | Liner Labelling                                   |               |
|---|---|---|---|---------------|
| Anti-oxidant UHMWPE Pinnacle® compatible liner (DePuy Synthes, UK)          | 36mm CoCr Articul/eze® femoral head (DePuy Synthes, UK) | 4 | AOPE 2<br>AOPE 3<br>AOPE 5<br>AOPE 6              | } AOPE liners |
| Anti-oxidant UHMWPE compression moulded acetabular cup (DePuy Synthese, UK) | 36mm CoCr Articul/eze® femoral head (DePuy Synthes, UK) | 4 | AOPE CM 1<br>AOPE CM 4<br>AOPE CM 9<br>AOPE CM 10 | } AOPE cups   |

The material was a prototype and therefore the exact composition was not disclosed by the manufacturer. However, the following details were known: the UHMWPE was gamma irradiated at 11.5Mrad and stabilised with anti-oxidant

hindered phenols to remove free radicals and lower the risk of oxidation. The density of the UHMWPE was 0.9403 g/cm<sup>3</sup>. Two different acetabular cup designs were studied (Figure 4-1), a Pinnacle compatible liner (AOPE liner; n=4) and a compression moulded acetabular cup (AOPE cup; n=4). The Pinnacle<sup>®</sup> compatible design comprised a 56mm outer diameter titanium shell and a press fit 36mm inner diameter anti-oxidant UHMWPE liner with taper lock and anti-rotation device (ARD) tabs that mate with scallops on the titanium shell. The liner thickness was 7.8mm at the apex and 5.1mm at the rim. This design was the same as the design of the XLPE and aged PE liners described in sections 2.2.1 and 3.2.1.



**Figure 4-1 A compression moulder acetabular cup (foreground; AOPE cup) and a Pinnacle<sup>®</sup> compatible liner with titanium shell (background; AOPE liner)**

The compression moulded acetabular cup design comprised a 36mm inner diameter non-removable compression moulded UHMWPE interior with Gription<sup>®</sup> porous coating on both the inner and outer surfaces of a 48mm outer diameter titanium shell (Figure 4-2). The UHMWPE in the compression moulded cup is 2.7mm thick.

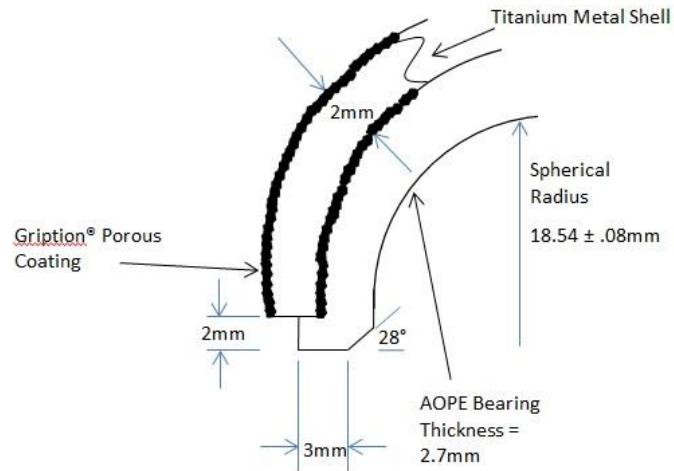


**Figure 4-2 Schematic of a cross-section of the compression moulded acetabular cup**

### 4.3 Methods

The anti-oxidant simulator test was carried out as described in section 3.3. The Pinnacle® shells were cemented directly into the mounts and the Pinnacle compatible liner could be removed at measurement points. The compression moulded cup was cemented directly into the mount and it was not possible to remove it at measurement points. The components were mounted on alternate stations to prevent machine bias (section 3.3.2). The simulator test was run for 4.8Mc under standard loading conditions (the test was stopped at 4.8Mc rather than 5Mc due to a power failure in the laboratory) and 5Mc under edge loading conditions. Measurement points were at 1, 2, 3, 4 and 4.8Mc for the standard loading tests and 1, 2, 3, 4 and 5Mc for the edge loading tests. As with the protocol development tests, all cups were removed and observed visually for evidence of cracking and/or subsurface damage at each measurement point. Total volume change was measured geometrically using a coordinate measuring machine (Legex 322, Mitutoyo, UK) for both cup designs and gravimetrically using a balance (Mettler Toledo, Leicester, UK) for the AOPE liner (as described in section 2.3.3). A

soak control for the AOPE liner was used in gravimetric assessment of volume change as previously described in section 3.3.6. Following testing, the rim profiles and subsurface damage were assessed in greater detail as described in sections 2.6 and 2.5.

Volume changes for the compression moulded components were not determined gravimetrically as the fixed UHMWPE design of the cup did not allow it to be removed from the simulator mount and too much fluid absorption would occur between UHMWPE and shell for accurate measurements to be taken.

#### **4.4 Results**

The following sections outline the results for the simulator test of the AOPE liners and the AOPE cups for 4.8Mc of standard loading and 5Mc of edge loading. The rim deformation, subsurface damage, surface damage and volume change of the acetabular liners are described.

##### **4.4.1 Rim Deformation**

Two dimensional contacting profilometry traces (Talysurf traces) were taken across the liner rim to measure deformation due to edge loading. The method is described in section 2.5.2. The penetration was measured at a user defined point on the inner rim and was described in section 2.5.3. Matlab plots of the traces over the inner rim and the mean penetration  $\pm$  confidence intervals are presented in this section.

The mean penetration for the AOPE liners was  $0.117 \pm 0.07\text{mm}$  (Figure 4-3). Furthermore, a sharp change in the radius of curvature at the point where the chamfer meets the bearing surface at the inner rim was observed on the worn profiles. This is in contrast to the unworn profile, which exhibited a more gradual change in gradient and a larger radius of curvature.

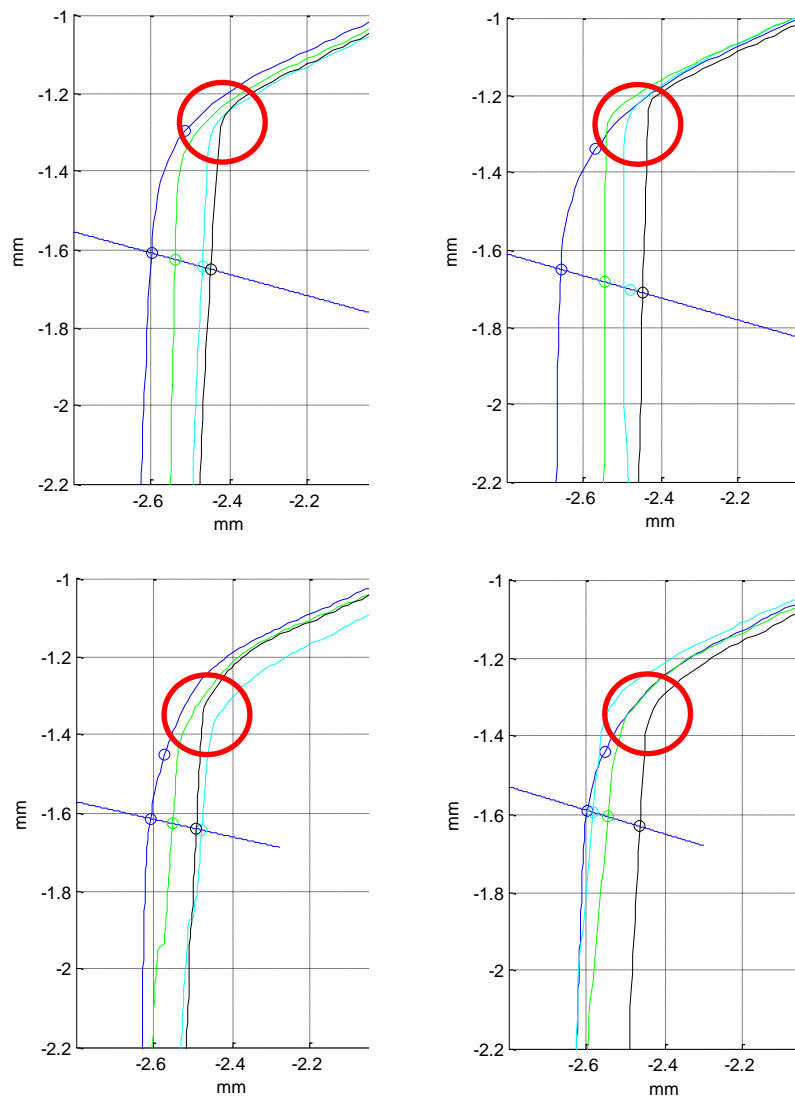


**Figure 4-3 4-4 A close up of the inner rim showing worn and unworn rim profiles for the AOPE liners. The point at which the penetration values were measured is shown and a sharp change in radius at the inner rim can be observed. The dark blue liner is the unworn profile and the green, cyan and black lines are the worn profiles.**

The mean penetration at the inner rim for the AOPE cups was  $0.07 \pm 0.05\text{mm}$  (Figure 4-5). Similar to the AOPE liners, a sharp change in the radius of curvature at the inner rim was observed on the worn profiles. This is in contrast to the unworn profile, which exhibited a more gradual change in gradient and a larger radius of curvature.

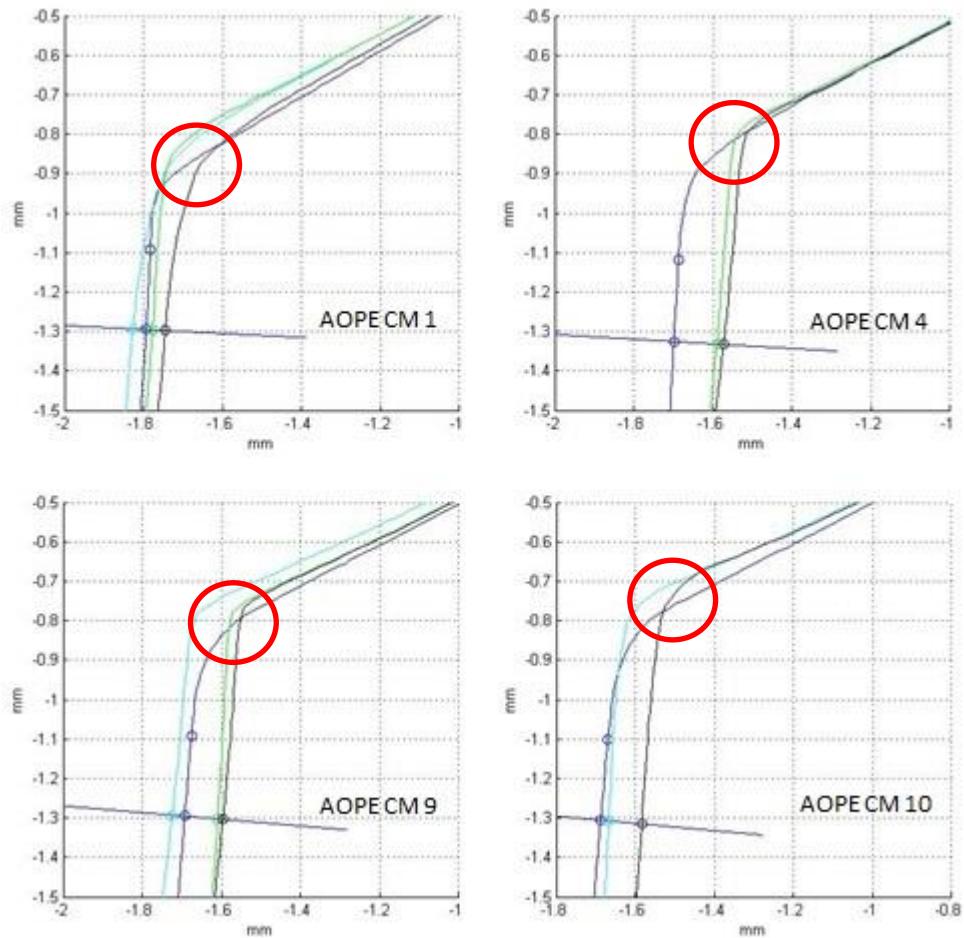


**Figure 4-5** A close up of the inner rim showing worn and unworn rim profiles for the AOPE cups. The point at which the penetration values were measured is shown and a sharp change in radius at the inner rim can be observed. The dark blue liner is the unworn profile and the green, cyan and black lines are the worn profiles.

#### **4.4.2 Subsurface Damage**

Subsurface damage on the AOPE liners was evaluated using MicroCT scans as described in section 2.6. Despite, the development of techniques to reduce metal artefacts in microCT scans, these were not investigated in this study and the AOPE cups were therefore not scanned because the different density of the titanium shells would produce an artefact and prevent visualisation of the UHMWPE.

No visible subsurface cracking or micro-cracking was observed on the AOPE liners when compared to the AOPE control described in section 2.6 (Figure 4-6).

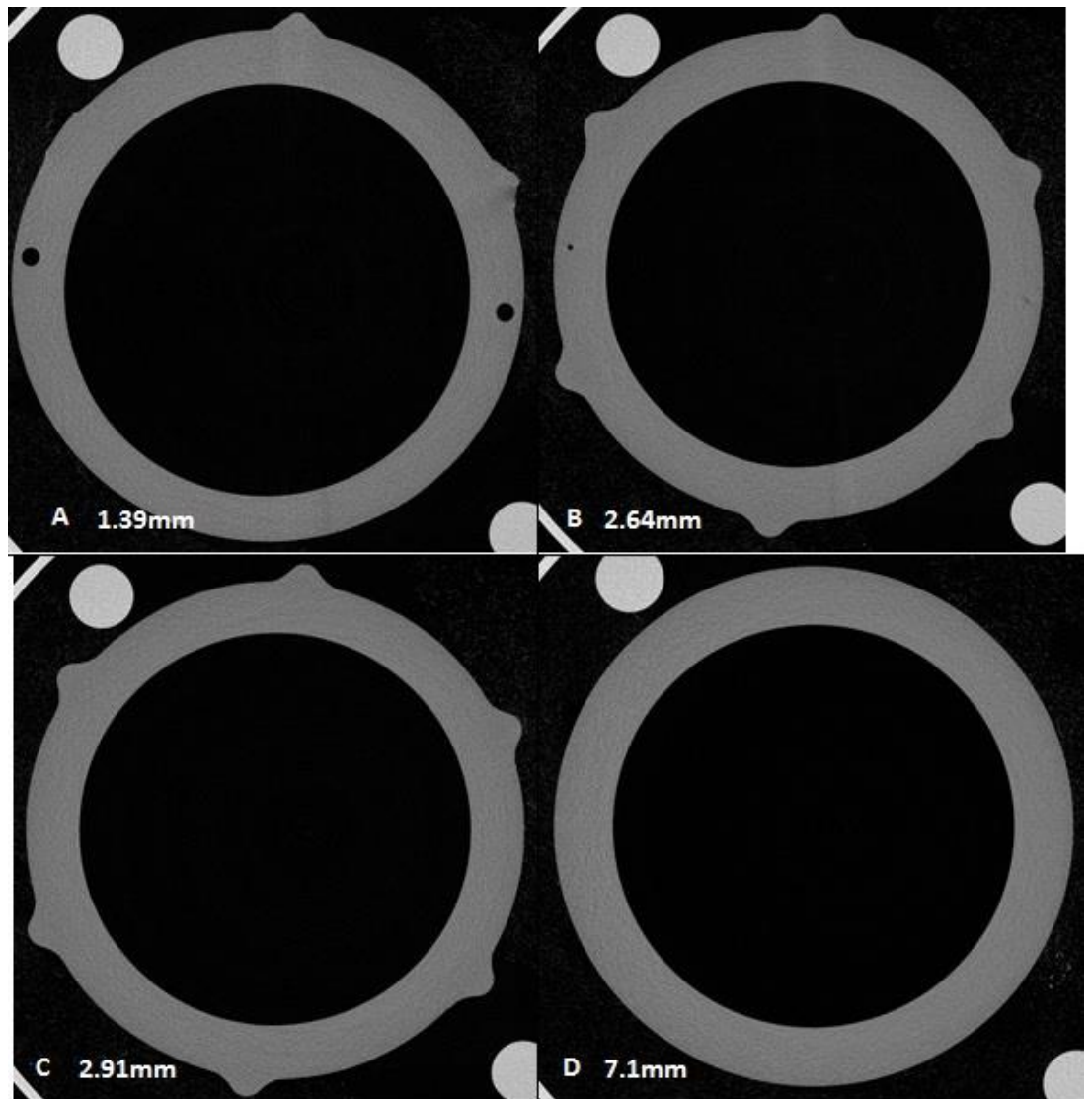


**Figure 4-6 MicroCT 2D reconstructed slices with no visible cracking: AOPE liner AOPE 5 at (A) 1.39mm. (B) 2.64mm, (C) 2.91mm and (D) 7.1mm below the horizontal surface of the rim. The holes are reference holes used in the CMM measurements. View is a cross section of the liner looking down onto the rim.**

#### **4.4.3 Damage to the acetabular liners and cups**

This section describes the wear and damage observed on the liners throughout the test and the location of wear and damage with respect to liner orientation.

A polishing or burnishing of the articulating surface in the superior region of the liner, characterised by a shiny appearance, was observed on all components,

both the AOPE liners and the AOPE cups. Fine multidirectional scratching was observed using a microscope on the bearing surfaces (Figure 4-7).

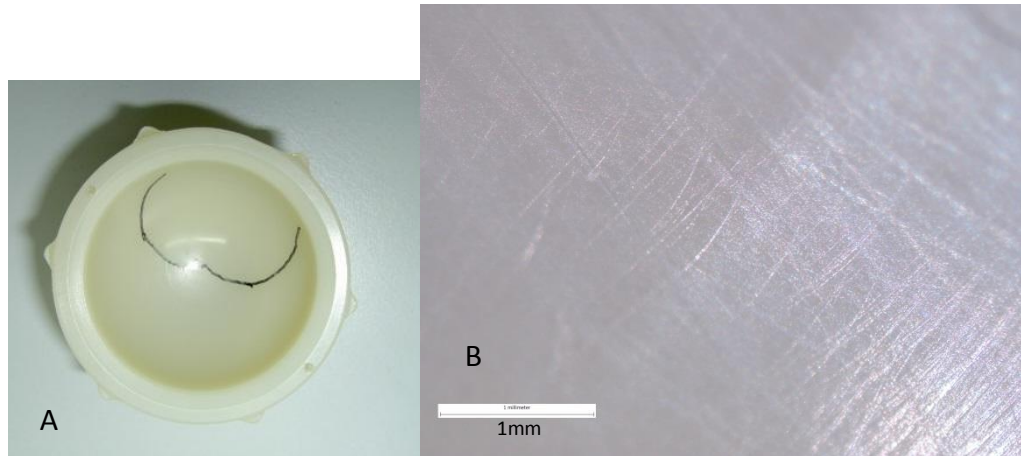


**Figure 4-7 An AOPE liner (AOPE 5) with (A) the wear area highlighted after standard loading and (B) a microscopy image of the polished bearing surface (x30 magnification)**

No other visible signs of damage on the bearing surface or the rim were observed on the liners or cups after standard or edge loading.

#### **4.4.4 Volume Changes**

The volume changes for the AOPE liners were calculated from the gravimetric measurements using the method described in section 2.3.3. They relate to material loss and compensation for fluid absorption was applied as described in section 3.3.6. The simulator tests for the AOPE liners and cups were run for 4.8Mc of standard loading and 5Mc of edge loading. For simplification of the results, these are discussed as 0 to 5Mc of standard loading and 5 to 10 Mc of edge loading. The mean volume change  $\pm$  the 95% confidence intervals are given and data sets are compared using a one-way ANOVA.

The mean total volume change for the AOPE liners after 5Mc of standard loading was  $25.4 \pm 1.9\text{mm}^3$  and the mean total volume change for the AOPE liners

between 0Mc and 5Mc of edge loading (5-10Mc of testing) was  $26.3 \pm 4.7\text{mm}^3$  (Figure 4-8).

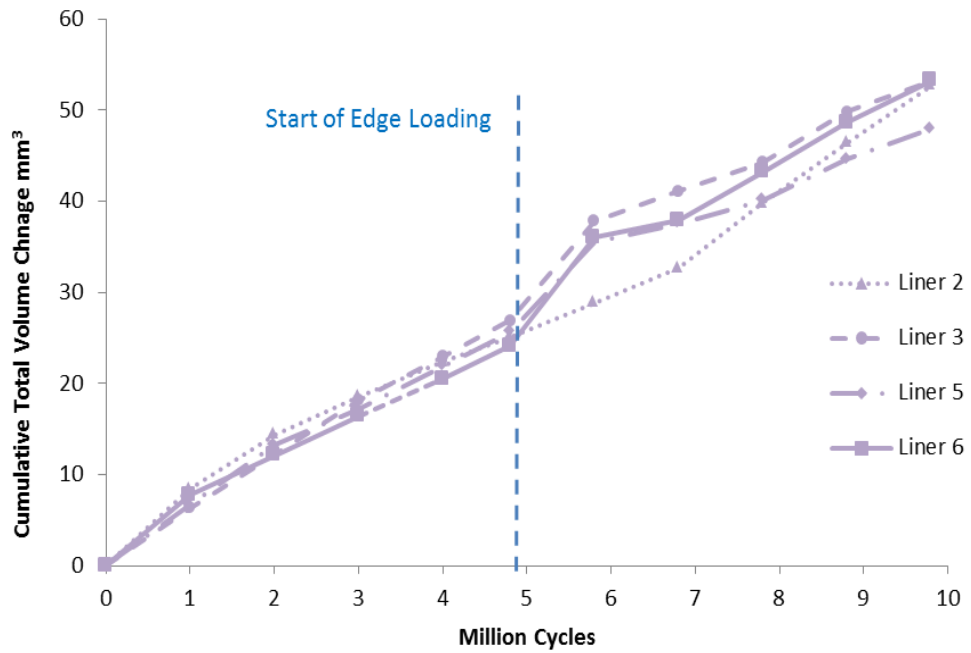


**Figure 4-8 Cumulative volume changes measured gravimetrically for the AOPE liners after 4.8Mc of standard loading (0-5Mc) and 5Mc of edge loading (5-10Mc) in a hip simulator**

The volume change of each AOPE liner and each AOPE cup was measured geometrically using a coordinate measuring machine as described in section 2.3.4. The geometric measurements assessed volume change relating to both wear and creep of the material.

The mean total volume change measured geometrically for the AOPE liners after 5Mc of standard loading was  $53 \pm 11\text{mm}^3$  and mean total volume change for the AOPE liners between 0Mc and 5Mc of edge loading (5-10Mc of testing) was  $36.4 \pm 5.22.9\text{mm}^3$  (Figure 4-9).

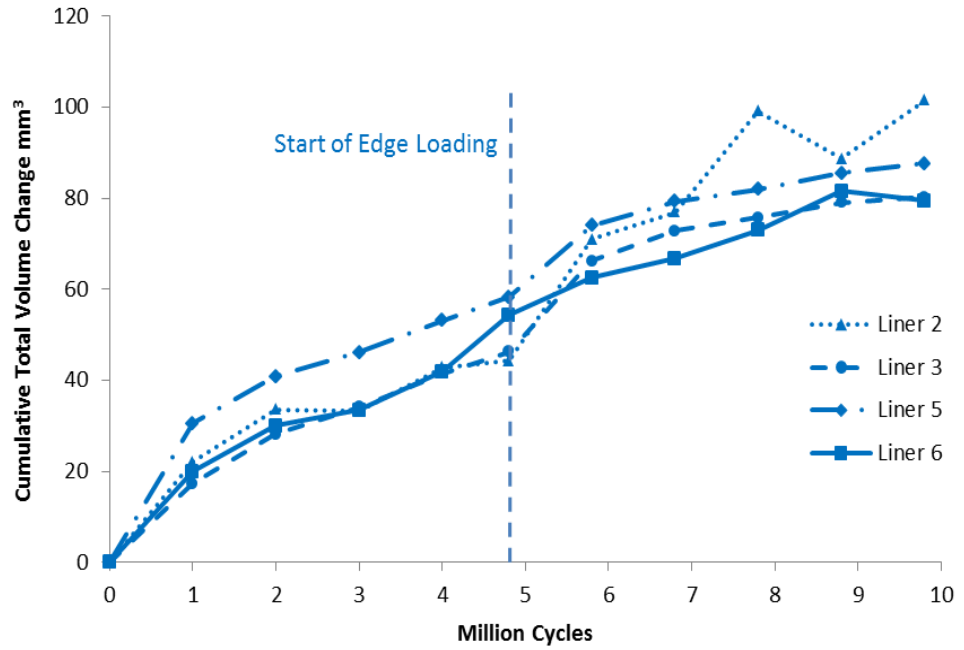


**Figure 4-9 Cumulative volume changes measured geometrically for the AOPE liners after 4.8Mc of standard loading (0-5Mc) and 5Mc of edge loading (5-10Mc) in a hip simulator**

The mean total volume change measured geometrically for the AOPE cups after 5Mc of standard loading was  $19.5 \pm 3.8\text{mm}^3$  and the mean total volume change for the AOPE cups between 0Mc and 5Mc of edge loading (5-10Mc of testing) was  $22.2 \pm 10.8\text{mm}^3$  (Figure 4-10).

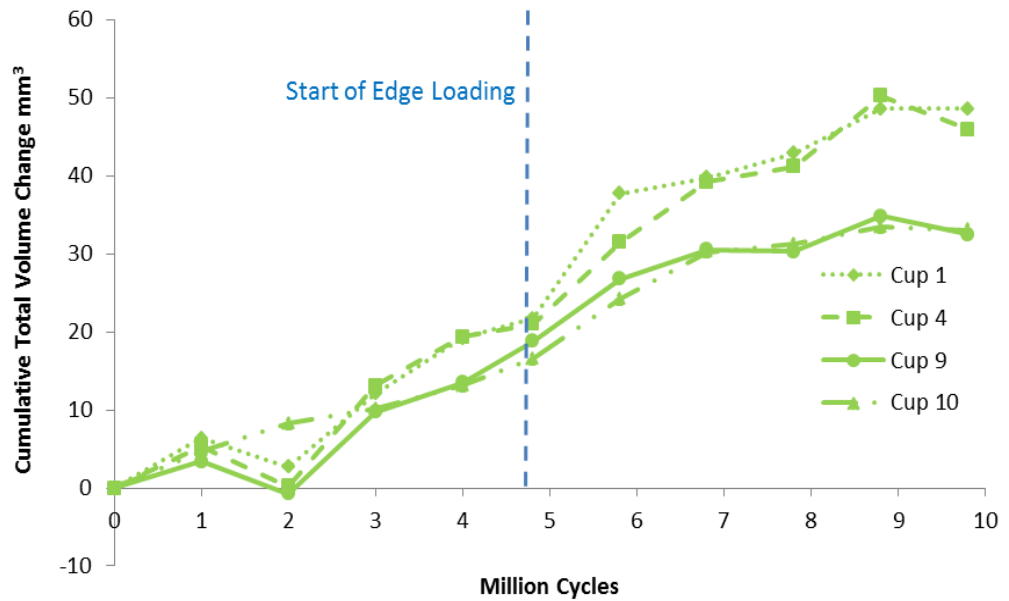


**Figure 4-10 Cumulative volume changes measured geometrically for the AOPE cups after 4.8Mc of standard loading (0-5Mc) and 5Mc of edge loading (5-10Mc) in a hip simulator**

The variation in the volume change measured geometrically between the AOPE cups increased during edge loading ( $19.5\text{mm}^2 \pm 11.9\% \text{RSD}$  for standard loading and  $20.5\text{mm}^2 \pm 15.7\% \text{RSD}$  for the edge loading conditions). This was also observed for the AOPE liners ( $50.8\text{mm}^2 \pm 13.1\% \text{RSD}$  and  $36.4 \pm 19.8\% \text{RSD}$  for standard and edge loading conditions, respectively).

The volume changes were converted to steady state wear rates as described in section 2.3.3. The steady state wear rates for the AOPE liners and AOPE cups calculated using both the gravimetric (AOPE liners only) and the geometric measurements are shown in Figure 4-11.

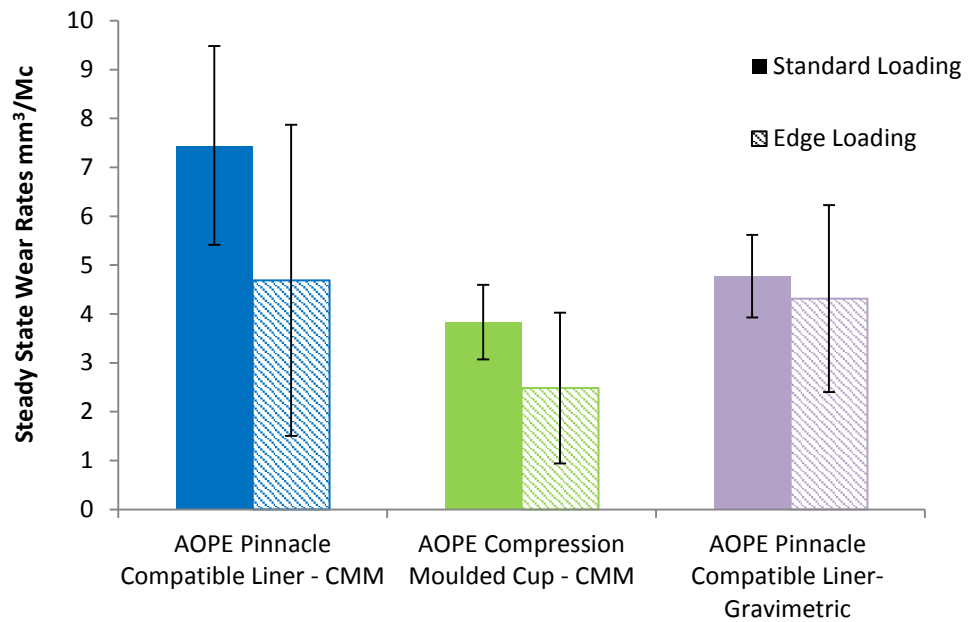


**Figure 4-11 Mean steady state wear rates for the AOPE liners and AOPE cups after 4.8Mc of standard and 5Mc of edge loading conditions calculated using geometric measurements and gravimetric measurements (AOPE liners only); ( $\pm$ 95% Confidence Intervals; n=4)**

The mean steady state wear rates for the AOPE cups were significantly lower than the AOPE liners under standard loading conditions ( $p < 0.01$ ) but the difference was not significant under edge loading conditions (measured geometrically;  $p = 0.09$ ). The mean steady state wear rates for the AOPE cups were significantly lower during edge loading than standard loading ( $p = 0.04$ ) but this difference for the AOPE liners was not significant when measured gravimetrically ( $p = 0.58$ ) or geometrically ( $p = 0.06$ ).

Volume change was observed on the superior region of the bearing surface after standard loading and in the form a thin narrow strip on the superior inner rim of all liners and cups after five million cycles of edge loading. This was observed on the SR3D geometric reconstructions (Figure 4-12).

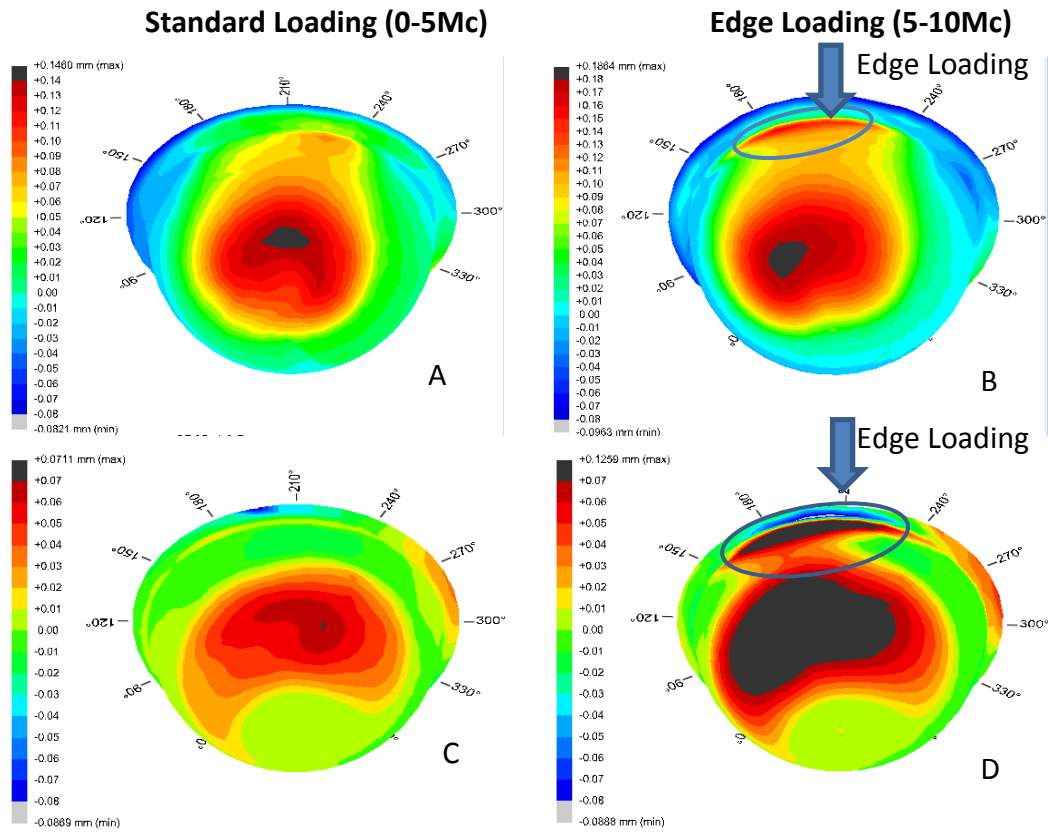


**Figure 4-12 SR3D geometric reconstructions of volume change after 5Mc standard loading and 5Mc edge loading conditions for the AOPE liners (A & B; AOPE 6) and AOPE cups (C & D; AOPE CM 2). Superior region of the liner/cup is at the top of the image.**

#### **4.4.5 Comparison of AOPE Study with Protocol Development Hip Simulator Study**

The results of the volume change and rim deformation assessments for the antioxidant tests were compared with the results of the protocol development tests in Chapter 3 and are presented in this Chapter. Very little surface or subsurface damage for the AOPE liners was observed and therefore these results were not compared.

The mean penetration at the inner rim for the AOPE liners and the AOPE cups ( $0.117\pm 0.07\text{mm}$  and  $0.07\pm 0.05\text{mm}$ , respectively) were not significantly different to the mean penetration at the inner rim for the XLPE liners or the aged PE liners ( $0.08\pm 0.04\text{mm}$  and  $0.18\pm 0.14\text{mm}$ , respectively; Figure 4-13; section 3.4.1)

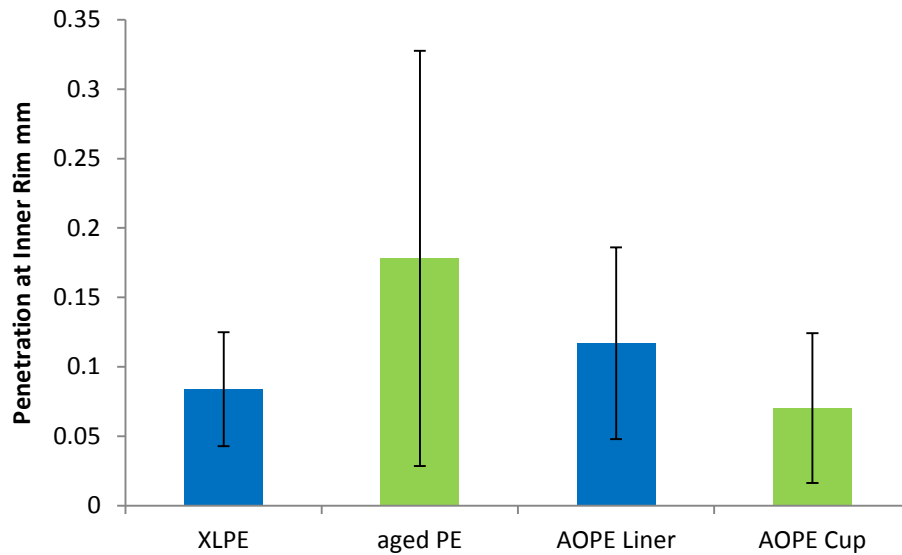


**Figure 4-13 Mean penetration values at the inner rim for the XLPE liners, Aged PE liners, AOPE liners and AOPE cups (95% Confidence Intervals; n=4)**

The AOPE liners and cups were lower wearing than the XLPE liners and the aged PE liners for the standard loading tests for both the gravimetric and geometric measurement methods (Figure 4-14; XLPE and aged PE data presented in sections 3.4.1). There was no significant difference in the wear of the different liners and cups under edge loading conditions.

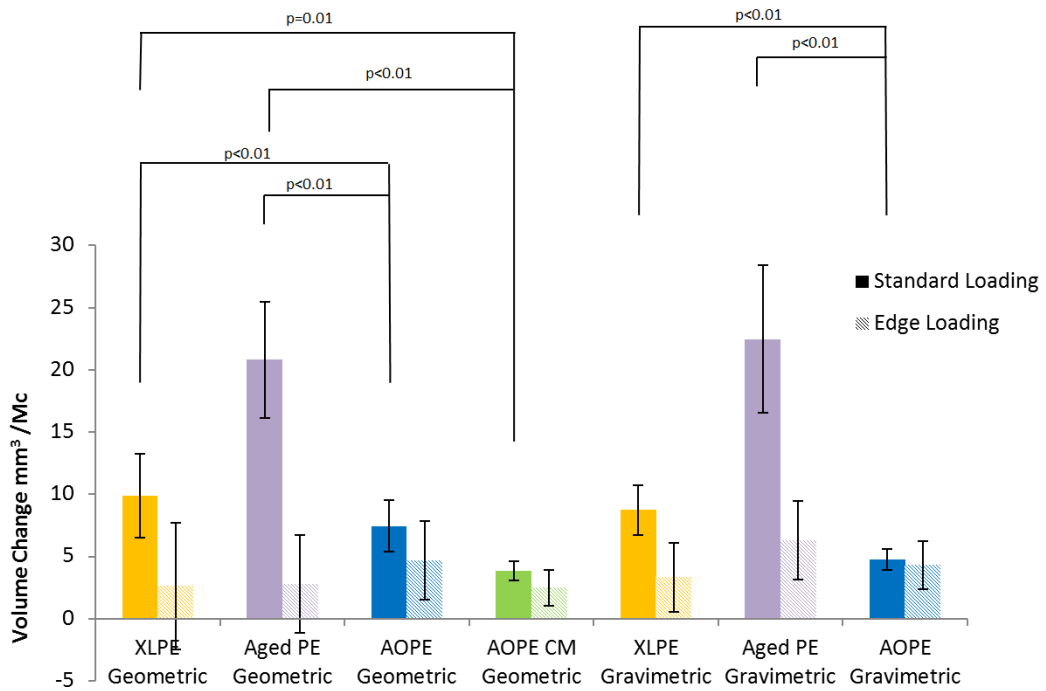


**Figure 4-14 Mean steady state wear rates measured gravimetrically and geometrically for the AOPE liners, AOPE cups, XLPE liners and aged PE liners for standard loading and edge loading conditions ( $\pm 95\%$  Confidence intervals;  $n=4$  for each liner/cup; all XLPE and aged PE data previously presented in results sections 3.4.1)**

## 4.5 Discussion

The aim of this study was to assess the wear and fatigue damage of a novel anti-oxidant UHMWPE of two different acetabular cup designs subjected to hip simulator testing under standard walking and edge loading conditions.

### 4.5.1 Volume Change

The AOPE cups exhibited lower volume change under standard loading conditions than the AOPE liners but there was no significant difference under edge loading conditions. Previous studies on compression moulded non modular cup designs have made similar observations and it was suggested in these studies that this may be due to increased shell-liner conformity, decreased micromotion and more favourable stress distributions due to design factors (Young et al., 2002;

Poultides et al., 2012). However, in terms of the decrease in wear due to micromotion, the absence of gravimetric measurements in the present study excludes any backside wear from the measured wear volume of the AOPE liners, so this is not factored into the results. Furthermore, a low sample size (n=4) means conclusions regarding better wear performance should be made with caution. However, further development of geometric measurement and analysis methods to more accurately establish wear volumes for these cups would be an interesting line of investigation.

The AOPE liners and cups were lower wearing than the XLPE liners and the aged PE liners for the standard loading tests for both the gravimetric and geometric measurement methods and there was no significant difference between any of the liners and cups under edge loading conditions. This result was expected as the material received a higher radiation dose than the wear resistant XLPE liners, resulting in a greater degree of crosslinking and wear resistance and the aged PE liners had undergone oxidative degradation. It is not known how the level of crosslinking compares to the XLPE liners, as the hindered phenols impede the crosslinking process (Narayan et al. 2009). However, the radiation dose is considerably higher (11.5Mrad for the AOPE compared to 5Mrad for the XLPE), so it is likely that the level of crosslinking is also greater.

Relatively little literature is available on anti-oxidant UHMWPE stabilised with hindered phenols, but previous studies on  $\alpha$ -tocopherol stabilised UHMWPE (Vitamin E) have reported no difference in wear rates compared to first generation crosslinked materials (Oral et al. 2006). Furthermore improved mechanical properties have also been reported for hindered phenol stabilised UHMWPE when compared to first generation highly crosslinked UHMWPE (Narayan et al. 2009; King et al. 2009; Narayan et al. 2009; King et al. 2009). It is likely that the difference in the volume change under edge loading conditions between the AOPE materials and the XLPE and Aged PE materials was not statistically significant because of the large variation in the volume change values under these conditions.

#### **4.5.2 Damage to Acetabular Liners and Cups**

Mild damage was observed on the AOPE liners and the AOPE cups in the form of fine scratching and a burnishing on the bearing surface. No cracking or visible damage to the rim was observed for either design.

The UHMWPE in this study was highly crosslinked and received a radiation dose of 11.5Mrad. Highly crosslinked UHMWPE acetabular components have a reduced toughness and fatigue crack propagation resistance (Baker et al., 1999; Pruitt, 2005) and may therefore be susceptible to rim fracture when edge loading occurs. Furthermore, as discussed in section 3.5.1, studies of retrieved acetabular liners have reported crack initiation at notched locking mechanisms that were similar to the ARDs on the components in this study (Tower et al., 2007; Furmanski et al., 2009; Furmanski et al., 2011). Hindered phenols have been shown to exhibit improved mechanical properties compared to crosslinked and re-melted UHMWPE including fatigue crack propagation resistance and these findings were supported in the present hip simulator study of edge loading conditions (King et al. 2009).

While the rim of the AOPE liners and the AOPE cups was not visibly deformed or damaged, the rim deformation analysis using 2D contacting profilometry (Talysurf traces) revealed some wear and/or deformation at the inner rim. This was comparable with the XLPE liners and the aged PE liners in the protocol development tests (Chapter 3) and therefore reinforces the visual analysis of the rim damage, which suggested that the AOPE liners and cups are no more susceptible to rim damage and wear than the clinically available XLPE liners.

The absence of cracking or fatigue type damage mechanisms in this study suggests that in terms of fatigue performance, the AOPE liners perform as well as the XLPE liners (negative controls) tested in Chapter 3. The lack of visible subsurface cracking when compared to the AOPE control liner in the MicroCT subsurface analysis further supports these findings.

## **4.6 Conclusion**

The aim of this study was to investigate the wear and fatigue mechanisms of a novel anti-oxidant UHMWPE of two different acetabular cup designs subjected to standard walking and edge loading conditions in hip simulator tests.

The anti-oxidant UHMWPE assessed in this study showed good wear and fatigue performance under standard and edge loading conditions when compared to the positive and negative controls in the protocol development tests described in Chapter 3. The volume change was comparable with the clinically available XLPE liners and no rim cracking was observed. Furthermore, the AOPE compression moulded cups showed comparatively good wear resistance when compared with the AOPE liners. Initial assessment of this anti-oxidant material is promising, further testing should be carried out to determine the wear and fatigue behaviour of the material following ageing and under more severe edge loading conditions.

## Chapter 5: **Wear and Damage Analysis of Explanted Acetabular Liners**

### **5.1 Introduction**

Pre-clinical simulator testing of total hip replacements is essential to understanding the clinical performance of new component designs and materials and is a requirement of legislative product approval. The analysis of explants retrieved at revision surgery can be used to inform and validate the design of these simulator tests and to ensure that clinically relevant damage mechanisms are being replicated. Furthermore, explant analyses can be used to identify trends and correlations in damage and failure mechanisms to predict early failure and inform future component design.

The aim of this study was to evaluate new methodologies for the analysis of explanted acetabular liners with specific emphasis on damage and deformation due to edge loading and to carry out primary failure analyses of explanted acetabular liners.

The study had the following objectives:

1. Apply and evaluate methodologies developed in Chapter 2 to assess explanted acetabular liners for wear, damage and deformation;
2. Identify damage mechanisms from analysis of sixteen liners retrieved at revision surgery along with the associated clinical data;
3. Determine whether specific risk factors for liner failures can be identified and if recommendations can be made to minimise such failures in future.

### **5.2 Methods and Materials**

This section describes the procedures that were implemented for collecting explants as well the methods of analysis that were specific to explants. General measurements and analyses were carried out as described in Chapter 2.

### **5.2.1 Ethical Approval and Explant Collection**

To comply with good clinical practice in research, ethical review by an appropriate ethics committee is required for all research involving human participants. For research involving NHS patients, ethical review is required by an NHS review committee. Favourable Ethical Approval was obtained from Leeds (West) Ethical Review Committee for the project “Wear Analysis of Explanted Orthopaedic Prostheses 09/H1307/60”. The protocol approved by the committee covered the retrieval of explanted orthopaedic components and associated tissue removed at revision surgery. The key elements of the collection procedure outlined in the protocol were the following:

- Pre-operative informed consent
- Maintaining patient anonymity
- Safe shipping and storage of retrieved explants.

The documents for obtaining consent and recording the details of the retrieved prostheses and associated tissue were approved by the research ethics committee and can be found in Appendix 6. Explants were assigned a code to maintain patient anonymity and recorded in a database. Consent forms were stored by Dr Sophie Williams, the chief investigator for the project.

Following favourable ethical opinion, R&D permission was obtained from each individual trust. Two sites were included in the present study: Musgrave Park Hospital, Belfast and Charlotte Maxeke Johannesburg Academic Hospital, Johannesburg, South Africa. These sites were selected based on the availability of retrieved joints.

The explants were carefully removed at revision surgery, packaged according to UN Packaging Instruction P650 and shipped according to UN3373 regulations for transportation of Biological Substances, Category B (Dept. for Transport, 2012). The explants were collected with pre and post-operative x-rays and selected patient and patient related data was recorded (Table 11; Explant Information Form, Appendix 6). On arrival in the department, the explants were decontaminated, cleaned and stored (section 2.3).

**Table 11 List of patient/implant data recorded and description of the data**

| <b>Details/Information collected with explants</b>                   | <b>Description of data provided</b>   |
|--|---|
| Name of Hospital   | Name of the hospital where the revision operation was carried out   |
| Name of Surgeon  | Name of the surgeon that carried out the revision operation   |
| Date of Birth  |   |
| Height/Weight  | The Patient's BMI (Body Max Index) was calculated from this data  |
| Gender   |   |
| Type of Prosthesis   | Bearing combination and product type if known (i.e. manufacturer and design name)   |
| Primary, 1 <sup>st</sup> , 2 <sup>nd</sup> revision explant or other | Was this the first revision operation for the patient and if not, how many previous revisions were there?                               |
| Implant and explant date   | Date that the joint was implanted and date of revision operation. Time in vivo was calculated from these dates.                         |
| Side operated on   | Left or right joint   |
| Initial Diagnosis  | The initial reason for the first joint replacement.   |
| Reason for Revision  | Why was the joint revised   |
| Patient Activity Level   | Surgeon selected from 6 different activity levels: immobile/wheelchair, 1 stick, 2 sticks, sedentary, reasonably active and very active |
| History of dislocation?  | YES/NO and details  |
| Evidence of Impingement?   | YES/NO and details  |
| Other information?   | Any other information that the surgeon or support staff deemed relevant to the failure of the joint.                                    |

### 5.2.2 Explant Selection

The explant collection at the Institute of Medical and Biological Engineering consisted of hip, knee and ankle joints collected over a period of six years. Sixteen explants were selected from this collection. To allow a better comparison between the simulator study and the explant study to be made (overall study aim and Chapter 6), explants of the same design as those tested in the simulator study in Chapter 3 & 4 were selected. The inclusion criteria for the study were material (UHMWPE) and design (Pinnacle®). The Pinnacle® design is described in section 3.2. A summary data set with relevant data for the explants is provided in Table 12. Images of the explants can be found in Appendix 5.

The explants were divided into three subsets (Figure 5-1): lipped liners (L; n=4; liners with an elevated rim region); dissociated neutral liners that had failed due to dissociation from the metal shell (D; n=5) and non-dissociated neutral liners that had failed for a variety of other reasons (N; n=7).

All of the neutral liners (dissociated and non-dissociated) had a flat face (no elevated rim) and the centre of rotation of the femoral head was concentric with the outer acetabular shell. In the lipped subset, three of the liners were Pinnacle® lipped liners (4mm build up for stability and 15° face change) and one was a +4 10° face changing liner (lateralisation of 4mm and 10° face change).

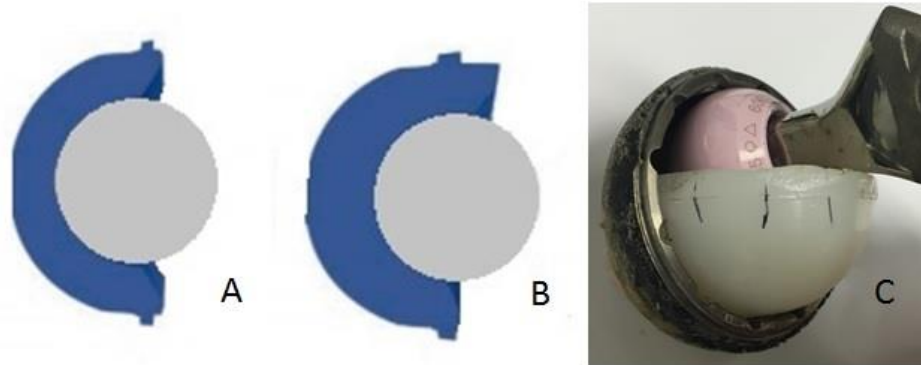


**Figure 5-1 Schematic of a (a) neutral liner, (B) lipped liner and (C) an image of a dissociated neutral liner (liner 10D)**

The subdivisions were selected to allow the identification of any trends and/or correlations in the damage mechanisms relating to the specific geometry of the components as well as to identify any damage mechanisms that were present on the dissociated neutral liners but not the non-dissociated neutral liners, thereby obtaining some insight into the failure of these components. Furthermore, the dissociated liners exhibited extensive damage that was sustained post-dissociation and it was therefore thought that this should be separated from the wider damage analysis as the damage mechanisms observed prior to dissociation were more useful to determine the cause of dissociation.

**Table 12 Summary details of all explants included in the study**

| Explant Code | Patient age (Years) | Time in vivo (Mnths) | BMI (Kg/m <sup>2</sup> ) | Cup Inclination (Degrees) | Activity level | PE thickness | Diameter | Sex | Side | Diagnosis | Reason for revision   | Bearing | Stem   | Subset |
|--------------|---------------------|----------------------|--------------------------|---------------------------|----------------|--------------|----------|-----|------|-----------|-----------------------|---------|--------|--------|
| 1N           | 79                  | 95                   | 35.9                     | 42                        | 3              | 9.5mm        | 28mm     | M   | R    | NA        | Lucency, infection    | MOP     | Corail | N      |
| 2N           | 78                  | 85                   | NA                       | 60                        | 3              | 8mm          | 28mm     | F   | R    | OA        | Stem lucency          | MOP     | Corail | N      |
| 3N*          | 68                  | 47                   | 28.3                     | 47                        | 4              | 8mm          | 28mm     | F   | L    | Pain      | Stem lucency          | MOP     | Corail | N*     |
| 4N           | 72                  | 101                  | 27.3                     | 50                        | 3              | 11mm         | 28mm     | M   | L    | OA        | Fall, Infection, pain | COP     | C-stem | N      |
| 5N           | 73                  | 101                  | 27                       | 48                        | 4              | 7mm          | 28mm     | F   | R    | NA        | Stem loosening        | COP     | Corail | N      |
| 6N           | 78                  | 95                   | 31                       | 55                        | 3              | 8.5mm        | 28mm     | M   | R    | Pain      | Stem loosening        | MOP     | Corail | N      |
| 7N*          | 70                  | 23                   | 37.6                     | 33                        | 5              | 9mm          | 32mm     | M   | L    | NA        | Dislocation           | MOP     | Corail | N*     |
| 8D*          | 78                  | 31                   | 33                       | 57                        | 3              | 8.5mm        | 32mm     | F   | R    | OA        | Dissociation          | MOP     | Corail | D*     |
| 9D           | 72                  | 71                   | 26                       | 49                        | 5              | 8.5mm        | 28mm     | M   | R    | NA        | Dissociation          | COP     | Corail | D      |
| 10D*         | 83                  | 63                   | 27.9                     | 43                        | 5              | 8.5mm        | 28mm     | M   | R    | OA        | Dissociation          | MOP     | Corail | D*     |
| 11D*         | 74                  | 58                   | 28                       | 43                        | 5              | 8.5mm        | 28mm     | F   | L    | OA        | Dissociation          | MOP     | Corail | D*     |
| 12D*         | 96                  | 97                   | 26                       | 50                        | 4              | 8.5mm        | 28mm     | M   | L    | OA        | Dissociation          | MOP     | Corail | D*     |
| 13L*         | 57                  | 85                   | 37.8                     | NA                        | 2              | 9.5mm        | 28mm     | F   | R    | OA        | Stem loosening        | COP     | Corail | L*     |
| 14L*         | 58                  | 60                   |                          | NA                        | 5              | 9.5mm        | 28mm     | F   | R    | OA        | Stem loosening        | COP     | Corail | L*     |
| 15L*         | 53                  | 7                    | 32.6                     | NA                        | NA             | 9.5mm        | 28mm     | F   | R    | OA        | Dislocation           | MOP     | NA     | L*     |
| 16L*         | 54                  | 6                    | 28                       | NA                        | 5              | NA           | 32mm     | F   | R    | OA        | Dislocation           | MOP     | NA     | L*     |

\*Crosslinked UHMWPE; NA =not applicable or not available

(N=Neutral, D=Dissociated, L=Lipped)

For the neutral liner subset, the average patient age was 75 years, the average BMI was 30 Kg/m<sup>2</sup> and the average activity level was 4, representing a sedentary patient population that did not use a mobility aid. The average time in vivo for these explants was 87 months and the reasons for revision were pain, loosening, lucency, infection and for one explant, recurrent dislocation. Five of seven liners were GVF<sup>®</sup> UHMWPE and the remaining two were a moderately crosslinked UHMWPE (Marathon<sup>®</sup>). Six of the seven neutral liners were 28mm diameter and one was 32mm diameter. For the dissociated liner subset, the average patient age was 81, the average BMI was 28 and the average activity level was 4. The average time in vivo for these explants was 64 months and the reason for revision was dissociation of the liner from the metal shell. A sudden onset of pain followed by a grinding or squeaking was reported for three of the five cases. The joint was revised at a mean of 6 months (4-8months) after this event. Four of five liners were crosslinked UHMWPE (Marathon<sup>®</sup>) and one liner was GVF<sup>®</sup> UHMWPE. Four of five dissociated liners were 28mm diameter and one was 32mm. For the lipped liner subset, the average patient age was 56, the average BMI was 33 and the average activity level was 4. The average time in vivo for these explants was 40 months and the reasons for revision were loosening for two of the explants and dislocation for two of the explants. All of the lipped liners were crosslinked. Three of four liners were diameter 28mm and one was 32mm diameter. Thirteen of the explants consisted of Corail<sup>®</sup> (DePuy, Warsaw, USA) cementless femoral stems (one was a DePuy C-stem<sup>®</sup> and two were unknown).

### **5.2.3 Analysis Methods for Explants**

An analysis protocol was followed for each of the selected explants and is summarised below:

- Components were photographed using a Canon 700D SLR Camera with a 100mm macro lens (Canon (UK) Ltd, Surrey, UK);
- The type of UHMWPE, diameter and UHMWPE thickness were determined from the lot numbers on the component and by consulting manufacturer product information sheets;
- Damage was graded and categorised as described in section 5.2.4;

- Geometric volume change measurements were taken as described in section 2.4.
- Rim profile traces were taken using contacting profilometry as described in section 2.5;
- MicroCT scans were carried out for a selection of the explants as described in section 2.6;
- The patient x-ray was inspected and the inclination angle of the acetabular component was determined using Sante DICOM Viewer FREE version 3.0.12 software. The transischial line was used as the horizontal reference as described by Murray (1993) and Loftus & Ghelman (2015) (Figure 5-2). A line was drawn along the horizontal reference and across the cup face and the angle between the two was calculated using the software angle tool;
- Any other relevant information or observations were noted.

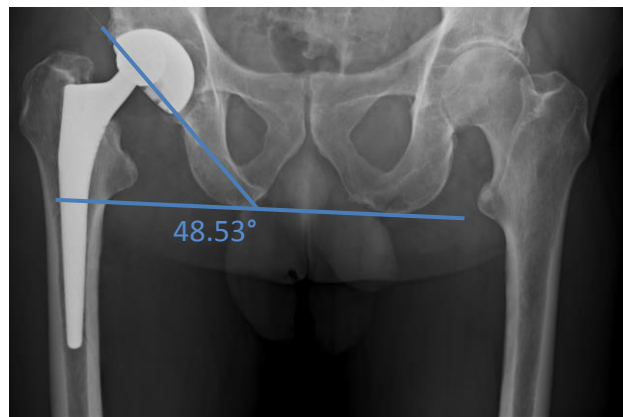


**Figure 5-2 Pre-operative x-ray showing the horizontal reference along the transischial line and the inclination angle of the acetabular cup**

#### **5.2.4 Semi-Quantative Damage Categorisation of Explants**

A macroscopic visual assessment of the explants was performed. A stereomicroscope (Nikon UK Ltd, Surrey, UK) was also used to help identify damage mechanisms if required. Each explant was awarded a damage score using an adaptation of a method described by Hood et al. (1983).

The explants were divided into four quadrants. If known, the wear area was located towards the superior aspect (identified from geometric reconstructions, see section 5.3.1; Figure 5-3). Each quadrant was subdivided into the bearing surface and the rim region with the rim region being defined as the flat rim section and the chamfer up to the inner rim.

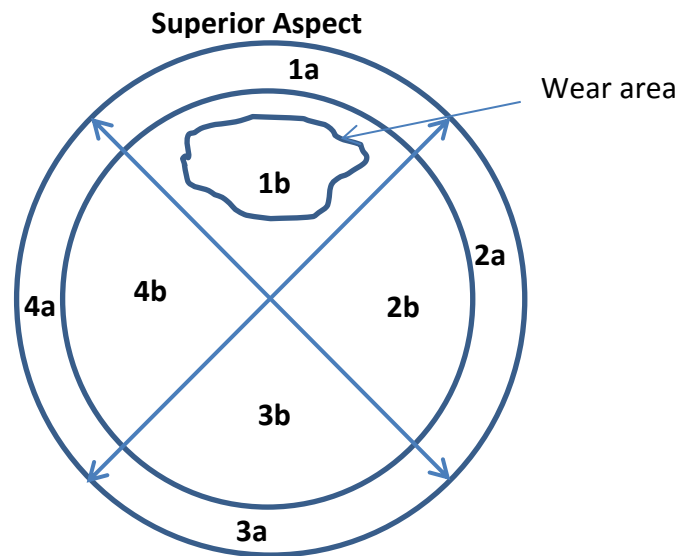


**Figure 5-3 Schematic of an acetabular liner divided into four quadrants with the wear area to the superior aspect where (a) denotes the rim subdivision and (b) the bearing surface subdivision**

Each subdivision of each quadrant was visually inspected for the following wear and damage mechanisms (Figure 5-4):

- **Deformation** - dimensional change due to plastic deformation
- **Pitting** - depressions in the surface
- **Embedded Debris** - third body particles embedded in the UHMWPE
- **Scratching** - multidirectional indentations into the UHMWPE
- **Burnishing** - highly polished appearance.
- **Abrasion** - visually roughened surface.
- **Delamination** - Subsurface failure together with removal of large sheet of UHMWPE

- **Cracking/Fracture** - small subsurface cracks to gross fracture of the component.

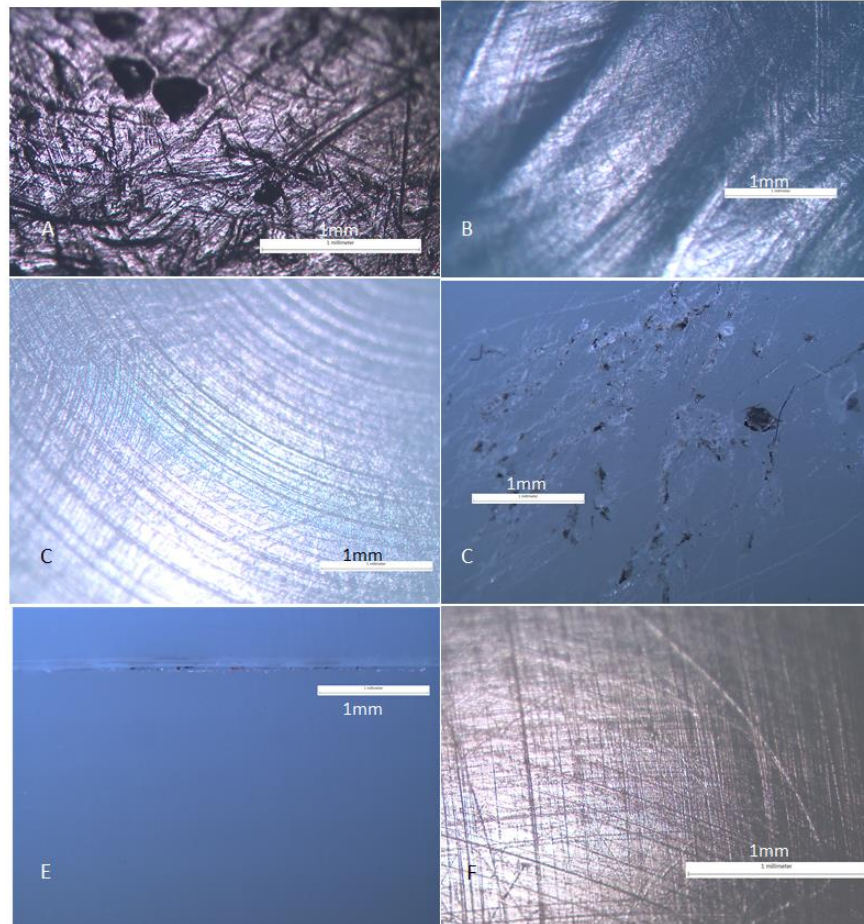


**Figure 5-4 Microscopy image taken at x30 magnification showing (A) pitting, (B) surface deformation (indentations), (C) unworn surface with machining marks still visible, (D) abrasion, scratching and embedded debris, (E) large scratch and (F) fine scratching and burnishing**

The presence and degree of each damage mechanism was graded on a scale of 0 to 3 depending on the percentage coverage of the quadrant (Table 13).

**Table 13 Scoring system for assessing damage mechanisms on explant bearing surfaces and rims**

| Damage Score | Extent of Damage            |
|--------------|-----------------------------|
| 0            | No damage                   |
| 1            | 10% coverage of quadrant    |
| 2            | 10-50% coverage of quadrant |
| 3            | >50% coverage of quadrant   |

The assessor's perception of severity was also taken into account in the final score. For example, if the damage mechanism only covered 10% of the surface but was deemed by the assessor to be particularly severe, this may have scored as highly as small scratches over more than 50% of the surface. The total possible score for each subdivision was 24, which equates to 48 for each quadrant and 192 for the whole acetabular liner.

The backside of the liners and other components (metal shell and femoral head) were visually inspected and any damage was noted. However, as the principal areas of interest in this study were the bearing surface and rim of the UHMWPE liner, a damage scoring was not performed. Femoral stems were excluded from the damage analysis because they were not available for all explants and because the focus of this study was the acetabular liners.

### 5.2.5 Calculation of Volume Change per Million Cycles for Explants

The volume change for the simulator samples was calculated by dividing the mean total volume change by the number of cycles. To obtain a comparative value for the explants, the formula developed by Dowson and Wallbridge (1982) to calculate the number of steps based on patient age and adapted by Hall & Pinder (1998) to determine the total number of cycles per year was applied (Equation 5.1):

$$N = 0.5(A_r - A_p)[6.58 - 0.032(A_r - A_p)] \times 10^6 \quad (5.1)$$

where  $A_r$  is the patient's age at revision and  $A_p$  is the patient's age at primary surgery.

A later study by Goldsmith et al. (2001) that observed the walking activities of patients with and without total hip replacements reported a decline in activity with age and results were "broadly consistent" with the earlier study by Dowson and Wallbridge. While it was acknowledged that patient activity may change over time, this reinforces the relevance of the formula for the present study.

The volume change per Mc for the explants was then calculated by dividing the total volume change by N.

### **5.3 Results**

The following sections outline the results of the explant analyses including rim deformation, subsurface damage, damage categorisation and volume change.

#### **5.3.1 Rim Deformation**

Two dimensional contacting profilometry traces were taken across the liner rims to measure wear and deformation due to edge loading as described in section 2.5.

##### Non-dissociated Neutral Liners

Five of the seven neutral liners did not exhibit evidence of edge loading on the rim region and the radius of curvature at the inner rim was relatively uniform around the circumference of the liner (explants 1N, 2N, 3N, 4N and 7N; Figure 5-5).

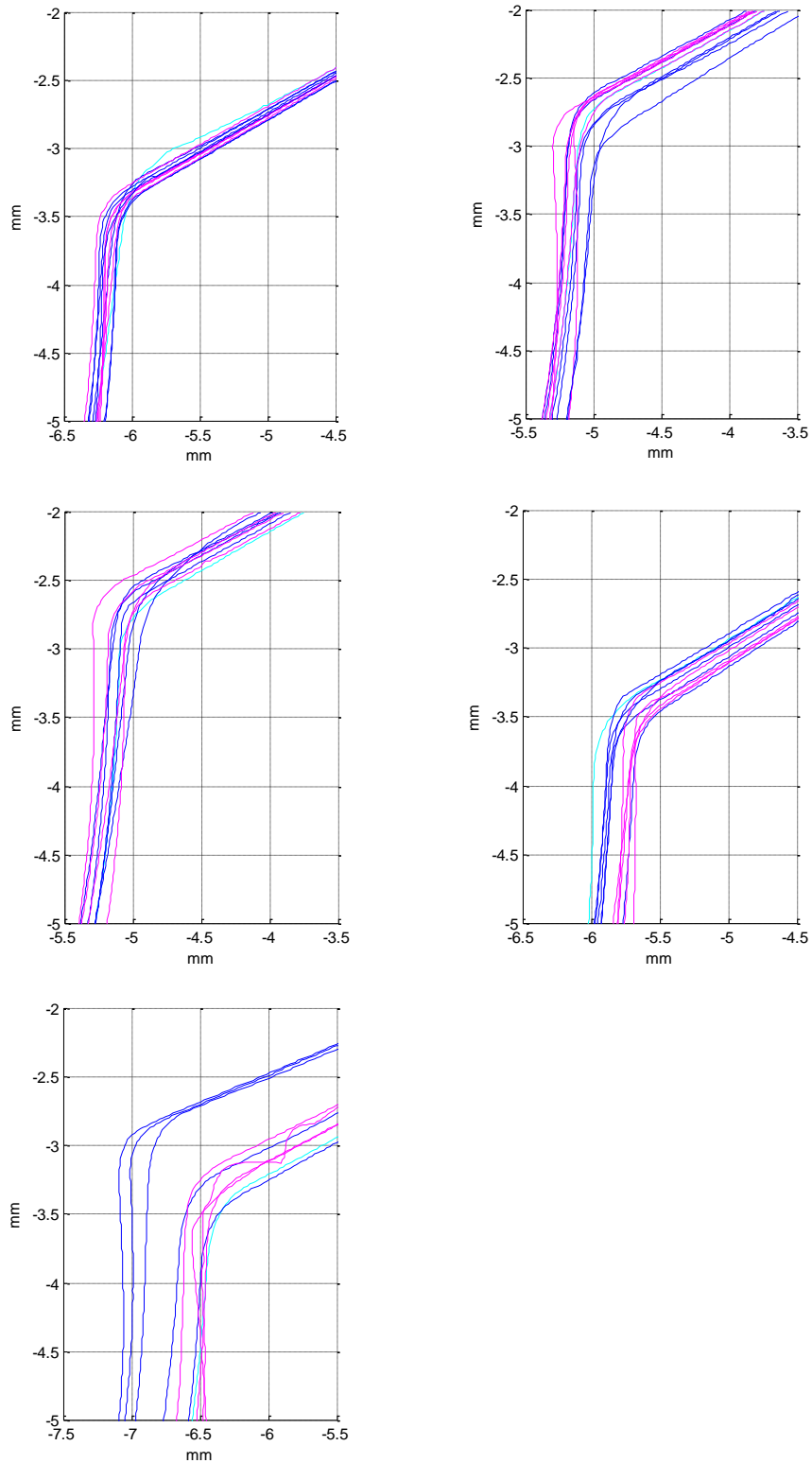


**Figure 5-5 Close up of the inner rims of five of the neutral liners with no visible deformation and/or wear. Blue traces are taken over the unworn region and pink traces over the worn region. Cyan traces are taken from the anterior and posterior unworn regions of the liner.**

A visible change in the radius of curvature and a sharpening of the inner rim was observed on two of the explants (explant 5N and explant 6N; Figure 5-6). For these two explants the mean distance from an unworn trace to the worn traces was 0.36mm and 0.5mm, respectively.

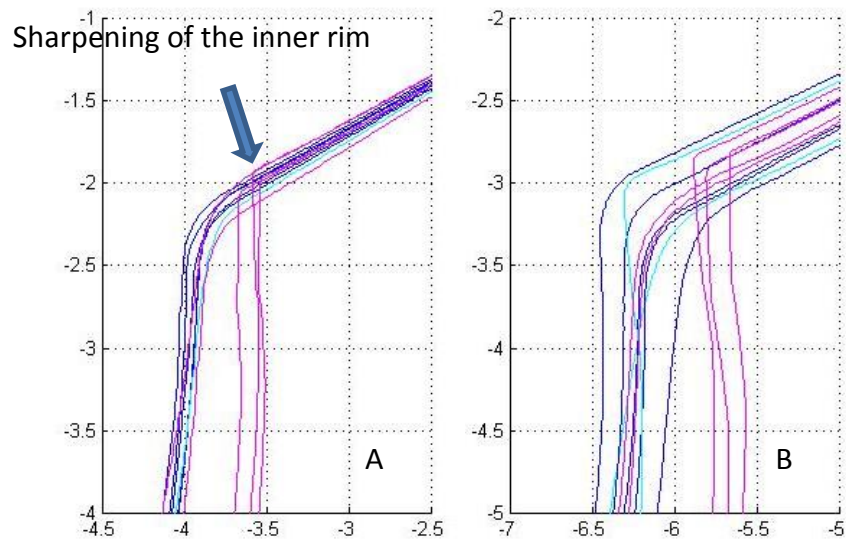


**Figure 5-6 A close up of the inner rim showing a sharpening of the rim for (A) explant 5N with a mean penetration distance of 0.36mm and (B) explant 6N with a mean penetration of 0.5mm. Blue traces are taken over the unworn region and pink traces over the worn region. Cyan traces are taken from across the anterior and posterior regions of the liner.**

#### Dissociated Neutral Liners

The extent of damage and deformation to the dissociated neutral liners made identification of the datum difficult and it was not possible to align and level the traces using the Matlab code (section 2.5). However, it was possible to plot the traces and qualitatively analyse the change in shape of the inner rim (Figure 5-7).

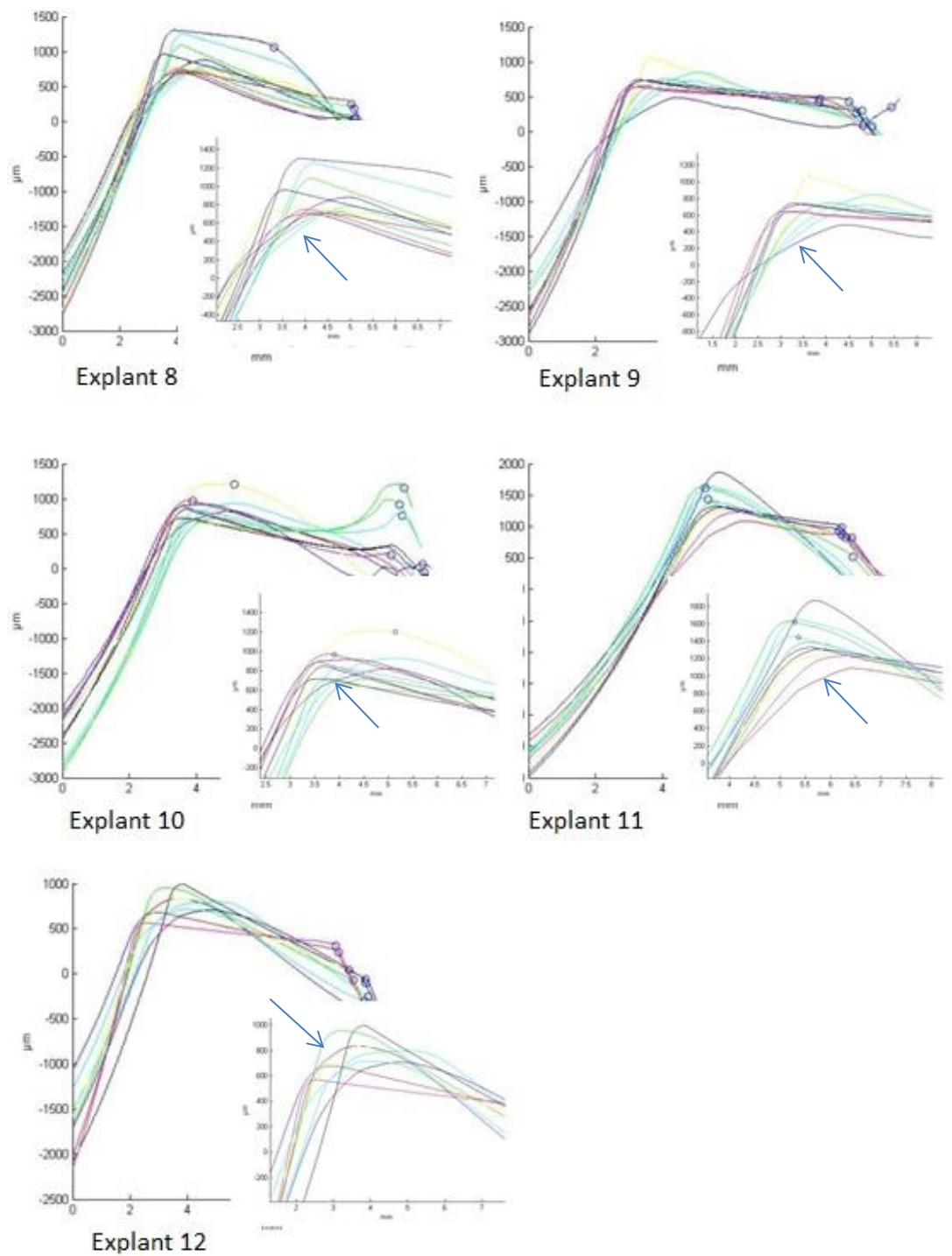


**Figure 5-7 Full traces and close up of the inner rims of the five dissociated neutral liners with large deformations in the form of a flattened curve on the superolateral rim (identified for one of the superolateral traces with an arrow)**

All of the dissociated neutral liners exhibited deformation at the inner superolateral rim, giving the rim a flattened appearance compared to other

undeformed or less deformed areas of the rim, such as the anterior and posterior sides (Figure 5-8).

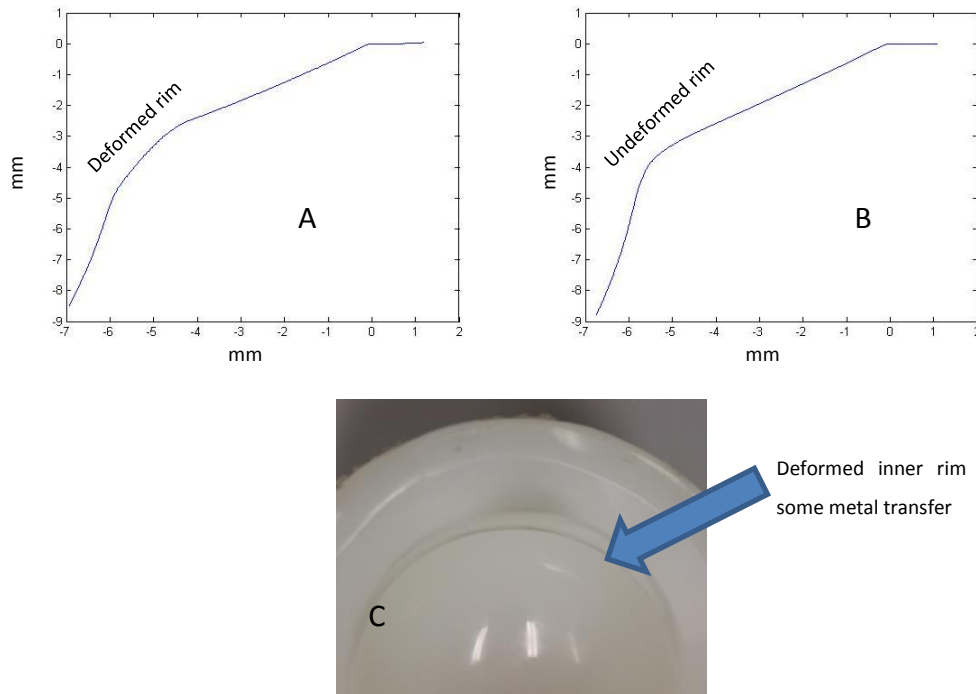


**Figure 5-8 Talysurf traces of (A) a flattened inner rim on the superior region of dissociated neutral liner, explant 12D, (B) an undeformed region of the same liner (or less deformed) and (C) a photographic image of the deformed inner rim (explant 12D)**

### **5.3.1 Subsurface damage**

Three non-dissociated neutral liners (explants 2N, 3N and 5N) and three dissociated neutral liners (explants 9D, 11D and 12D) were selected for subsurface damage assessment using MicroCT. This is described in section 2.6.

#### Non-dissociated Neutral liners

No obvious subsurface micro-cracking or damage was observed on explant 3N when compared with the XLPE control liner in 2.6.2 (Figure 5-9).

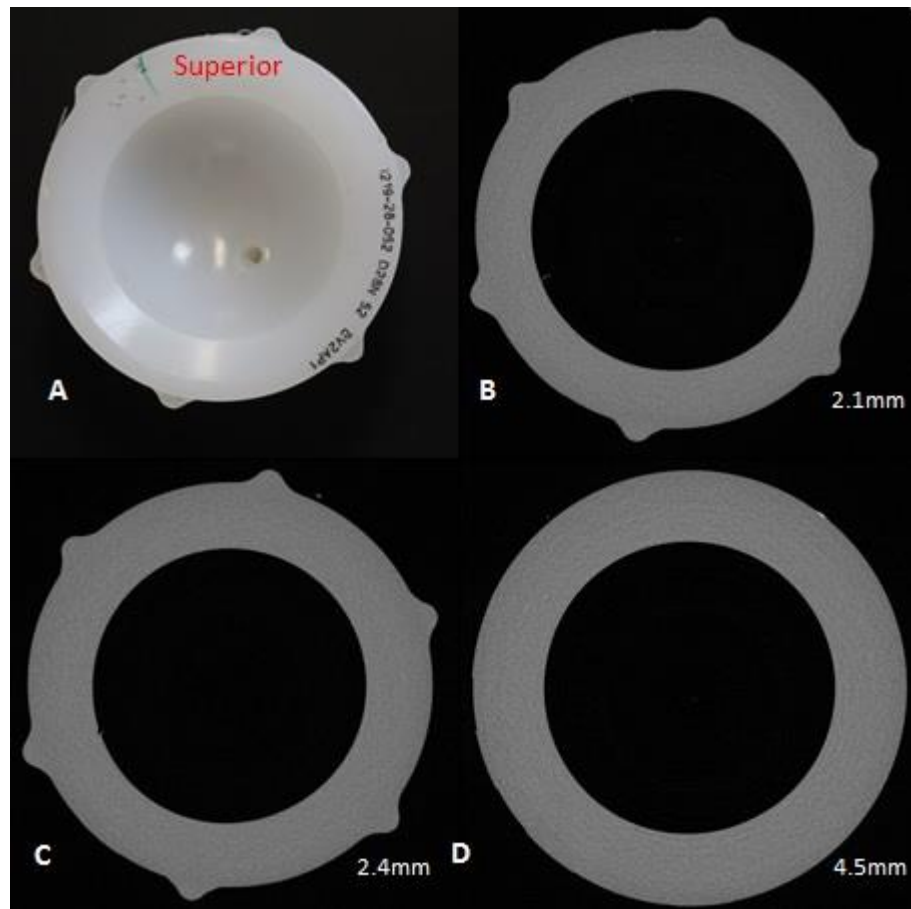


**Figure 5-9 A** Photographic image and MicroCT images of the subsurface damage observed on a non-dissociated neutral liner (explant 3N) showing (A) a photo of the component and orientation *in vivo*, (B, C & D) visibly undamaged sections of the liner between 2.1mm and 4.5mm below the horizontal rim.

No visible micro-cracking or subsurface damage was observed in the superior region of explant 2N. However, significant subsurface damage was observed in the posterior rim region, beneath the damage that was observed on the surface (Figure 5-10). Large cracks and cracks propagating circumferentially, originating from the larger cracks, were observed. This damage was observed up to 2.2mm below the horizontal surface of the liner rim.

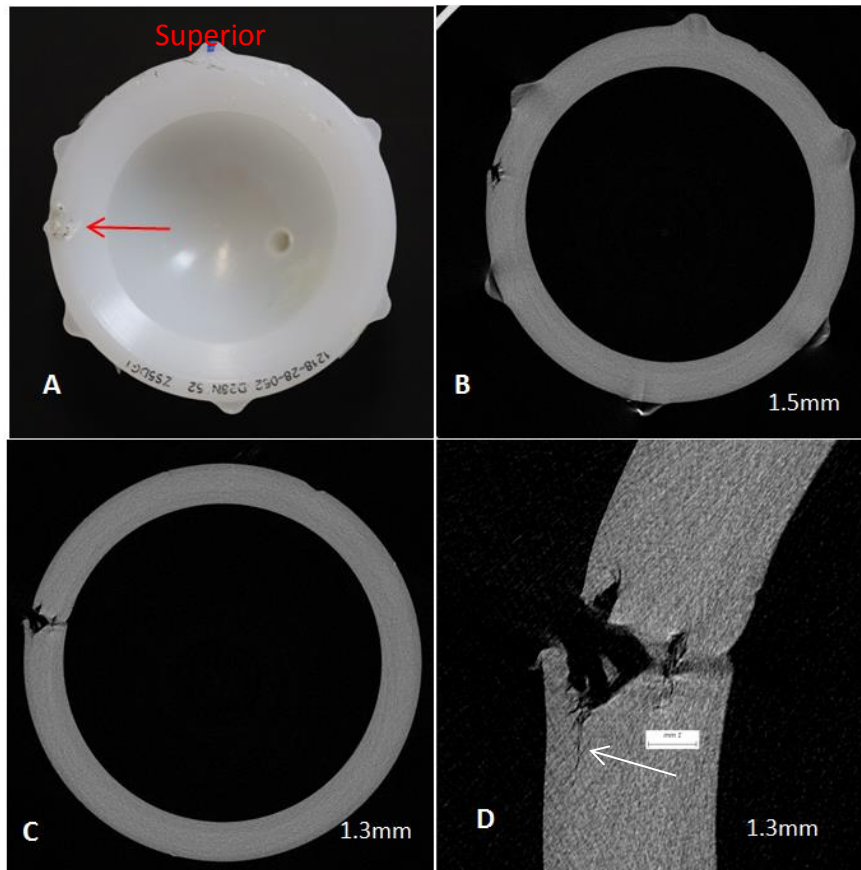


**Figure 5-10 A Photographic image and MicroCT images of the subsurface damage observed on a non-dissociated neutral liner (explant 2N) showing (A) a photo of the component and orientation *in vivo*, (B) visibly undamaged section of the liner 5mm below the horizontal rim (C) a visibly damaged section showing cracking 1.3mm beneath the surface damage and (D) a close up of the damage in (C) showing cracks extending circumferentially and perpendicular to the outer rim (arrow; scale bar 1mm).**

No significant micro-cracking or subsurface damage was observed in the superior region of explant 5N. However, significant subsurface damage was observed in the posterior rim region, beneath the damage that was observed on the surface (Figure 5-11). Cracks propagating circumferentially and multi directional cracking were observed up to 2.5mm below the surface of the liner rim. This damage appeared to originate at the outer edge of the liner rim and no cracking was observed close to or originating from the inner rim. Damage and cracking was

observed in the upper rim region only and did not extend more than a few millimetres below the horizontal rim.

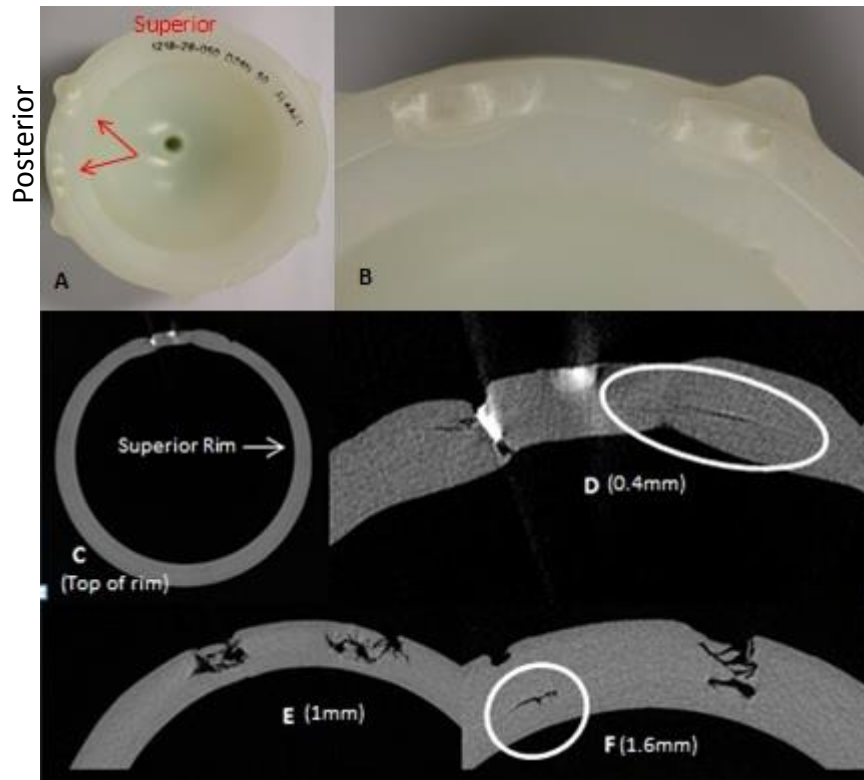
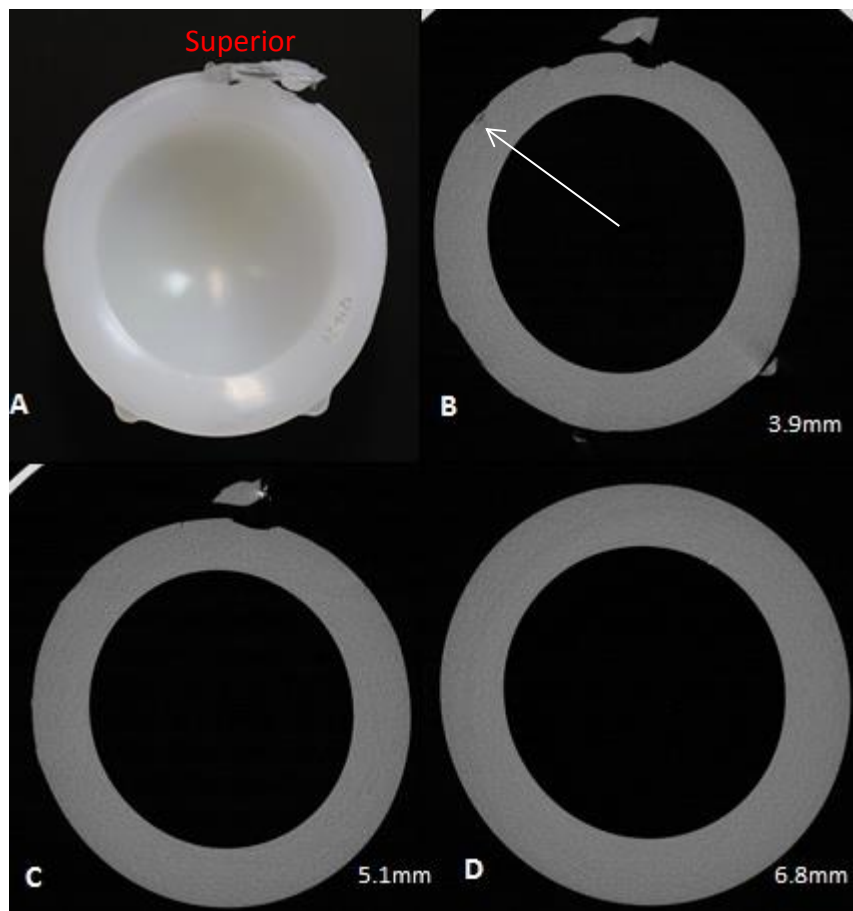


Figure 5-11 Photographic images and MicroCT images of the subsurface damage observed on a non-dissociated neutral liner (explant 5N) showing (A) a photo of the component and orientation *in vivo*, (B) a close up photographic section of the damaged rim showing surface damage in the posterior region, (C) a complete MicroCT slice at the top (horizontal section) of the liner rim, (D) a crack propagating circumferentially 0.4mm beneath the surface damage, (E) extensive multi-directional cracking 1mm underneath the surface damage and (F) a crack propagating circumferentially 1.6mm below the surface damage.

#### Dissociated Neutral Liners

Subsurface cracking adjacent to an absent anti-rotation tab was observed on explant 11D (Figure 5-12). This explant had a fractured superior rim. However, very little subsurface damage was observed though the thickness of the liner in the superior or inferior rim.



**Figure 5-12 Photographic images and MicroCT images of the subsurface damage observed on a dissociated neutral liner (explant 11D) showing (A.1) a photo of the fractured superior rim with absent anti-rotation tabs, (B) the fractured superior rim and cracking adjacent to the location of an absent anti-rotation tab 3.9mm below the horizontal liner rim, (C) a visibly undamaged section, except for the fracture in the superior region, 5.1mm below the horizontal rim, (D) a visibly undamaged section 6.8mm below the horizontal liner rim**

Extensive subsurface damage was observed on explant 9D, beneath the damage that was visible on the surface (Figure 5-13). On the superior rim, cracks propagating circumferentially parallel to the outer rim and embedded debris were observed. These cracks appeared to originate at the outer rim and extended up to 3mm below the horizontal liner rim. Multi directional cracking was observed in the most extensively damaged areas. On the inferior rim, multi-directional cracking was

observed beneath the delamination. Unlike the cracking on the superior rim this did not appear to initiate at the outer rim.

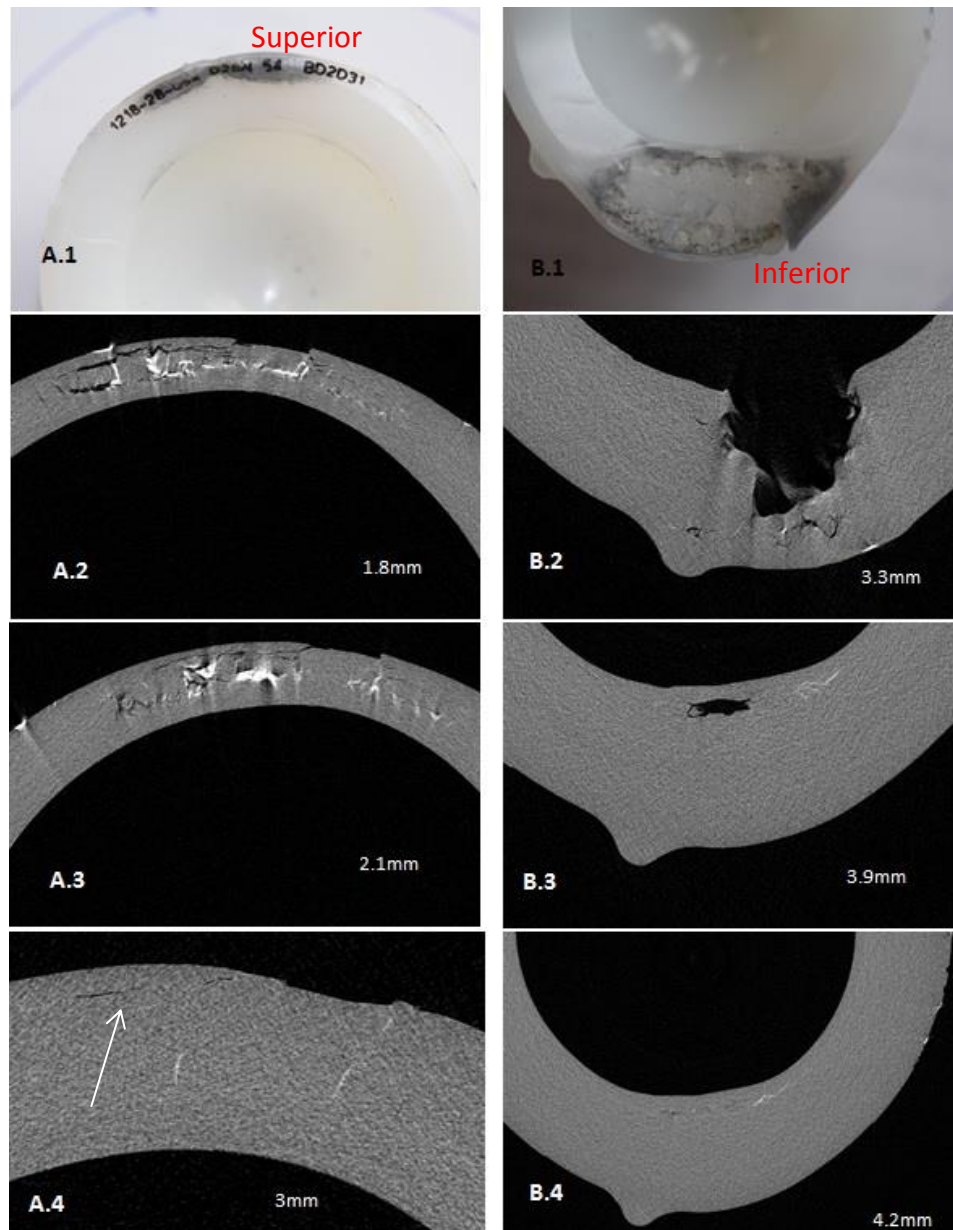


**Figure 5-13 Photographic images and MicroCT images of the subsurface damage observed on a dissociated neutral liner (explant 9D) showing (A.1) a photo of the superior rim with cracking, absent antirotation tabs and embedded debris, (B.1) a photo of the inferior rim with delamination and embedded debris, (A.2, A.3 & A.4) MicroCT images of circumferential cracking propagating parallel to the outer rim and multi-directional cracking with embedded debris at 1.8mm, 2.1mm and 3mm (B.2, B.3) multi-directional cracking 3.3mm and 3.9mm below the horizontal rim and (B.4) circumferential cracking near the inferior inner rim**

Extensive subsurface damage was observed on explant 12D, beneath the damage that was visible on the surface (Figure 5-14). On the superior rim, no subsurface micro-cracking or damage was observed. On the inferior rim, multi-directional cracking and embedded debris were observed beneath the delamination and cracks were also observed adjacent to an anti-rotation tab.

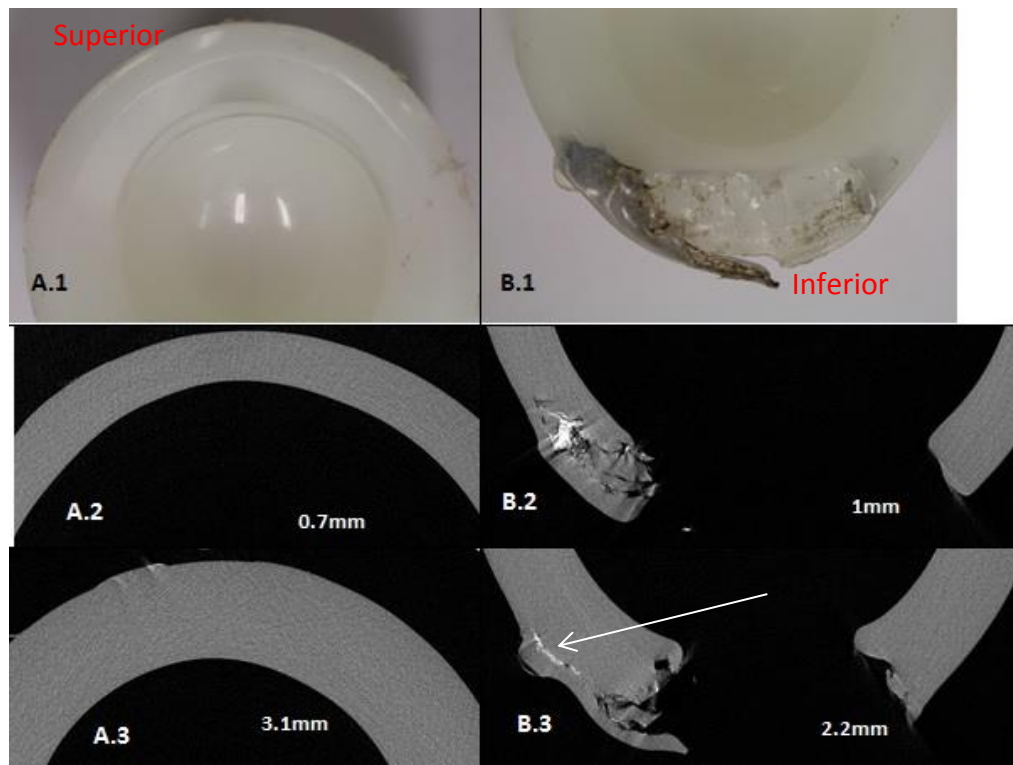


Figure 5-14 Photographic images and MicroCT images of the subsurface damage observed on a dissociated neutral liner (explant 12D) showing (A.1) a photo of the deformed superior rim (B.1) a photo of the inferior rim with delamination and embedded debris, (A.2 & A.3) the visibly undamaged superior rim at 0.7mm and 3.1mm below the horizontal liner rim (B.2 & B.3) extensive multi-directional cracking on the inferior rim and cracking adjacent to an anti-rotation tab (arrow)

### **5.3.2 Damage Categorisation**

Damage categorisation was carried out using an adaption of the Hood method (Hood et al., 1983) to assess wear and damage mechanisms as described in section 5.2.3.

#### Non-dissociated Neutral liners

The mean damage score for the non-dissociated neutral liners was 15 (Table 14; Page 181). All of the non-dissociated neutral liners appeared to be relatively undamaged with no evidence of gross failure. Mild to moderate scratching was observed on the bearing surface and the rim of all of the non-dissociated neutral liners (Figure 5-15A). Abrasion was observed on the bearing surface of one of the liners (explant 2N) and embedded debris was observed on the bearing surface and the rim of two of the liners (explants 2N and 4N; Figure 5-15C). An elongation of the bearing surface was observed on three of the liners (explants 3N, 5N and 6N; Figure 5-15D) and two gouge like cracks (Figure 5-15E) were observed on the rim area of one of the liners (explant 5N). The femoral heads were relatively undamaged with only very light scratching or metal transfer observed. Very little damage was observed on the backside of the neutral liners and the machining marks were still visible on the backside of all the liners.

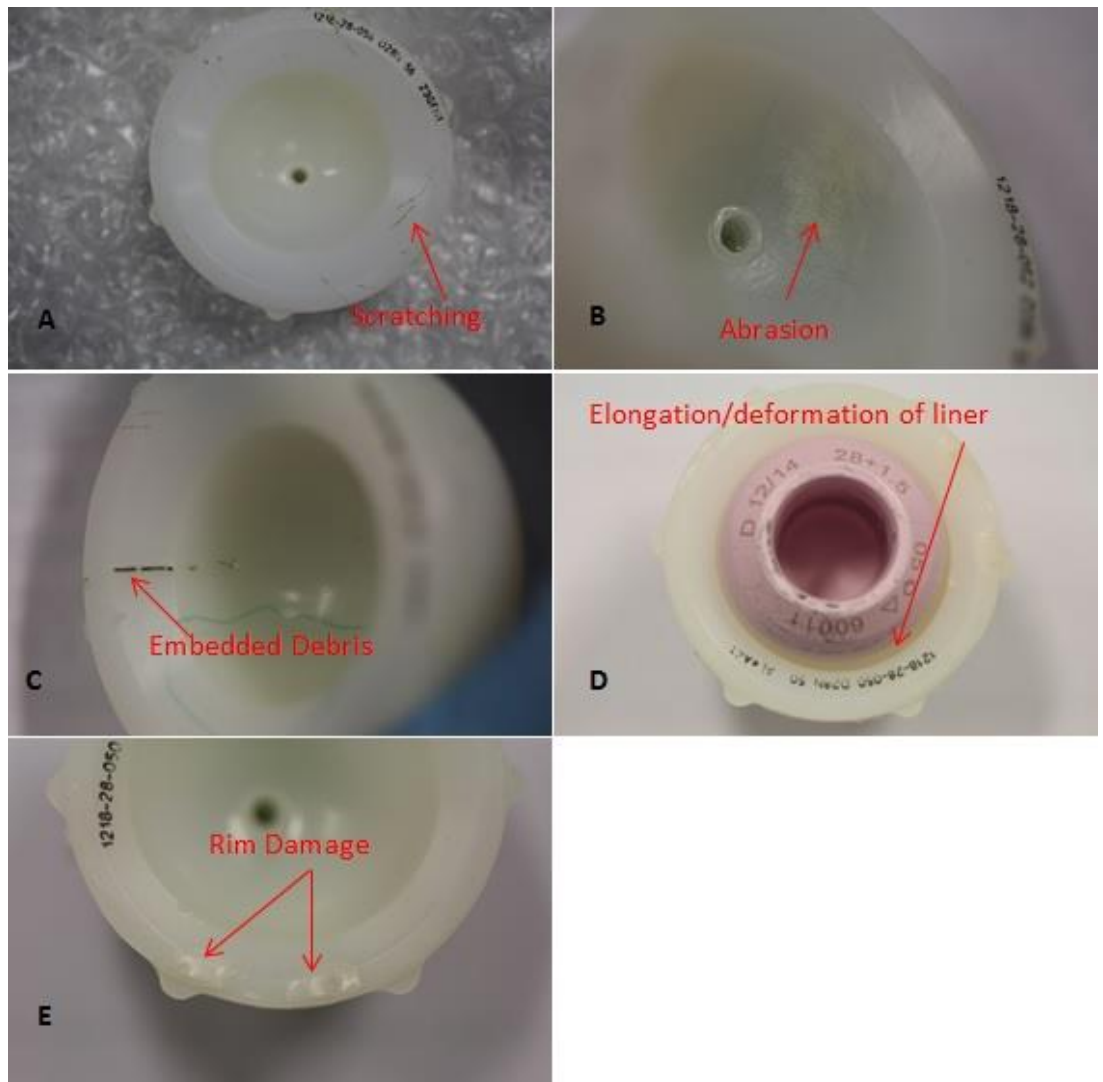


**Figure 5-15 Examples of damage modes observed on the non-dissociated neutral liners (A) Scratching with some embedded particles (explant 1N), (B) Abrasion (explant 2N), (C) embedded debris (explant 4N), (D) elongation of the bearing surface (explant 5N) and (E) rim damage in the form of two gouge like cracks (explant 5N)**

#### Dissociated Neutral Liners

The mean damage score of the dissociated neutral liners was 22 (Table 14; page 181). Deformation, delamination, fracture, scratching and embedded particles were observed on the rim of the dissociated neutral liners (Figure 5-16). Deformation of the inner rim was observed on all liners, predominately along the superior region of the liner (Figure 5-16A). Damage was observed at the periphery

of the superior rim in the form of deformation (all liners), metal transfer/embedded particles (all liners; Figure 5-16A) and fracture (explants 9D and 12D; Figure 5-16B). The ARD tabs on the superior rim were absent from all liners, leaving only one or two tabs from an original six. Further damage was observed on the inferior rim of all liners: deformation (all liners); embedded particles (explants 8D, 9D and 12D); a gouge like material removal (explant 8D; Figure 5-16C); and delamination (explants 9D and 12D; Figure 5-16D). The bearing surface remained relatively undamaged with common damage mechanisms such as pitting, abrasion and burnishing either not being observed or being very mild. Very light scratching was observed on the bearing surface of all of the dissociated neutral liners. One of the liners exhibited a slight discoloration to one side of the bearing surface (explant 11D). An elongation of the liner into an oval shape was observed for all of the liners.

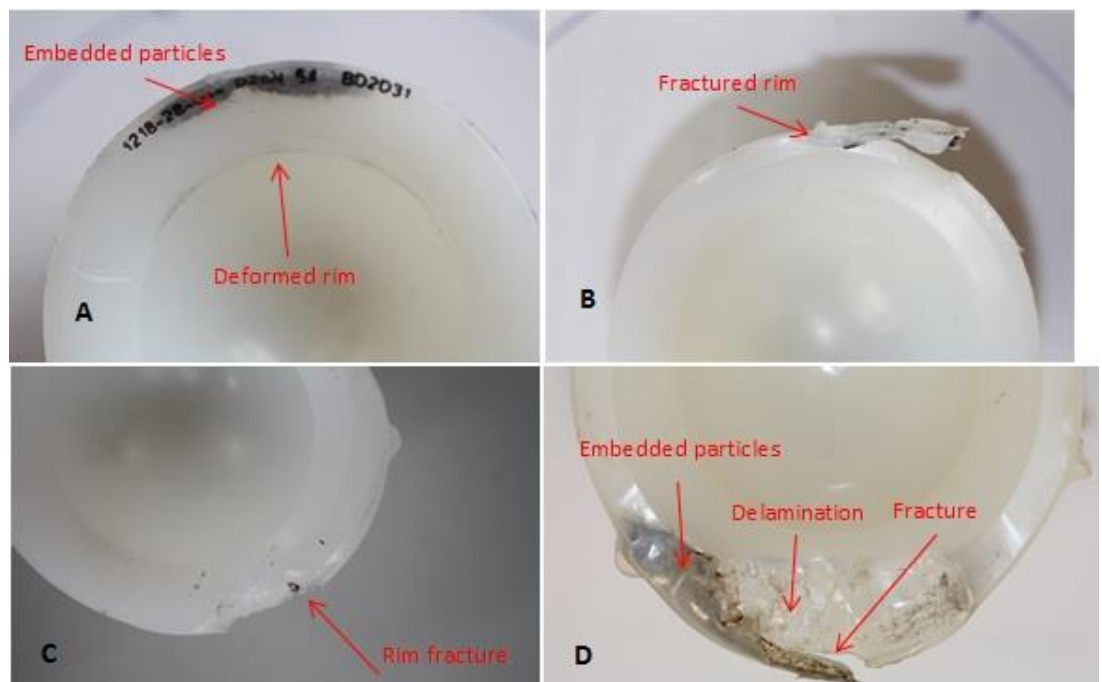


**Figure 5-16 Examples of damage mechanisms on the dissociated neutral liners: (A) Deformation at inner rim and embedded particles at the outer superior rim (explant 9D), (B) fractured superior rim (explant 11D) (C) gouge like rim fracture on the superior rim (explant 8D) and (D) Delamination, fracture and embedded particles on the inferior rim (explant 12D)**

Damage in the form of scratching, deformation and a prominent ridge was also observed on one side of the backside of the liners Figure 5-17.

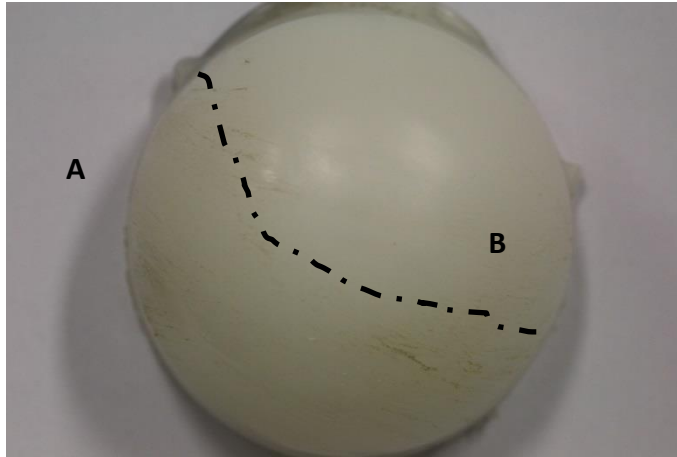


**Figure 5-17 (A) Deformation, scratching and a ridge across the backside of the liner. (B) The other side of the liner was less damaged**

Significant material transfer from the titanium shell was observed on all femoral heads and scratching was observed on all of the metal heads. This corresponded to a deformed and worn area on the superior region of the titanium shell as shown in Figure 5-18. This was observed on all the dissociated neutral explants with the exception of explant 11D and explant 12D, for which the shell was not available for analysis.

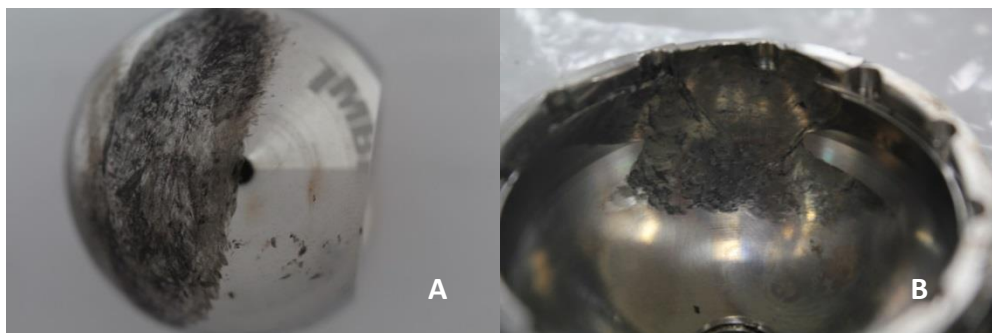


**Figure 5-18 (A) Femoral head with typical metal transfer and scratching and (B) metal shell showing with deformation caused by articulation of the femoral head**

### Lipped Liners

The mean damage score for the lipped liners was 15 (Table 14; page 64). All of the lipped liners exhibited mild scratching on the bearing surface and the rim. Very mild abrasion was observed on the rim of one of the liners (explant 16L). Machining marks were still visible on the bearing surface of two of the liners (explant 15L and 16L). Three of the four liners exhibited an area of deformation on the extended rim (explants 13L, 14L and 15L), consistent with damage caused by femoral neck impingement (Figure 5-19). Circular indentations were observed on the bearing surface of one of the lipped liners (explant 14L; Figure 5-19B). One of the liners was grossly deformed around the outer edge of the superolateral rim (explant 16L; Figure 5-19D).

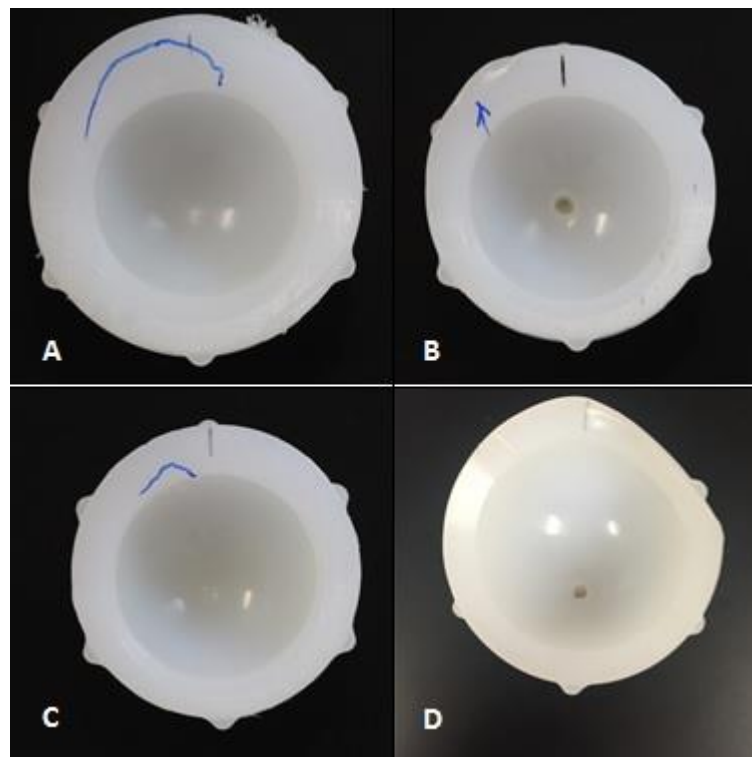


**Figure 5-19 Images of lipped explants showing (A), (B), (C) areas of rim deformation (highlighted with blue pen) possibly due to impingement and (D) gross deformation to the superolateral rim**

The backsides of the lipped liners were relatively undamaged with only very light scratching being observed. Light metal transfer was observed around the base of the two ceramic femoral heads (explants 13L and 14L). Heavy scratching was observed to one side of the two metal femoral heads (explants 15L and 16L; Figure 5-20).

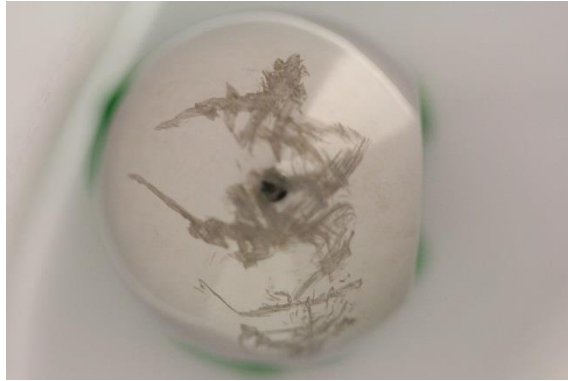


**Figure 5-20 A femoral head that articulated with a lipped liner (explant 15L) with heavy scratching to one side**

**Table 14 Summary of damage scores for each quadrant and subdivision for all explanted liners (mean is rounded to nearest whole number)**

| Explant Code | Damage Score |                 |           |
|--------------|--------------|-----------------|-----------|
|              | Rim          | Bearing Surface | Total     |
| 1 N          | 7            | 6               | 13        |
| 2 N          | 8            | 8               | 16        |
| 3 N*         | 6            | 8               | 14        |
| 4 N          | 7            | 13              | 20        |
| 5 N          | 8            | 7               | 15        |
| 6 N          | 4            | 10              | 14        |
| 7 N*         | 9            | 5               | 14        |
| Mean (N)     | <b>7</b>     | <b>8</b>        | <b>15</b> |
| 8 D*         | 14           | 6               | 20        |
| 9 D          | 20           | 5               | 25        |
| 10 D*        | 17           | 5               | 22        |
| 11 D*        | 10           | 7               | 17        |
| 12 D*        | 17           | 6               | 23        |
| Mean (D)     | <b>16</b>    | <b>6</b>        | <b>22</b> |
| 13 L*        | 14           | 11              | 25        |
| 14 L*        | 7            | 12              | 19        |
| 15 L*        | 5            | 1               | 6         |
| 16 L*        | 6            | 4               | 10        |
| Mean (L)     | <b>8</b>     | <b>7</b>        | <b>15</b> |

\*crosslinked (Non-Dissociated Neutral =N; D = Dissociated Neutral; L = Lipped)

The overall damage score for the dissociated neutral liners (22) was higher than that of the neutral liners (15) and the lipped liners (15) but the difference was not significant. The rim region was more damaged than the bearing surface for the dissociated neutral subset ( $p < 0.01$ ) but the difference was not significant for the neutral or lipped subsets. The mean damage scores for each liner subset and each location (bearing surface and rim) are given in Table 15. The most prevalent damage mechanisms were scratching and deformation on the bearing surface and scratching, deformation and embedded debris on the rim. Scratching and embedded debris were observed over all quadrants. Deformation was observed predominantly on the superior region of the liner.

**Table 15 Mean damage scores for each different mechanisms and liner subset, divided into bearing surface and rim region**

| Damage Mechanism | Bearing Surface |          |          | Rim Region  |             |             |
|------------------|-----------------|----------|----------|-------------|-------------|-------------|
|                  | N*              | D*       | L*       | N           | D           | L           |
| Deformation      | 0.86            | 2.40     | 2        | 0.71        | <b>5.64</b> | <b>3.25</b> |
| Pitting          | -               | -        | 1        | -           | -           | -           |
| Embedded Debris  | 0.14            | -        | 0.25     | 0.71        | <b>3.4</b>  | 0.25        |
| Scratching       | <b>5.57</b>     | <b>3</b> | <b>3</b> | <b>5.14</b> | 2.2         | <b>3.75</b> |
| Burnishing       | 1.29            | 0.2      | -        | -           | 0.2         | -           |
| Abrasion         | 0.43            | -        | 0.75     | -           | 0.8         | 0.25        |
| Delamination     | -               | -        | -        | 0.14        | 1.2         | -           |
| Cracking/Failure | -               | -        | -        | 0.43        | 2           | -           |

\*N = Non-dissociated Neutral liner; D=Dissociated neutral liner; L = lipped liner

### 5.3.3 Volume change

The volume change was assessed geometrically and geometric reconstructions were created using Redlux software. The method is described in section 2.4. Negative volume change was defined as volume change due to penetration into the liner when viewed looking onto the bearing surface, such as wear, and positive volume change as change protruding from the liner such as creep. This corresponds to the Redlux histogram. It is recognised that many areas of volume change may comprise a combination of both, but the nomenclature highlights the dominant volume change for a particular area.

A distinct negative volume change on what is thought to be the superior region of the bearing surface, most likely due to both wear and creep, was observed on all of the neutral liners (Figure 5-21). A secondary area of negative volume change was observed near the rim opposite the principal area of volume change. A positive volume change, likely due to creep, was observed on other areas of the bearing surface for all liners. The volume change values for the principal and secondary volume change areas for all neutral liners, measured using the method described in section 2.4, are given in Table 16.

**Table 16 Volume changes for the non-dissociated neutral acetabular liners with the mean of the non-crosslinked liner  $\pm$  95% CI**

| Explant | Principal volume change on area of articulation (mm <sup>3</sup> ) | Secondary volume change (mm <sup>3</sup> ) | Total volume change (mm <sup>3</sup> ) | Rate of volume change (mm <sup>3</sup> /Mc) |
|---------|--|--|--|---|
| 1       | 33.28  | 1.88                                       | 35.16                                  | 4.94  |
| 2       | 24.78  | 1.94                                       | 26.72                                  | 4.21  |
| 3*      | 21.59  | 3.08                                       | 24.67                                  | 5.24*                                       |
| 4       | 53.73  | 2.11                                       | 55.84                                  | 6.27  |
| 5       | 153.86   | 4.07                                       | 157.93                                 | 18.25                                       |
| 6       | 183.75   | 12.31                                      | 196.06                                 | 26.58                                       |
| 7*      | 55.17  | 1.76                                       | 56.93                                  | 26.31*                                      |
|         |  |  | <b>Mean**</b>                          | <b>12.1 <math>\pm</math> 12.3</b>           |

\*Crosslinked liner \*\*Mean excluding crosslinked liners

The mean volume change per year for the non-crosslinked non-dissociated neutral liners was 12.1mm<sup>3</sup>/Mc (n=5; 11.63mm<sup>3</sup>/yr; 95% CI  $\pm$  12.3; range 4.2 - 26.6mm<sup>3</sup>/Mc). Only two crosslinked neutral liners were studied and the volume change per year for these were 5.24mm<sup>3</sup>/Mc and 26.3mm<sup>3</sup>/Mc.

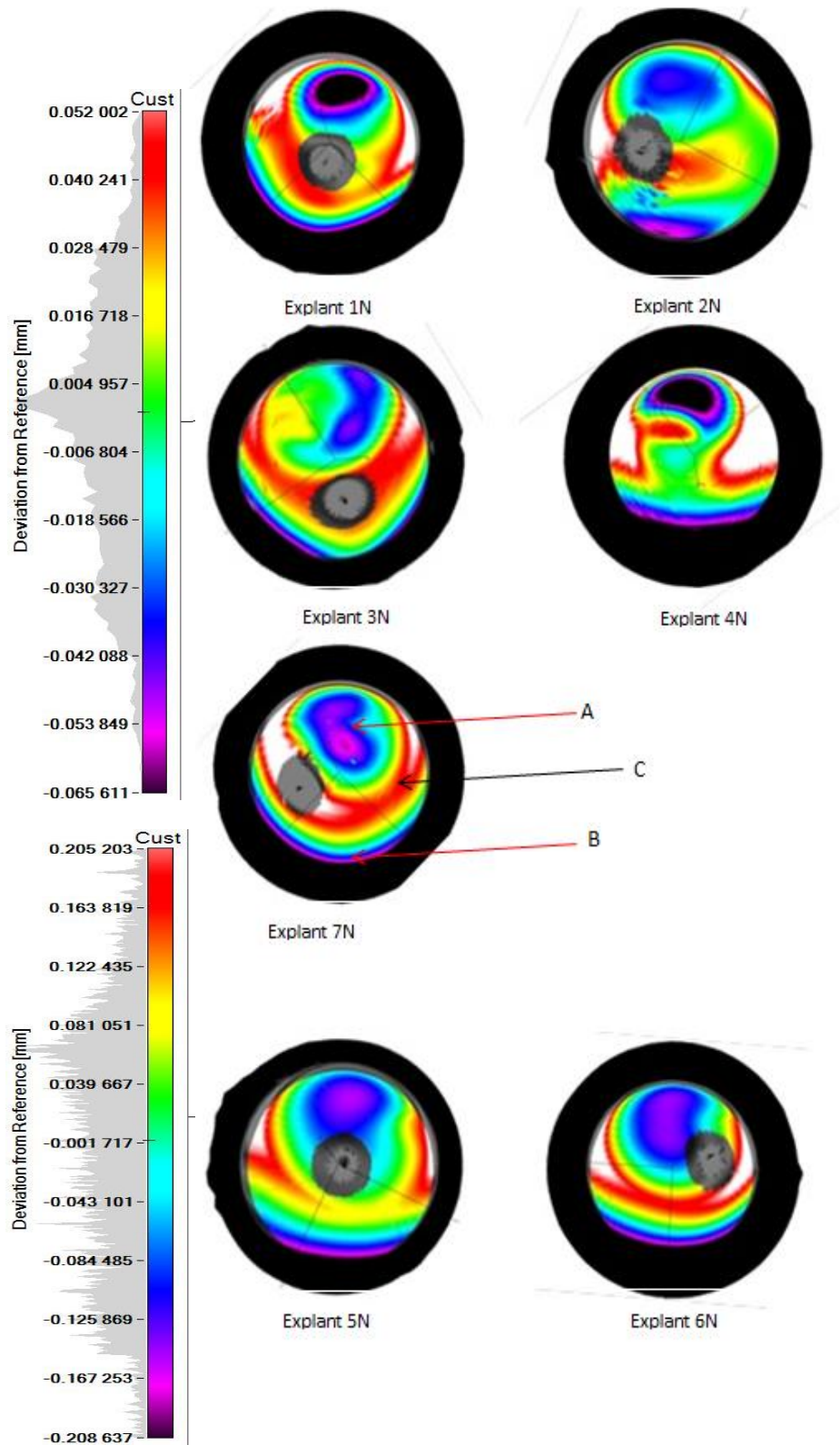


**Figure 5-21** Redlux geometric reconstructions of the explanted non-dissociated neutral acetabular liners. Annotations apply to all liners: (A) a principal area of volume change due to wear and creep, (B) a secondary area of volume change and (C) creep on the bearing surface (red, white). Grey areas are screw holes excluded from the calculations. View looks down onto the bearing surface

No distinct area of volume change relating to wear or deformation due to articulation on the bearing surface was observed for three of the five dissociated neutral liners (explants 8D, 10D, and 11D; Figure 5-22), reflecting the elongated 'oval' shape of these liners (section 5.3.2). One of the dissociated neutral liners had atypical volume change (compared to other explants and simulator samples in this study) on the articulating surface in the form of four distinct regions of negative volume change (explant 9D). One of the liners had an area of negative volume change on the bearing surface similar to the neutral liners (explant 12D). Areas of negative and positive volume change around the circumference of the liners were observed on all of these liners. Volume change for the dissociated neutral liners was not obtained as no obvious volume change associated with a wear area was observed on the bearing surface for most of the liners.

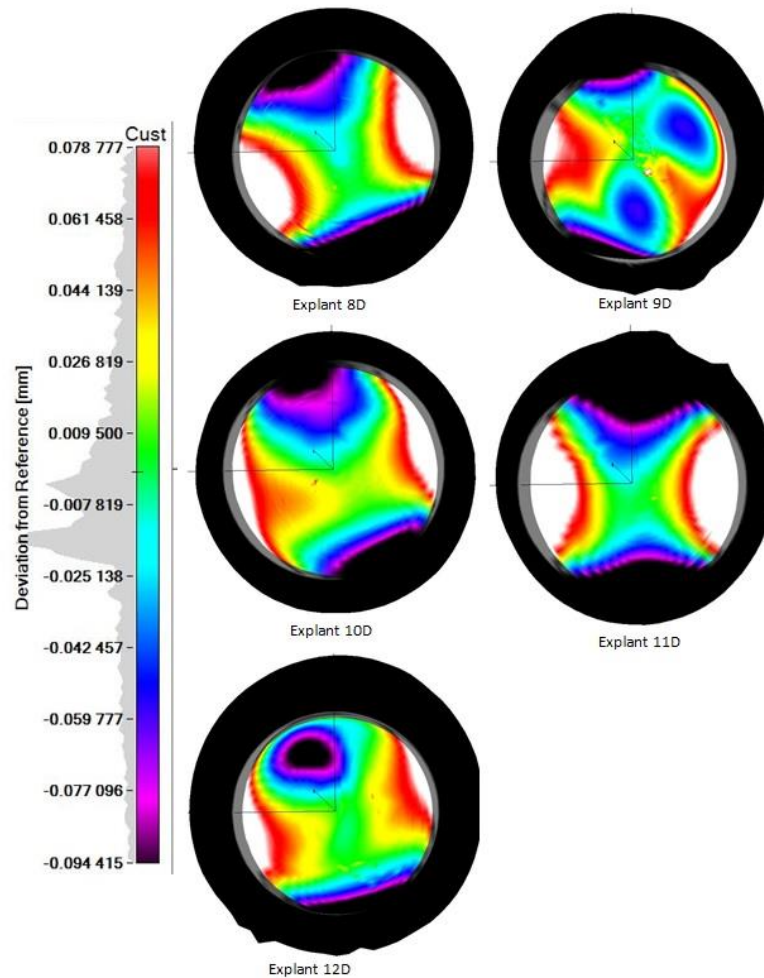


**Figure 5-22 Redlux geometric reconstructions of the explanted dissociated neutral acetabular liners showing areas of wear/deformation near the rim and extending on to the bearing surface (explants 8D, 10D & 11D), atypical volume change on the bearing surface (explant 9D) and “typical” volume change on the bearing surface (explant 12D). View looks down onto the bearing surface**

No distinct volume change associated with wear or deformation due to articulation on the bearing surface was observed on the lipped liners, with the exception of one liner for which there is a small area of volume change on the superior region of the bearing surface (explant 15L; Figure 5-23). An area of damage due to circular indentations was observed on the bearing surface of one of the liners (explant 14L) and some machining marks were still visible on the surface of two of the liners (explants 15L and 16L). Volume change of the lipped liners was not obtained as no distinct volume change associated with a wear area was observed on the bearing surface for most of the liners.

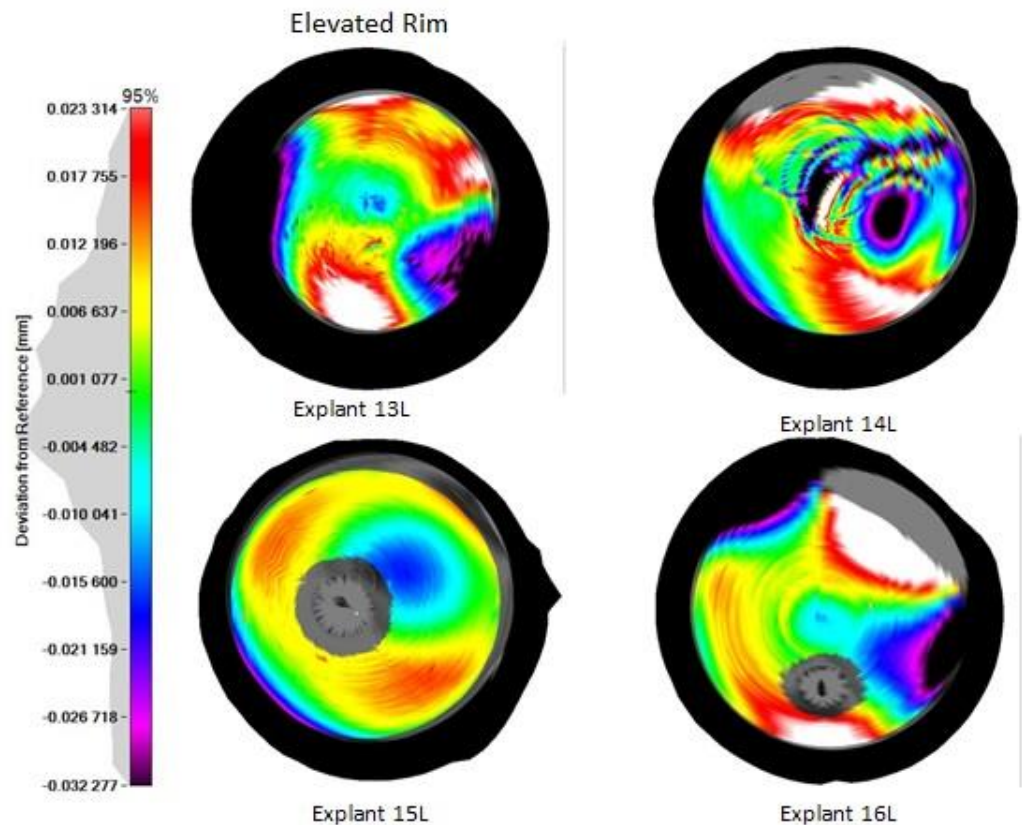


**Figure 5-23 Redlux images of the explanted lipped acetabular liners showing areas of volume change. The elevated rim is positioned at the top of the image and view looks down onto the bearing surface.**

### **5.3.4 Statistical Analyses and Correlations**

Statistical analyses were carried out as described in section 2.3.5.

No correlations between volume change, volume change per year or damage score and time *in vivo*, patient age, patient activity levels, patient BMI, liner thickness or cup inclination angle were observed.

The patient age associated with the lipped liners was significantly younger than the non-dissociated neutral and dissociated neutral liners ( $p < 0.01$ ).

Most of the dissociated neutral liners were crosslinked UHMWPE (five of seven), most of the neutral liners were non crosslinked GVF UHMWPE (four of five)

and all of the lipped liners were crosslinked UHMWPE. The time *in vivo* was significantly shorter for the crosslinked liners over all subsets ( $p < 0.01$ ). The mean values for each variable are shown in Table 17. The value is in bold and the p number is given where the difference in the means is significant.

**Table 17 Mean values of patient and explant data for each subset (the p number is given where there is a statistically significant difference;  $p < 0.05$ )**

|  | <b>Non-dissociated Neutral</b>   | <b>Dissociated neutral</b>           | <b>Lipped</b>         |
|--|----------------------------------|--------------------------------------|-----------------------|
| Volume change per year (mm <sup>3</sup> /Mc) | 16 (Crosslinked)<br>12.1 (GVF)   | NA                                   | NA                    |
| Time in vivo (months)                        | 87                               | 64                                   | 40                    |
| Mean damage score                            | 14 (crosslinked)<br>15.6(GVF)    | 21.4                                 | 15.8                  |
| Age  | 75                               | 81                                   | <b>56 (P&lt;0.01)</b> |
| Activity levels                              | 4                                | 4                                    | 4                     |
| BMI  | 30                               | 28                                   | 33                    |
| Liner thickness (mm)                         | 8.7                              | 8.5                                  | 9.5                   |
| Cup Inclination angle (°)                    | 48                               | 46                                   | NA                    |
|  | <b>Crosslinked (all subsets)</b> | <b>Non crosslinked (all subsets)</b> |                       |
| Time in vivo (months)                        | 44                               | <b>91(p&lt;0.01)</b>                 |                       |

\*NA = Not available

There was no difference in the damage scores between crosslinked and non crosslinked liners for the non-dissociated neutral liners. However, this was not statistically determined as only two of the non-dissociated neutral liners were crosslinked. The mean volume change per Mc for the non-dissociated neutral ceramic on UHMWPE explants was lower than the metal on UHMWPE explants (5.8mm<sup>3</sup>/Mc and 16.1mm<sup>3</sup>/Mc for the COP and the MOP explants, respectively).

However, this was not statistically significant as only two of the neutral liners were ceramic on UHMWPE and the volume change per year was not determined for the dissociated neutral and lipped liners, so these subsets could not be included in the analysis.

#### **5.4 Discussion**

Explant analysis can be used to determine wear and failure mechanisms and to identify correlations with component design, positioning and patient factors such as age and activity levels. Furthermore, it can be used to validate and inform the design of pre-clinical hip simulator testing. In this study, measurement methodologies were developed and have been used to assess damage and deformation to the rims of UHMWPE acetabular liners, to understand subsurface damage in the rim region and to measure wear volume in components where no pre-wear measurement exists. These methods are non-destructive and are therefore particularly appropriate for analysing explants. These methodologies can be developed further and used in future studies to better understand the prevalence of different types of edge loading and damage mechanisms and their role in the failure of acetabular liners.

Sixteen Pinnacle® acetabular liners were retrieved and assessed for damage and wear. These explants were selected because they were the same design and material as the acetabular liners tested in the simulator tests in this study (Chapter 3 & 4), allowing a more direct comparison to be made between the simulator studies and the explant study, which is one of the overall aims of this project (Chapter 6).

The liners were subdivided into three groups: non-dissociated neutral liners (n=7), dissociated neutral liners (n=5) and lipped liners (n=4). The subsets were selected because it is known that the geometry of the lipped liners may make them more susceptible to femoral neck impingement rather than edge loading mechanisms (Takaoka and Ueno, 1998; Chu et al., 2002; Birman et al., 2005; Duffy et al., 2009) and while useful information relating to more general damage

mechanisms may be gained from including them in the study, it was important to acknowledge that this difference in geometry may influence the results. Similarly, the dissociated neutral liners sustained significant damage following dissociation. This post-dissociation damage does not provide information relating to the cause of dissociation and for this reason they were assessed separately in order not to influence the results of the wider damage categorisation analysis. The small cohorts for each type of liner in this study meant that it was not possible to determine statistical correlations and cause of failure for the liners. Often the reason for revision provided some insight into the failure (for example dissociation and stem loosening) but determining if these failures were secondary to specific liner design characteristics and/or positioning factors was challenging. Despite this, some interesting observations were made that could be used to inform the design of future explant and simulator studies.

#### **5.4.1 Rim Deformation of Explanted Acetabular Liners**

Rim deformation and damage indicative of edge loading or impingement were observed on a small cohort of UHMWPE acetabular liners in this study. Edge loading and impingement may result in increased wear and/or loosening of the femoral stem or dissociation of the liner and it is important to understand the cause of failure in these instances. Furthermore, high stress concentrations in areas where edge loading has occurred may result in fatigue failure and fracture of the liners and this should be included in design considerations and component positioning recommendations.

Further understanding of the rim deformation and edge loading mechanisms was gained by comparing the edge damage of the non-dissociated neutral and dissociated neutral subsets. The rim deformation observed on the non-dissociated neutral liners and the dissociated neutral liners revealed two distinct geometries (Figure 5-24). A sharpening of the inner rim was observed on two of the non-dissociated neutral liners (no deformation was observed on the remaining non-dissociated neutral liners) and a flattening of the inner rim was observed on the dissociated neutral liners. This suggests that the mechanism of damage is different for each type of liner.

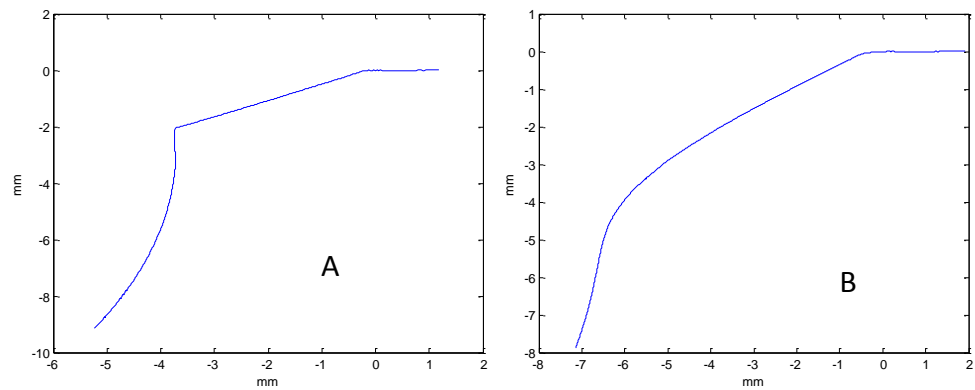


**Figure 5-24 Talysurf trace over the deformed region of (A) a non-dissociated neutral liner and (B) a dissociated neutral liner revealing distinct geometries between the two types of liner at the inner rim**

The dissociated neutral liners were badly damaged at the time of retrieval. However, the majority of this damage was caused after the liners had dissociated. Information about the extent and type of damage prior to dissociation was more valuable when attempting to identify the cause of dissociation. It was therefore necessary to identify when the flattening of the rim occurred. For all the dissociated neutral liners, the femoral head articulated against the metal shell after dissociation. This is indicated by scratching and metal transfer on the femoral head as well as damage to the inside of the metal shell (Figure 5-18). When the bearing couple was reassembled in the dissociated position using the ridge on the backside of the liner and the area of damage on the metal shell as landmarks, it could be argued that damage to the inner rim was not caused post-dissociation, because in this position there was no contact between head and inner rim and a much greater degree of damage would be expected across the entire superior rim region if there was articulation in this area (Figure 5-25). For example, the product reference numbers and machining marks would no longer be visible. It could therefore be hypothesised that damage to the inner rim was sustained before the dissociation event. This would support the hypothesis that the mechanism of edge damage to

the dissociated neutral liners prior to dissociation was different to the edge damage sustained by the non-dissociated neutral liners.



**Figure 5-25 (A) Reassembled dissociated neutral explant (explant 10D) showing (A) the position of the head with respect to the liner following the dissociation, (B) the deformed region of the inner rim and (C) a close up of the relatively undamaged rim region and (D) a microscope image of the rim area with machining marks still visible (x30 magnification)**

Two distinct edge damage mechanisms were described by Hall et al. (1998) for explanted cemented Charnley cups: a blunted edge due to impingement and a sharpened edge due to articular wear. The rim sharpening due to articular wear was more pronounced where the direction of wear was close to the rim of the cup. The findings of the present study were consistent with these descriptions. The flattened deformed rim on the dissociated neutral liners may therefore have been caused by impingement. Impingement of the femoral neck against the rim of the liner has been reported to cause fatigue failure of the locking mechanism and push-out of the liner from the shell (Malik et al. 2009; Gray et al. 2012). The exact prevalence of impingement is difficult to determine but some studies have estimated that it occurs in 39% to 60% of total hip replacements (Isaac et al., 1992; Yamaguchi et al., 2000; Shon et al., 2005; Usrey et al., 2006). Where cups are lateralised or not sufficiently inclined the risk is greater.

An alternative hypothesis is that the sharpening effect on the inner rim of the non-dissociated neutral subset could be caused by microseparation of the femoral head and acetabular cup leading to edge loading of the rim, rather than articular

wear. However, it is suggested that the degree of microseparation was small resulting in the femoral head not fully subluxating onto the chamfered region of the rim. It could therefore be hypothesised that two of the neutral liners experienced edge loading while the dissociated neutral liners experienced impingement on the superior rim. There are some limitations to the impingement theory. Firstly, deformation due to impingement is often observed as a notch like deformation on the rim, as is the impingement observed on the lipped liners in this study (Yamaguchi et al., 2000; Shon et al., 2005; Marchetti et al., 2011). In the present study, the deformation on the inner rim of the dissociated neutral liners was not notch-like; extending as much as 90° around the rim and indicating that the deformation may have been caused by the femoral head and not the femoral neck. Secondly, the posterosuperior region is a common site for impingement, but impingement in the superior region has not to the author's knowledge been widely reported in the literature and it is difficult to imagine what movement would cause this type of impingement. It therefore may be more plausible that, rather than impingement, the deformation was a result of a greater degree of edge loading than that experienced by the neutral liners, giving the deformation a different shape.

This raised the question, is it possible that the dissociation resulted from fatigue failure of the liner rim following microseparation and a high degree of repetitive edge loading? Fluoroscopic studies have shown a microseparation of the femoral head and cup during gait that leads to edge loading of the superior rim (Dennis et al., 2001; Komistek et al., 2002; Lombardi et al., 2000). Simulator studies have shown that high inclination angles and joint centre mismatch such as medialisation are risk factors for edge loading (Nevelos et al., 2000; M Al-Hajjar et al., 2013; Al-Hajjar et al., 2010; Mazen Al-Hajjar et al., 2013). In addition, increased torque has also been reported when there was a mismatch between the centres of rotation of head and cup and edge loading (Al-Hajjar et al. 2011), which may also contribute to fatigue failure of the locking mechanism (Burroughs et al., 2006). It is therefore reasonable to suggest that the deformation observed on the inner rim of the retrieved liners in this study may have been caused entirely or in part by edge loading where the femoral head subluxated to such a degree that the contact was

made on the chamfered region of the liner resulting in an increase in torque that was sufficient to induce failure of the locking mechanism.

Lewinnek et al. (1978) recommended a safe range of  $40^\circ \pm 10^\circ$  to minimise the risk of dislocation in total hip replacements. This safe range has been widely adopted and recommended by manufacturers. High inclination angles have since been linked with edge loading for hard on hard bearings (Williams et al. 2008; Leslie et al. 2009; Al-Hajjar et al. 2010). The inclination angles in this study fall within the safe range recommended by Lewinnek with the exception of three liners (Lewinnek et al. 1978; explants 2N, 6N & 8D;  $60^\circ$ ,  $55^\circ$  and  $57^\circ$ , respectively) and there is no difference in the mean inclination angle of the non-dissociated neutral subset and the dissociated neutral subset. Furthermore, no correlation between inclination angle and edge wear or dissociation was observed. It is therefore possible that edge loading and dissociation can occur in well positioned components. Furthermore, the 'safe range' recommended by Lewinnek was to avoid dislocation secondary to impingement. Given the evidence presented in this study for different edge loading mechanisms, perhaps the recommended safe range should also consider risk factors for edge loading such as high inclination angles, medialisation of the cup and head offset deficiencies.

Edge loading is a clinical concern due to the potential for fatigue failure of the rim. The dissociated neutral liners in this study exhibited deformation at the inner rim on the superior region of the liner and four of the five dissociated neutral liners in this study were crosslinked, which increased the risk of fatigue failure (and fracture of ARDs) due to the reduction in mechanical properties associated in with this material (Bradford et al., 2004; Baker et al., 1999; Pruitt, 2005; Furmanski et al., 2011; Furmanski et al., 2009). Furthermore, while impingement has commonly been linked to liner dissociation (Gray et al., 2012; Yun et al., 2015), it should be noted that impingement is a sporadic event, only occurring when the patient performs an unusual activity that challenges the range of motion of the joint. In contrast, edge loading could potentially occur every single step.

The rim deformation observed in this study gave insight into the different mechanisms of damage to liner rims. The cohort assed in this study was too small

to make any firm conclusions. However, this study provided insight into potential failure mechanisms and further work should therefore aim to identify the prevalence of each type of rim damage mechanism and to determine a link with failure. This work should include simulator testing to investigate more severe edge loading and whether this would result in a flattened rim, similar to that observed in the explants in this study.

#### **5.4.2 Subsurface Damage to Explanted Acetabular Liners**

The 2D microCT reconstructions did not reveal visually identifiable subsurface micro-cracking in the explanted liners (where micro-cracking was defined as cracks smaller than 1mm). However, the microCT scans allowed a non-destructive analysis of the initiation, propagation and severity of cracking beneath any damage that was visible on the surface to be performed.

The microCT scans revealed information about the extent of cracking that could not be determined from the surface using microscopes or other optical methods. Where subsurface cracking was present in the non-dissociated neutral liners, it was often observed propagating circumferentially, close to and parallel with the outer edge of the rim and appeared to initiate at areas of extensive surface damage (Figure 5-26) or around anti-rotation tabs. This type of damage may leave the liner susceptible to rim fracture as observed in some explant studies (Tower et al., 2007; Furmanski et al., 2009) or dissociation (Yun et al., 2015). Minimal subsurface damage was observed in the liners that did not also exhibit surface damage, it could therefore be hypothesised that surface damage, such as that caused by femoral neck impingement, resulted in initiation of cracks that propagated through the thickness of the material in areas of high stresses such as anti-rotation tabs and areas of thin UHMWPE.

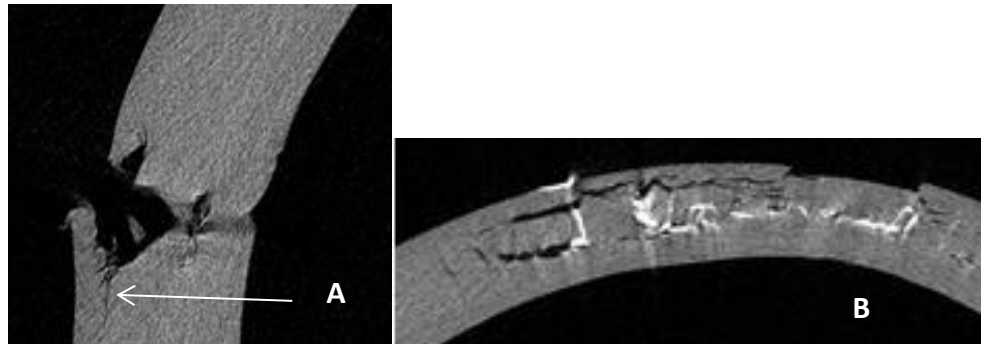


**Figure 5-26 (A) MicroCT image of a crack propagating circumferentially, appearing to initiate at an area of extensive damage (B) Cracks propagating circumferentially and parallel to the outer edge of the rim**

It is difficult to determine the exact initiation and propagation behaviour of the cracks in this microCT study because of the small sample size and the lack of data for regular time points throughout the lifetime of the component. However, it does support existing studies regarding stress concentrations at anti-rotation tabs and thin rims and subsequent cracking and rim fracture in these areas (Yun et al., 2015). Furthermore, the subsurface cracking observed in the dissociated neutral liners may have occurred following dissociation and is therefore not necessarily representative of cracking during implantation. However it does provide information relating to the initiation and propagation of cracks in UHMWPE acetabular liners that have been subjected to adverse loading.

MicroCT scanning of explanted UHMWPE acetabular cups can be used to non-destructively analyse subsurface damage and identify damage mechanisms that may cause fatigue failure and/or fracture in these components. Micro-cracking was not observed in this microCT study when compared to the untested control liners (section 2.6). However, the limitations of this method (discussed in section 2.6.5) for observing micron sized cracks mean that it is possible that micro-cracking was present and not observed, either because it was less than 10 $\mu$ m in size or larger in size but failed to be distinguished by the observer from the surrounding material. Further work to improve the method to identify micro-cracking or confirm the lack of micro-cracking would still be an interesting line of investigation.

### **5.4.3 Damage and Volume Change to Explanted Acetabular Liners**

All seven non-dissociated neutral liners exhibited mild damage, predominantly in the form of scratching to the rim and bearing surface and similarly only very mild damage in the form of light scratching was observed on the backside of the liners. No obvious cause of liner failure due to damage (such as rim cracking or fatigue failure) was observed for any of the non-dissociated neutral liners. The mean volume change of  $12.1\text{mm}^3/\text{Mc}$  for the five non-crosslinked neutral UHMWPE explants was lower than previously observed in hip simulator studies and other explant studies (Hall & Pinder 1998; Endo et al. 2002; Bowden et al. 2005; Galvin et al. 2007; Engh et al. 2012; Glyn-Jones et al. 2015) and volume change was therefore deemed not to be excessive for this cohort of liners. Only two of the neutral subsets were crosslinked and so a mean volume change was not obtained ( $6.3\text{mm}^3/\text{Mc}$  and  $26.3\text{mm}^3/\text{Mc}$  for each crosslinked liner). It should be noted that the volume change calculations in this study do not include wear and deformation in the rim region and these may increase if edge loading was taken into consideration. Furthermore, the relative standard deviation from the mean of 12.42% (section 2.4.5) should be taken into consideration when interpreting the volume changes as this may have contributed to the variation in values. Furthermore, the measurement accuracy may be further affected by the complex damage mechanisms observed in explants.

Six of the non-dissociated neutral liners were coupled with Corail® (DePuy Synthes, Warsaw, USA) cementless stems and were revised for lucency around the stem or stem loosening (the other Corail stem was revised for dislocation and the remaining stem was a c-stem revised for infection). It is therefore possible that these acetabular liners were functioning well at the time of revision and the failure of these explants is a result of failure of the femoral fixation. A study by Canton et al (2015) found that aseptic loosening of stems was significantly higher in lateralised stems (high offset and varus stems). However, the stems that were available for analysis in this study were all standard offset.

The four lipped liners exhibited only mild damage in the form of scratching and abrasion on the bearing surface and the rim. An area of deformation on the

extended rim that was consistent with damage caused by femoral neck impingement was observed on three of the four lipped liners. Lipped liners are designed to prevent dislocation but result in a smaller range of motion and an increased risk of impingement on the extended rim (Yamaguchi et al., 2000; Shon et al., 2005; Malik, 2007). Femoral stem loosening secondary to impingement has previously been observed on liners with an extended rim (Bosco and Benjamin, 1993; Messieh et al., 1994; Takaoka and Ueno, 1998). Two of the four lipped liners were revised for stem loosening, which may have been secondary to femoral neck impingement on the lipped region of the liners and the deformation observed on the rim in this study supports this hypothesis. Interestingly none of the lipped liners in this study dissociated despite the evidence of impingement, which reinforces the observation that edge loading caused the liner dissociation rather than impingement.

The series of round indentations that were observed on the bearing surface of one of the lipped liners (explant 14L) may have been caused by third body debris between the femoral head and bearing surface. Heiner et al. (2009) reported that third body debris in the bearing space greatly increased with subluxation of the femoral head and Lundberg et al. (2007) described an association between lever out subluxation due to impingement and third body debris. The deformation observed on the extended rim of the liner in this study suggested that third body debris may have entered the bearing space as described in these studies, causing deep scratching. In this case, the extensive wear caused by both third body debris and femoral neck impingement may have contributed to osteolysis in the femoral region and loosening of the stem.

All five dissociated neutral liners exhibited damage as a result of the dissociation. While characterisation of the damage on the liners was relatively straightforward, the cause of the dissociation was less clear. Previous studies on ceramic liners have linked early liner dissociation to malseated components and subsequent fracture (Miller et al., 2009). However, recent studies have reported late liner dissociations (UHMWPE) as much as 8 years postoperatively, indicating a fatigue type failure mechanism rather than malseating of the component at the time of implantation (Mesko, 2009; Gray et al., 2012; Mayer et al., 2012; O'Neill et

al., 2015; Yun et al., 2015). The present study describes a cohort of five liner dissociations with a mean implantation time of 64 months (range 31-97months) for which the failure of the locking mechanism and shearing of the ARD tabs was consistent with previous observations in this type of failure. While it is plausible that malseated components may perform well for extended periods of time before failure, the relatively long mean implantation time reported in the literature and in this study suggest that correctly seated liners may experience failure of the locking mechanism due to longer term fatigue mechanisms. Whether this is a result of adverse loading or malpositioning of the anti-rotation tabs or both is less clear and not something that is answered within the scope of this study. However, simulator testing that investigates the potential failure mechanisms of malseated components would be a useful line of investigation.

#### **5.4.4 Damage and Wear of Crosslinked and Non-crosslinked Acetabular Liners**

Most of the dissociated neutral liners were crosslinked UHMWPE (five of seven) and most of the non-dissociated neutral liners were not (four of five). Crosslinked UHMWPE liners have previously been reported to be more susceptible to cracking and rim fracture as a result of the reduced fatigue properties of crosslinked UHMWPE (Bradford et al., 2004; Furmanski et al., 2009; Atwood et al., 2011; Pruitt et al., 2013). It is therefore possible that the findings in the present study support the hypothesis that crosslinked liners are more susceptible to dissociation due to the reduced fatigue properties. However, a much larger cohort would be required to confirm this finding.

Previous studies, have reported no difference in damage between crosslinked and conventional polyethylene acetabular components (Schroder et al., 2011; Pang et al., 2015). The findings in the present study support this because there was no significant difference between the mean damage scores over all subsets for the crosslinked and non-crosslinked liners ( $p=0.56$ ). However, it should be noted that the distinct geometries of the liners may also influence damage scores and not just the material type.

An interesting finding in this study is the correlation between the use of crosslinked UHMWPE and a shorter implantation time (for all subsets). Again, with such small cohorts it is difficult to identify crosslinked UHMWPE as a factor in early failure in acetabular cups, particularly those that have dissociated. However, this would be an important line of investigation for future retrievals studies.

#### **5.4.5 Statistical Analyses**

No correlations between volume change, volume change per year or damage score and time *in vivo*, patient age, patient activity levels, patient BMI, liner thickness or cup inclination angle were observed. This contrasts with previous studies that reported a correlation between wear and time *in vivo* (Bowden et al. 2005). The cohorts in this study are too small to determine strong correlations and a larger cohort would likely reveal more information regarding failure factors.

#### **5.4.6 Limitations to Explant Analysis Methodologies**

There were limitations to the analysis methods used in this study. The limitations of the rim profile measurements, the MicroCT measurements and the volume change measurements are discussed in sections 2.4, 2.5 and 2.6.

The Hood method for damage categorisation only considers the degree of coverage when assessing damage (Hood et al., 1983) and not the severity of the damage. Furthermore, it assesses an entire quadrant and therefore does not distinguish between rim damage and damage to the bearing surface. The method was adapted in this study to divide each quadrant into rim and bearing surface, allowing rim damage to be assessed separately, and to introduce an assessment of severity as well as coverage. A recent study by Childs et al. 2016 evaluated four different methods for categorising shoulder explants (Hood et al., 1983; Wasielewski et al., 1994; Lombardi et al., 2008; Brandt et al., 2012) and concluded that the Hood method was subjective and did not allow for differences in severity and prevalence. Childs concluded that the method developed by Brandt et al. 2012 was the best method for assessing both. These authors also highlighted the importance of using more than one observer to maintain consistency and minimising viewing time to reduce observer fatigue. Based on these findings, while

attempts were made to improve on the basic Hood method, the method used in the present study would be improved by using multiple observers and using a less subjective assessment of severity. However, as the focus of this study was to develop methodologies to measure and analyse rim damage, it was felt that the damage categorisation was adequate to give an overview prior to performing more specific measurement techniques.

#### **5.4.7 Summary and Conclusion**

New measurement and analysis methods were evaluated in this study to help understand rim deformation and wear of explanted acetabular liners. Non-destructive methods to determine wear, rim deformation and subsurface cracking in the rim area were evaluated and the preliminary results of a small cohort of acetabular liners were obtained using these methods. Key areas of method development were identified for use in future studies. This study serves as a primary investigation into the validity of methods for analysing explants and going forward the results of this study can be used to help develop more specific research questions.

One of the principal findings in this explant study was the existence of two distinct edge loading deformation mechanisms. While current thinking often implicates impingement as the cause of liner dissociation, this study proposes edge loading due to subluxation of the femoral head as a potential cause of fatigue failure of the locking mechanism. The sharpened rim on the non-dissociated neutral liners may indicate low levels of edge loading where the head does not pass onto the chamfered region and the flattened rim may indicate edge loading where the head passes onto the chamfered region of the rim. Certainly, clinical evidence suggests that such a degree of edge loading is possible. The cracking around anti-rotation tabs observed on the microCT images support the existence of high stress in these areas and while the liner could potentially function normally without ARDs, the circumferential cracking around the perimeter could ultimately result in fracture of the rim as previously observed clinically.

Edge loading has been shown to be a significant concern clinically and in the presence of material degradation such as oxidation or following thermal

processing, fatigue failure could be accelerated. To fully understand the edge loading mechanisms in this study, future simulator tests should include a greater degree of microseparation to attempt to replicate the flattened rims observed in this study. Simulation of impingement should also be considered.

## Chapter 6: Discussion and Future Work

### 6.1 Introduction

Currently, international ISO standards outline loading and displacement recommendations for a standard walking cycle. However, studies have observed a microseparation of the head and cup *in vivo* resulting from rotational and/or translational malposition of the components leading to edge loading of the acetabular rim (Lombardi et al., 2000; Dennis et al., 2001; Komistek et al., 2002). Translational malposition refers to a mismatch in the centres of rotation of the femoral head and acetabular cup and rotational malposition is described as excessive inclination and/or version of the acetabular component (Nevelos et al., 2000; Stewart et al., 2001; Leslie et al., 2009; Al-Hajjar et al., 2010; M Al-Hajjar et al., 2013; Al-hajjar, Lancaster-jones, et al., 2015). Furthermore, previous studies of explanted acetabular liners reported cracking and fracture of the rim, which may have been caused by edge loading of the component (Tower et al., 2007; Furmanski et al., 2009; Furmanski et al., 2011). A requirement for pre-clinical testing that replicates these edge loading conditions and the damage mechanisms observed *in vivo* has been identified.

The hip simulator tests in this study developed a method for testing acetabular components under edge loading conditions. These tests allowed an assessment of the wear and damage sustained by components that are subjected to edge loading conditions in hip simulator tests to be made. Cracking and rim damage was observed on the positive controls, the aged PE liners, but not on the negative controls, the XLPE liners. In further tests of AOPE cups and liners, no cracking or rim damage was observed. Wear and deformation was observed on the bearing surface and rims of all simulator components.

A comparison of the wear, deformation and damage to the simulator components was compared with a small cohort of explanted acetabular liners of similar design to the simulator components and similarities and differences in wear and damage mechanisms were assessed. To perform the comparative analysis, measurement methodologies were developed for analysing explanted acetabular

liners. The analysis of explants presents challenges that are not encountered when measuring simulator samples. Many of the standard methods for measuring simulator samples involve measuring the cups or liners prior to testing on the simulator and then comparing the pre-test measurements with the post-test measurements. However, unlike simulator samples, the pre-wear measurements are not available for explants and it is often difficult to define the original profile of the component. The new measurement and analysis methods in this study were developed to attempt to overcome these challenges and were developed using the simulator test samples as a comparison. These methods can be used in the future to inform standard operating protocols for analysis of explanted acetabular components. The results of the analyses can be used to inform the design of clinically relevant hip simulator tests. Few studies have previously compared simulator samples and explants and so this is a novel aspect of the present study.

The overall aim of this study was to develop and evaluate a hip simulator protocol for edge loading by testing a range of crosslinked UHMWPE acetabular components and to evaluate and compare damage mechanisms observed on explanted components. This section discusses the comparison between the wear and damage observed on the simulator samples and the explants and the clinical relevance of the hip simulator protocols in this study. The data has previously been presented in results sections 3.4, 4.4 and 5.3.

## **6.2 Comparative Analysis of Simulator Components and Explants**

The following sections compare simulator components with explants using the methods developed in Chapter 2. Due to measurement difficulties relating to damage, deformation and geometrical features (discussed in sections 5.3.1, 5.3.1 and 5.3.1) for the dissociated and lipped liners, only the non-dissociated neutral liners were assessed for volume change.

### **6.2.1 Rim Deformation of Simulator Components and Explants**

A principal focus of this study was to compare the wear damage caused by edge loading in hip simulator studies with wear damage potentially caused by

subluxation and edge loading of the femoral head *in vivo*. A sharpening of the inner rim was observed on all the simulator components following edge loading tests (Figure 6-1A). Similarly, a sharpened rim was observed on two of the non-dissociated neutral explanted liners (explant 5N & explant 6N; Figure 6-1B). The mean penetration at the inner rim for the explants (0.43mm) was larger than the mean penetration of the simulator liners (0.08mm, 0.13mm, 0.12mm and 0.06mm for the XLPE, aged PE, AOPE and AOPE Cups, respectively). This may be due to the relatively low dynamic microseparation used in the simulator tests in these studies, as discussed in section 3.5. Interestingly, the simulator liners did not dissociate under the edge loading conditions in this simulator study, which indicate that the conditions may be less severe than those experienced by the dissociated explanted liners. The more severe wear and deformation observed on the rim of these explants may support findings in previous fluoroscopy studies that reported larger microseparation of the femoral head and acetabular cup *in vivo* than those used in the simulator tests in this study (Lombardi et al., 2000; Dennis et al., 2001; Komistek et al., 2002).

A larger cohort of explants would be required to fully understand the prevalence and degree of penetration and rim damage due to edge loading *in vivo* but initial findings suggest that hip simulator testing of edge loading conditions with larger microseparations may be more clinically relevant. Nonetheless, initial results regarding the mechanism of rim wear suggest that the simulator studies in this project produced clinically relevant wear and deformation mechanisms on the acetabular rims.

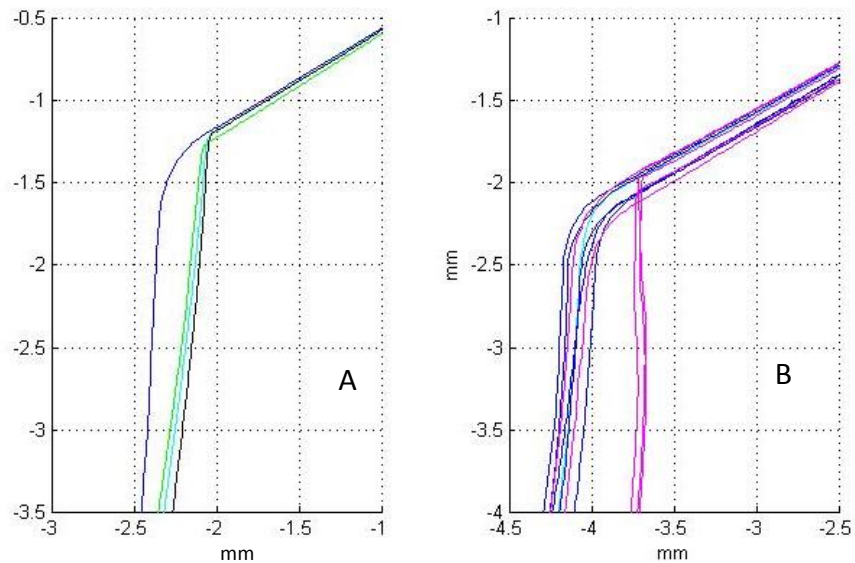


**Figure 6-1 Talysurf rim traces of (A) a simulator sample (aged PE liner A10) and (B) an explanted liner (explant 5N) showing similar rim wear and/or deformation in the form of a sharpening of the inner rim and reduced radius of curvature**

### **6.2.2 Subsurface Damage of Simulator Liners and Explants**

MicroCT scans of the XLPE and AOPE liners taken at a resolution of 10 $\mu$ m did not reveal subsurface micro-cracking when compared with untested controls. Similarly, it was not possible to identify subsurface micro-cracking in the selected explanted liners where no surface damage was observed. However, where surface damage was observed, on both simulator samples and explants, the microCT scans revealed information about initiation and propagation of subsurface cracking that would otherwise be difficult to obtain without using destructive methods. In both the aged PE liners and explants with surface damage (from both the non-dissociated and dissociated neutral subset), cracking was observed near the outer edge of the liner rim and around anti-rotation tabs (Figure 6-2). Incidences of cracks propagating circumferentially around the rim were observed on both aged PE liners and explants. The similarities in crack initiation and propagation for simulator components and explants suggest that the damage mechanisms sustained by acetabular liners *in vivo* are replicated to a degree by the hip simulator edge loading protocol developed in this study. Larger cohorts would be

required to confirm these initial findings, as well as further method development to visualise micro-cracking. Furthermore, measuring simulator samples at regular intervals during testing would provide additional information relating to initiation and propagation.

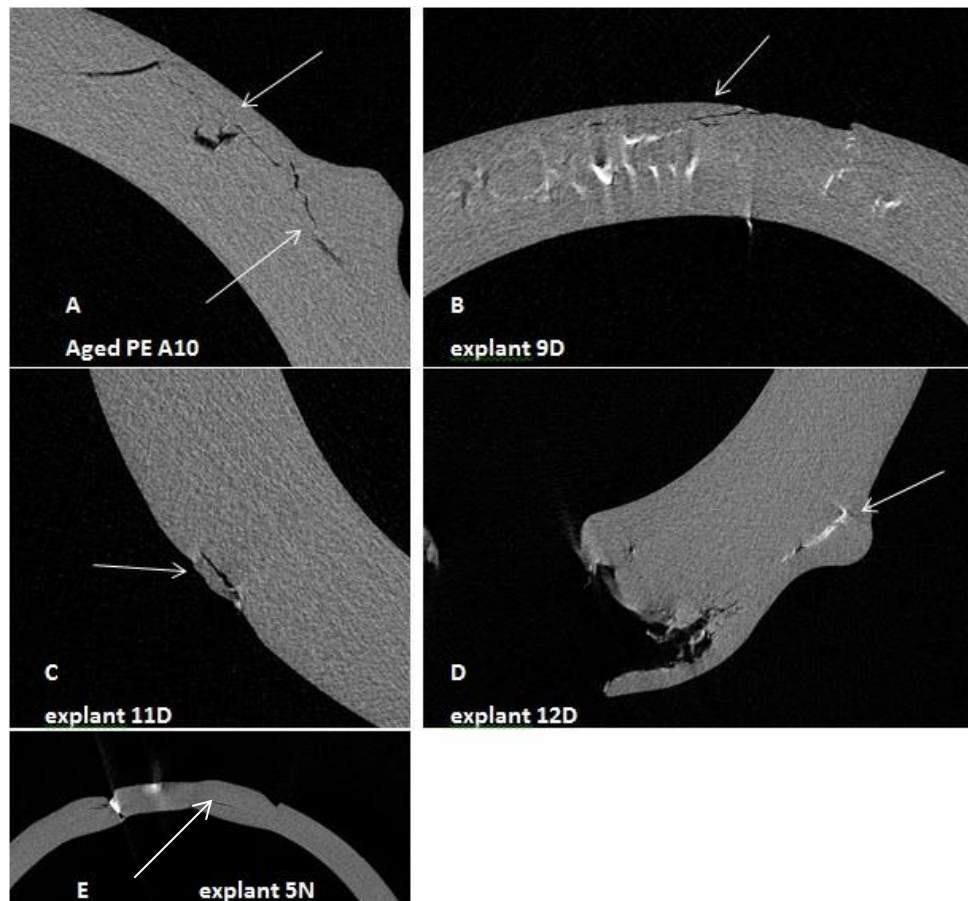


**Figure 6-2 MicroCT images of (A) cracks propagating circumferentially around the liner rim and at an anti-rotation tab on the superior rim of an aged PE liner (simulator sample A10), (B) a crack propagating circumferentially close to the outer edge of the superior rim of a dissociated explant (9D), (C) a crack along an anti-rotation tab on the inferior rim of a dissociated explant (11D), (D) a crack filled with third body debris along an anti-rotation tab on the inferior rim of an explant (12D) and (E) a crack propagating circumferentially around a non-dissociated explant (5N).**

### 6.2.3 Surface Damage to Simulator Liners and Explants

Following 5Mc of testing under standard loading conditions and 5Mc of testing under edge loading conditions in a hip simulator, relatively minimal surface damage was observed on the XLPE and the AOPE acetabular liners in this study. Cracking was observed on the backside of the aged PE liners, around anti-rotation tabs and at the inner rim but the bearing surface was relatively undamaged. In comparison, more surface damage was observed on the explanted liners.

A polishing or burnishing and fine scratching was observed on the surface of the simulator components. Other damage mechanisms such as pitting, embedded debris, fracture and deformation that weren't present on the simulator samples were observed on the explants. Scratching in particular was more severe on the explants. A fine scratching (visible using a microscope) was observed on the bearing surface of all simulator liners but much larger, deeper scratches that were visible to the eye were observed on the explants (Figure 6-3).

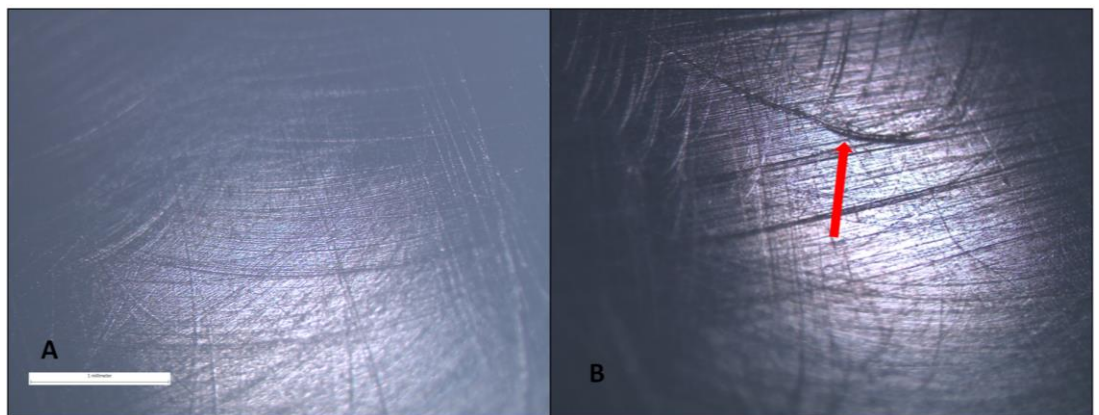


**Figure 6-3 Microscope images of the surface of (A) an XLPE simulator liner with fine scratching on the surface (XLPE AM1) and (B) an explant with fine scratching as well as larger, deeper scratches (arrow; explant 4N; x30 magnification)**

It is suggested that the most likely cause of scratching was third body debris in the joint space. Sources of third body debris include metal particles from wear of the metallic components and porous coatings. Light scratching was observed on

the femoral heads during simulator testing and this suggests that some third body damage was sustained during these tests. Explant and simulator studies have reported increased wear due to third body damage (Minakawa et al. 1998; Morscher et al. 1998; Bragdon et al. 2003). The difference in the appearance of scratching to the bearing surface suggests that more third body damage is sustained by the explants than the simulator components. Therefore, to better replicate *in vivo* conditions, introducing third body wear testing into ISO standards for hip simulator testing should be considered.

Fracture and deformation was observed on the rims of some of the non-dissociated neutral explants and a deformation of the inner rim was observed on the dissociated neutral explants that may have been attributable to severe edge loading or femoral neck impingement (Figure 6-4).



**Figure 6-4 Rim damage on (A) a non-dissociated neutral explanted liner and a (B) dissociated neutral liner that may have been cause by femoral neck impingement.**

Femoral neck impingement has been reported in several explant studies and is estimated to occur in as many as 60% of cups (Isaac et al., 1992; Yamaguchi et al., 2000; Shon et al., 2005; Usrey et al., 2006). Impingement is known to cause loosening of both femoral stems and acetabular cups and has been implicated in fatigue fracture of liners rims (Duffy et al., 2009). Deformation in this study was observed close to the outer rim of the explanted liners and in some cases, resulted in minor cracking and/or fracture of the components. The microCT measurements provided information about the initiation and propagation of subsurface cracks when damage was sustained on the surface of the component. Simulator

technology has only recently advanced sufficiently to replicate damage due to impingement. The harsh nature of the tests can be damaging to some simulator designs and require a range of motion beyond that for which most simulators were designed. Nevertheless, observations regarding the damage sustained by implants *in vivo* in previous studies and the present study indicate that development of tests to replicate impingement conditions may be required.

#### **6.2.4 Volume Change of Simulator Components and Explants**

The mean volume change per Mc calculated for the XLPE liners, AOPE liners and the AOPE cups was lower than the mean volume change per Mc calculated for the five non-dissociated non-crosslinked neutral explanted liners (data for the crosslinked explants was not included as only two were crosslinked; Figure 6-5). The mean volume change per Mc for the aged PE liners was higher than the explants. These results were expected as the XLPE and AOPE liners had a greater degree of crosslinking, and therefore wear resistance, and a reduction in wear resistance caused by ageing of the aged PE liners has previously been discussed (section 3.4.1). However, differences in wear rates were not significant due to the large range of values for the explants (range 4.21mm<sup>3</sup>/Mc-26.58 mm<sup>3</sup>/Mc; Figure 6-5).

The measurement methodology developed for measuring volume change in explants did not take into account any volume change at the rim and therefore the actual volume change for the explants may be higher. However, the comparison is made with simulator samples that were tested under standard loading conditions only, excluding volume change at the rim and therefore representing an equivalent rate of volume change.

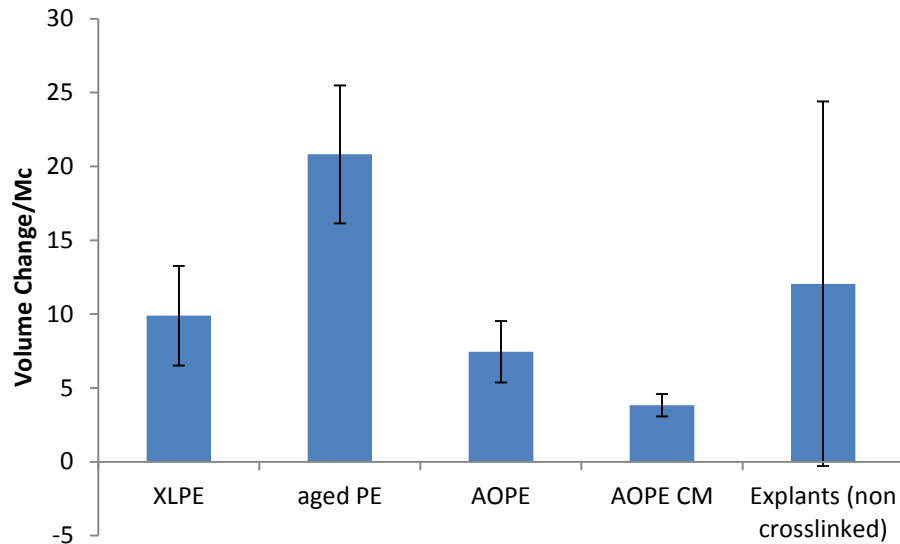


**Figure 6-5 Volume change per million cycles measured geometrically under standard loading conditions for all simulator components (n=4) and for the non-crosslinked non-dissociated neutral explanted liners (n=5; ±95% Confidence Intervals)**

It should also be noted that the volume change values for the simulator samples were performed using SR3D software, by comparing a pre-wear liner with a worn liner, and therefore the volume change comparison with the explants is comparing two different methods for calculating volume change. Furthermore, volume change results can vary from one simulator to another, so it is likely that the same simulator components would yield different results if tested on a different simulator (Ali et al., 2016).

A large variation in the volume change of explants has previously been reported. In a commentary by Schmalzried et al. (1998) a number of studies on UHMWPE wear *in vivo* were assessed: Sychterz et al. (1997) reported a penetration range of 0.02-0.45mm/yr in one study of 96 hips and Woolson & Murphy (1995) reported a penetration range of 0-0.30mm/yr in a study of 80 hips. The authors of the commentary Schmalzried et al. attributed these variations to the multifactorial

nature of UHMWPE wear, including patient variables, operative procedures and long-term loosening of implants. Similarly, in a separate study of UHMWPE acetabular cups by Bowden et al. (2005) a range of volumetric wear rates of 27-98mm<sup>3</sup>/yr measured using microCT was reported. More recently, Pace et al. (2013) reported a penetration range of 0.11-0.88mm/yr for metal on UHMWPE acetabular cups.

The large range of values for volume change that has been observed in explant studies makes meaningful comparisons with simulator studies challenging. The small cohort and the large variation observed in this study meant it was not possible to draw firm conclusions regarding the clinical relevance of the volume changes in the simulator tests in this study.

### **6.3 Study Limitations**

A hip simulator edge loading protocol was developed in this study that allowed UHMWPE acetabular cups and liners to be tested under more clinically relevant loading conditions. New methods were developed in this study to measure and analyse explants for wear, deformation and damage and to compare explants with simulator components. However, there were some limitations to the study methods that may influence the results of this comparison. These limitations are discussed in the relevant chapters and summarised in this section.

In the hip simulator edge loading tests, it was not possible to measure lateral sliding distance during the test because the components were surrounded by serum. It was possible for the lateral sliding to be adjusted by eye during the test and verified at serum changes and measurement points but the test may have run for short periods of time outside of the target sliding distance of 0.5-1mm.

In the hip simulator edge loading test, the aged PE liners were deformed and rocked in the shell. This may have resulted in atypical stress distributions in the liner, possibly causing the backside cracking that was observed.

A further limitation of the hip simulator studies was that not all materials were aged and therefore the wear and deformation to the rim was not assessed for

these components where oxidative degradation existed. It is known that the wear and fatigue performance of UHMWPE is compromised under these conditions and this would therefore be a valuable follow up study.

There were limitations to the measurement methodologies used to measure the simulator samples. The gravimetric measurements were subject to error arising from fluid absorption of the components and the geometric measurements did not distinguish between wear and deformation of the material.

There were also limitations to the measurement methodologies used to analyse the explants. The volume change of the explants was assessed geometrically without the pre-wear profile for comparison. The volume change was therefore calculated from a best fit estimation of the pre-wear data, which is unlikely to be an exact representation of the unworn liner. The methodology for measuring volume change in explants in the present study was validated using gravimetric data (section 2.4). However, there were limitations to the method: the validation using the untested, unsoaked control liner (liner NA14) did not take into account the effect of plastic deformation on the accuracy of the method and in contrast the validation using the hip simulator tested liner (liner AM1) would have been susceptible to error due to fluid absorption (despite the use of a soak control for compensation).

The rim deformation measurement methodology was subject to error due to positioning of the liner during measurements. If the liner was not positioned in exactly the same place between traces a difference in gradient along the chamfer was observed, which affected the measurement of penetration at the inner rim. Furthermore, the rim deformation was assessed by comparing the worn region of the liner with an unworn region of the same liner. This assumes that no wear or deformation occurred in the “unworn” region, which may not have been the case.

The microCT method was limited by the resolution achieved by the scanner, which was limited by the size of the components.

The damage categorisation method did not effectively separate prevalence and severity of damage.

Observer variability was a limitation of the volume change method, the damage categorisation method and the MicroCT method.

#### **6.4 Conclusion**

Simulator tests were not intended to exactly mimic the kinematics and operating conditions of the human body but rather replicate the wear and damage observed *in vivo* for a specific set of conditions. Current ISO standard simulator tests replicate an average set of conditions to achieve average wear and/or damage but do not necessarily replicate conditions that might result in failure or revision. In this study, similar damage mechanisms were observed on explants and simulator samples: a rim sharpening at the inner rim and crack initiation at the outer rim and around anti-rotation tabs, both indicative of edge loading. This reinforces the importance of current developments to ISO standards to introduce an edge loading protocol for hip simulator testing that replicates the rim wear and damage observed *in vivo* for an adverse set of conditions.

The surface damage observed on the simulator components suggests that tribological conditions in the hip simulator test were less harsh than those experienced *in vivo* and therefore caused less surface damage such as cracking and pitting. Volume change calculations for the explants were more varied than those obtained from simulator components and further study to determine whether this is a result of a variation in wear and deformation in explants or a limitation of the measurement technique is required

Areas where simulator testing and/or measurement techniques could be further developed were identified, such as testing under larger microseparations, third body wear tests to better replicate tribological conditions *in vivo* and impingement tests to fully replicate rim wear. Furthermore, improving volume change measurement protocols to include volume change at the rim would be a useful line of investigation.

## 6.5 Future Work

Measurement methodologies have been developed in this study that can be used to assess the wear and damage of explanted acetabular liners and to compare wear and damage mechanisms observed on explants with those observed in hip simulator studies. The work carried out can be used to inform the development and evaluation of future explant studies as well as the design of future simulator tests. This section discusses the work that could be carried out in the future to build on the findings of this study.

### 6.5.1 Simulator Studies

Future developments of simulator studies should consider introducing a range of adverse testing conditions:

- Larger microseparations;
- Accelerated ageing of UHMWPE components;
- Impingement tests;
- Testing with malseated components;
- Third body wear testing.

In addition, the use of simulators to better understand explants should be considered. Simulator tests using explanted components to compare *in vivo* and *in vitro* wear and damage would help to understand differences between the tribology and kinematics of simulators and *in vivo* conditions.

Wear debris isolation and analysis should be considered in order to compare the size and concentration of wear particles produced for conventional and cross-linked UHMWPE in simulators as well as comparing this with wear debris collected from tissue surrounding explanted liners.

### 6.5.2 Explant Studies

One of the main limitations of this explant study was the cohort size. Larger collections of explants of similar design should be analysed in order to identify correlations between wear and damage mechanisms and patient factors, time *in*

*vivo*, design factors, etc. Implant failures are multi-factorial and therefore larger cohorts are required to identify trends in failure mechanisms.

Further work to develop explant categorisation methods for acetabular liners should be carried out. This should include designing a method that assesses wear and damage on the backside, rim and bearing surface independently. The method should carefully consider the damage mechanisms that are relevant to acetabular liners, as existing methods are often biased towards damage mechanisms observed on total knee replacements. The standard ASTM F561-05a: Standard Practice for Retrieval and Analysis of Medical Devices, and Associated Tissues and Fluids, should be consulted but should be adapted to consider damage mechanisms resulting from adverse loading conditions. The method should include separate scores for prevalence (% coverage) and severity. Further to this, repeatability and reproducibility should be assessed. The development of a reproducible categorisation method will allow an initial assessment of explanted liners to be carried out, which in turn can be used to select explants for study based on severity and type of damage mechanism.

The Matlab code that was developed in this study can be used to qualitatively and quantitatively assess rim wear and deformation on simulator components and explants. However, issues regarding alignment of the components following rotation between traces were highlighted. To resolve this issue, a measurement fixture that allowed rotation of the component between traces without moving it from the fixture should be designed. The fixture should be able to accommodate a range of acetabular liner sizes and shapes (i.e. different locking mechanisms) and should enable alignment of the component prior to measurement, specifically, ensuring the liner is perfectly horizontal before being tilted to 45° for measuring. An appropriate fixture should resolve the issues that were encountered relating to a difference in gradient along the chamfer and allow a more accurate value for penetration at the rim to be determined. An alternative to designing a fixture for the Talysurf would be to develop measurement methods using equipment that moves around the circumference of the liner, rather than moving the liner itself. Possible equipment would be the CMM (although this is likely to be less accurate than the Talysurf) or the Talyrond (Taylor Hobson, Leicester, UK).

The MicroCT scans carried out during this study revealed information relating to crack initiation and propagation beneath surface damage on both simulator samples and explants. It was not possible to positively identify micro-cracking in this study. To investigate further, a smaller section of the liner should be identified using existing scans and then scanned at a higher resolution. In addition, the absorption of dye into the material to highlight smaller subsurface cracks should be investigated and the use of computer algorithms to automatically detect and highlight small voids and micro-cracking should be considered.

Further work should be carried out to develop the method for measuring volume change to include volume change at the rim. In addition, attempts should be made to distinguish between volume change due to wear and volume change due to plastic deformation of the components. Possible methods would include heating the components to recover any plastic deformation through the shape memory effect of UHMWPE (Muratoglu et al., 2004).

## 6.6 Final Summary

The aim of this study was to develop and evaluate clinically relevant simulation methods for edge loading conditions, to investigate the wear and rim damage of a range of different types of UHMWPE acetabular liners under these conditions and to compare this wear and damage with that observed *in vivo* by analysing explanted UHMWPE liners.

- A simulator edge loading protocol was developed that simulated subsurface damage and rim cracking in aged UHMWPE acetabular liners but not in non-aged crosslinked liners. This supported previous findings that edge loading of UHMWPE components may cause rim deformation, cracking and failure as observed *in vivo*, particularly where component positioning is sub-optimal or in the case of material degradation.
- The edge loading protocol was used to assess the wear and fatigue mechanisms of a novel antioxidant UHMWPE of two different acetabular cup designs. These cups exhibited rim wear and/or deformation, similar to that observed clinically and on the non-aged crosslinked liners in the previous simulator tests, but did not crack or fracture at the rim.
- New measurement methodologies were assessed and used to measure wear and damage mechanisms in a small cohort of explanted acetabular liners. These were compared with the damage mechanisms observed in the simulator tests. Clinically relevant damage mechanisms were observed on simulator samples after edge loading and key areas of method development and investigation for explants were identified from these initial studies, including developing microCT and rim deformation measurement methodologies and developing damage analysis protocols to include damage mechanisms relating to adverse loading.
- Key developments in future simulator testing were identified including assessing the wear and rim damage of acetabular components under larger microseparations, after accelerated ageing, subjected to femoral neck impingement and subjected to liner malseating.

## References

- Affatato, S., Vandelli, C., Bordini, B. and Toni, A. 2000. Fluid absorption study in ultra-high molecular weight polyethylene ( UHMWPE ) sterilized and unsterilized acetabular cups. *Proceedings Of the Institution Of Mechanical Engineers Part H-Journal Of Engineering In Medicine*. **215**,pp.107–111.
- Al-hajjar, M., Clarkson, P., Williams, S., Jennings, L.M., Thompson, J., Isaac, G.H., Ingham, E. and Fisher, J. 2015. Increased Torque in Hip Replacement Bearings due to Translational Surgical Mal-Positioning; ORS Poster No. 1759.
- Al-Hajjar, M., Fisher, J., Tipper, J.L., Williams, S. and Jennings, L.M. 2013. Wear of 36-mm BIOLOX (R) delta ceramic-on-ceramic bearing in total hip replacements under edge loading conditions. *Proceedings Of the Institution Of Mechanical Engineers Part H- Journal Of Engineering In Medicine*. **227**(H5),pp.535–542.
- Al-Hajjar, M., Jennings, L.M., Begand, S., Oberbach, T., Delfosse, D. and Fisher, J. 2013. Wear of novel ceramic-on-ceramic bearings under adverse and clinically relevant hip simulator conditions. *Journal of Biomedical Materials Research - Part B Applied Biomaterials*. **101**(8),pp.1456–1462.
- Al-hajjar, M., Lancaster-jones, O.O.D., Williams, S. and Jennings, L.M. 2015. Different levels of Rotational and Translational Surgical Mal-Positioning Affects the Occurrence and Severity of Edge Loading and Wear in Total Hip Replacements: ORS Poster No. 899 *In: Orthopaedic Research Society Annual Meeting (2015)*.
- Al-Hajjar, M., Leslie, I.J., Tipper, J., Williams, S., Fisher, J. and Jennings, L.M. 2010. Effect of cup inclination angle during microseparation and rim loading on the wear of BIOLOX(R) delta ceramic-on-ceramic total hip replacement. *J Biomed Mater Res B Appl Biomater*. **95**(2),pp.263–268.
- Ali, M., Al-hajjar, M., Partridge, S., Williams, S., Fisher, J. and Jennings, L.M. 2016. Influence

of hip joint simulator design and mechanics on the wear and creep of metal-on-polyethylene bearings. *Proceedings Of the Institution Of Mechanical Engineers Part H-Journal Of Engineering In Medicine*. **230**(5),pp.389–397.

Amstutz, H., Campbell, P., Kossovsky, N. and Clarke, I.C. 1992. Mechanism and Clinical Significance of Wear Debris-Induced Osteolysis. *Clinical orthopaedics and related research*. **276**,pp.7–18.

Archard, J.F. 1953. Contact and rubbing of flat surfaces. *Journal of Applied Physics*. **24**(8),pp.981–988.

Arthritis Research UK 2014. Arthritis in the UK – facts and statistics. *Arthritis Research UK*,pp.1–4.

ASTM F2003-02(2015) 2015. *Standard Practice for Accelerated Aging of Ultra-High Molecular Weight Polyethylene after Gamma Irradiation in Air*.

Atwood, S.A., Citters, D.W. Van, Patten, E.W., Furmanski, J., Ries, M.D. and Pruitt, L.A. 2011. Tradeoffs amongst fatigue , wear , and oxidation resistance of cross-linked ultra-high molecular weight polyethylene. *Journal of the Mechanical Behavior of Biomedical Materials*. **4**(7),pp.1033–1045.

Auger, D.D., Dowson, D., Fisher, J. and Jin, Z. 1993. Friction and lubrication in cushion form bearings for artificial hip joints. *Proceedings Of the Institution Of Mechanical Engineers Part H-Journal Of Engineering In Medicine*. **207**,pp.25–33.

Babovic, N. and Trousdale, R.T. 2013. Total Hip Arthroplasty Using Highly Cross-Linked Polyethylene in Patients Younger Than 50 Years With Minimum 10-Year Follow-Up. *Journal of Arthroplasty*. **28**(5),pp.815–817.

Baker, D.A., Bellare, A. and Pruitt, L. 2003. The effects of degree of crosslinking on the fatigue crack initiation and propagation resistance of orthopedic-grade. *J Biomed Mater*

*Res A. 2003 Jul 1;66(1):146-54. Biomed Mater Res A. 2003 Jul 1;66(1):146-54. 66(1),pp.146–154.*

Baker, D. a, Hastings, R.S. and Pruitt, L. 1999. Study of fatigue resistance of chemical and radiation crosslinked medical grade ultrahigh molecular weight polyethylene. *Journal of biomedical materials research.* **46(4)**,pp.573–81.

Barbour, P.S., Stone, M.H. and Fisher, J. 1999. A hip joint simulator study using simplified loading and motion cycles generating physiological wear paths and rates. *Proceedings of the Institution of Mechanical Engineers. Part H, Journal of engineering in medicine.* **213(6)**,pp.455–467.

Barbour, P.S.M., Barton, D.C. and Fisher, J. 1995. The influence of contact stress on the wear of UHMWPE for total replacement hip prostheses. *Wear.* **181–183(PART 1)**,pp.250–257.

Barrack, R.L., Burak, C. and Skinner, H.B. 2004. Concerns about Ceramics in THA. *Clinical Orthopaedics and Related Research.* **429**,pp.73–79.

BBC 2014. Bitesize: The Body in Action. [Accessed 2 September 2016]. Available from: [http://www.bbc.co.uk/bitesize/standard/biology/the\\_body\\_in\\_action/movement/revision/3/](http://www.bbc.co.uk/bitesize/standard/biology/the_body_in_action/movement/revision/3/).

Bell, C.J., Wlaker, P.S., Aberysundra, M.R., Simmons, J.M., King, P.M. and Blunn, G.W. 1998. Effect of Oxidation on Delamination of Ultrahigh-molecular-weight polyethylenen Tibial Componenets. *Journal of Arthroplasty.* **13(3)**,pp.280–290.

Bergmann, G., Graichen, F. and Rohlmann, a. 2004. Hip joint contact forces during stumbling. *Langenbeck's Archives of Surgery.* **389(1)**,pp.53–59.

Bergmann, G., Graichen, F. and Rohlmann, a. 1995. Is staircase walking a risk for the fixation of hip implants? *Journal of Biomechanics.* **28(5)**,pp.535–553.

Biresaw, G. 2008. Part IV: Polymeric and Bio-Based Surfactants: Tribological Properties of Ag-Based Amphiphiles *In: Surfactants in Tribology: ISBN 978-1-4200-6008-9.*

Birman, M. V., Noble, P.C., Conditt, M. a., Li, S. and Mathis, K.B. 2005. Cracking and impingement in ultra-high-molecular-weight polyethylene acetabular liners. *Journal of Arthroplasty*. **20**(7),pp.87–92.

Bladen, C.L., Tzu-Yin, L., Fisher, J. and Tipper, J.L. 2013. In vitro analysis of the cytotoxic and anti-inflammatory effects of antioxidant compounds used as additives in ultra high-molecular weight polyethylene in total joint replacement components. *Journal of Biomedical Materials Research - Part B Applied Biomaterials*. **101 B**(3),pp.407–413.

Blunn, G., Joshi, A.B., Lilley, P.A., Engelbrecht, E., Ryd, L., Lidgren, L., Hardinge, K., Nieder, E. and Walker, P.S. 1992. Polyethylene wear in unicondylar knee prostheses. 106 retrieved Marmor, PCA, and St Georg tibial components compared. *Acta orthopaedica Scandinavica*. **63**(3),pp.247–255.

Blunn, G.W., Joshi, a. B., Minns, R.J., Lidgren, L., Lilley, P., Ryd, L., Engelbrecht, E. and Walker, P.S. 1997. Wear in retrieved condylar knee arthroplasties: A comparison of wear in different designs of 280 retrieved condylar knee prostheses. *Journal of Arthroplasty*. **12**(3),pp.281–290.

Bosco, J.A. and Benjamin, J.B. 1993. Loosening of a femoral stem associated with the use of an extended lip acetabular cup liner: A case report. *The Journal of arthroplasty*. **8**(1),pp.91–93.

Bottner, F., Su, E., Nestor, B., Azzis, B., Sculco, T.P. and Bostrom, M. 2005. Radiostereometric Analysis: The Hip. *HSS Journal*. **1**(1),pp.94–99.

Bowden, A.E., Kurtz, S.M. and Edidin, A.A. 2005. Validation of a Micro-CT Technique for Measuring Volumetric Wear in Retrieved Acetabular Liners. *Journal of Biomedical Materials Research - Part B Applied Biomaterials*. **75**,pp.205–209.

- Bowden, A.E., Kurtz, S.M. and Edidin, A.A. 2005. Validation of a micro-CT technique for measuring volumetric wear in retrieved acetabular liners. *Journal of Biomedical Materials Research - Part B Applied Biomaterials*. **75**(1),pp.205–209.
- Brach del Prever, E.M., Bistolfi, A., Bracco, P. and Costa, L. 2009. UHMWPE for arthroplasty: Past or future? *Journal of Orthopaedics and Traumatology*. **10**(1),pp.1–8.
- Bradford, L., Baker, D. a, Graham, J., Chawan, A., Ries, M.D. and Pruitt, L. a 2004. Wear and surface cracking in early retrieved highly cross-linked polyethylene acetabular liners. *The Journal of bone and joint surgery. American volume*. **86–A**,pp.1271–1282.
- Bragdon, C.R., Connor, D.O., Lowenstein, J.D., Jasty, M. and Syniuta, W.D. 1996. The importance of multidirectional motion on the wear of polyethylene. *Proceedings Of the Institution Of Mechanical Engineers Part H-Journal Of Engineering In Medicine*. **210**,pp.157–165.
- Bragdon, C.R., Jasty, M., Muratoglu, O.K., Connor, D.O.O. and Harris, W.H. 2003. Third-Body Wear of Highly Cross-Linked Polyethylene in a Hip Simulator. *The Journal of arthroplasty*. **18**(5),pp.553–561.
- Brandt, J., Haydon, C.M., Harvey, E.P., Mccalden, R.W. and Medley, J.B. 2012. Tribology International Semi-quantitative assessment methods for backside polyethylene damage in modular total knee replacements. *Tribology International*. **49**,pp.96–102.
- BS ISO 14242:2002 2002. Implants for surgery — Wear of total hip-joint prostheses —.
- BS ISO 14242-1:2014 2014. *BSI Standards Publication Implants for surgery — Wear of total hip-joint prostheses Part 1 : Loading and displacement parameters for wear-testing machines and corresponding environmental conditions for test*.
- Burroughs, B.R., Muratoglu, O.K., Bragdon, C.R., Wannomae, K.K., Christensen, S., Lozynsky, A.J. and Harris, W.H. 2006. In vitro comparison of frictional torque and torsional

resistance of aged conventional gamma-in-nitrogen sterilized polyethylene versus aged highly crosslinked polyethylene articulating against head sizes larger than 32 mm. *Acta orthopaedica*. **77**(5),pp.710–718.

Calvert, G.T., Devane, P.A., Fielden, J., Hon, M.A., Adams, K., Horne, J.G. and Fracs, C. 2009. A Double-Blind , Prospective , Randomized Controlled Trial Comparing Highly Cross-Linked and Conventional Polyethylene in Primary Total Hip Arthroplasty. *Journal of Arthroplasty*. **24**(4),pp.505–510.

Childs, K., Crosby, L. and Goswami, T. 2016. Quantitative Analysis of Retrieved Glenoid Liners. *Lubricants*. **4**,pp.1–11.

Chu, C., Huang, G., Chang, J., Wu, S. and Lee, C. 2002. Aseptic Loosening of the Prosthetic Femoral Stem Resulting from Impingement of the Prosthetic Femoral Neck onto the Rim of the Polyethylene Cup in Total Hip Arthroplasty. *Journal of Medical Science*. **22**(325),pp.131–133.

Chuter, G.S.J., Cloke, D JMahomed, A., Partington, P.F. and Green, S.M. 2007. Wear analysis of failed acetabular polyethylene. *The Journal of bone and joint surgery. American volume*. **89**(2),pp.273–279.

Clarke, I.C., Manaka, M., Tateiwa, T., Williams, P. and Gustafson, G. 2005. Micro-separation hip kinematics had no adverse wear affect on XLPE cups Poster No . 0828 • 51st Annual Meeting of the Orthopaedic Research Society.

Collier, J.P., Sperling, D.K., Currier, J.H., Sutula, L.C., Saum, K. a and Mayor, M.B. 1996. Impact of gamma sterilization on clinical performance of polyethylene in the knee. *The Journal of arthroplasty*. **11**(4),pp.377–89.

Costa, L., Bracco, P., Maria, E., Kurtz, S.M. and Gallinaro, P. 2006. Oxidation and Oxidation Potential in Contemporary Packaging for Polyethylene Total Joint Replacement Components. *Journal of Biomedical Materials Research - Part B Applied Biomaterials*.

**78B**,pp.20–26.

Currier, B.H. 2007. Evaluation of Oxidation and Fatigue Damage of Retrieved Crossfire Polyethylene Acetabular Cups. *The Journal of Bone and Joint Surgery (American)*. **89(9)**,p.2023.

Currier, B.H., Van Citters, D.W., Currier, J.H., Carlson, E.M., Tibbo, M.E. and Collier, J.P. 2013. In vivo oxidation in retrieved highly crosslinked tibial inserts. *Journal of Biomedical Materials Research - Part B Applied Biomaterials*. **101 B(3)**,pp.441–448.

Currier, B.H., Currier, J.H., Mayor, M.B., Lyford, K. a., Van Citters, D.W. and Collier, J.P. 2007. In Vivo Oxidation of  $\gamma$ -Barrier-Sterilized Ultra-High-Molecular-Weight Polyethylene Bearings. *Journal of Arthroplasty*. **22(5)**,pp.721–731.

Currier, B.H., Currier, J.H., Mayor, M.B., Lyford, K. a, Collier, J.P. and Van Citters, D.W. 2007. Evaluation of oxidation and fatigue damage of retrieved crossfire polyethylene acetabular cups. *The Journal of bone and joint surgery. American volume*. **89(9)**,pp.2023–2029.

Currier, J.H., Duda, J.L., Sperling, D.K., Collier, J.P., Currier, B.H. and Kennedy, F.E. 1998. In vitro simulation of contact fatigue damage found in ultra-high molecular weight polyethylene components of knee prostheses. *Proceedings Of the Institution Of Mechanical Engineers Part H-Journal Of Engineering In Medicine*. **212**,pp.293–302.

D’Lima, B.Y., Urquhart, A.G., Buehler, K.O. and Walker, R.H. 2000. The Effect of the Orientation of the Acetabular and Femoral Components on the Range of Motion of the Hip at Different Head-Neck Ratios \*. *The Journal of Bone and Joint Surgery (American)*. **82–A(3)**,pp.315–321.

Dennis, D. a., Komistek, R.D., Northcut, E.J., Ochoa, J. a. and Ritchie, A. 2001. ‘In vivo’ determination of hip joint separation and the forces generated due to impact loading conditions. *Journal of Biomechanics*. **34(5)**,pp.623–629.

Dept. for Transport 2012. *GUIDANCE NOTE NUMBER : 17 / 2012 [ REV . 7 ] TRANSPORT OF INFECTIOUS SUBSTANCES UN2814 ,.*

DePuy Orthopaedics Inc. 2009. Polyethylene Compendium.

Derbyshire, B., Fisher, J., Dowson, D., Hardaker, C. and Brummitt, K. 1994. Comparative study of the wear of UHMWPE with zirconia ceramic and stainless steel femoral heads in artificial hip joints. *Medical engineering & physics*. **16**,pp.229–236.

Dorr, L., Wan, Z., Shahrदार, C., Sirianni, L., Boutary, M. and Yun, A. 2005. Clinical Performance of a Durasul Highly Cross-Linked Polyethylene Acetabular Liner for Total Hip Arthroplasty at Five Years. *Journal of Bone and Joint Surgery, Am.*,pp.1816–1821.

Dowson, D. 1982. The walking activity of patients with artificial hip joints. *Engineering in Medicine*. **11**(2),pp.95–96.

Duffy, G.P., Wannomae, K.K., Rowell, S.L. and Muratoglu, O.K. 2009. Fracture of a cross-linked polyethylene liner due to impingement. *The Journal of arthroplasty*. **24**(1),p.158.e15-9.

Eddin, A.A., Jewett, C.W., Kalinowski, A., Kwarteng, K. and Kurtz, S.M. 2000. Degradation of mechanical behavior in UHMWPE after natural and accelerated aging. *Biomaterials*. **21**(14),pp.1451–1460.

Endo, M., Tipper, J.L., Barton, D.C., Stone, M.H., Ingham, E. and Fisher, J. 2002. Comparison of wear, wear debris and functional biological activity of moderately crosslinked and non-crosslinked polyethylenes in hip prostheses. *Proceedings Of the Institution Of Mechanical Engineers Part H-Journal Of Engineering In Medicine*. **216**,pp.111–122.

Engh, C.A., Hopper, R.H., Huynh, C., Ho, H., Sritulanondha, S. and Engh, C.A. 2012. Winner of the Dorr Award A Prospective, Randomized Study of Cross-Linked and Non – Cross-Linked Polyethylene for Total Hip Arthroplasty at 10-Year Follow-Up. *Journal of*

*Arthroplasty*. **27**(8),p.2–7.e1.

Estok, D.M., Bragdon, C.R., Plank, G.R., Huang, A., Muratoglu, O.K. and Harris, W.H. 2005. The Measurement of Creep in Ultrahigh Molecular Weight Polyethylene A Comparison of Conventional Versus Highly Cross-Linked Polyethylene. *Journal of Arthroplasty*. **20**(2),pp.239–243.

Fauci, A. 2006. *Harrison's: Rheumatology: ISBN 978-0071814843*. The McGraw-Hill Companies.

Fehrig, T., Smith, S., Braun, E., Mobley, C., Wang, P. and Griffin, W. 1999. Motion at the Modular Acetabular Shell and Liner Interface: A Comparative Study. *Clinical Orthopaedics and Related Research*. **367**,pp.306–314.

Fisher, J. 1994. Wear of Ultra High Molecular Weight Polyethylene in Total Artificial Joints. *Current Orthopaedics*. **8**(Biomechanics masterclass 3),pp.164–169.

Fisher, J., Al-Hajjar, M., Williams, S., Jennings, L.M. and Ingham, E. 2012. In vitro measurement of wear in joint replacements: A stratified approach for enhanced reliability 'safer' pre-clinical simulation testing. *Seminars in Arthroplasty*. **23**(4),pp.286–288.

Furmanski, J., Anderson, M., Bal, S., Greenwald, a. S., Halley, D., Penenberg, B., Ries, M. and Pruitt, L. 2009. Clinical fracture of cross-linked UHMWPE acetabular liners. *Biomaterials*. **30**(29),pp.5572–5582.

Furmanski, J., Kraay, M.J. and Rimnac, C.M. 2011. Crack Initiation in Retrieved Cross-Linked Highly Cross-Linked Ultrahigh-Molecular-Weight Polyethylene Acetabular Liners. *The Journal of Arthroplasty*. **26**(5),pp.796–801.

Galvin, a L., Jennings, L.M., Tipper, J.L., Ingham, E. and Fisher, J. 2010. Wear and creep of highly crosslinked polyethylene against cobalt chrome and ceramic femoral heads.

*Proceedings of the Institution of Mechanical Engineers, Part H: Journal of Engineering in Medicine.* **224**(10),pp.1175–1183.

Galvin, a L., Tipper, J.L., Jennings, L.M., Stone, M.H., Jin, Z.M., Ingham, E. and Fisher, I. 2007. Wear and biological activity of highly crosslinked polyethylene in the hip under low serum protein concentrations. *Proceedings of the Institution of Mechanical Engineers. Part H, Journal of engineering in medicine.* **221**,pp.1–10.

García-Rey, E., García-Cimbrelo, E. and Cruz-Pardos, A. 2012. New polyethylenes in total hip replacement: A TEN- TO 12-YEAR FOLLOW-UP STUDY. *Journal of Bone and Joint Surgery, Am.* **95–B**(3),pp.326–332.

Gencur, S.J., Rimnac, C.M. and Kurtz, S.M. 2006. Fatigue crack propagation resistance of virgin and highly crosslinked , thermally treated ultra-high molecular weight polyethylene. *Biomaterials.* **27**,pp.1550–1557.

Glyn-Jones, S., Garfield-roberts, P., Gundle, R., Taylor, A., Mclardy-smith, P. and Murray, D.W. 2015. Highly Crosslinked Polyethylene in Total Hip Arthroplasty Decreases Longterm Wear: A Double-blind Randomized Trial. *Clinical Orthopaedics and Related Research.* **473**,pp.432–438.

Glyn-Jones, S., McLardy-Smith, P., Gill, H.S. and Murray, D.W. 2008. The creep and wear of highly cross-linked polyethylene. *Journal of Bone and Joint Surgery, Br.* **90–B**,pp.556–561.

Goldsmith, A.A.J., Dowson, D., Wroblewski, B.M., Siney, P.D., Fleming, P.A., Lane, J.M., Stone, M.H., Ed, F. and Walker, R. 2001. Comparative Study of the Activity of Total Hip Arthroplasty Patients and Normal Subjects. *Journal of Arthroplasty.* **16**(5),pp.613–619.

Gray, C.F., Moore, R.E. and Lee, G.-C. 2012. Spontaneous dissociation of offset, face-changing polyethylene liners from the acetabular shell: a report of four cases. *The Journal of bone and joint surgery. American volume.* **94**(9),pp.841–5.

- Grupp, T.M., Holderied, M., Mulliez, M.A., Streller, R., Jäger, M., Blömer, W. and Utzschneider, S. 2014. Biotribology of a vitamin E-stabilized polyethylene for hip arthroplasty – Influence of artificial ageing and third-body particles on wear. *Acta Biomaterialia*. **10**(7),pp.3068–3078.
- Hall, M. and Pinder, I.M. 1998. Wear in Retrieved Acetabular Components Effect of Femoral Head Radius and Patient Parameters. *The Journal of arthroplasty*. **13**(3),pp.291–295.
- Hall, R.M., Siney, P., Unsworth, a and Wroblewski, B.M. 1998. Prevalence of impingement in explanted Charnley acetabular components. *Journal of orthopaedic science : official journal of the Japanese Orthopaedic Association*. **3**(4),pp.204–8.
- Hall, R.M. and Unsworth, A. 1995. Measurement of wear in retrieved acetabular sockets. *Proceedings Of the Institution Of Mechanical Engineers Part H-Journal Of Engineering In Medicine*. **209**,pp.233–242.
- Heiner, A.D., Lundberg, H.J., Baer, T.E., Douglas, R., Callaghan, J.J. and Brown, T.D. 2009. Effects od Episodic Subluxation Events on Third Body Ingress and Embedment in the THA Bearing Surface. *Journal of Biomechanics*. **41**(10),pp.2090–2096.
- Hood, R., Wright, T. and Burstein, A. 1983. Retrieval analysis of total knee prostheses: a method and its application to 48 total condylar prostheses. *Journal of biomedical materials research*. **17**(5),pp.829–842.
- Hua, X., Li, J., Wang, L., Jin, Z., Wilcox, R. and Fisher, J. 2014. Contact mechanics of modular metal-on-polyethylene total hip replacement under adverse edge loading conditions. *Journal of Biomechanics*. **47**(13),pp.3303–3309.
- Ingham, E. and Fisher, J. 2000. Biological reactions to wear debris in total joint replacement. *Proceedings of the Institution of Mechanical Engineers. Part H, Journal of engineering in medicine*. **214**,pp.21–37.

Ingram, J.H., Stone, M., Fisher, J. and Ingham, E. 2004. The influence of molecular weight, crosslinking and counterface roughness on TNF-alpha production by macrophages in response to ultra high molecular weight polyethylene particles. *Biomaterials*. **25**(17),pp.3511–3522.

Isaac, G.H., Wroblewski, B.M., Atkinson, J.R. and Dowson, D. 1992. Isaac. A tribological study of retrieved hip prostheses 1992.pdf. *Clinical orthopaedics and related research*.,p.115.

Jalali-Vahid, D., Jagatia, M., Jin, Z.M. and Dowson, D. 2001. Prediction of lubricating film thickness in a ball-in- socket model with a soft lining representing human natural and artificial hip joints. *Proceedings Of the Institution Of Mechanical Engineers Part H- Journal Of Engineering In Medicine*. **215**(October 2000),pp.363–372.

Jedenmalm, A., Noz, M.E., Olivecrona, H., Olivecrona, L., Jedenmalm, A., Noz, M.E., Olivecrona, H. and Olivecrona, L. 2009. A new approach for assessment of wear in metal-backed acetabular cups using computed tomography: A phantom study with retrievals A new approach for assessment of wear in metal- backed acetabular cups using computed tomography. *Acta Orthopaedica*. **3674**(August 2016),pp.218–224.

Jennings, L.M., Al-Hajjar, M., Brockett, C.L., Williams, S., Tipper, J.L., Ingham, E. and Fisher, J. 2012. (iv) Enhancing the safety and reliability of joint replacement implants. *Orthopaedics and Trauma*. **26**(4),pp.246–252.

Jin, Z.M., Dowson, D. and Fisher, J. 1996. Analysis of fluid film lubrication in artificial hip joint replacements with surfaces of high elastic modulus. *Proceedings Of the Institution Of Mechanical Engineers Part H-Journal Of Engineering In Medicine*. **211**,pp.247–256.

Kabo, J., Gebhard, J., Loren, G. and Amstutz, H. 1993. In vivo wear of polyethylene acetabular components. *Journal of Bone and Joint Surgery, Br*. **75–B**,pp.254–258.

King, R., Narayan, V.S., Aust, S. and Hanes, M. 2009. • Assessment of Oxidative Stability of

Gamma-Irradiated , Antioxidant-Stabilized UHMWPE Tibial Component Poster No . 463

• 55th Annual Meeting of the Orthopaedic Research Society.

King, R., Narayan, V.S., Ernsberger, C. and Hanes, M. 2009. • Characterization of Gamma-Irradiated UHMWPE Stabilized with a Hindered-Phenol Antioxidant Paper No . 19 • 55th Annual Meeting of the Orthopaedic Research Society.

Komistek, R.D., Dennis, D.A., Ochoa, J.A., Haas, B.D. and Hammill, C. 2002. In vivo comparison of hip separation after metal-on-metal or metal-on-polyethylene total hip arthroplasty. *The Journal of bone and joint surgery. American volume.* **84–A(10)**,pp.1836–41.

Kurtz, S.M. 2009. *UHMWPE Biomaterials Handbook: ISBN 978-0-12-374721-1 Second Edition* 2nd ed. Elsevier.

Kurtz, S.M., Hozack, W.J., Purtill, J.J., Marcolongo, M., Kraay, M.J., Goldberg, V.M., Sharkey, P.F., Parvizi, J., Rimnac, C.M. and Edidin, A.A. 2006. Significance of In Vivo Degradation for Polyethylene in Total Hip Arthroplasty. *Journal of Clinical Orthopaedics and Related Research.* **453(453)**,pp.47–57.

Kurtz, S.M., MacDonald, D.W., Mont, M.A., Parvizi, J., Malkani, A.L. and Hozack, W. 2014. Retrieval Analysis of Sequentially Annealed Highly Crosslinked Polyethylene Used in Total Hip Arthroplasty. *Clinical Orthopaedics and Related Research.* **473(3)**,pp.962–971.

Kurtz, S.M., Muratoglu, O.K., Evans, M. and Edidin, A.A. 1999. Advances in the processing , sterilization , and crosslinking of ultra-high molecular weight polyethylene for total joint arthroplasty. *Biomaterials.* **20**,pp.1659–1688.

Kurtz, S.M., Ochoa, J.A., Hovey, C.B. and White, C. V 1999. Simulation of initial frontside and backside wear rates in a modular acetabular component with multiple screw holes. *Journal of Biomechanics.* **32**,pp.967–976.

- Kurtz, S.M., Ochoa, J. a., White, C. V., Srivastav, S. and Cournoyer, J. 1998. Backside nonconformity and locking restraints affect liner/shell load transfer mechanisms and relative motion in modular acetabular components for total hip replacement. *Journal of Biomechanics*. **31**(5),pp.431–437.
- Kurtz, S.M., van Ooij, A., Ross, R., de Waal Malefijt, J., Pelozo, J., Ciccarelli, L. and Villarraga, M.L. 2007. Polyethylene wear and rim fracture in total disc arthroplasty. *Spine Journal*. **7**(1),pp.12–21.
- Kurtz, S.M., van Ooij, A., Ross, R., de Waal Malefijt, J., Pelozo, J., Ciccarelli, L. and Villarraga, M.L. 2007. Polyethylene wear and rim fracture in total disc arthroplasty. *The spine journal : official journal of the North American Spine Society*. **7**(1),pp.12–21.
- Kurtz, S.M., Pelozo, J., Siskey, R. and Villarraga, M.L. 2005. Analysis of a retrieved polyethylene total disc replacement component. *Spine Journal*. **5**(3),pp.344–350.
- Lancaster, J.K. 1973. Dry bearings: a survey of materials and factors affecting their performance. *Tribology*. **6**(6),pp.219–251.
- Leslie, I.J., Williams, S., Isaac, G., Ingham, E. and Fisher, J. 2009. High cup angle and microseparation increase the wear of hip surface replacements. *Clinical Orthopaedics and Related Research*. **467**(9),pp.2259–2265.
- Lewinnek, G.E., Lewis, J.L., Tarr, R., Compere, C.L. and Zimmerman, J.R. 1978. Dislocations after total hip-replacement arthroplasties. *The Journal of bone and joint surgery. American volume*. **60**(2),pp.217–20.
- Lewis, R.. 1964. Predicting Wear. *Mech. Eng.* **80**,pp.32–35.
- Liao, Y.S., Benya, P.D. and McKellop, H.A. 1999. Effect of protein lubrication on the wear properties of materials for prosthetic joints. *Journal of Biomedical Materials Research*. **48**(4),pp.465–473.

- Lieberman, J.R., Kay, R.M., Hamlet, W.P., Park, S. and Kabo, J.M. 1996. Wear of the Polyethylene Liner-Metallic Shell Interface in Modular Acetabular Components An in vitro Analysis. *Journal of Arthroplasty*. **11**(5),pp.602–608.
- Loftus, M. and Ghelman, B. 2015. Acetabular Version Measurement in Total Hip Arthroplasty: the Impact of Inclination and the Value of Multi-Planar. *The Musculoskeletal Journal of Hospital for Special Surgery*. **11**,pp.65–70.
- Lombardi, A.V.J., Ellison, B.S. and Berend, K.R. 2008. Polyethylene Wear Is Influenced by Manufacturing Technique in Modular TKA. *Clinical Orthopaedics and Related Research*. **466**,pp.2798–2805.
- Lombardi, a V, Mallory, T.H., Dennis, D. a, Komistek, R.D., Fada, R. a and Northcut, E.J. 2000. An in vivo determination of total hip arthroplasty pistoning during activity. *The Journal of arthroplasty*. **15**(6),pp.702–709.
- Lu, Z. and McKellop, H. 1997. Frictional heating of bearing materials tested in a hip joint wear simulator. *Proceedings of the Institution of Mechanical Engineers. Part H, Journal of engineering in medicine*. **211**(1),pp.101–108.
- Malik, A. 2007. Impingement with Total Hip Replacement. *The Journal of Bone and Joint Surgery (American)*. **89**(8),p.1832.
- Malik, A., Dorr, L.D. and Long, W.T. 2009. Impingement as a Mechanism of Dissociation of a Metasul Metal-on-Metal Liner. *Journal of Arthroplasty*. **24**(2),p.323.e13-6.
- Manaka, M., Clarke, I.C., Yamamoto, K., Shishido, T., Gustafson, A. and Imakiire, A. 2004. Stripe Wear Rates in Alumina THR—Comparison of Microseparation Simulator Study with Retrieved Implants. *J Biomed Mater Res Part B: Appl Biomater*. **69**,pp.149–157.
- Manning, D.W., Chiang, P.P., Martell, J.M., Galante, J.O. and Harris, W.H. 2005. In vivo comparative wear study of traditional and highly cross-linked polyethylene in total hip

arthroplasty. *The Journal of arthroplasty*. **20**(7),pp.880–6.

Marchetti, E., Krantz, N., Berton, C., Bocquet, D., Fouilleron, N., Migaud, H. and Girard, J. 2011. Component impingement in total hip arthroplasty: frequency and risk factors. A continuous retrieval analysis series of 416 cup. *Orthopaedics & traumatology, surgery & research : OTSR*. **97**(2),pp.127–33.

Martell, J.M. and Berdia, S. 1997. Determination of polyethylene wear in total hip replacements with use of digital radiographs. *Journal of Bone and Joint Surgery - Series A*. **79**(11),pp.1635–1641.

Martell, J.M., Berkson, E., Berger, R. and Jacobs, J. 2003. Comparison of two and three-dimensional computerized polyethylene wear analysis after total hip arthroplasty. *Journal of Bone and Joint Surgery - Series A*. **85**(6),pp.1111–1117.

Martell, J.M., Verner, J.J. and Incavo, S.J. 2003. Clinical Performance of a Highly Cross-linked Polyethylene at Two Years in Total Hip Arthroplasty : A Randomized Prospective Trial. *Journal of Arthroplasty*. **18**(7),pp.55–59.

Masaoka, T., Clarke, I.C., Yamamoto, K., Tamura, J., Williams, P.A., Good, V.D., Shoji, H. and Imakiire, A. 2003. Validation of volumetric and linear wear-measurement in UHMWPE cups - A hip simulator analysis. *Wear*. **254**(5–6),pp.391–398.

Mayer, S.W., Wellman, S.S., Bolognesi, M.P. and Attarian, D.E. 2012. Late liner disassociation of a Pinnacle system acetabular component. *Orthopedics*. **35**(4),pp.e561-5.

Mayor, B., Currier, B.H., Citters, D.W. Van, Currier, J.H. and Collier, J.P. 2003. Oxidation of Ultra-High Molecular Weight Polyethylene and Its Influence on Contact Fatigue and Pitting of Knee Bearings. *Tribology Transactions*. **1**,pp.111–118.

Mazzucco, D. and Spector, M. 2003. Effects of contact area and stress on the volumetric wear of ultrahigh molecular weight polyethylene. *Wear*. **254**(5–6),pp.514–522.

- McKellop, H.A., Campbell, P., Park, S., Schmalzreid, T.P., Grigoris, P., Amstutz, H. and Sarmiento, A. 1995. The Origin of Submicron Polyethylene Wear Debris in Total Hip Arthroplasty. *Clinical Orthopaedics and Related Research*. **311**,pp.3–20.
- McKellop, H. a. 2007. The lexicon of polyethylene wear in artificial joints. *Biomaterials*. **28**,pp.5049–5057.
- McKellop, H., Shen, F.W., Lu, B., Campbell, P. and Salovey, R. 1999. Development of an extremely wear-resistant ultra high molecular weight polyethylene for total hip replacements. *Journal of orthopaedic research : official publication of the Orthopaedic Research Society*. **17**(2),pp.157–167.
- Mesko, J.W. 2009. Acute liner disassociation of a Pinnacle acetabular component. *The Journal of arthroplasty*. **24**(5),pp.815–8.
- Messieh, M., Mattingly, D.A., Turner, R.H., Scott, R., Fox, J. and Slater, J. 1994. Wear Debris From Bipolar Femoral Impingement A Cause of Femoral Stem Loosening. *The Journal of arthroplasty*. **9**(1).
- Miller, A.N., Su, E.P., Bostrom, M.P.G., Nestor, B.J. and Padgett, D.E. 2009. Incidence of Ceramic Liner Malseating in Trident 1 Acetabular Shell. *Clinical Orthopaedics and Related Research*.,pp.1552–1556.
- Minakawa, H., Stone, M.H., Wroblewski, B.M., Lancaster, J.G., Ingham, E. and Fisher, J. 1998. Quantification of third-body damage and its effect on UHMWPE wear with different types of femoral head. *Journal of Bone and Joint Surgery, Am*. **80-B**,pp.894–899.
- Morscher, E.W., Hefti, A. and Aebi, U. 1998. Severe osteolysis after third-body wear due to hydroxyapatite particles from acetabular cup coating. *Journal of Bone and Joint Surgery, Br*. **80**(March),pp.267–272.
- Muratoglu, O.K., Bragdon, C.R., O'Connor, D.O., Jasty, M., Harris, W.H., Rizwan, G. and

- McGarry, F. 1999. Unified wear model for highly crosslinked ultra-high molecular weight polyethylenes (UHMWPE). *Biomaterials*. **20**(16),pp.1463–1470.
- Muratoglu, O.K., Greenbaum, E.S., Bragdon, C.R., Jasty, M., Freiberg, A. a and Harris, W.H. 2004. Surface analysis of early retrieved acetabular polyethylene liners. *The Journal of Arthroplasty*. **19**(1),pp.68–77.
- Murray, D.W. 1993. THE DEFINITION AND ORIENTATION MEASUREMENT OF ACETABULAR ORIENTATION. *The Journal of bone and joint surgery. British volume*. **75–B**,pp.228–232.
- Narayan, V.N. and King, R. 2009. Oxidative Stability Studies in UHMWPE - ASTM Protocol Aging Poster No . 2316 • 56th Annual Meeting of the Orthopaedic Research Society.
- Narayan, V.S., Ernsberger, C. and King, R. 2009. Pin-on-Disk Wear Studies of Antioxidant-Stabilized UHMWPE Materials Poster No . 462 • 55th Annual Meeting of the Orthopaedic Research Society.
- Narayan, V.S., King, R., Warner, D. and Sharp, M. 2009. Evaluation of Antioxidant-Stabilized UHMWPE Materials Poster No . 459 • 55th Annual Meeting of the Orthopaedic Research Society.
- National Joint Registry 2014. 12th Annual Report. . (December 2014).
- Nevelos, J., Ingham, E., Doyle, C., Streicher, R., Nevelos, a, Walter, W. and Fisher, J. 2000. Microseparation of the centers of alumina-alumina artificial hip joints during simulator testing produces clinically relevant wear rates and patterns. *The Journal of arthroplasty*. **15**(6),pp.793–795.
- Nevelos, J.E., Ingham, E., Doyle, C., Fisher, J. and Nevelos, a. B. 1999. Analysis of retrieved alumina ceramic components from Mittelmeier total hip prostheses. *Biomaterials*. **20**(19),pp.1833–1840.

Nevelos, J.E., Ingham, E., Doyle, C., Nevelos, a. B. and Fisher, J. 2001. The influence of acetabular cup angle on the wear of 'BIOLOX Forte' alumina ceramic bearing couples in a hip joint simulator. *Journal of Materials Science: Materials in Medicine*. **12**(2),pp.141–144.

Office for National Statistics 2014. Health Expectancies at Birth and at Age 65 in the United Kingdom : 2009-11. ,pp.1–16.

O'Neill, C.K.J., Napier, R.J., Diamond, O.J., Brien, S.O., Beverland, D.E. and Presentation, C. 2015. Case Report: Acetabular Liner Dissociation following Total Hip Arthroplasty : A Rare but Serious Complication That May Be Easily Misinterpreted in the Emergency Department. *Case Reports in Emergency Medicine*.,pp.1–4.

Ong, C.S. and Sa, N. 1998. Ultrasonic evaluation of ultra-high molecular weight polyethylene used in medical prostheses. *Proceedings Of the Institution Of Mechanical Engineers Part H-Journal Of Engineering In Medicine*. **212**(September 1997),pp.65–69.

Oral, E., Christensen, S.D., Malhi, A.S., Wannomae, K.K. and Muratoglu, O.K. 2006. Wear Resistance and Mechanical Properties of Highly Cross-linked , Ultrahigh – Molecular Weight Polyethylene Doped With Vitamin E. *Journal of Arthroplasty*. **21**(4),pp.580–591.

Oral, E., Malhi, A.S. and Muratoglu, O.K. 2006. Mechanisms of decrease in fatigue crack propagation resistance in irradiated and melted UHMWPE \$. *Biomaterials*. **27**,pp.917–925.

Oral, E., Neils, A.L., Doshi, B.N., Fu, J. and Muratoglu, O.K. 2016. Effects of simulated oxidation on the in vitro wear and mechanical properties of irradiated and melted highly crosslinked UHMWPE. *Journal of Biomedical Materials Research - Part B Applied Biomaterials*. **104B**,pp.316–322.

Pace, T.B., Keith, K.C., Alvarez, E., Snider, R.G., Tanner, S.L., Desjardins, J.D., Carolina, S., System, G.H. and Box, P.O. 2013. Comparison of Conventional Polyethylene Wear and

Signs of Cup Failure in Two Similar Total Hip Designs. *Advances in Orthopedics*. **2013**.

Pang, H., Naudie, D.D.R., Mccalden, R.W., Macdonald, S.J. and Teeter, M.G. 2015. Highly Crosslinked Polyethylene Improves Wear But Not Surface Damage in Retrieved Acetabular Liners. *Clinical Orthopaedics and Related Research*. **473**,pp.463–468.

Patil, S., Bergula, A., Chen, P.C., Colwell, C.W. and D'Lima, D. 2003. Polyethylene Wear and Acetabular Component Orientation. *The Journal of Bone and Joint Surgery (American)*. **85**,pp.56–63.

Patten, E.W., Atwood, S.A., Citters, D.W. Van, Pruitt, L.A. and Ries, M.D. 2010. Delamination of a highly cross-linked polyethylene liner associated with titanium deposits on the cobalt-chromium modular femoral head following dislocation. *Journal of Bone and Joint Surgery, Br.* **92–B(9)**,pp.1306–1311.

Paul, J. 1976. Force actions transmitted by joints in the human body. *Proceedings of the Royal Society London B*. **192**,pp.163–172.

Pedersen, D.R., Rourke, M.R.O., Goetz, D.D., Vittetoe, D.A., Clohisy, J.C. and Brown, T.D. 2007. Association of Third Body Embedment with Rim Damage in Retrieved Acetabular Liners. *Clinical Orthopaedics and Related Research*. (465),pp.133–139.

Pooley, C.. and Tabor, D. 1972. Friction and molecular structure: the behaviour of some thermoplastics. *Proceedings of the Royal Society A*. **329**,pp.251–274.

Poultides, L. a., Sioros, V., Anderson, J. a., Bruni, D., Beksac, B. and Sculco, T.P. 2012. Ten- to 15-Year Clinical and Radiographic Results for a Compression Molded Monoblock Elliptical Acetabular Component. *Journal of Arthroplasty*. **27(10)**,pp.1850–1856.

Premnath, V., Harris, W.H., Jasty, M. and Merrill, E.W. 1996. Gamma sterilization of UHMWPE articular implants: An analysis of the oxidation problem. *Biomaterials*. **17(18)**,pp.1741–1753.

- Pruitt, L.A., Ansari, F., Kury, M., Mehdizah, A., Patten, E.W., Huddlestein, J., Mickelson, D., Chang, J., Hubert, K. and Ries, M.D. 2013. Review Article Clinical trade-offs in cross-linked ultrahigh-molecular-weight polyethylene used in total joint arthroplasty. *Journal of biomedical materials research Part B*. **101**,pp.476–484.
- Pruitt, L. a. 2005. Deformation, yielding, fracture and fatigue behavior of conventional and highly cross-linked ultra high molecular weight polyethylene. *Biomaterials*. **26**(8),pp.905–915.
- Puolakka, T., Juhola, K., Keränen, J., Nevalainen, K.J., Pajamäki, K., Halonen, P., Saikko, V., Lehto, M., Nevalainen, J.K. and Järvinen, V. 2003. Increased volumetric wear of polyethylene liners with more than 3 years of shelf-life time. *International Orthopaedics*. **27**,pp.153–159.
- Raimondi, M.T., Sassi, R. and Pietrabissa, R. 2000. A method for the evaluation of the change in volume of retrieved acetabular cups. *Proceedings Of the Institution Of Mechanical Engineers Part H-Journal Of Engineering In Medicine*. **214**,pp.577–587.
- Revell, P. a, al-Saffar, N. and Kobayashi, a 1997. Biological reaction to debris in relation to joint prostheses. *Proceedings of the Institution of Mechanical Engineers. Part H, Journal of engineering in medicine*. **211**(2),pp.187–197.
- Ries, M.D., Scott, M.L. and Jani, S. 2001. Relationships Between Gravimetric Wear and Particle Generation in Hip Simulators : Conventional Compared with Cross-Linked Polyethylene. *Journal of Bone and Joint Surgery*. **83–A**(Supplement 2),pp.116–122.
- Rose, R.M., Goldfarb, H.V., Ellis, E. and Crugnola, A.M. 1983. On the pressure dependence of the wear of ultrahigh molecular weight polyethylene. *Wear*. **92**(1),pp.99–111.
- Rostoker, W. and Galante, J.O. 1979. Contact pressure dependence of wear rates of ultra high molecular weight polyethylene. *Journal of Biomedical Materials Research*. **13**(6),pp.957–964.

- Saikko, V. 2014. Effect of shelf versus accelerated aging of UHMWPE on delamination in knee wear simulation. *Tribology International*. **73**,pp.10–16.
- Schmalzried, T.P., Scott, D.L., Zahiri, C. and Dorey, F. 1998. Variables Affecting Wear In Vivo: Analysis of 1,080 Hips with Computer-Assisted Technique. *Transactions of the Society of Biomaterials*. **21**,p.216.
- Schroder, D.T., Kelly, N.H., Wright, T.M. and Parks, M.L. 2011. Retrieved highly crosslinked UHMWPE acetabular liners have similar wear damage as conventional UHMWPE. *Clinical Orthopaedics and Related Research*. **469**(2),pp.387–394.
- Shibata, N., Tomita, N., Onmori, N., Kato, K. and Ikeuchi, K. 2003. Defect initiation at subsurface grain boundary as a precursor of delamination in ultrahigh molecular weight polyethylene. *Journal of biomedical materials research. Part A*. **67**(1),pp.276–84.
- Shon, W.Y., Baldini, T., Peterson, M.G., Wright, T.M. and Salvati, E.A. 2005. Impingement in Total Hip Arthroplasty. *The Journal of Arthroplasty*. **20**(4),pp.427–435.
- Simon, J., Dayan, A., Ergas, E., Stuchin, S. and Di Cesare, P. 1998. Case Report Catastrophic Failure of the Acetabular Component in a Ceramic-Polyethylene Bearing Total Hip Arthroplasty. *The Journal of Arthroplasty*. **13**(1),pp.108–113.
- Sobieraj, M.C., Murphy, J.E., Brinkman, J.G., Kurtz, S.M. and Rimnac, C.M. 2013. Monotonic and fatigue behavior of five clinically relevant conventional and highly crosslinked UHMWPEs in the presence of stress concentrations. *Journal of the Mechanical Behavior of Biomedical Materials*. **28**,pp.244–253.
- Stewart, T., Tipper, J., Streicher, R., Ingham, E. and Fisher, J. 2001. Long-term wear of HIPed alumina on alumina bearings for THR under microseparation conditions. *Journal of Materials Science: Materials in Medicine*. **12**,pp.1053–1056.
- Sutula, L.C., Collier, J.P., Sperling, D.K., Currier, J.H., Saum, K.A. and Mayor, M.B. 1996.

Impact of gamma sterilization on clinical performance of polyethylene in the hip. *The Journal of arthroplasty*. **11**(4),pp.377–89.

Sychterz, B.Y.C.J., E, M.S., Engh, C.A., D, M., Shah, N. and S, B. 1997. Radiographic Evaluation of Penetration by the Femoral Head into the Polyethylene Liner over Time \*. *The Journal of Bone and Joint Surgery (American)*. **79–A**(7),pp.1040–1046.

Takaoka, S.K.K. and Ueno, A.T.M. 1998. Polyethylene wear from femoral bipolar neck-cup impingement as a cause of femoral prosthetic loosening. *Archives of orthopaedic and trauma surgery*. **117**,pp.390–391.

Talmo, C.T., Shanbhag, A.S. and Rubash, H.E. 2006. Nonsurgical Management of Osteolysis. *Clinical Orthopaedics and Related Research*. **453**,pp.254–264.

Teeter, M.G., Milner, J.S., Au, J.A., Lorusso, D. and Holdsworth, D.W. 2011. Regional Measurements of Surface Deviation Volume in Worn Polyethylene Joint Replacement Components: ORS Poster No. 1136

Teeter, M.G., Naudie, D.D.R., Charron, K.D. and Holdsworth, D.W. 2010. Three-Dimensional Surface Deviation Maps for Analysis of Retrieved Polyethylene Acetabular Liners Using Micro-Computed Tomography. *Journal of Arthroplasty*. **25**(2),pp.330–332.

Teeter, M.G., Yuan, X., Naudie, D.D.R. and Holdsworth, D.W. 2010. Technique to quantify subsurface cracks in retrieved polyethylene components using micro-CT. *Journal of long-term effects of medical implants*. **20**(1),pp.27–34.

Tipper, J.L., Ingham, E., Hailey, J.L., Besong, a a, Fisher, J., Wroblewski, B.M. and Stone, M.H. 2000. Quantitative analysis of polyethylene wear debris, wear rate and head damage in retrieved Charnley hip prostheses. *Journal of materials science. Materials in medicine*. **11**(2),pp.117–24.

Tower, S.S., Currier, J.H., Currier, B.H., Lyford, K. a, Van Citters, D.W. and Mayor, M.B. 2007.

Rim cracking of the cross-linked longevity polyethylene acetabular liner after total hip arthroplasty. *The Journal of bone and joint surgery. American volume.* **89**(10),pp.2212–2217.

Tuke, M., Taylor, A., Roques, A. and Maul, C. 2010. 3D linear and volumetric wear measurement on artificial hip joints — Validation of a new methodology. *Precision Engineering.* **34**(4),pp.777–783.

Uddin, M.S. 2014. Wear Measurement and Assessment of Explanted Cross-Linked PE Acetabular Cups Using a CMM Wear Measurement and Assessment of Explanted Cross-Linked PE Acetabular Cups Using a CMM. *Tribology Transactions.* **57**:5,pp.767–777.

Usrey, M.M., Noble, P.C., Rudner, L.J., Conditt, M. a., Birman, M. V., Santore, R.F. and Mathis, K.B. 2006. Does Neck/Liner Impingement Increase Wear of Ultrahigh-Molecular-Weight Polyethylene Liners? *Journal of Arthroplasty.* **21**(6 SUPPL.),pp.65–71.

V.N., N., R., K. and Senyurt, A.. 2010. Oxidative Stability Studies in UHMWPE - ASTM Protocol Aging In: *56th Annual Meeting of the Orthopaedic Research Society.*

Vassiliou, K. and Unsworth, a 2004. Is the wear factor in total joint replacements dependent on the nominal contact stress in ultra-high molecular weight polyethylene contacts? *Proceedings of the Institution of Mechanical Engineers. Part H, Journal of engineering in medicine.* **218**(2),pp.101–7.

Wang, A. 2001. A unified theory of wear for ultra-high molecular weight polyethylene in multi-directional sliding. *Wear.* **248**(1–2),pp.38–47.

Wang, A., Sun, D.C., Yau, S., Edwards, B., Sokol, M., Essner, A., Polineni, V.K., Stark, C. and Dumbleton, J.H. 1997. Orientation softening in the deformation and wear of ultra-high molecular weight polyethylene. *Wear.* **203–204**,pp.230–241.

Wang, a, Essner, a, Polineni, V., Stark, C. and Dumbleton, J.. 1998. Lubrication and wear of

ultra-high molecular weight polyethylene in total joint replacements. *Tribology International*. **31**(1–3),pp.17–33.

Wannomae, K.K., Bhattacharyya, S., Freiberg, A., Estok, D., Harris, W.H. and Muratoglu, O. 2006. In Vivo Oxidation of Retrieved Cross-linked Ultra – High-Molecular-Weight Polyethylene Acetabular Components with Residual Free Radicals. *Journal of Arthroplasty*. **21**(7),pp.1005–1011.

Wasielowski, R., Galante, J., Liegthy, R., Natarajan, R. and Rosenberg, A. 1994. Wear Patterns on Retrieved Polyethylene Tibial Inserts and Their Relationship to Technical Considerations During Total Knee Arthroplasty. *Clinical Orthopaedics and Related Research*®. **299**,pp.31–43.

Willert, H., Friedrichsheim, O.U., Main, F., Germany, W. and Semlitsch, M. 1977. Reactions of the Articular Capsule to Wear Products of Artificial Joint Prostheses. *Journal of biomedical materials research*. **11**,pp.157–164.

Williams, S., Butterfield, M., Stewart, T., Ingham, E., Stone, M. and Fisher, J. 2003. Wear and deformation of ceramic-on-polyethylene total hip replacements with joint laxity and swing phase microseparation. *Proceedings of the Institution of Mechanical Engineers. Part H, Journal of engineering in medicine*. **217**,pp.147–153.

Williams, S., Jalali-Vahid, D., Brockett, C., Jin, Z., Stone, M.H., Ingham, E. and Fisher, J. 2006. Effect of swing phase load on metal-on-metal hip lubrication, friction and wear. *Journal of Biomechanics*. **39**(12),pp.2274–2281.

Williams, S., Leslie, I., Isaac, G., Jin, Z., Ingham, E. and Fisher, J. 2008. Tribology and wear of metal-on-metal hip prostheses: influence of cup angle and head position. *The Journal of bone and joint surgery. American volume*. **90 Suppl 3**,pp.111–117.

Woolson, S.T. and Murphy, M.G. 1995. of the Polyethylene Components of Harris-Galante Inserted without Acetabular. *The Journal of Bone and Joint Surgery (American)*. **77**(9).

Yamaguchi, M., Akisue, T., Bauer, T.W. and Hashimoto, Y. 2000. The spatial location of impingement in total hip arthroplasty. *The Journal of arthroplasty*. **15**(3),pp.305–313.

Young, A., Sychterz, C., Hopper, R. and Engh, C.A. 2002. Effect of Acetabular Modularity on Polyethylene Wear and Osteolysis in Total Hip Arthroplasty. *The Journal of Bone and Joint Surgery (American)*. **84–A**(1),pp.58–63.

Yun, A., Koli, E.N., Moreland, J., Iorio, R., Tilzey, J.F., Mesko, J.W., Lee, G.-C. and Froimson, M. 2015. Polyethylene Liner Dissociation Is a Complication of the DePuy Pinnacle Cup: A Report of 23 Cases *In: Clinical Orthopaedics and Related Research: Symposium 2015 Hip Society Proceedings*. Springer US.

## Appendix 1: Simulator Components with Station Numbers and Labelling

Table 1 Details of XLPE Pinnacle acetabular liners for protocol development study (Chapter 3)

| Sample ID | Description                      | Diameter | LOT#   | REF#        |
|-----------|----------------------------------|----------|--------|-------------|
| AM1       | Marathon UHMWPE acetabular liner | 36mm     | FK7F91 | 1219-36-056 |
| AM3       | Marathon UHMWPE acetabular liner | 36mm     | FH5FJ1 | 1219-36-056 |
| AM5       | Marathon UHMWPE acetabular liner | 36mm     | FH5FJ1 | 1219-36-056 |
| AM7       | Marathon UHMWPE acetabular liner | 36mm     | 114854 | 1219-36-056 |
| AM9       | Marathon UHMWPE acetabular liner | 36mm     | 114854 | 1219-36-056 |
| AM11      | Marathon UHMWPE acetabular liner | 36mm     | 224893 | 1219-36-056 |

Table 2 Details of aged GVF UHMWPE Pinnacle compatible acetabular liners for protocol development study (Chapter 3)

| Sample ID | Description                      | Diameter | Gamma Process Run ID | LOT#               | REF         |
|-----------|----------------------------------|----------|----------------------|--------------------|-------------|
| A2        | Aged GVF UHMWPE acetabular liner | 36mm     | 68403A               | 4420722<br>4418276 | 1219-36-056 |
| A4        | Aged GVF UHMWPE acetabular liner | 36mm     | 68403A               | 4420722<br>4418276 | 1219-36-056 |
| A6        | Aged GVF UHMWPE acetabular liner | 36mm     | 68403A               | 4420722<br>4418276 | 1219-36-056 |
| A8        | Aged GVF UHMWPE acetabular liner | 36mm     | 68403A               | 4420722<br>4418276 | 1219-36-056 |
| A10       | Aged GVF UHMWPE acetabular liner | 36mm     | 68403A               | 4420722<br>4418276 | 1219-36-056 |
| A12       | Aged GVF UHMWPE acetabular liner | 36mm     | 68403A               | 4420722<br>4418276 | 1219-36-056 |

Table 3 Details of CoCr femoral heads articulating with XLPE and aged PE liners for protocol development study (Chapter 3)

| Sample ID  | Description | Diameter | Taper | LOT#    | REF         |
|------------|-------------|----------|-------|---------|-------------|
| XLPE 1     | ARTICUL/EZE | 36mm     | 12/14 | 3167851 | 1365-52-000 |
| Aged PE 2  | ARTICUL/EZE | 36mm     | 12/14 | 3167851 | 1365-52-000 |
| XLPE 3     | ARTICUL/EZE | 36mm     | 12/14 | 3003038 | 1365-52-000 |
| Aged PE 4  | ARTICUL/EZE | 36mm     | 12/14 | 3155929 | 1365-52-000 |
| XLPE 5     | ARTICUL/EZE | 36mm     | 12/14 | 3155929 | 1365-52-000 |
| Aged PE 6  | ARTICUL/EZE | 36mm     | 12/14 | 3167851 | 1365-52-000 |
| XLPE 7     | ARTICUL/EZE | 36mm     | 12/14 | 2513886 | 1365-52-000 |
| Aged PE 8  | ARTICUL/EZE | 36mm     | 12/14 | 2513886 | 1365-52-000 |
| XLPE 9     | ARTICUL/EZE | 36mm     | 12/14 | 2513886 | 1365-52-000 |
| Aged PE 10 | ARTICUL/EZE | 36mm     | 12/14 | 2513886 | 1365-52-000 |

Table 4 Details of Pinnacle metal shells for protocol development study (Chapter 3)

| Sample ID | Description    | Outer diameter | LOT       | REF         |
|-----------|----------------|----------------|-----------|-------------|
| Shell 1   | Pinnacle Shell | 56mm           | FA4F91000 |             |
| P1        | Pinnacle Shell | 56mm           | D3VEM1000 | 1217-01-056 |
| Shell 3   | Pinnacle Shell | 56mm           | FA4F91000 |             |
| P2        | Pinnacle Shell | 56mm           | D3VEM1000 | 1217-01-056 |
| Shell 5   | Pinnacle Shell | 56mm           | FB5R41000 |             |
| P3        | Pinnacle Shell | 56mm           | D3KDA1000 | 1217-01-056 |
| Shell 7   | Pinnacle Shell | 56mm           | FA4F91000 |             |
| P4        | Pinnacle Shell | 56mm           | D3VEM1000 | 1217-01-056 |
| Shell 9   | Pinnacle Shell | 56mm           | FA4F91000 |             |
| P5        | Pinnacle Shell | 56mm           | D3KDA1000 | 1217-01-056 |

Table 5 Details of AOPE compression moulded acetabular cups for AOPE study (Chapter 4)

| Sample ID | Description | Diameter | LOT#         | Other ref |
|-----------|-------------|----------|--------------|-----------|
| AOPE CM1  | Monoblock   | 36mm     | DE 022309248 | MD-E0601a |
| AOPE CM2  | Monoblock   | 36mm     | DE 022309248 | MD-E0601a |
| AOPE CM3  | Monoblock   | 36mm     | DE 022309248 | MD-E0601a |
| AOPE CM4  | Monoblock   | 36mm     | DE 022309248 | MD-E0601a |
| AOPE CM9  | Monoblock   | 36mm     | DE 022309248 | MD-E0601a |
| AOPE CM10 | Monoblock   | 36mm     | DE 022309248 | MD-E0601a |

Table 6 Details of AOPE Pinnacle compatible acetabular liners for AOPE study (Chapter 4)

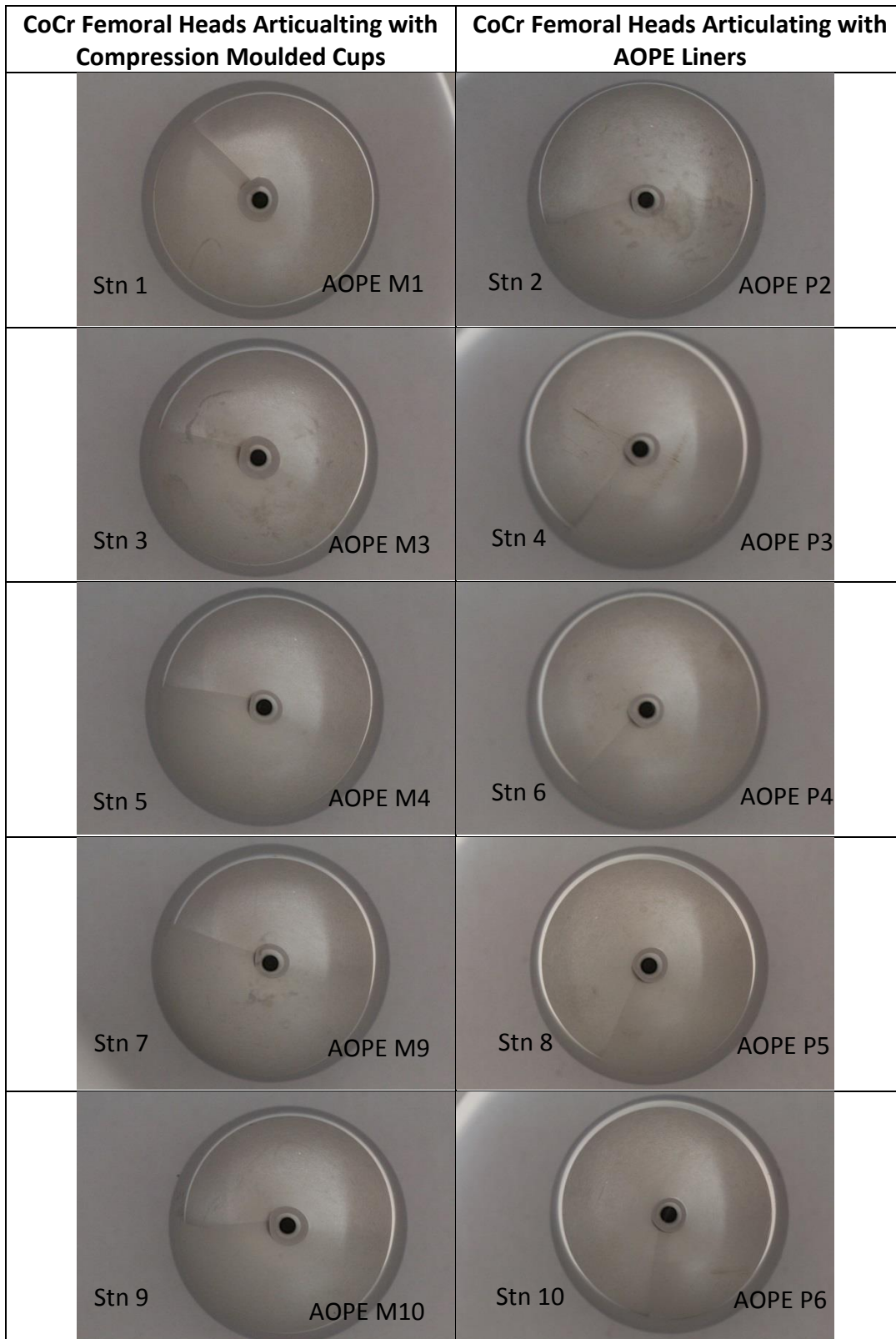
| Sample ID | Description | Diameter | LOT#  | REF |
|-----------|-------------|----------|---|-----|
| AOPE 1    | Pinnacle    | 36mm     | AO Pinnacle LOT and REF numbers not provided by DePuy |     |
| AOPE 2    | Pinnacle    | 36mm     |   |     |
| AOPE 3    | Pinnacle    | 36mm     |   |     |
| AOPE 4    | Pinnacle    | 36mm     |   |     |
| AOPE 5    | Pinnacle    | 36mm     |   |     |
| AOPE 6    | Pinnacle    | 36mm     |   |     |

Table 7 Details of Pinnacle metal shells for AOPE study (Chapter 4)

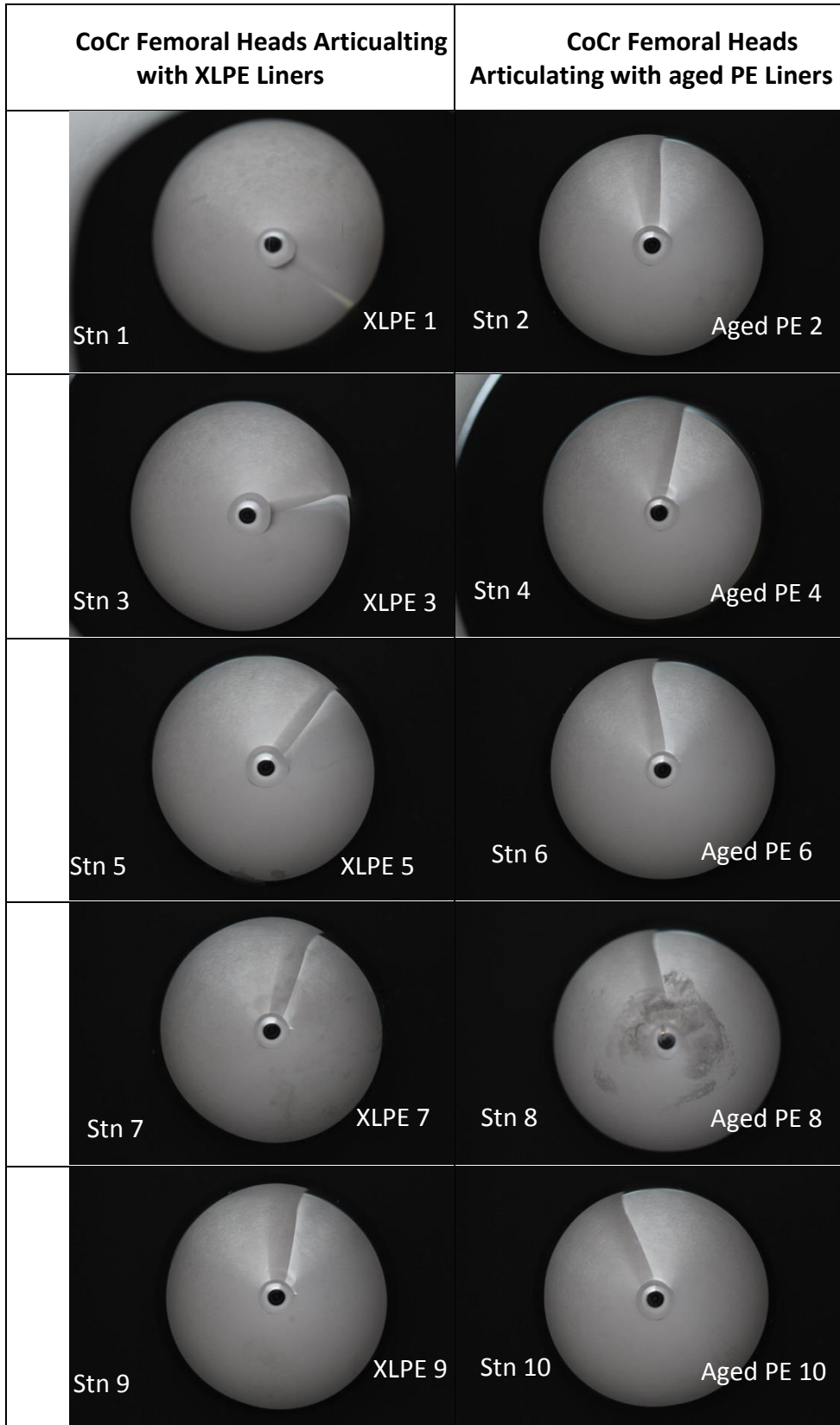
| Sample ID | Description    | Outer diameter | LOT       | REF         |
|-----------|----------------|----------------|-----------|-------------|
| P1        | Pinnacle Shell | 56mm           | D3VEM1000 | 1217-01-056 |
| P2        | Pinnacle Shell | 56mm           | D3VEM1000 | 1217-01-056 |
| P3        | Pinnacle Shell | 56mm           | D3KDA1000 | 1217-01-056 |
| P4        | Pinnacle Shell | 56mm           | D3VEM1000 | 1217-01-056 |
| P5        | Pinnacle Shell | 56mm           | D3KDA1000 | 1217-01-056 |

Table 8 Details of CoCr femoral heads for AOPE study (Chapter 4)

| <b>Sample ID</b> | <b>Description</b> | <b>Diameter</b> | <b>Taper</b> | <b>LOT#</b> | <b>REF</b>  |
|------------------|--------------------|-----------------|--------------|-------------|-------------|
| M1               | ARTICUL/EZE        | 36mm            | 12/14        | 3013699     | 1365-52-000 |
| M2               | ARTICUL/EZE        | 36mm            | 12/14        | 3013699     | 1365-52-000 |
| M3               | ARTICUL/EZE        | 36mm            | 12/14        | 3010300     | 1365-52-000 |
| M4               | ARTICUL/EZE        | 36mm            | 12/14        | 3000245     | 1365-52-000 |
| M9               | ARTICUL/EZE        | 36mm            | 12/14        | 3000245     | 1365-52-000 |
| M10              | ARTICUL/EZE        | 36mm            | 12/14        | 3013699     | 1365-52-000 |
| P1               | ARTICUL/EZE        | 36mm            | 12/14        | 3010300     | 1365-52-000 |
| P2               | ARTICUL/EZE        | 36mm            | 12/14        | 3010300     | 1365-52-000 |
| P3               | ARTICUL/EZE        | 36mm            | 12/14        | 3010300     | 1365-52-000 |
| P4               | ARTICUL/EZE        | 36mm            | 12/14        | 3013699     | 1365-52-000 |
| P5               | ARTICUL/EZE        | 36mm            | 12/14        | 3010300     | 1365-52-000 |
| P6               | ARTICUL/EZE        | 36mm            | 12/14        | 3000245     | 1365-52-000 |



**Figure 1 CoCr Femoral heads that articulated with the AOPE compression moulded cups and AOPE liners for 5Mc of standard loading and 5Mc of edge loading with corresponding stations and component labelling (Chapter 4)**



**Figure 2 CoCr Femoral heads that articulated with XLPE and Aged PE liners for 5Mc of standard loading and 5Mc of edge loading with corresponding stations and component labelling (Chapter 3)**

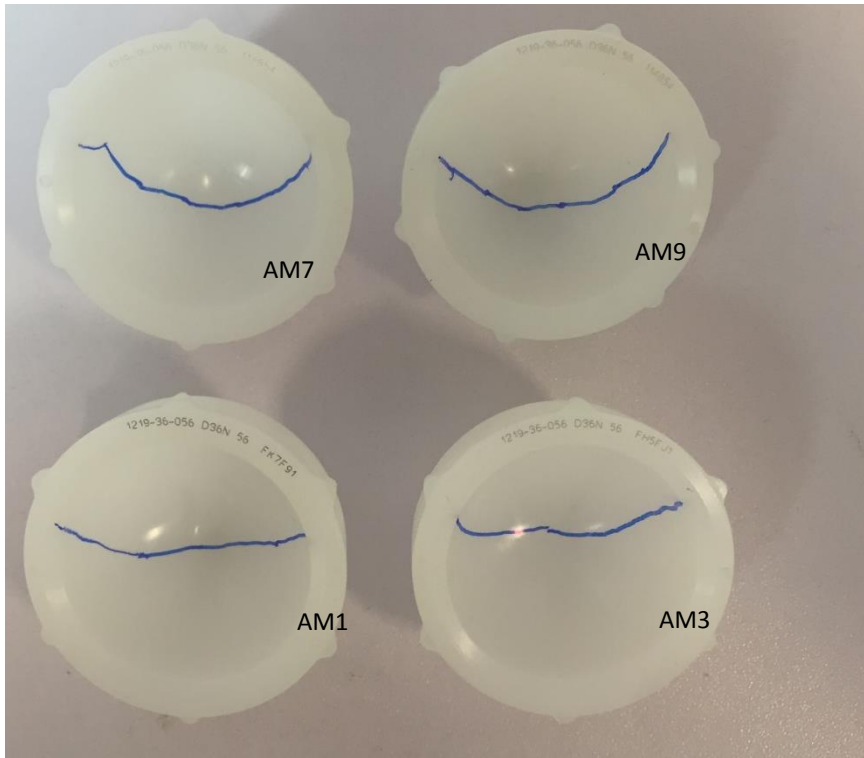


**Figure 3 XLPE acetabular liners with polished wear area highlighted (Chapter 3)**

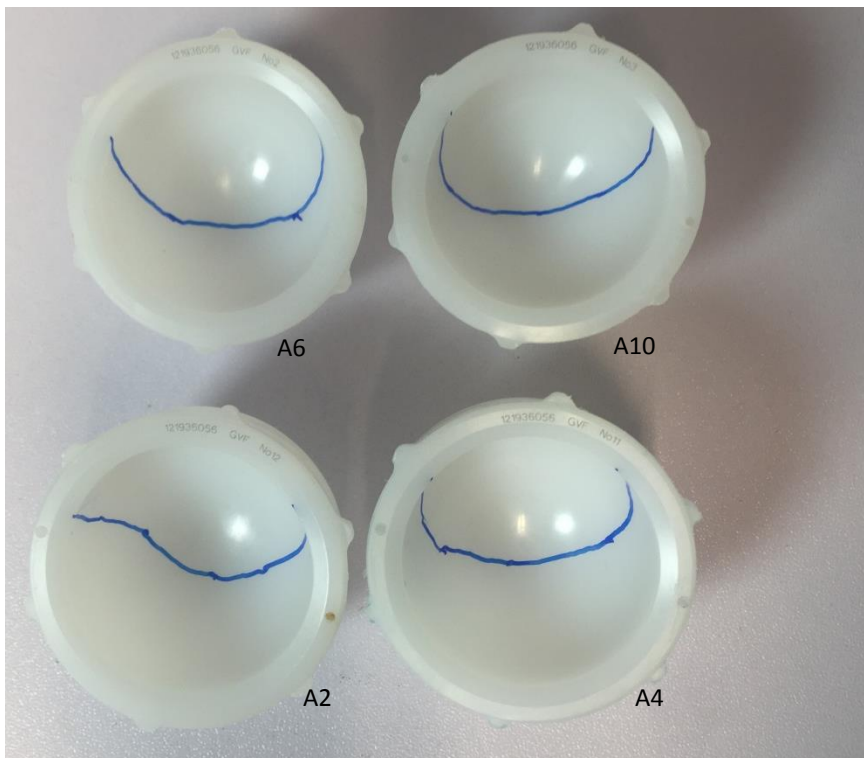


**Figure 4 Aged PE Acetabular liners with polished wear area highlighted (Chapter 3)**

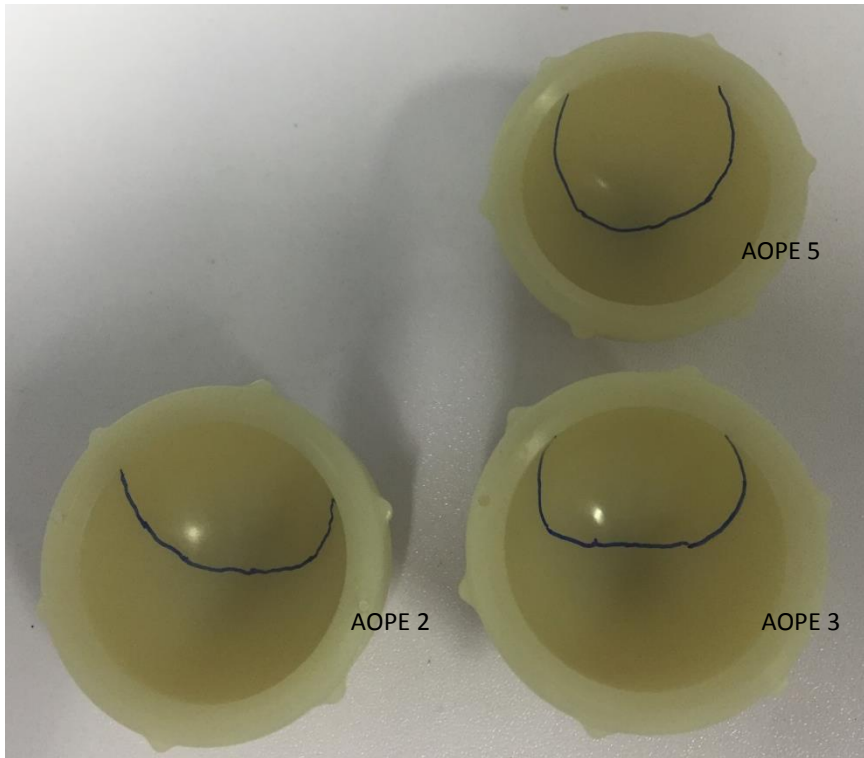


**Figure 5 AOPE Acetabular liners with polished wear area highlighted (Chapter 4). Note one liner was returned to Depuy following testing and analysis prior to taking this picture.**

Table 9: Simulator test set-up for protocol development study

| <b>Station Number</b>    | <b>Femoral Head</b> | <b>Acetabular Cup/Liner</b> |
|--------------------------|---------------------|-----------------------------|
| Station 1                | AOPE M1             | AOPE CM 1                   |
| Station 2                | AOPE P1             | AOPE 6                      |
| Station 3 (load control) | AOPE M3             | AOPE CM 3                   |
| Station 4                | AOPE P2             | AOPE 2                      |
| Station 5                | AOPE M4             | AOPE CM 4                   |
| Station 6                | AOPE P3             | AOPE 3                      |
| Station 7                | AOPE M9             | AOPE CM 9                   |
| Station 8 (load control) | AOPE P4             | AOPE 4                      |
| Station 9                | AOPE M10            | AOPE CM 10                  |
| Station 10               | AOPE P5             | AOPE 5                      |

Table 10: Simulator test set-up for AOPE study

| <b>Station Number</b>    | <b>Femoral Head</b> | <b>Acetabular Cup/Liner</b> |
|--------------------------|---------------------|-----------------------------|
| Station 1                | XLPE 1              | AM1                         |
| Station 2                | Aged PE 2           | A2                          |
| Station 3 (load control) | XLPE 2              | AM3                         |
| Station 4                | Aged PE 4           | A4                          |
| Station 5                | XLPE 5              | AM5                         |
| Station 6                | Aged PE 6           | A6                          |
| Station 7                | XLPE 7              | AM7                         |
| Station 8 (load control) | Aged PE 8           | A8                          |
| Station 9                | XLPE 9              | AM9                         |
| Station 10               | Aged PE 10          | A10                         |

**Appendix 2: Inter and Intra-user variability of volume change measurements on explant 6N**

**Table 1: Mean volume change ± %RSD of explant 6N for three repeats of four different protocols by four different users using Redlux analysis software.**

| Explant 6 | Protocol 1 (mm <sup>3</sup> ) | Protocol 2 (mm <sup>3</sup> ) | Protocol 3 (mm <sup>3</sup> ) | Protocol 4 (mm <sup>3</sup> ) |
|-----------|-------------------------------|-------------------------------|-------------------------------|-------------------------------|
| User 1    | <u>75 ± 4.4%</u>              | 184 ± 16%                     | 47 ± 14.7%                    | 128 ± 14.2%                   |
| User 2    | 63 ± 23.8%                    | 182 ± 32.1%                   | <u>40 ± 20%</u>               | 128 ± 28.4%                   |
| User 3    | 142 ± 14.5%                   | <u>310.2 ± 5.8%</u>           | 108.3 ± 26.7%                 | 278 ± 9.2%                    |
| User 4    | 93.8 ± 13.9%                  | 236.5 ± 16.7%                 | 57.5 ± 11.9%                  | <u>261.9 ± 6.2%</u>           |

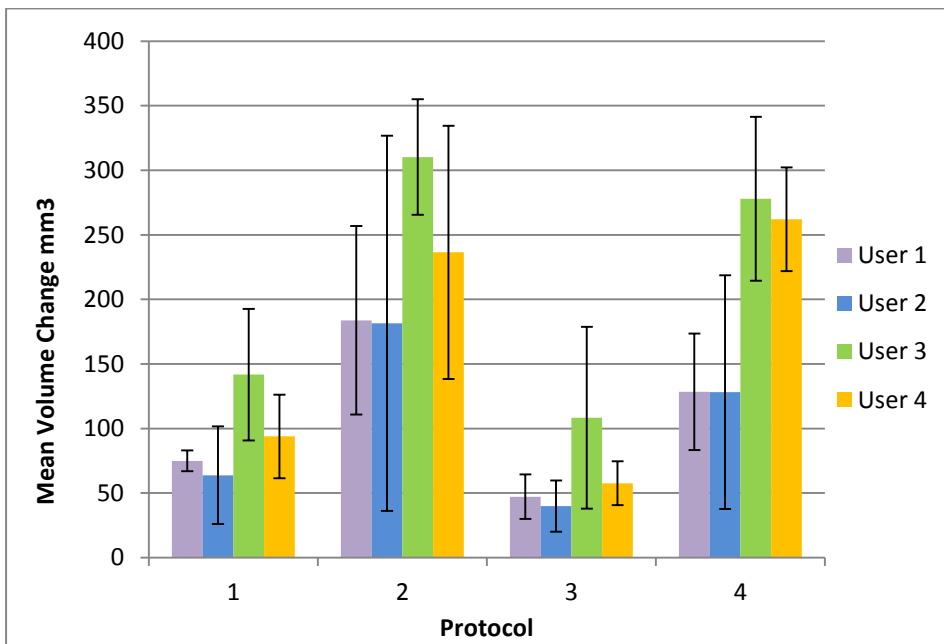


**Figure 1: Inter-user variability of the four protocols for each user for explant 6N (±95% Confidence intervals)**

## Appendix 3: Analysing Volume Change in Explants with Redlux

### Protocol 2: Defining the reference Sphere

1. Import .dat file using “[R&D] Import CMM data” script.
2. Remove rim using local radius tool and the exclusion tool from the analysis tab (Figure 1). Areas are excluded by right clicking in the area to be excluded and clicking exclude.

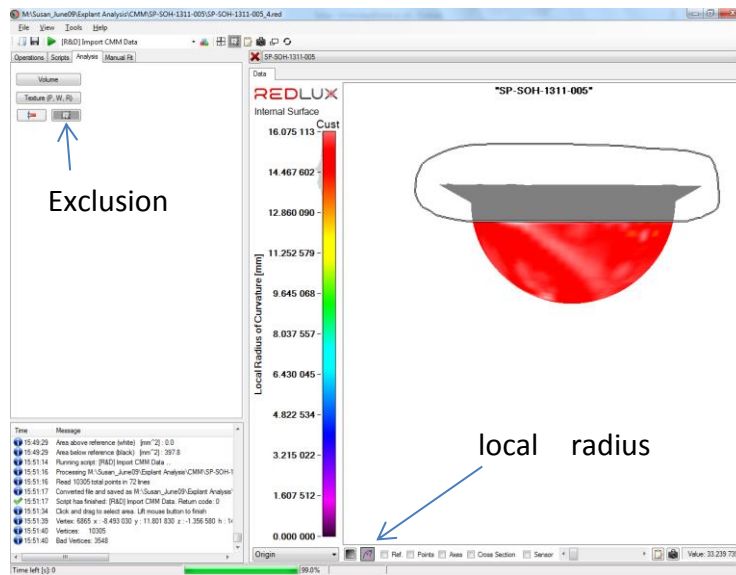


Figure 1 Exclusion of the rim area with local radius tool selected.

3. Exclude any screws holes (or major damage to the bearing surface; Figure 2).

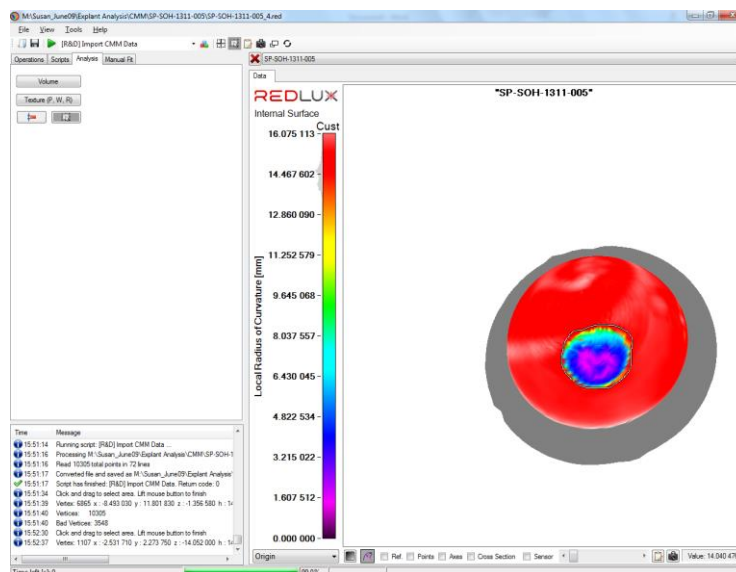
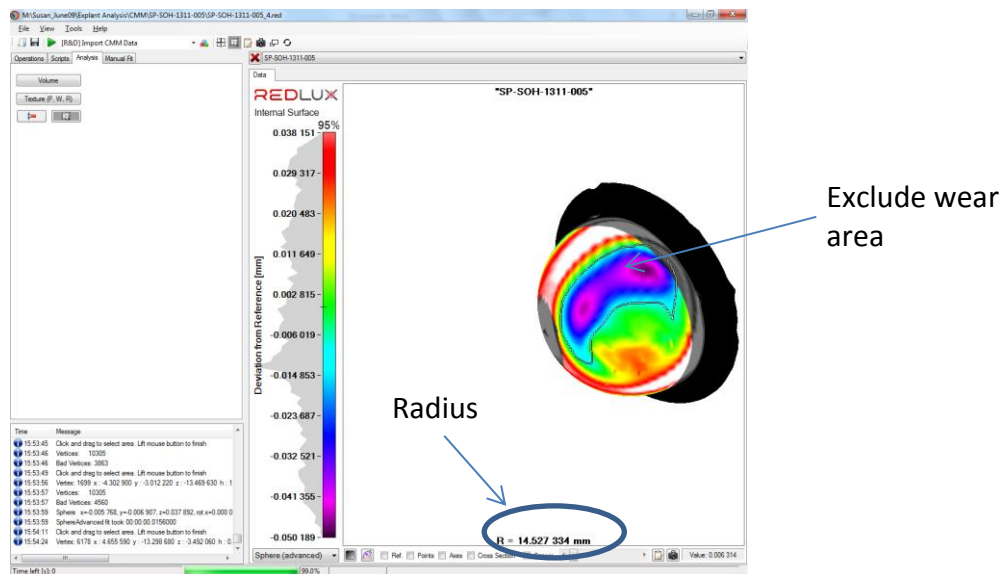


Figure 2 Exclusion of a screw hole with local radius tool selected

4. Deselect local radius tool and click on Fit to Sphere (advanced) and note radius.
5. Exclude wear area and note radius (Figure 3)



**Figure 3 Exclusion of the wear area**

6. Repeat step 5 by increasing the size of the excluded wear area until the radius stops increasing or the excluded area is too big to continue.
7. Right click on work area and select "Include All"
8. Save the file and note radius.

### Protocol 2: Calculating the Volume Change

9. Draw round the wear area and exclude the rest of the cup. Do this on the inside of the cup so that all other areas are excluded (Figure 4).
10. Right click on the histogram and set minimum so that the wear area turns black (this is usually somewhere in the purple region of the histogram).

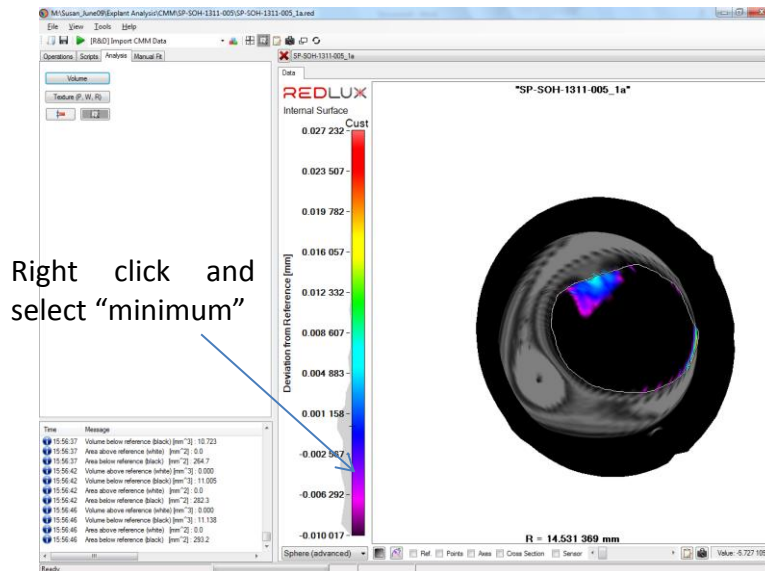
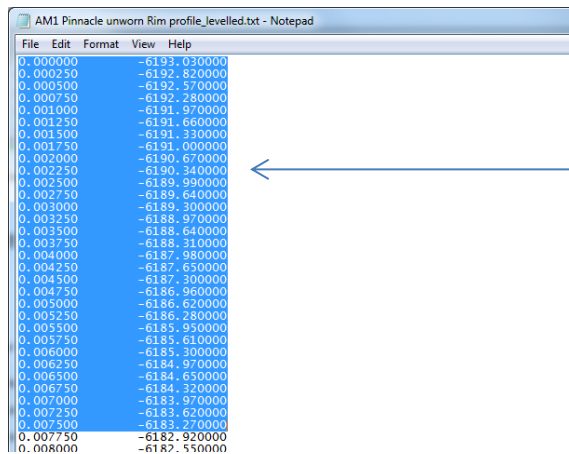


**Figure 4 Selection of the wear area from the inside of the cup with the remaining areas of the cup excluded**

11. Click on "Volume" tool. Observe volume and area.
12. Repeat step 10 until the volume stops increasing.
13. Note Volume and Area.

## Appendix 4: Analysing Rim Deformation in UHMWPE Liners

1. Export raw data file from Talysurf and save as .PRF (export original file and not analysed file)
2. In Talymap Gold -> Open blank document -> Open studiable -> Save profile as .txt
3. For each liner, copy the x and y coordinates for all rim traces from text files (Figure 1)



The screenshot shows a Notepad window titled "AM1 Pinnacle unworn Rim profile\_levelled.txt - Notepad". The window contains a list of x and y coordinates for a trace. The x-axis values range from 0.000000 to 0.008000 in increments of 0.000250. The y-axis values range from -6193.030000 to -6182.550000, with a general upward trend. An arrow points from the text on the right to the y-axis values in the screenshot.

| x        | y            |
|----------|--------------|
| 0.000000 | -6193.030000 |
| 0.000250 | -6192.820000 |
| 0.000500 | -6192.970000 |
| 0.000750 | -6192.280000 |
| 0.001000 | -6191.970000 |
| 0.001250 | -6191.660000 |
| 0.001500 | -6191.230000 |
| 0.001750 | -6191.000000 |
| 0.002000 | -6190.670000 |
| 0.002250 | -6190.340000 |
| 0.002500 | -6189.990000 |
| 0.002750 | -6189.640000 |
| 0.003000 | -6189.300000 |
| 0.003250 | -6188.970000 |
| 0.003500 | -6188.640000 |
| 0.003750 | -6188.310000 |
| 0.004000 | -6187.980000 |
| 0.004250 | -6187.650000 |
| 0.004500 | -6187.300000 |
| 0.004750 | -6186.960000 |
| 0.005000 | -6186.620000 |
| 0.005250 | -6186.280000 |
| 0.005500 | -6185.950000 |
| 0.005750 | -6185.610000 |
| 0.006000 | -6185.300000 |
| 0.006250 | -6184.970000 |
| 0.006500 | -6184.650000 |
| 0.006750 | -6184.320000 |
| 0.007000 | -6183.970000 |
| 0.007250 | -6183.620000 |
| 0.007500 | -6183.270000 |
| 0.007750 | -6182.920000 |
| 0.008000 | -6182.550000 |

x and y coordinates for a trace taken across the unworn region of an XLPE liner

Figure 1 Text file showing the x and y coordinates of the Talysurf trace

4. For each liner paste the x and y coordinates into a spreadsheet. The unworn trace (or the trace to which all other traces will be compared) should be pasted in columns A & B and then two columns should be left blank between each consecutive trace (Figure 2). Name the Excel file and the worksheet and save in the same folder as the Matlab program file.

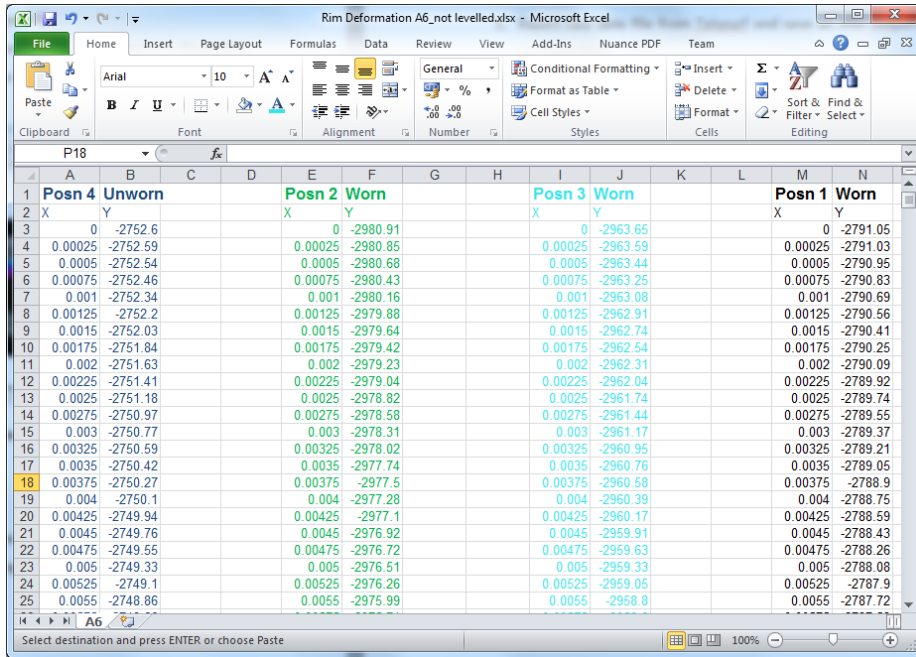


Figure 2 Spreadsheet showing the x and y coordinates of the traces. The colours represent the colours of the traces in the Matlab plots and all traces will be compared to the traces in the first column (usually the unworn trace)

5. Open Matlab and Open the relevant program (AGEDGVF\_notlevelled\_5.m in this example).

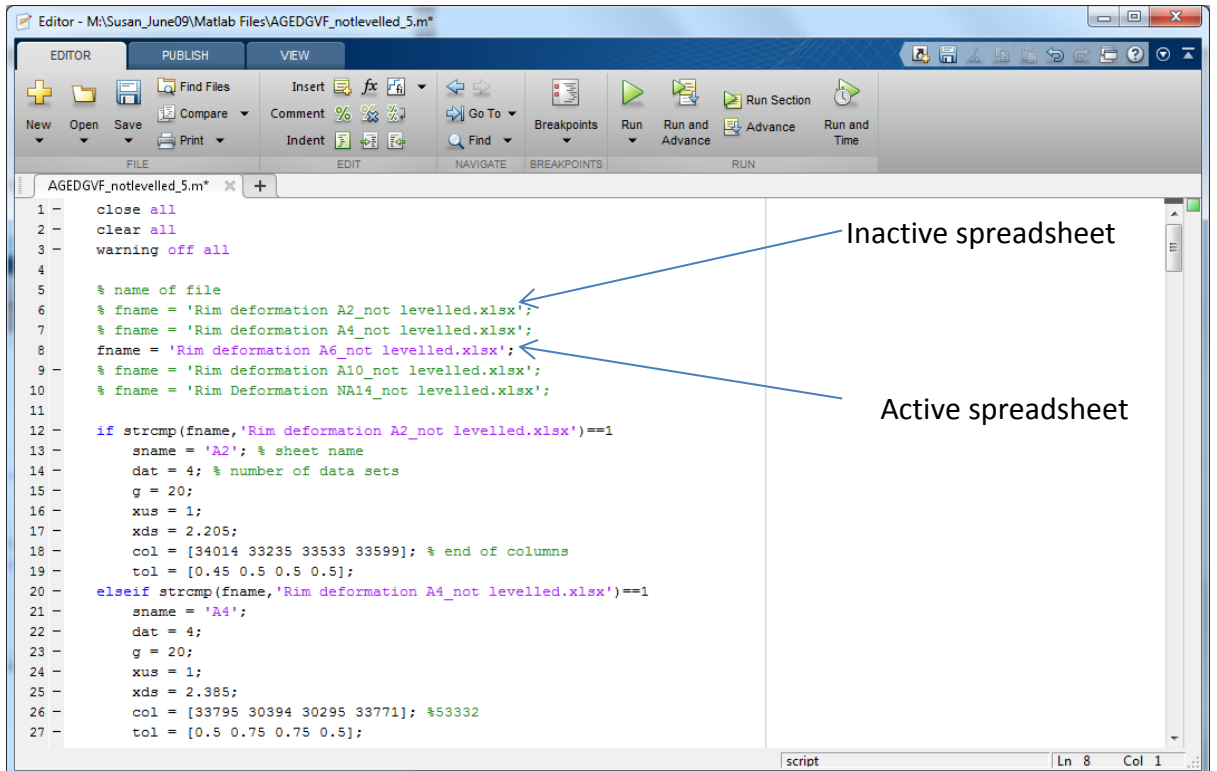


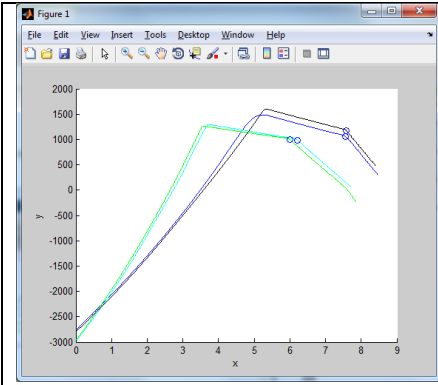
Figure 3 First few lines of the Matlab code with the names of the active and inactive spreadsheets highlighted

6. Enter the name of the Excel file in the first section under %name of file. Anything after % will be ignored so several spreadsheets can be entered at this stage (Figure 3).
7. For each spreadsheet in the 'if' and 'elseif' sections enter the following details (Figure 4):
  - a. The name of the file after 'fname'
  - b. The name of the worksheet 'sname'
  - c. The number of data sets (dat =?)
  - d. The number of the last cell in each column; col = [.....]

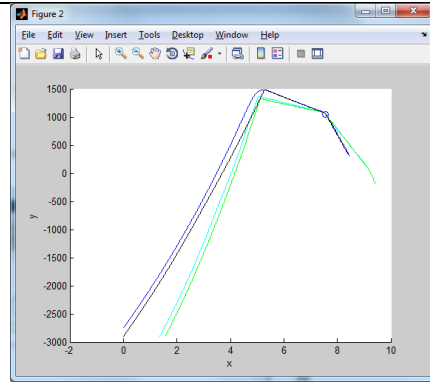
```
if strcmp(fname, 'Rim deformation A2_not levelled.xlsx')==1
    sname = 'A2'; % sheet name
    dat = 4; % number of data sets
    g = 20;
    xus = 1;
    xds = 2.205;
    col = [34014 33235 33533 33599]; % end of columns
    tol = [0.45 0.5 0.5 0.5];
```

**Figure 4 Code relating to the details of each spreadsheet and trace data**

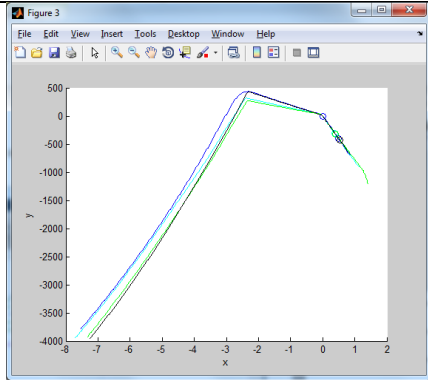
8. Run the program (click Run or press F5) ensuring the correct spreadsheet is active.
9. A series of graphs will appear:



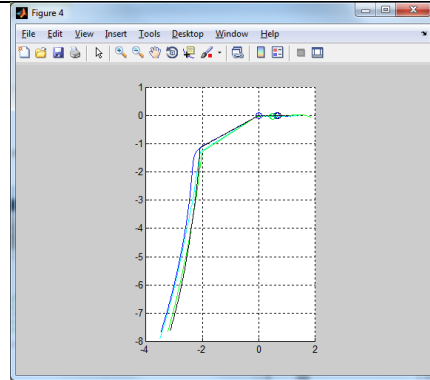
The raw data plotted for each trace



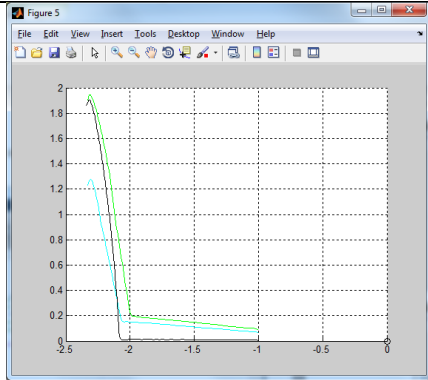
The reference point matched for each trace



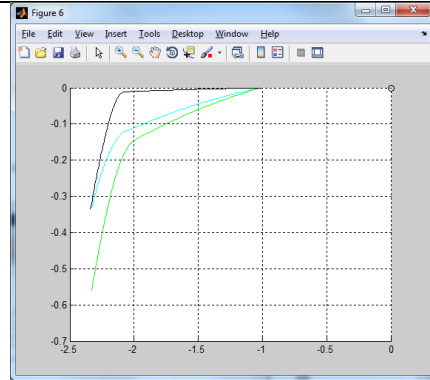
The horizontal rim of the worn traces rotated round the reference point to match the worn trace



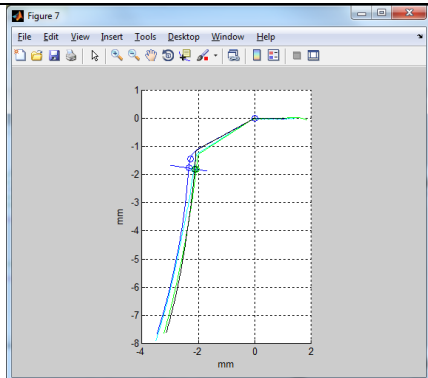
All traces levelled and scaled (both axes in mm)



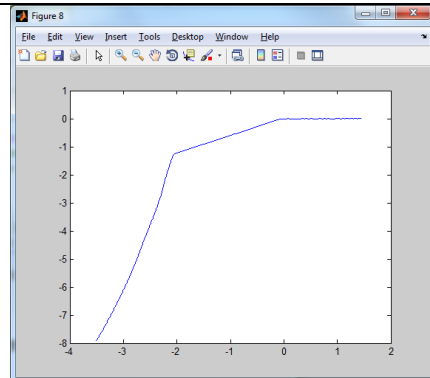
Plot of penetration distance between traces



Plot of volume between traces (not used)



Traces aligned with the penetration distance marked at a user defined point



A single trace

10. Seven colours are available in Matlab and each colour corresponds to the column in spreadsheet in the following order Dark Blue, Green, Cyan, Black, Magenta, Red, Yellow. Colours can be changed in by changing the variable c (Figure 5).

```
62 - % for all data sets
63 - figure
64 - hold on
65 - xlabel('x')
66 - ylabel('y')
67 - p = 10;
68 - dsr = 100;
69 - R = cell(1,dat);
70 - S = cell(1,dat);
71 - R = zeros(dat,2);
72 - K = zeros(1,dat);
73 - c = [98 99 103 107 109 114 121 98 99 103 107 109]; % blue cyan green black magenta red yellow blue.....(again!)
74
```

Figure 5 section of the code where the trace colours are defined

11. If the reference point is not located in the correct location (Figure 6A). Then changing the tolerance will move the reference point (Figure 6B & C).

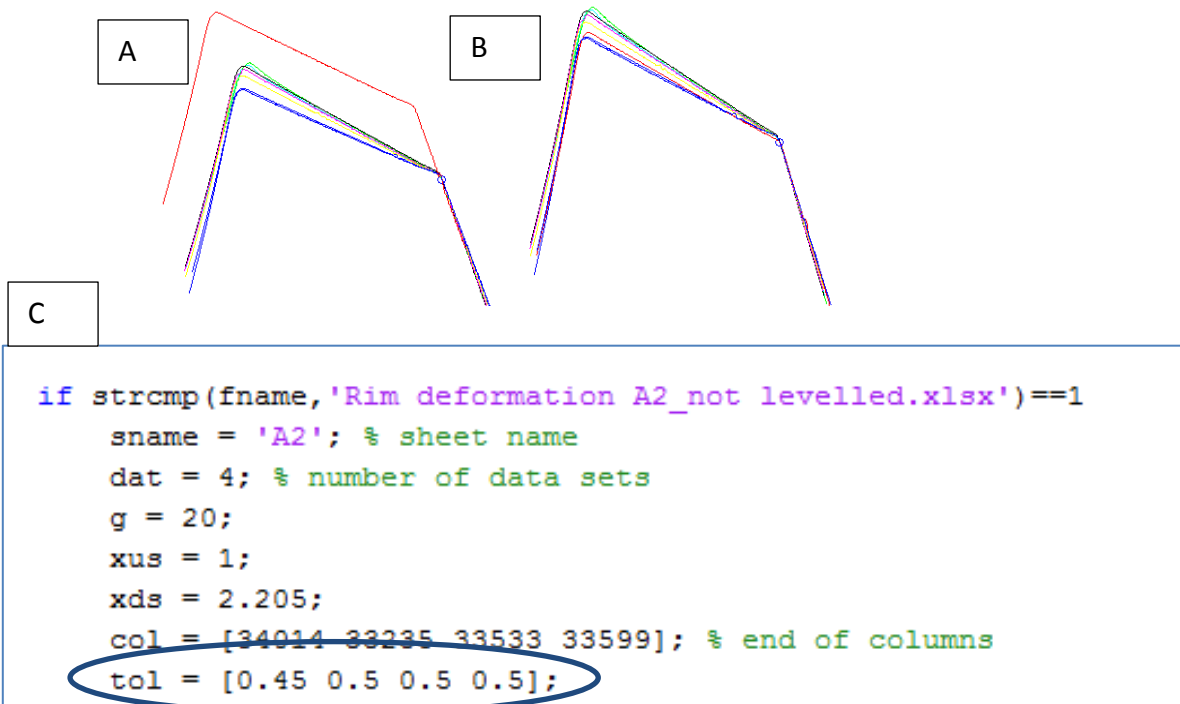


Figure 6A, B & C: A trace with the reference point located in the wrong place, B the corrected reference point and C the section of code where the tolerance can be modified.

12. The point at which the penetration distance is calculated can be defined by the user by entering the x value into the code (use the zoom feature to refine; Figure 7)

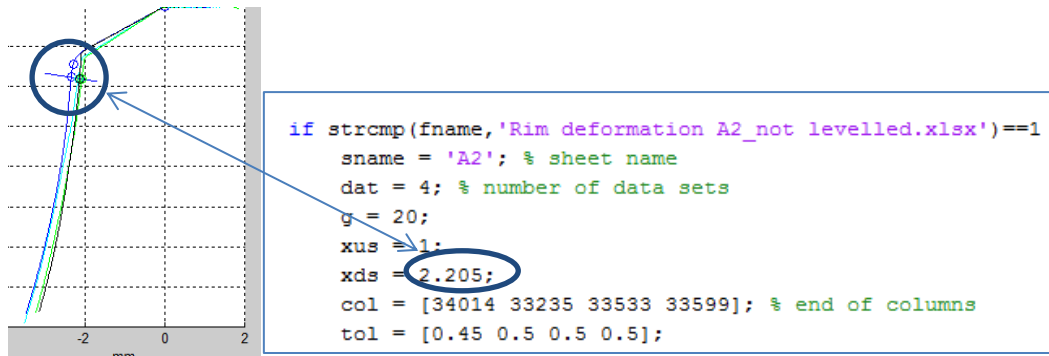


Figure 7 the point where the penetration (distance between the unworn and worn traces is calculated and the section of code where this is defined.

13. The penetration is obtained by entering N into the command prompt (Figure 8):

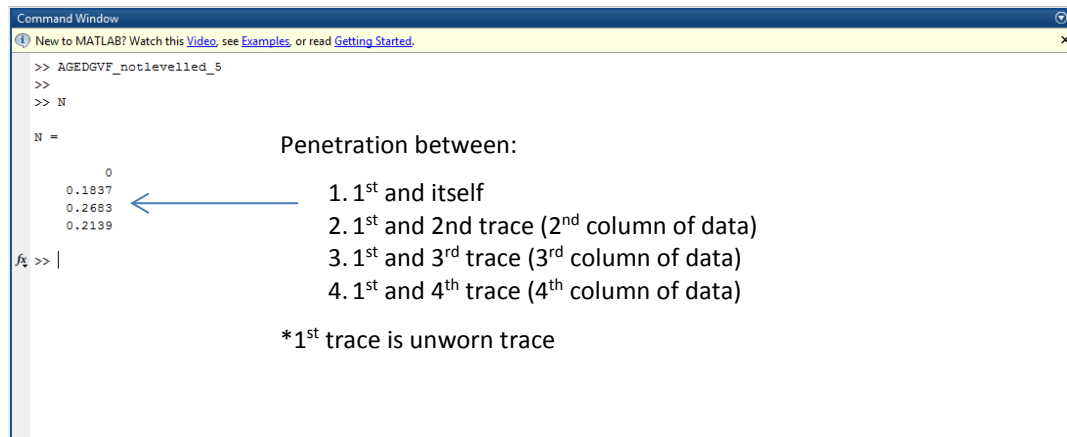
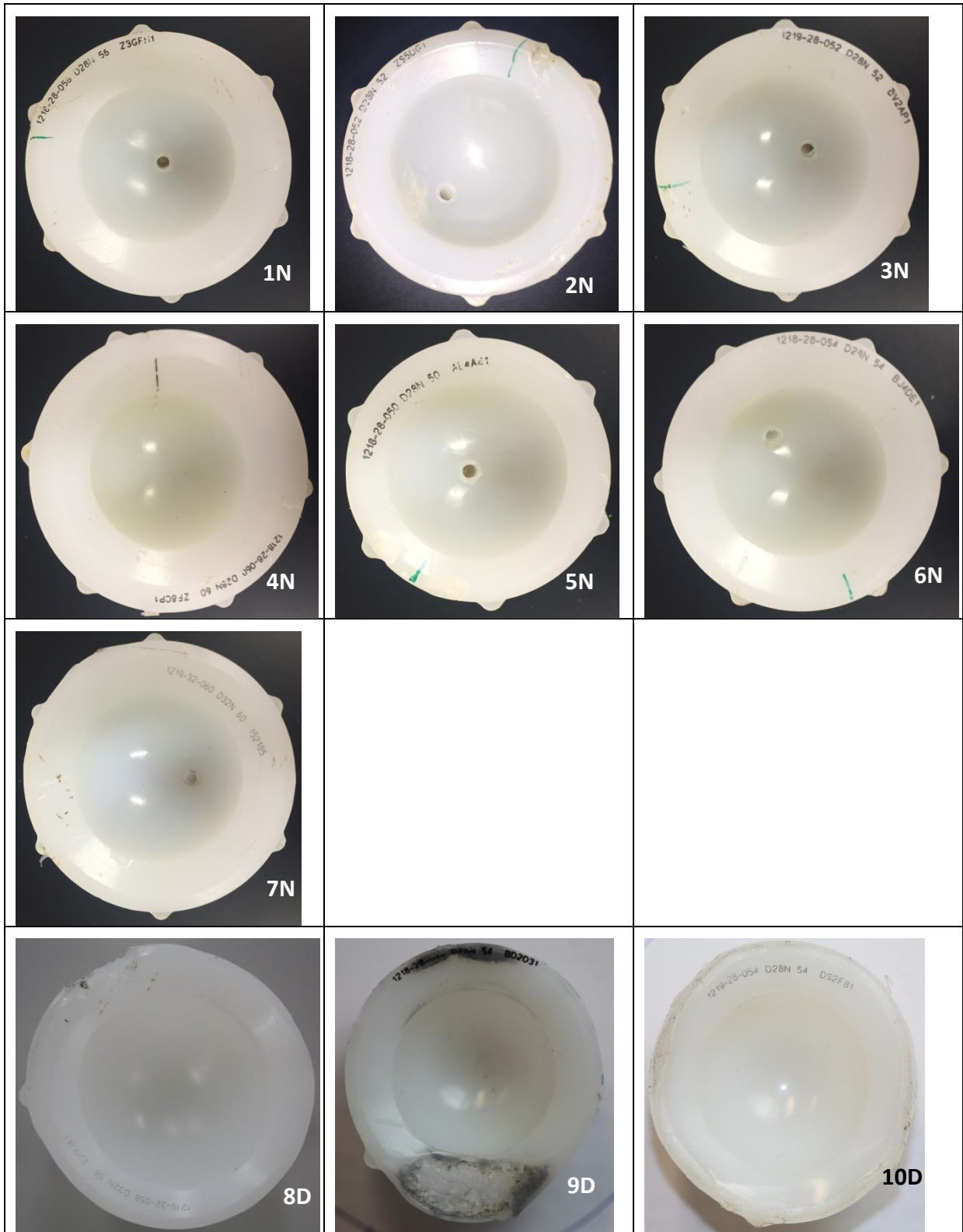
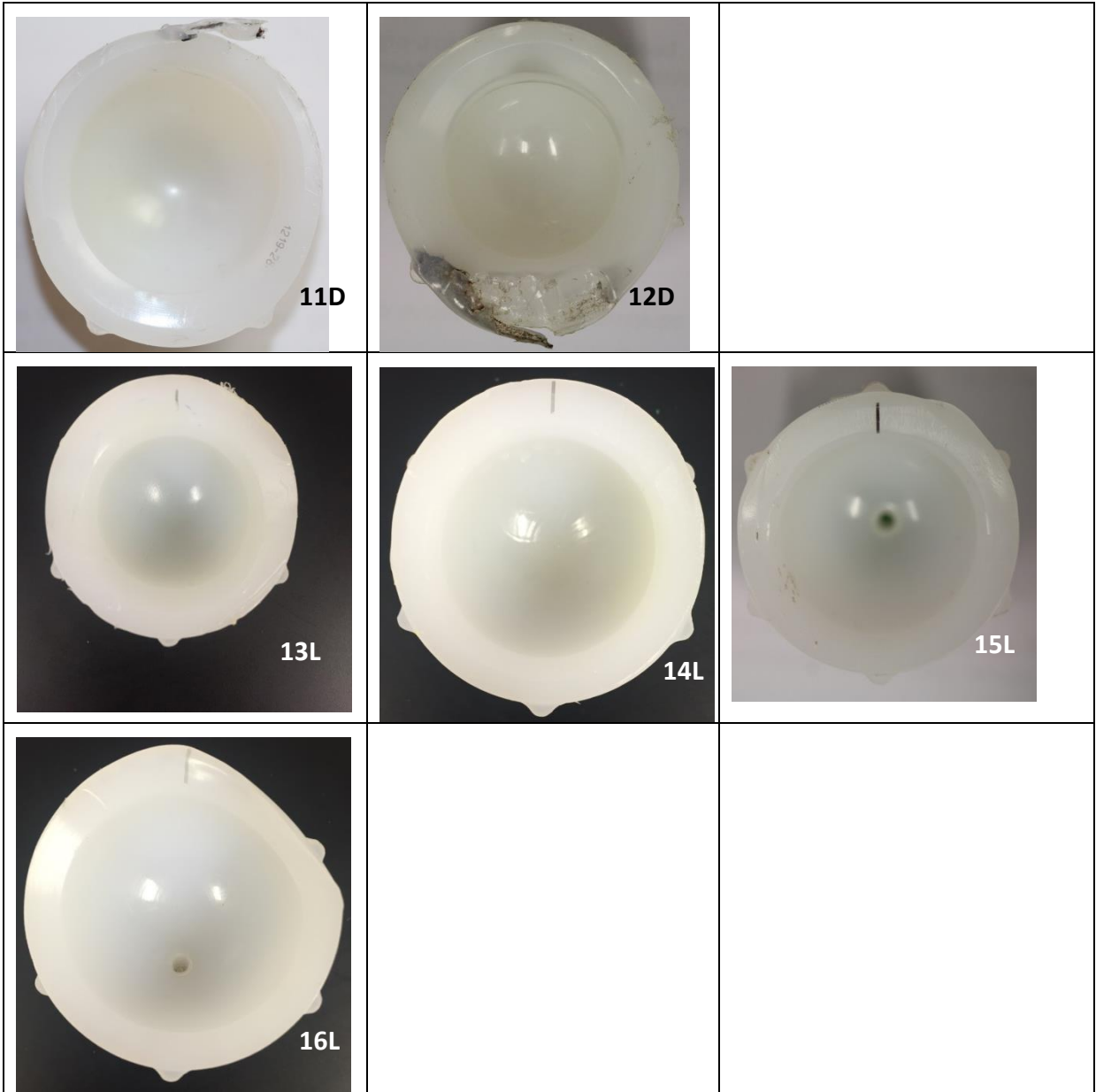


Figure 8 The command prompt window with the penetration distances displayed (all distances are relevant to the unworn trace or first column of data.

14. Standard Matlab features can be used to save and print graphs.

### Appendix 5: Images of Explanted Acetabular Liners





## **Appendix 6: Informed Consent and Explant Collection Documents**

### **Patient Information Sheet: Wear Analysis of Explanted Orthopaedic Implants**

#### **Information for the patient**

You are being invited to take part in a research study. Before you decide whether to take part you need to understand why the research is being done and exactly what it will involve. Please take the time to read the following information carefully and please do not hesitate to ask any questions if required.

#### **Background information**

Over 1 million artificial hips and knees are implanted into patients each year around the world. These can be made of plastic, metal and/or ceramic components. Hip replacement was one of the most successful operations of the 20<sup>th</sup> Century, however artificial hip and knee implants sometimes require replacement for a number of reasons. Your surgeon should discuss this with you.

#### **What is the purpose of the research?**

We are research scientists from the Institute of Medical and Biological Engineering at the University of Leeds. We want to improve our understanding of why implants fail. This is done by analysing the surfaces of your old implant for damage, along with the wear particles from the tissues from around your implant. Completing this research may allow us to improve joint replacements for future patients.

#### **Why have I been chosen?**

You have been chosen because you are a patient undergoing joint replacement revision surgery. Approximately 200 other patients will be invited to participate in this research.

#### **Do I have to take part?**

It is up to you to decide if you would like to take part. If you decide to take part, you will be given this information sheet to keep and you will be asked to sign a consent form to show you have agreed to take part. You are free to withdraw at any time and without giving a reason. A decision not to take part, or to withdraw at any time, will not affect the standard of care you receive.

#### **What are the benefits or risks involved?**

There are no benefits to you if you choose to take part. This research may however lead to improvements in joint replacements for future patients. There are no risks to you if you choose to take part. The tissue (bone, cartilage and soft tissue) we would like to analyse is routinely removed by the surgeon to prepare the implantation site for your new joint replacement. This tissue would normally be discarded following your operation.

#### **What will happen if I take part?**

You do not have to do anything. Your old joint replacement device and discarded tissue will be collected from the operating theatre after your operation and taken to the laboratory at the University of Leeds for analysis. No part of the surgical procedure will be different if you choose to participate in this study or not.

Personal information, relevant to this study, will also be collected, stored and processed to help us with our research. Your information, failed implant and discarded tissue will be assigned a code so that you will remain anonymous to researchers at the University of Leeds. Only the project co-ordinator at the University of Leeds will have access to your consent form, which will remain in a sealed envelope and kept in a locked cabinet. All researchers at the University of Leeds will have a duty of confidentiality to you as a research participant.

Your old joint replacement will be examined for wear and surface measurements will be taken, the components will then be stored in a locked cabinet in a locked room. Your tissue will be analysed to characterise the wear particles present and will also be stored in a locked cupboard in a locked laboratory. After the analysis has taken place we will record the results and your tissue sample will either be incinerated or stored for future research. If your sample is deemed suitable for future research it will be stored under the same conditions as mentioned above and used in similar studies by researchers at the University of Leeds. There will be no genetic analysis of the tissue.

If your joint replacement has failed prematurely, this will be reported to the manufacturer. Your personal data will not be disclosed by researchers at the University of Leeds and the manufacturer will be referred to your orthopaedic surgeon should they require further information.

The duration of the study is 5 years in total. Your data and explants will be stored for a further 5 years to allow for the research to be published at the end of the study.

#### **What if my operation is unsuccessful?**

The surgery itself does not form part of this study. As no part of the surgical procedure or the care that you will receive will be different should you choose to participate, researchers at the University of Leeds are not responsible for the success or otherwise of your operation and any matters relating to your surgery or treatment should be discussed with your surgeon in the normal way.

#### **Will my taking part be confidential?**

Yes. We will follow legal and ethical practice and all information about you will be handled in confidence and in accordance with the Caldicott Principles and the Data Protection Act 1998.

#### **What will happen to the results of the research?**

Results of the research will be used in internal scientific reports. It is also anticipated that results will be submitted to peer reviewed scientific journals. Participant identity will remain confidential. Your surgeon will be sent a summary of research findings. Should you wish to receive a copy of the results please request them from your surgeon. Alternatively, in time research may be published in scientific journals, visit the iMBE website for details. No patients will be identifiable.

#### **Who has reviewed the study and who is funding the research?**

All research in the NHS is looked at by an independent group of people, called a Research Ethics Committee to protect your safety, rights, wellbeing and dignity. This study has been reviewed and given favourable opinion by a Research Ethics Committee. This research is being funded by the National Institute for Health Research (NIHR).

#### **Further Information**

Please contact Dr Sophie Williams at the University of Leeds [REDACTED] or email [REDACTED] should you require any further information regarding the research.

If you are unhappy with your treatment at any time and wish to complain formally, you can do this through the NHS Complaints Procedure. Details can be obtained from the hospital.

## Patient Consent Form: Wear Analysis of Explanted Orthopaedic Implants

Centre: \_\_\_\_\_

iMBE code: \_\_\_\_\_

### Patient consent

Please initial box

- |    |   |                          |
|----|---|--------------------------|
| 1. | I confirm that I have read and understand the Patient Information Sheet (version 3) for the above research study. I have had the opportunity to ask questions and have had these answered satisfactorily.   | <input type="checkbox"/> |
| 2. | I understand that my participation is voluntary and that I am free to withdraw at any time without giving any reason, without my medical care or legal rights being affected.   | <input type="checkbox"/> |
| 3. | I understand that sections of any of my medical notes may be looked at by responsible individuals from [Leeds Teaching Hospitals NHS Trust] or from the regulatory authorities, where it is relevant to my taking part in research. I give permission for these individuals to have access to my records. | <input type="checkbox"/> |
| 4. | I understand that researchers at the University of Leeds will analyse my explanted joint replacement device.  | <input type="checkbox"/> |
| 5. | I understand that researchers at the University of Leeds will analyse tissue from around my implant for wear particles.   | <input type="checkbox"/> |
| 6. | I agree to have my tissue sample stored at the University of Leeds for future research.   | <input type="checkbox"/> |
| 7. | I understand that researchers at the University of Leeds will process personal information that that is relevant to the research. I give permission for these individuals to obtain, store and process such information.  | <input type="checkbox"/> |
| 8. | I agree to take part in the above study.  | <input type="checkbox"/> |

---

Name of Patient

Date

Signature

---

Name of Person Taking Consent

Date

Signature

**Explant information: Wear Analysis of Explanted Orthopaedic Implants**

Patient code (designated by iMBE): \_\_\_\_\_

Name of Hospital (Revision Operation) \_\_\_\_\_

Name of Surgeon (Revision Operation) \_\_\_\_\_

Date of Birth \_\_\_\_\_

Height / Weight \_\_\_\_\_

Patient Sex      M    F

Type of Prosthesis \_\_\_\_\_

Is this explant the Primary explant?  1st revision explant?  2nd revision explant?  
 Other?

Implant Date \_\_\_\_\_

Explant Date \_\_\_\_\_

Time of prosthesis in vivo \_\_\_\_\_

Side Operated On \_\_\_\_\_

Pre-revision x-ray available?    YES    NO

Initial Diagnosis \_\_\_\_\_

Reason for Revision \_\_\_\_\_

Patient Activity level before revision. Please tick to indicate level of activity.

|     | Immobile/<br>Wheelchair | 2 Sticks (Zimmer<br>frame) | 1 stick | Sedentary | Reasonably<br>active | Very active |      |
|-----|-------------------------|----------------------------|---------|-----------|----------------------|-------------|------|
| Low |                         |                            |         |           |                      |             | High |

**Hip only:**                      Is there a history of dislocation?                      YES    NO \_\_\_\_\_

Is there evidence of impingement at time of revision?                      YES    NO \_\_\_\_\_

**Knee only:**                      Is there evidence of medial and/or lateral laxity?                      YES    NO \_\_\_\_\_

If yes, to what degree? mild  moderate  severe

Is there evidence of gross surgical malalignment?                      YES    NO \_\_\_\_\_

Any other information

Thank you for your help

